

AISC E&R Library



7344

1206



→ RESEARCH LIBRARY

key words:

- 1- tubular members
- 2- bracing, fldgs.
- 3- seismic design



---

**Department of Civil Engineering**

The University of Michigan  
College of Engineering

Ann Arbor, Michigan 48109

---

RR1206

7344

AISC - 2068

PDF/FTG - Type 1

Project: AISC

Year:

Filename: 7344-01

Files:

Document Title: Special Instructions from Local Building Official Perspective

Scan & Pre-Process:

- Prep Document      Insertions?       Yes       No
- Canon Scan
- Color/Grayscale Scan
- Image Enhance

FineReader Operations

zk

- Zoning       start @ \_\_\_\_\_ of \_\_\_\_\_ /  start @ \_\_\_\_\_ of \_\_\_\_\_
- Spell Check       start @ \_\_\_\_\_ of \_\_\_\_\_ /  start @ \_\_\_\_\_ of \_\_\_\_\_
- Save to PDF

HC Page #	Page of File	Error (missing page, pixedit error, crashed page, etc.) Note errors, be clear and brief. Bring complex issues to project manager.	OK

- Insert Images       Final Quality Control
- Proof
- Rename / Add/Remove Index Data, move to Delivery Area, Update Worksheet

Additional Notes:

# AISC - 2068

# PDF/FTG - Type 1

Project: AISC

Year: 98

Filename: 7344-02

Files:

Document Title: An Energy Design Approach to Reduce the Ductility Demands of Steel Moment Frames Subjected to Severe Earthquakes.

### Scan & Pre-Process:

- Prep Document      Insertions?       Yes       No
- Canon Scan
- Color/Grayscale Scan
- Image Enhance

### FineReader Operations

- Zoning       start @ <sup>156</sup> 25 of 114 / 1      start @ \_\_\_\_\_ of \_\_\_\_\_
- Spell Check       start @ <sup>157</sup> 25 of 114 / 1      start @ \_\_\_\_\_ of \_\_\_\_\_
- Save to PDF

HC Page #	Page of File	Error (missing page, pixedit error, crashed page, etc.) <i>Note errors, be clear and brief. Bring complex issues to project manager.</i>	OK
78	190	Skew.	

- Insert Images       Final Quality Control
- Proof
- Rename / Add/Remove Index Data, move to Delivery Area, Update Worksheet

Additional Notes:

00249  
69  
April 1987

Research Report UMCE 87-3

INVESTIGATION OF CONCRETE-FILLED  
STEEL TUBES UNDER  
CYCLIC BENDING AND BUCKLING

Zhiyuan Liu  
Subhash C. Goel *author*

A Report on Research Sponsored by  
National Science Foundation  
Grant No. CEE-8300684

---

Department of Civil Engineering

The University of Michigan  
College of Engineering  
Ann Arbor, Michigan 48109

---

ABSTRACT

INVESTIGATION OF CONCRETE-FILLED  
STEEL TUBES UNDER CYCLIC BENDING AND BUCKLING

by

Zhiyuan Liu

and

Subhash C. Goel

In recent years cold-formed rectangular tubular bracing members have become popular for steel structures in seismic regions. It is known that these bracing members can provide considerable strength and lateral stiffness to a structure in an economical manner. But tubular bracing members with large width-thickness ratio (yet within the limits specified by current codes) are susceptible to early cracking due to local buckling and subsequent loss of ductility and strength when subjected to cyclic deformation. This study was concerned with finding a suitable solution to premature fracture problem in cold-formed rectangular tubular bracing members.

Review of the past related studies and results of preliminary concrete-filled beam and stub column tests in this study gave a clue that filling concrete in tubular bracing members might improve the local buckling behavior. A series of hollow and concrete-filled tubular beams, stub columns, and full size bracing specimens were tested in this study to understand how concrete and steel work together in these composite bracing members.

On the basis of the test results it was concluded that

the presence of concrete could change the local buckling mode, reduce its severity, and increase the plastic hinge moment capacity, energy dissipation capacity and fracture life. Concrete filling also increased compression forces and tensile forces depending on the ratio of area of concrete to steel and the slenderness ratio. The strength of concrete and steel fibers did not have significant effect on the behavior of these composite bracing members.

An empirical hysteresis model is proposed for concrete-filled tubular bracing members. This model considers the increases in tension and compression forces and "fuller" shape of hysteresis loops due to the presence of concrete.

## ACKNOWLEDGMENTS

This report was submitted by the senior author in partial fulfillment of the requirements for the degree of Doctor of Philosophy (Civil Engineering) in the Horace H. Rackham School of Graduate Studies at The University of Michigan. Dr. Liu wishes to express his sincere appreciation to Professor Goel, chairman of his doctoral committee, for his invaluable guidance, encouragement and assistance throughout this study. The authors would like to thank Professors Will Hansen, Robert D. Hanson, Antoine E. Naaman, and Alan S. Wineman, (members of the doctoral committee) for reviewing the report and offering helpful suggestions.

The investigation was sponsored by the National Science Foundation through Grant No. CEE-8300684 for which the authors are most grateful. The conclusions and opinions expressed in this report are solely those of the authors and do not necessarily represent the views of the sponsor.

The authors also wish to express their thanks to a number of students in the Department of Civil Engineering who helped in the test program at various stages. These are: Stephen Gorsuch, Hacksoo Lee, Sangsoo Lee and Peixin Xu. The help and cooperation received from Ray Allen, Kevin Schmidt and James Wanzeck in the G.G. Brown Laboratory is gratefully

acknowledged.

The senior author wishes to express his special thanks to his wife, Jin Shi, for her keen interest, understanding and encouragement during his four years of graduate study at The University of Michigan. His little son, Andrew, missed him during his play hours and deserves special thanks.

TABLE OF CONTENTS

ACKNOWLEDGMENTS . . . . . ii

LIST OF TABLES . . . . . vii

LIST OF FIGURES . . . . . viii

LIST OF APPENDICES . . . . . xvii

NOTATION . . . . . xviii

CHAPTER

I. INTRODUCTION . . . . . 1

    1.1 Introduction . . . . . 1

    1.2 Review of Related Studies . . . . . 3

        1.2.1 Research on Hollow Tubular  
            Bracing Members . . . . . 4

        1.2.2 Research on Tube and Concrete  
            Composite Members . . . . . 5

        1.2.3 Summary of Related Studies . . . . . 7

    1.3 Objectives and Scope . . . . . 8

II. PRELIMINARY TEST PROGRAM . . . . . 11

    2.1 Introduction . . . . . 11

    2.2 Hollow And Concrete-Filled Tubular Beams . . . . . 12

        2.2.1 Apparatus And Procedure . . . . . 13

        2.2.2 Summary of Experimental Observation . . . . . 13

            2.2.2.1 General Behavior . . . . . 14

            2.2.2.2 Local Buckling Modes . . . . . 14

            2.2.2.3 Ultimate Moments . . . . . 15

            2.2.2.4 Ductility And Energy  
                Absorption . . . . . 16

    2.3 Concrete-Filled Stub Columns . . . . . 16

        2.3.1 Experimental Program . . . . . 17

	2.3.1.1	Specimens . . . . .	17
	2.3.1.2	Apparatus And Procedure . . . . .	18
2.3.2		Summary of Experimental Observation . . . . .	19
	2.3.2.1	General Behavior . . . . .	19
	2.3.2.2	Peak Forces . . . . .	20
	2.3.2.3	Local Buckling Modes . . . . .	22
	2.3.2.4	Plateau of Peak Compression Force . . . . .	23
	2.3.2.5	Effect of Steel Fibers . . . . .	25
2.3.3		Summary of Conclusions . . . . .	26
III. MAIN EXPERIMENTAL PROGRAM . . . . .			28
3.1		Introduction . . . . .	28
3.2		Test Specimens . . . . .	29
3.3		Material Properties . . . . .	31
	3.3.1	Steel Tube . . . . .	31
	3.3.2	Concrete . . . . .	33
3.4		Fabrication Process . . . . .	34
	3.4.1	Tubes Filled with Concrete . . . . .	34
	3.4.2	Hollow Tubular Specimens . . . . .	35
3.5		Test Set-Up . . . . .	36
	3.5.1	Loading System . . . . .	36
	3.5.2	Instrumentation . . . . .	37
	3.5.3	Data Acquisition System . . . . .	39
3.6		Loading History . . . . .	39
	3.6.1	Consideration of Loading History . . . . .	39
	3.6.2	Definition of $\Delta_y^*$ . . . . .	40
	3.6.3	Deformation Sequences Used . . . . .	42
IV. EXPERIMENTAL RESULTS OF MAIN TEST PROGRAM . . . . .			44
4.1		Introduction . . . . .	44
4.2		General Observations and Discussions . . . . .	45
	4.2.1	General Observations . . . . .	46
	4.2.2	Failure Modes of Specimens . . . . .	47
4.3		Buckling Modes . . . . .	50
	4.3.1	Overall Buckling . . . . .	50
	4.3.2	Local Buckling . . . . .	52
		4.3.2.1 Hollow Specimens . . . . .	52
		4.3.2.2 Concrete-Filled Specimens . . . . .	54
4.4		Behavior of Specimens under Tension . . . . .	55
	4.4.1	First Yield Force . . . . .	55
	4.4.2	Cyclic Peak Tension Forces . . . . .	60
4.5		Behavior of Specimens under Compression . . . . .	60
	4.5.1	First Buckling Load . . . . .	60
		4.5.1.1 Tangent Modulus Method . . . . .	62
		4.5.1.2 Approximate Method . . . . .	66
	4.5.2	Cyclic Peak Compression Forces . . . . .	68
4.6		Hysteresis Behavior . . . . .	73

V.	MODELING THE HYSTERESIS LOOPS . . . . .	74
5.1	Introduction . . . . .	74
5.2	Review of Jain's Model . . . . .	76
5.2.1	Basic Assumptions . . . . .	76
5.2.2	Detailed Procedure . . . . .	78
5.2.3	Comparison of Test Results with Jain's Model . . . . .	80
5.3	Proposed Model . . . . .	82
5.3.1	Modifications in Jain's Model . . . . .	82
5.3.2	Verification of Proposed Model . . . . .	87
5.3.3	Limitations of Proposed Model . . . . .	88
5.4	Summary . . . . .	88
VI.	SUMMARY AND CONCLUSION . . . . .	90
6.1	Introduction . . . . .	90
6.2	Summary . . . . .	91
6.3	Conclusions . . . . .	93
6.4	Suggestion for Further Studies . . . . .	95
	TABLES . . . . .	97
	FIGURES . . . . .	105
	APPENDICES . . . . .	191
	REFERENCES . . . . .	222

LIST OF TABLES

Table

2-1	Geometrical Properties of Beam Specimens . . . . .	98
2-2	Ultimate Moments of Beam Specimens . . . . .	98
2-3	Number of Cycles and Energy Absorbed by Beams . . . . .	99
2-4	Geometrical Properties of Stub Columns . . . . .	100
3-1	Geometrical Properties of Bracing Specimens . . . . .	101
3-2	Results of Coupon Tests of Steel . . . . .	102
3-3	Mix Proportions and Strength of Concrete . . . . .	103
4-1	Energy Absorbed by Specimens T633H and T633C6 . . . . .	104

00254

LIST OF FIGURES

Figure

2.1	Typical Beam Specimen . . . . .	106
2.2	Test Set-Up for Beam Testing . . . . .	106
2.3	Schematic Drawing of the Test Set-Up for Beam Testing . . . . .	107
2.4	Load History for Beam Testing . . . . .	107
2.5	Hysteresis Loops of Group 1 Beam Specimens . . . (a) Specimen BH (b) Specimen BHA	108
2.6	Hysteresis Loops of Group 2 Beam Specimens (1) . (a) Specimen BC6 (b) Specimen BC6F	109
2.7	Hysteresis Loops of Group 2 Beam Specimens (2) . (a) Specimen BC8F (b) Specimen BC6A	110
2.8	Local Buckling Mode of Hollow Beams . . . . .	111
2.9	Local Buckling Mode of Beams Filled with Concrete . . . . .	111
2.10	Maximum Cyclic Moments of Group 1 Beams . . . . . (a) Specimen BH (b) Specimen BHA	112
2.11	Maximum Cyclic Moments of Group 2 Beams (1) . . . (a) Specimen BC6 (b) Specimen BC6F	113
2.12	Maximum Cyclic Moments of Group 2 Beams (2) . . . (a) Specimen BC8F (b) Specimen BC6A	114
2.13	Test Set-Up for Column Tests . . . . .	115

Figure

2.14	Typical Stub Column Specimen and Specimen C633HS . . . . .	115
	(a) Typical Specimen	
	(b) Specimen C633HS	
2.15	Force-Deformation Curves for Group 1 Stub Column Specimens . . . . .	116
2.16	Force-Deformation Curves for Group 2 Stub Column Specimens . . . . .	117
2.17	Different Local Buckling Modes Between Hollow and Concrete-Filled Stub Columns . . . . .	118
2.18	Local Buckling Mode of Specimen C633HS . . . . .	118
2.19	The Difference in Stability of the Peak Force between Column Specimens with Different Width-Thickness Ratios . . . . .	119
2.20	Difference in Stability of Peak Force between Hollow and Concrete-Filled Stub Columns . . . . .	120
2.21	Comparison between Column Specimens with and without Steel Fibers . . . . .	121
3.1	Hollow Bracing Specimen T633H . . . . .	122
3.2	Concrete-Filled Bracing Specimen T633C6 . . . . .	123
3.3	Concrete-Filled Bracing Specimen T633C4 . . . . .	124
3.4	Concrete-Filled Bracing Specimen T633C4F . . . . .	125
3.5	Concrete-Filled Bracing Specimen T633C6F . . . . .	126
3.6	Concrete-Filled Bracing Specimen T633C8F . . . . .	127
3.7	Hollow Bracing Specimen T424H . . . . .	128
3.8	Concrete-Filled Bracing Specimen T424C6 . . . . .	129
3.9	Hollow Bracing Specimen T422H . . . . .	130
3.10	Gusset Plate for 6x3" Tubular Specimens . . . . .	131
3.11	Gusset Plate for 4x2" Tubular Specimens . . . . .	131
3.12	Typical Stress-Strain Curves for Tube Material from Coupon Tests . . . . .	132

Figure

3.13	Cracking in Concrete-Filled Columns Made from Different Tubes . . . . .	133
3.14	Steel Fibers . . . . .	133
3.15	Concrete Cylinder Test Results . . . . .	134
3.16	Tube End Treatment for Filling Concrete . . . . .	135
3.17	Assembly Jig for Bracing Specimens . . . . .	135
3.18	Test Frame for Bracing Specimens . . . . .	136
3.19	Schematic Drawing of the Testing Frames . . . . .	137
3.20	Data Acquisition System of Main Testing . . . . .	138
3.21	Loading History of Bracing Specimens . . . . .	139
3.22	Definition of Yield Stress for Tubes . . . . .	140
4.1	Failure Mode and Hysteresis Loops of T633H . . . . . (a) Cycle Numbers of Crack and Failure (b) Hysteresis Loops	141
4.2	Failure Mode and Hysteresis Loops of T633C6 . . . . . (a) Cycle Numbers of Crack and Failure (b) Hysteresis Loops	142
4.3	Failure Mode and Hysteresis Loops of T633C4 . . . . . (a) Cycle Numbers of Crack and Failure (b) Hysteresis Loops	143
4.4	Failure Mode and Hysteresis Loops of T633C8F . . . . . (a) Cycle Numbers of Crack and Failure (b) Hysteresis Loops	144
4.5	Failure Mode and Hysteresis Loops of T424H . . . . . (a) Cycle Numbers of Crack and Failure (b) Hysteresis Loops	145
4.6	Failure Mode and Hysteresis Loops of T422H . . . . . (a) Cycle Numbers of Crack and Failure (b) Hysteresis Loops	146
4.7	Computing Length of Bracing Specimens and Equivalent Sections . . . . . (a) Bending in the In-Plane Direction (b) Bending in the Out-of-Plane Direction	147

Figure

4.8	Overall Buckling Modes after Formation of Plastic Hinges . . . . .	148
	(a) Hollow Specimen T633H	
	(b) Concrete-Filled Specimen T633C6	
4.9	Local Buckling Modes for Hollow Specimens . . . . .	149
	(a) Specimen T633H with $b/t = 30$	
	(b) Specimen T424H with $b/t = 14$	
4.10	Local Buckling in Concrete-Filled Specimen T633C6 . . . . .	150
	(a) First Local Buckling on Broad Sides	
	(b) Second Local Buckling on Narrow Sides	
4.11	Buckled Sections of Bracing Specimens . . . . .	151
	(a) Hollow Specimen	
	(b) Concrete-Filled Specimens	
4.12	First Yield Force for Hollow and Concrete-Filled Specimens . . . . .	152
	(a) Specimens T424H and T424C6	
	(b) Specimens T633H and T633C6	
4.13	Equivalent Section of Concrete-Filled Specimen for Tension . . . . .	153
4.14	Stress State of One Side of Tube Wall Subjected to Lateral Restraint from Concrete under Tension . . . . .	153
4.15	Cyclic Tension Forces . . . . .	154
	(a) Specimens T633H and T633C6	
	(b) Specimens T424H and T424C6	
4.16	Measured Buckling Stress in the First Cycle for Hollow Specimens . . . . .	156
4.17	First Buckling Load from Tests for All Specimens . . . . .	157
4.18	Typical Stress-Strain Relationship for Tubes . . . . .	158
4.19	Typical Stress-Strain Relationship for Concrete . . . . .	158
4.20	First Buckling Load Comparison between Computed Value and Test Results . . . . .	159
4.21	Definition of Drop of Cyclic Compression Force. . . . .	160
4.22	Suggested Loading History for Producing Steady Drop of Cyclic Compression Force . . . . .	161

Figure

4.23	Expected Cyclic Peak Compression Force Drop Line . . . . .	161
4.24	Cyclic Compression Force for Specimens T633H and T633C6 . . . . .	162
4.25	Cyclic Compression Force for Specimens T424H and T424C6 . . . . .	163
4.26	Cyclic Compression Force for Specimens T636H and T422H . . . . .	164
4.27	Cyclic Compression Force for Specimens T424H and T422H . . . . .	165
4.28	Cyclic Compression Force at Reversal Point for Specimens T633H and T633C6 . . . . .	166
4.29	Cyclic compression Force at Reversal Point for Specimens T424H and T424C6 . . . . .	167
4.30	Hysteresis Loops for Specimens T633H and T633C6 in Cycle 1 . . . . .	168
4.31	Hysteresis Loops for Specimens T633H and T633C6 in Cycle 2 . . . . .	168
4.32	Hysteresis Loops for Specimens T633H and T633C6 in Cycle 4 . . . . .	169
4.33	Hysteresis Loops for Specimens T633H and T633C6 in Cycle 9 . . . . .	169
5.1	Different Types of Analytical Model for Steel Bracing Members . . . . . (a) Finite Element Model (b) Physical Theory Model (c) Phenimenological Model	170
5.2	Initial Tensile Loading and Unloading Path . . . . .	171
5.3	Jain's Hysteresis Model for Steel Members . . . . .	172
5.4	Comparison with Jain's Hysteresis Model for Specimen T633H, Cycle 1 . . . . .	173
5.5	Comparison with Jain's Hysteresis Model for Specimen T633H, Cycle 2 . . . . .	173
5.6	Comparison with Jain's Hysteresis Model for Specimen T633H, Cycle 5 . . . . .	174

Figure

5.7	Comparison with Jain's Hysteresis Model for Specimen T422H, Cycle 1 . . . . .	175
5.8	Comparison with Jain's Hysteresis Model for Specimen T422H, Cycle 2 . . . . .	176
5.9	Comparison with Jain's Hysteresis Model for Specimen T422H, Cycle 5 . . . . .	177
5.10	Comparison with Jain's Hysteresis Model for Specimen T424H, Cycle 1 . . . . .	178
5.11	Comparison with Jain's Hysteresis Model for Sepcimen T424H, Cycle 2 . . . . .	179
5.12	Comparison with Jain's Hysteresis Model for Specimen T424H, Cycle 5 . . . . .	180
5.13	Comparison with Jain's Hysteresis Model for Specimen T424H, Cycle 10 . . . . .	181
5.14	Relationship between Increase in Tension Force vs. Ac/As Ratio . . . . .	182
5.15	Assumed Relationship between Increase in Tension Force vs. Ac/As Ratio . . . . .	182
5.16	Proposed Hysteresis Model for Concrete-Filled Tubular Members . . . . .	183
5.17	First Buckling Load from Tests and SSRC Formulas . . . . .	184
5.18	Comparison with Proposed Hysteresis Model for Specimen T633C6, Cycle 1 . . . . .	185
5.19	Comparison with Proposed Hysteresis Model for Specimen T633C6, Cycle 5 . . . . .	186
5.20	Comparison with Proposed Hysteresis Model for Specimen T633C6, Cycle 10 . . . . .	187
5.21	Comparison with Proposed Hysteresis Model for Specimen T424C6, Cycle 1 . . . . .	188
5.22	Comparison with Proposed Hysteresis Model for Specimen T424C6, Cycle 5 . . . . .	189
5.23	Comparison with proposed Hysteresis Model for Specimen T424C6, Cycle 10 . . . . .	190

Figure

A.1	Stress at Plastification Limit . . . . .	201
	(a) Stress in Steel lies in Non-Linear Stage, Point a, But below the Yield Point b	
	(b) Stress in Concrete Just Reaches $f_c'$ , Point a'	
A.2	Limiting Slenderness Ratio of 6x3x3/16 Tubes Filled with Different Strengths of Concrete . . .	202
B.1	Hysteresis Loops for Specimens T633H and T633C6, Cycle 1 . . . . .	203
B.2	Hysteresis Loops for Specimens T633H and T633C6, Cycle 2 . . . . .	203
B.3	Hysteresis Loops for Specimens T633H and T633C6, Cycle 3 . . . . .	204
B.4	Hysteresis Loops for Specimens T633H and T633C6, Cycle 4 . . . . .	204
B.5	Hysteresis Loops for Specimens T633H and T633C6, Cycle 5 . . . . .	205
B.6	Hysteresis Loops for Specimens T633H and T633C6, Cycle 6 . . . . .	205
B.7	Hysteresis Loops for Specimens T633H and T633C6, Cycle 7 . . . . .	206
B.8	Hysteresis Loops for Specimens T633H and T633C6, Cycle 8 . . . . .	206
B.9	Hysteresis Loops for Specimens T633H and T633C6, Cycle 9 . . . . .	207
B.10	Hysteresis Loop for Specimen T633C6, Cycle 10 . . . . .	207
B.11	Hysteresis Loop for Specimen T633C6, Cycle 11 . . . . .	208
B.12	Hysteresis Loop for Specimen T633C6, Cycle 12 . . . . .	208
B.13	Hysteresis Loop for Specimen T633C6, Cycle 13 . . . . .	209
B.14	Hysteresis Loop for Specimen T633C6, Cycle 14 . . . . .	209
B.15	Hysteresis Loops for Specimens T424H and T424C6, Cycle 1 . . . . .	210

Figure

B.16	Hysteresis Loops for Specimens T424H and T424C6, Cycle 2 . . . . .	210
B.17	Hysteresis Loops for Specimens T424H and T424C6, Cycle 3 . . . . .	211
B.18	Hysteresis Loops for Specimens T424H and T424C6, Cycle 4 . . . . .	211
B.19	Hysteresis Loops for Specimens T424H and T424C6, Cycle 5 . . . . .	212
B.20	Hysteresis Loops for Specimens T424H and T424C6, Cycle 6 . . . . .	212
B.21	Hysteresis Loops for Specimens T424H and T424C6, Cycle 7 . . . . .	213
B.22	Hysteresis Loops for Specimens T424H and T424C6, Cycle 8 . . . . .	213
B.23	Hysteresis Loops for Specimens T424H and T424C6, Cycle 9 . . . . .	214
B.24	Hysteresis Loops for Specimens T424H and T424C6, Cycle 10. . . . .	214
B.25	Hysteresis Loops for Specimens T424H and T424C6, Cycle 11. . . . .	215
B.26	Hysteresis Loops for Specimens T424H and T424C6, Cycle 12. . . . .	215
B.27	Hysteresis Loops for Specimens T424H and T424C6, Cycle 13. . . . .	216
B.28	Hysteresis Loops for Specimens T424H and T424C6, Cycle 14. . . . .	216
B.29	Hysteresis Loops for Specimens T424H and T424C6, Cycle 15. . . . .	217
B.30	Hysteresis Loop for Specimen T422H, Cycle 1 . . . . .	218
B.31	Hysteresis Loop for Specimen T422H, Cycle 2 . . . . .	218
B.32	Hysteresis Loop for Specimen T422H, Cycle 3 . . . . .	219

Figure

B.33 Hysteresis Loop for Specimen T422H,  
Cycle 4 . . . . . 219

B.34 Hysteresis Loop for Specimen T422H,  
Cycle 5 . . . . . 220

B.35 Hysteresis Loop for Specimen T422H,  
Cycle 6 . . . . . 220

B.36 Hysteresis Loop for Specimen T422H,  
Cycle 7 . . . . . 221

B.37 Hysteresis Loop for Specimen T422H,  
Cycle 8 . . . . . 221

LIST OF APPENDICES

Appendix

A.	First Buckling Load Calculation . . . . .	192
B.	Experimental Hysteresis Loops . . . . .	200

09259

## NOTATION

$A, A_s$	Cross-section area of steel
$A_c$	Cross-section area of concrete
$b$	Width of tube section
$C_c$	Slenderness ratio that separates elastic and inelastic buckling
$E$	Modulus of elasticity of steel
$E_{ct}$	Tangent modulus of concrete
$E_e$	Equivalent modulus for considering concrete
$E_{st}$	Tangent modulus of steel
$f_c'$	Strength of concrete
$F_y$	Yield strength of steel
$h$	Depth of tube section
$I_c$	Moment of inertia of concrete
$I_s$	Moment of inertia of steel
$K$	Effective length factor of member
$K_x$	Effective length factor in out-of-plane direction
$K_y$	Effective length factor in in-plane direction
$L$	Computing Length of a member
$L'$	Length of a tube

$m$	Ratio of moment of inertia of concrete to steel
$n$	Ratio of area of concrete to steel
$P$	Axial force
$P_c$	Peak compression force of stub column
$P_a$	Actuator force applied to the testing frame
$P_{al}$	Axial load applied to the specimen
$P_b$	The first buckling load of bracing members
$P_y$	Yield force of steel
$P_{yc}$	Yield force of tube filled with concrete
$r$	The radius of gyration of tube section
$r_t$	The radius of gyration of transformed section
$t$	Thickness of tube
$\alpha$	The angle which the brace makes with the horizontal
$\beta$	Increase in tension force due to concrete
$\Delta$	Axial deformation
$\Delta_y$	Yield deformation
$\delta$	Initial elastic slop, equal to $AE/L$
$\Delta_y^*$	Normalizing yield deformation
$\epsilon$	Residual strain
$\epsilon_c$	Strain of concrete

$\epsilon_s$	Strain of steel
$\epsilon_1$	Strain in steel in longitudinal direction
$\epsilon_2$	Strain in steel in lateral direction
$\theta_p'$	Initial plastic rotation
$\mu$	Poisson's ratio of steel
$\phi$	Curvature of member, equal to $d^2y/dx^2$
$\sigma_c$	Stress of concrete
$\sigma_s$	Stress of steel
$\sigma_1$	Stress in steel in longitudinal direction
$\sigma_2$	Stress in steel in lateral direction

CHAPTER I  
INTRODUCTION

1.1 Introduction

In recent years, braced frames have become popular in seismic regions especially for high rise structures. It is well known that bracing members can provide considerable strength and lateral stiffness to a structure in an economical manner (9,10,12,16,20,30). However, in the event of a severe earthquake it is the bracing members which experience severe cyclic deformations. As a result, the survival of a braced frame during a severe earthquake strongly depends on the energy dissipation capacity of the bracing members through their post-buckling hysteresis behavior.

Recently, cold-formed rectangular steel tubes have become increasingly common for bracing members (13,15,18,34,40). There are several structural and non-structural advantages that these tubes have over other shapes, for example:

1). Tubes are more efficient compression members due to their larger radius of gyration for the same cross section area compared with other shapes.

2). The closed shape of tube sections provides greater torsional strength and stiffness.

3). Their smooth outside surface reduces potential corrosion, and minimizes the surface area that may need to be

painted and maintained.

In spite of having the above advantages, steel tubes are susceptible to early cracking due to local buckling and subsequent loss of ductility and strength. Past studies have shown that the hysteresis behavior of tubes depends heavily on the slenderness ratio and width-thickness ratio. A member with small slenderness ratio may not be able to withstand a severe shaking without fracture when subjected to cyclic post-buckling deformation (9,11,13). On the other hand, members with large slenderness ratio may not provide enough strength due to overall buckling. A balance between strength and ductility is sought in earthquake resistant structural members.

Past studies have also shown that cracking in rectangular tubes starts at the corners of the compression flange and webs soon after local buckling because of cold work and concentration of strains (11,13). Preventing severe local buckling is the key to solving this problem. Review of past studies on concrete-filled columns provides the clue that concrete filling might be an effective way to delay or prevent early cracking caused by severe local buckling. The concrete inside the tubes can change the mode of local buckling of thin steel tubes and the steel tube in turn provides confinement to concrete. Therefore, such members should have excellent ductility and strength.

In order to study the behavior and to evaluate the ductility and strength of concrete-filled rectangular steel tubular bracing members under cyclic loads, experimental and

theoretical studies are needed. For this purpose a series of concrete-filled beams, stub columns, and bracing members were tested. This report will focus on presenting and discussing the results of this study in detail.

### 1.2 Review of Related Studies

There have been numerous experimental and analytical studies related to steel tubes in the past. In general these studies can be divided into three groups: The first group is hollow steel tubes used as bracing members. The second group is concrete-filled tubular columns, in which tubes provide confinement to concrete. For this reason a more appropriate name for members in this group might be tube-confining concrete columns rather than concrete-filled tubular columns. The third group is very slender concrete-filled tubes, such as bracing members, in which the primary purpose of concrete filling is to prevent severe local buckling of the flat walls of tubes. Most of the past studies were limited to the first two groups. Almost no research has been conducted to-date on members in the third group.

It is believed that through reviewing the earlier studies on members in the first two groups (hollow tubular bracing members and tube-confining concrete columns), some concepts can be identified that can be related to the third group (concrete-filled rectangular tubular bracing members). In the following three sections research on the first two groups will be reviewed and discussed with the main points being summarized in regards to how rectangular tubular bracing

members can be improved and what needs to be carried out in this study for such composite members.

### 1.2.1 Research on Hollow Tubular Bracing Members

Cold-formed rectangular tubes have become quite popular in recent years especially as bracing members in multi-story steel structures. Nevertheless, it has been recognized that these members may not possess adequate ductility or energy absorption capacity to survive severe earthquake motions. In a few of the more recent studies (9,11,13), bracing members of rectangular section showed premature fractures following severe local buckling in regions of plastic deformation. Experimental results show:

1). Rectangular tubes fractured much earlier than the wide-flange and other shapes.

2). Specimens with small slenderness ratios cracked earlier than those with larger slenderness ratios.

3). The larger the width-thickness ratio, the shorter the fracture life. For example, even when a width-thickness ratio of 30 was used, which is within the AISC Specification (3) limit, the tubes cracked very early.

From these studies, it can be seen that the fracture life of hollow tubular bracing members is, in some way, proportional to the slenderness ratio and inversely proportional to width-thickness ratio. In conclusion, tubular bracing members are favored, but further studies are needed. The main concern will center on how to delay or lessen local buckling to prevent premature fractures.

### 1.2.2 Research on Tube and Concrete Composite Members

Most of the past studies on concrete-filled steel tubes have focused on ultimate capacity and maximum deformation under monotonic loading for round columns. The purpose is to provide confinement to concrete from steel and to increase the ductility of concrete (21,23,27). In these cases round tubes have been found to be desirable. However, no studies have been made on concrete-filled rectangular tubular bracing members in which the main purpose of concrete is to change the mode of local buckling and lessen its severity. This section focuses on reviewing studies on tube-confining concrete beams and columns.

In the U.S.A., Chen's work (6,7) provides a good summary of the work done. According to Chen limited experimental results and analyses are available only for monotonic loads. Theoretically, these analyses have focused on some specified sections and did not take into account the local or overall buckling. The members were treated just like normal reinforced concrete sections except that because the concrete was encased in steel tubes a higher value was used for the strength of the concrete and concrete was considered more ductile.

In Japan, several experimental studies were carried out by Masahide Tomii, et al (28,35,36,37). Most of their work was limited to very stocky columns or beam-columns and main conclusions can be summarized as follows:

- 1). Compressive strength of the concrete core cured in steel tubes may have a higher value than that of concrete

cylinders cured otherwise.

2). The magnitude of axial force and width-thickness ratio of tubes had a significant effect on the inelastic behavior of the concrete-filled tubular beam-columns.

3). The existence of encased concrete can prevent or delay severe local buckling in steel tubes. This increases the ductility of such members.

In China, researchers led by Zhong (41,42) have carried out much research on concrete-filled tubular columns both experimentally and theoretically. Their results and findings can be summarized as follows:

1). Several strength calculation methods to predict the capacity of these composite members were formulated by using different theories and verified by experiments.

2). Different types of tests for the composite material of concrete-filled steel tube were carried out. The microdeformation behavior was analyzed and integrated to understand the working mechanism.

3). Their tests showed that the load bearing capacity is greater than the sum of the capacity of the two alone, and is in fact approximately 1.7 to 2 times greater.

4). These composite members have good toughness and plasticity.

On the analytical side the available formulas for the concrete-filled steel tubular columns can give the ultimate capacity under monotonic loads. There are no procedures available for determining the hysteresis relationship between force and deformation under cyclic loads. Park (24) in New

Zealand has not only carried out a series of experiments to investigate the hysteresis behavior of concrete-filled tubular beams, but has also developed a computer program to determine the relationship between moment and curvature. In his program idealized stress-strain relationship for both concrete and steel were used. But again, no overall and local buckling behavior was considered.

### 1.2.3 Summary of Related Studies

Earlier studies mentioned in the Section 1.2.1 show that the main weakness of hollow tubular bracing members is premature cracking caused by severe local buckling. In order to lessen local buckling it is necessary to either increase the slenderness ratio or decrease the width-thickness ratio. However, the former is at the expense of lower strength and the latter simply means more steel used.

On the other hand, the research on the concrete-filled columns mentioned in Section 1.2.2 showed that apart from the increase in strength caused by using concrete, the mode of local buckling was changed and the local buckling was much less severe. Although, the behavior of columns and bracing members differs, it is expected that concrete filling should also improve the behavior of bracing members, particularly in regards to local buckling.

In conclusion, it can be said that steel tubes, particularly those with small slenderness ratios and large width-thickness ratios crack very early under cyclic loads due to local buckling. Filling with concrete is a potential way

to delay or alleviate local buckling and to prevent premature fractures.

Since no tests and studies have been carried out for the hysteresis behavior of concrete-filled steel tubular bracing members under cyclic loads, it is necessary to understand how concrete helps steel tubes and how the two work together. In other words, further research is needed in this area in order to develop more rational models for the behavior of such members and to find the most effective way to use concrete and steel tubes together.

### 1.3 Objectives and Scope

The present research focuses on studying experimentally the behavior of concrete-filled steel tubular bracing members under cyclic loading. The main parameters in this study are the mode of local buckling and the effects of varying strength of concrete. Although most of the specimens have equal slenderness ratio and width-thickness ratio, the effect of slenderness ratio and width-thickness ratio on the behavior was also studied.

The primary objectives of this study are:

- 1). To experimentally study the hysteresis behavior and modes of buckling and failure for concrete-filled steel tubular bracing members under cyclic loading.
- 2). To theoretically develop procedures to synthesize the hysteresis behavior of these composite members.
- 3). To recommend practical ways to prevent or delay local buckling of steel tubes thereby improving their ductility and

energy dissipation capacity.

The scope of this research is limited to rectangular tubes made of A500 Grade B steel and concrete made of Portland Type I cement. The effective slenderness ratio of most of the specimens is about 60. A few specimens with an effective slenderness ratio of about 100 were also tested. The width-thickness ratio of all the specimens was 30, except for one pair of specimens which had width-thickness ratio of 14. Quasi-static cyclic loading was used for the tests because little difference between results from static and dynamic loadings has been reported by a number of investigators in the past (14,18,19).

Bracing members have their unique behavior under cyclic loading. This is due to their geometric characteristics and the nature of the force. From the geometric point of view, they are slender enough to experience overall buckling in compression and relatively large lateral deformation which introduces bending. Under cyclic axial force and bending moments, local buckling strongly influences the fracture life. The behavior of bracing members combines the characteristics of beams and columns at different stages of loading. Therefore, test on concrete-filled columns and beams can be very helpful in studying the behavior of concrete-filled bracing members.

Past studies on concrete-filled beams and columns focused their attention mainly on overall behavior under monotonic loading. Since local buckling is a key factor influencing the hysteresis behavior of bracing members preliminary tests on

hollow and concrete-filled tubular beams and stub columns were also carried out to supplement the main tests on bracing members. Special attention was paid to local buckling modes under different conditions. The purpose was to find the change in pattern of local buckling due to the presence of concrete under bending and compression.

Therefore, this study was performed in two phases. The first phase was the preliminary tests, in which both hollow and concrete-filled beams and stub columns made of rectangular tubes were tested. In the second phase, which is the main part of this study, full-scale hollow and concrete-filled rectangular steel tubular bracing members were tested. Chapter II will discuss the preliminary test program. Preparation and processes for the main tests are presented in Chapter III. The results and observations of the main tests are presented in Chapter IV, and an empirical hysteresis model is proposed in Chapter V.

CHAPTER II  
PRELIMINARY TEST PROGRAM

2.1 Introduction

As discussed in the previous chapter, due to lack of test results on concrete-filled tubular bracing members, series of preliminary tests were performed on beams and stub columns as an aid to understand the basic behavior of composite tubular bracing members. Although beams and stub columns work in ways different from bracing members, the bracing members are kind of special beam-columns under combined axial forces and bending. Furthermore, these preliminary beam and stub column tests show more clearly the effect of each parameter one at a time. It is much easier to study the effect of a combination of parameter by knowing their individual effects.

For this purpose, six hollow and concrete-filled tubular beams, and eight stub columns were tested in the preliminary program of this study. During the preliminary tests, both overall and local behaviors of the specimens were carefully observed. Special attention was paid to recognizing the difference in local buckling modes between hollow and concrete-filled beams and stub columns. This chapter will present test observations and discussion of results for beam specimens first and then stub column specimens. Following these preliminary tests, the main full-scale hollow and

concrete-filled tubular bracing member tests were carried out. The next chapter, Chapter III, will present the details of the test set-up and procedure for the main test program. The test observations and discussion of results of the main test program will be presented in Chapter IV.

## 2.2 Hollow And Concrete-Filled Tubular Beams

In the following first half part of this chapter, the test program on hollow and concrete-filled tubular beams is presented. The test program on hollow and concrete-filled stub columns will be presented in the second half of this chapter, beginning with Section 2.3.

Six square steel tubes of size 2.5x2.5x0.105" (64x64x2.7 mm) were used. A typical specimen is shown in Figure 2.1. The tubes were made of A500 Grade C steel by cold-forming. These specimens are divided into two groups, Group 1 and Group 2. In Group 1 there are two specimens designated BH and BHA, where B stands for "Beam"; H for "Hollow"; and A for "Annealed". In Group 2 there are four specimens designated BC6, BC6F, BC6A, and BC8F, where B stands for "Beam"; C for "Concrete-filled"; the number following C for the strength of concrete in unit of ksi; A for "Annealed"; and F for "Fibers". Group 1 specimens are hollow and Group 2 specimens were filled with different types of concrete. The properties of the specimens are listed in Table 2-1.

In both groups, only lateral loading was applied to the specimens. The variable parameters were the presence of concrete, the strength of concrete, the annealing of the steel

tubes, and the existence of steel fibers.

The concrete was compacted on a vibrating table during and after placement. A number of 2x2x2" (51x51x51 mm) concrete cubes were taken from each batch in order to determine the properties of concrete.

#### 2.2.1 Apparatus and Procedure

Figure 2.2 shows the test set-up, and Figure 2.3 schematically shows the test machine and specimen. The specimens were placed on two roller supports. A dial gage reading 1/1000 inch (0.025 mm) was placed at the mid point of the specimen to measure the vertical deflection. When the hydraulic table moved up, the loading beam which reacted against the top beam of the test machine applied two concentrated downward forces on the specimen at the third-points. The beam span was 30 inches (76 cm).

The loading history was controlled by the deflection of the beam at the middle. Each time when the deflection reached the specified value the load was brought to zero. Then the specimen was turned upside down. In this way the test machine applied force on the specimen in the "opposite" direction, thus, simulating reversed cyclic loading. The history of loading is shown in Figure 2.4.

#### 2.2.2 Summary of Experimental Observation

From the observation of the experiment, it is clear that specimens in two groups have large differences in local buckling modes, ductility, and ultimate moment capacity. But

within each group, the differences are small. These features are discussed in detail in the following:

#### 2.2.2.1 General Behavior

As shown in Figures 2.5 to 2.7, the hysteresis curves exhibit a linear response early in the virgin state of loading until the initial yielding. The decrease in resistance (moment capacity) due to cyclic loading occurred more rapidly in the first group than in the second group. After yielding, the specimens in Group 1 were divided by two concentrated plastic hinges into three almost straight segments. Also, major inelastic local deformation occurred under the two load points where both moments and shear forces reached their maximum values, Figure 2.8. On the other hand, in Group 2 specimens the plastification or local buckling was spread over the entire middle segment where the beam had the maximum moment, Figure 2.9. The failure mechanism for both groups was low cycle fatigue. After certain number of cycles of loading small cracks formed at the bottom of the specimens under load points, which then propagated very quickly into the webs of the specimen. Concrete fill in the specimens changed the mode of local buckling, reduced its severity, and lengthened the fracture life, and thus increased their strength and ductility.

#### 2.2.2.2 Local Buckling Modes

There was large difference in the local buckling modes between specimens in the two groups. In the first group the

main local buckling was concentrated under the load points. However, for the second group the local buckling was spread over the mid segment of the specimen and some bumps formed, (Figure 2.9), and when the loads were applied in the opposite direction these bumps disappeared. The other point is that the compression flange of specimens in Group 1 buckled inwards, while that in Group 2 buckled outwards forming several waves. The severe local buckling in the first group was the principal cause of rapid deterioration of strength and failure of the specimens. The local buckling in the second group was not that severe. This showed that the presence of concrete could change the local buckling mode and reduce its severity.

#### 2.2.2.3 Ultimate Moments

The measured ultimate moments were defined as values corresponding to unloading points on the hysteresis curves. Figures 2.10 to 2.12 show the ultimate moment capacity in each half cycle. It can be seen from these figures that for the specimens in Group 1 the maximum moments decreased rapidly with each cycle. However, in Group 2 the ultimate moments in each cycle remained very stable. But within each group, the differences are very small. This can be explained by the presence of concrete which prevented severe local buckling and crumbling and allowed the steel to undergo strain hardening over much larger length of the beam.

The theoretical ultimate moments were calculated by a simple method proposed in Reference 24. Rectangular stress

blocks of concrete and steel were assumed. The results from the tests and the theoretical values are summarized in Table 2-2.

#### 2.2.2.4 Ductility and Energy Absorption

Table 2-3 shows the number of cycles and the energy absorbed per cycle by specimens at each displacement amplitude. It is clear that the energy absorbed by the tubular beams filled with concrete was much higher than the beams without concrete. But the concrete inside the tube did not increase the number of cycles by very much except when high strength concrete was used. Possible explanation is given in the following:

The failure mechanism of test specimens under two point loads is mainly due to low cycle fatigue and local deformation under load points. The higher the strength of concrete the more effectively the concrete prevents the local deformation and increases the number of cycles to failure.

Because the main function of concrete is to prevent tube from local buckling and crumbling in compression, the steel fibers (in the amounts as used in these specimens) did not help much.

### 2.3 Concrete-Filled Stub Columns

In the preceding sections, the test results of hollow and concrete-filled tubular beams were presented. Beginning with this section, the test program and results of hollow and concrete-filled tubular stub columns are summarized:

### 2.3.1 Experimental Program

#### 2.3.1.1 Specimens

Eight hollow and concrete-filled tubular stub columns were tested. All specimens were made of A500 Grade B cold-formed tubes which were cut in lengths of 9 inches (23 cm) from the same tubes used as bracing members in the main test program (Chapter III). These column specimens are also divided into two groups. In the first group, there are four columns designated C633HS, C424H, C633H, and C422H, where C stands for "Column"; the first two numbers following C for width and depth of tube section in unit of inch, respectively; the third number for the thickness of tube wall in unit of 1/16 inch (1.6 mm); H for "Hollow"; and S for "Stiffened by angles". In this group, no tubes are filled with concrete, but each tube has different section. Specimen C633HS was made from 6x3x3/16" (152x76x4.8 mm) tube and two 1x1x1/10" (25x25x2.5 mm) angles which were welded on both broad sides of the tube in the longitudinal direction as shown in Figure 2.14(b). The effect of width-thickness ratio on the local buckling behavior is studied in this group. In the second group, there are also four specimens designated CC4, CC4F, CC6F, and CC8F, where the first C stands for "Column"; the second C for "Concrete-filled"; the number for the strength of concrete in unit of ksi; and F for "Fibers". All of them had the same tube size of 6x3x3/16" (152x76x4.8 mm) but each was filled with different grade of concrete with or without steel fibers. The purpose of using specimens in this group was to investigate the influence of different types of concrete.

Comparison between results from these two groups could show how concrete changes the overall and local behavior of these stub columns. A typical specimen is shown in Figure 2.14(a). Table 2-4 gives the summary of all specimens used in this series.

Concrete used for Group 2 specimens was from the same batch as for bracing members in the main test program for different types of concrete. Chapter III gives more detailed information on mixing and curing of concrete.

Two to four strain gages were used for each stub column, which were mounted in the center of each side of the tube. The purpose of this was twofold: 1) Strain gages indicated how much force was carried by steel alone in a concrete-filled column particularly in the linear stage, 2) The strain level could be measured at which local buckling started for specimens with different width-thickness ratios.

#### 2.3.1.2 Apparatus and Procedure

Figure 2.13 shows the test set-up for stub column testing. The column was placed into a hydraulic compression-only machine. When the central piston moved up it applied the compression force to the column which sat on the piston. All specimens were subjected to monotonic compression load until failure or deformation reached 2 inches (51 mm). Two dial gages were placed on in each side of the column to measure the axial deformation.

Test was controlled by the force at the step of 5 (22 KN) or 10 kips (44 KN) depending on the cross-section area of

specimens. At each load level the readings of dial gages were taken manually. Strain gage readings were scanned by an HP data acquisition system, stored onto a tape, and also printed on paper.

### 2.3.2 Summary of Experimental Observation

#### 2.3.2.1 General Behavior

Figure 2.15 shows the relationship between force and deformation for the specimens in Group 1. From zero loading to yield force the relationship between force and deformation remains linear and no any local buckling was observed. After yielding the load was maintained for a while depending on different width-thickness ratio till local buckling occurred. As soon as first local buckling occurred outwards on two wider sides of the tube, the force began to drop at rates depending on the width-thickness ratio. Then the local buckling occurred on the two narrow sides which buckled inwards. The force decreased continuously but at lower rate. When deformation reached about 1 inch (25 mm) the force ceased to drop because the loss due to local buckling was offset by strain hardening. The force at 1 inch (25 mm) deformation was about 30% to 50% of the peak force depending on the width-thickness ratio.

Figure 2.16 shows the relationship between force and deformation for the specimens in Group 2. The concrete-filled stub columns in this group exhibited essentially similar behavior as the specimens in the first group except for the following differences:

1). Larger peak force was observed compared with the hollow counterpart. The difference is mainly attributed to concrete.

2). Although the first local buckling in the wide sides was outwards as in hollow sections, the second local buckling in the narrow sides was also outwards due to the presence of concrete rather than inwards as in hollow specimens.

3). The compression force had chance to go up back after the second local buckling. This was because the loss of compression capacity of the tube due to local buckling was compensated by not only strain hardening of steel tube but also due to concrete filling in the local buckled region.

#### 2.3.2.2 Peak Forces

The slenderness ratio of stub columns in the study ranges from 6 to 9, as such overall buckling is not a problem. The peak force was almost equal to the yield force for the hollow specimens in Group 1. According to coupon tests yield stress and ultimate stress were very close for the steel of these cold-formed tubes, which is around 60 ksi (41 KN/cm<sup>2</sup>). Previous researchers had made similar observation (13). Therefore, the peak force of hollow stub columns can be calculated as the product of cross-section area and the yield stress.

On the other hand, the peak force of Group 2 specimens was slightly larger than the sum of forces taken by concrete and steel if they experienced compression independently. According to the test results the following formula can be

used to calculate the peak force for concrete-filled rectangular tubular stub columns.

$$P_C = A_C f_C' + A_S F_Y \quad f_C' \leq 6 \text{ ksi} \quad (2.1)$$

where,

$P_C$  = Peak compression force

$A_C$  = Cross-section area of concrete

$f_C'$  = Strength of concrete

$A_S$  = Cross-section area of steel tube

$F_Y$  = Yield strength of steel

$f_C'$  is the strength of concrete from standard cylinder tests. If it is larger than 6 ksi (4.1 KN/cm<sup>2</sup>), it is taken equal to 6 ksi (4.1 KN/cm<sup>2</sup>). The reason why higher strength of concrete does not increase the compression capacity of stub column specimens can be explained as follows:

When high strength concrete approaches its ultimate strength, it develops relatively large lateral deformation which pushes rectangular tube walls to local buckling, in turn, concrete loses confinement from the tube. This is different from a round section, the lateral expansion of concrete introduces hoop stress in round tube wall which in turn provides very good confinement to concrete to help reach its high strength. This has been verified in previous studies (21,44).

### 2.3.2.3 Local Buckling Mode

All specimens, with or without concrete, had local buckling outwards on two broad sides of the tube first. As the axial deformation increased, the hollow columns had the second local buckling inwards on the narrow two sides, while concrete-filled columns buckled outwards due to the presence of concrete, Figure 2.17. This difference in the mode of local buckling between hollow and concrete-filled specimens is of major importance.

The strain level at which local buckling occurred was mainly dependent on width-thickness ratio of the tube walls and had no significant relationship to the presence of concrete. The larger the width-thickness ratio, the lower the strain level at which local buckling occurred. The hollow column specimen C633H made from 6x3x3/16" (152x76x4.8 mm) tube with width-thickness ratio of 30 had the first buckling at average strain level of about 0.008, while specimen C424H made from 4x2x4/16" (102x51x6.4 mm) tube which had width-thickness ratio of 14 did not show any local buckling until strain reached up to 0.03.

Specimen C633HS was made from 6x3x3/16" (152x76x4.8 mm) tube with width-thickness ratio of 30. Two 1x1x1/10" (25x25x2.5 mm) angle stiffeners were welded on both broad sides. Although this specimen followed similar local buckling pattern as other hollow tubular columns, shown in Figure 2.18, it did not exhibit any local buckling until strain reached up to 0.03 as in specimen C424H which had width-thickness ratio of 14. Thus, it is evident that use of angle stiffeners may

be as effective in delaying local buckling as decreasing width-thickness ratio. However, the use of stiffeners in the way described above does not change the local buckling mode.

All specimens in Group 2 had the same width-thickness ratio of 30 and were filled with different types of concrete. Test results showed that concrete could not delay the occurrence of local buckling. All of them had local buckling at strain of about 0.008 which was the same as in hollow specimen C633H with width-thickness of 30.

The reason why concrete could not delay the local buckling can be explained as follows. When compression force is small and before steel yields, both concrete and steel work independently. In other words, the interaction between concrete and steel is negligible. As compression force increases, the poisson's ratio of concrete finally becomes larger than that of steel. Then concrete tries to push the tube walls out causing bending in the tube walls. Since the thin tube walls have low stiffness for bending, the tube walls would buckle out until enough membrane stress develops to offset the outward force from concrete. Therefore, concrete can not delay the time local buckling occurs. But the important difference between hollow columns and concrete-filled columns lies in that concrete can change the local buckling mode. This will be discussed in more detail in Chapter IV.

#### 2.3.2.4 Plateau of Peak Compression Force

As mentioned earlier, the peak force for all hollow

columns was almost equal to their yield force. But how long the peak force could be maintained before dropping as deformation increases is another question. In other words, what is the duration between yielding up to local buckling when the force begins to drop? Here the duration refers to the length of plateau of peak compression force.

For hollow specimens in Group 1, width-thickness ratio is the dominant factor effecting the plateau of peak forces. Specimens C422H and C633H were made from 4x2x2/16" (102x51x3.2 mm) and 6x3x3/16" (152x76x4.8 mm) tubes, respectively, which had the same width-thickness ratio of 30. Both specimens showed very similar behavior at peak force. Soon after the load reached the yield value it began to drop as shown in Figure 2.19(a). That means that local buckling which caused the decrease of the force occurred immediately after yielding. On the other hand, specimen C424H was made of 4x2x4/16" (102x51x6.4 mm) tube with width-thickness ratio of 14, and the peak force remained very stable before dropping as shown in Figure 2.19(b). Local buckling did not occur until strain reached about 0.03.

The behavior of specimen C633HS is quite interesting. Although it is made from the same tube as specimen C633H with width-thickness ratio of 30, two 1x1x1/10" (25x25x2.5 mm) angles were welded as stiffeners. From the point of view of stability of peak compression force, it behaved just like specimen C424H with width-thickness ratio of 14. The peak force did not drop as immediately and suddenly as it did in specimen C633H. It remained stable until local buckling

occurred later as shown in Figure 2.19(b).

Figure 2.20 shows the test results for all Group 2 specimens and one Group 1 specimen C633H for comparison. All curves for Group 2 specimens are very similar except for different peak forces due to different strength of encased concrete. Like hollow specimens C633H and C422H, local buckling occurred soon after yielding following which force began to drop. The reason is that concrete could not delay the local buckling in a rectangular tubular column as was discussed earlier in Section 2.3.2.3. But unlike the hollow tubes the force in concrete-filled columns dropped some after local buckling, but started increasing as soon as the force taken by confined concrete was enough to offset the loss of the force due to local buckling.

It is clear that larger the width-thickness ratio less stable is the peak force, and the more quick the drop after local buckling. On the other hand, smaller the width-thickness ratio more stable the peak force, and slower the drop of force. Thus, the width-thickness ratio dominates the stability of peak compression force for stub columns. An alternative way may be to stiffen the tube walls as was done in specimen C363HS. The presence of concrete does not affect the yield plateau, but it reduces the force drop after local buckling and in fact the force increases after some drop.

#### 2.3.2.5 Effect of Steel Fibers

According to the test results, the effect of steel fibers was negligible in tubular columns. Specimens CC4 and CC4F

were identical except that specimen CC4F had 2.5% steel fibers mixed in concrete. Figure 2.21 shows the force and deformation relationship for the two specimens. Like beam tests discussed in Section 2.1, no significant difference can be seen. This phenomenon can be explained as following. The basic purpose of using fibers is to improve the ductility of concrete for large deformation. But in a concrete-filled column, the steel tube provides confinement to concrete and make it behave in a ductile manner. Because of this the difference between tubular columns with and without fibers becomes rather insignificant.

### 2.3.3 Summary of Conclusions

From the observation of tests of hollow and concrete-filled steel tubular beams and stub columns the following conclusions can be drawn:

1). Width-thickness ratio is a key factor influencing local buckling and the stability of peak compression force. The severity of local buckling could be reduced by either using smaller width-thickness ratio or stiffening the tube walls.

2). Concrete can change the local buckling modes in both beams and columns by preventing tube walls from buckling inwards. This reduces the severity of local buckling. Nevertheless, concrete can not delay local buckling and can not improve the plateau of peak compression force very much in stub columns.

3). Concrete can increase the load capacity in both beams

and columns. It also prevents the load from dropping continually. High strength concrete and steel fibers did not provide extra benefit in either preventing local buckling or increasing strength in rectangular tubular beams and columns.

These observations and conclusions are only based on limited tests. More tests are needed for more general conclusions and quantitative analyses, such as developing mathematical relationship between width-thickness ratio and strain level at which local buckling occurs.

Although more study and tests may be needed to have more rational and general conclusions, the test results discussed in this chapter have shown quite clearly that concrete filling can change the mode of local buckling and reduce its severity. This aspect could be very helpful in improving the hysteresis behavior of tubular bracing members. In testing of full-scale hollow and concrete-filled steel tubular bracing members, these concepts were utilized. The detailed procedure and results of the main test program are presented in the following two chapters, Chapters III and IV.

CHAPTER III  
MAIN EXPERIMENTAL PROGRAM

3.1 Introduction

Previous research has shown that local buckling in tubular bracing members occurs at locations of plastic hinges soon after overall buckling. Cracking caused by severe local buckling starts at the corners between compression flange and webs just after a few cycles and propagated very quickly into the flange and the webs. Such early cracking could be delayed or prevented by either increasing the slenderness ratio of the member or decreasing width-thickness ratio. But the former is at the expense of reduced compression strength and the latter will require more steel. A better solution is desired.

From the preliminary tests presented in the previous chapter it was learned that filling tubular beams and columns with concrete could change the mode of local buckling and delay or prevent premature fractures so that these members could absorb more energy after local buckling. This gave a clue that tubular bracing members should have similar improvement in their performance if they are also filled with concrete as the behavior of bracing members combines the characteristics of beams and columns.

The purpose of the main test program is to experimentally verify the above idea which is based on the past related

studies and the preliminary tests. It is also desired to understand how concrete changes the local buckling mode and lessen its severity, and what is the hysteresis behavior of these composite bracing members. Based on these test results a theoretical hysteresis model can be formulated for dynamic analysis for structures with these members. This study can also provide information for further research in this area.

In the main test program a series of full-scale hollow and concrete-filled tubular bracing members were tested. This chapter will present the procedure for the main tests. This includes preparation of specimens, test set-up and loading history. The test observation and discussion of results will be presented in Chapter IV, and an empirical hysteresis model will be proposed in Chapter V.

### 3.2 Test Specimens

Nine specimens were selected for this study. The specimens were selected to fit the existing test set-up and designed to reflect the effects of major parameters on behavior of concrete-filled steel tubular bracing members when subjected to severe cyclic loading. The main parameters were: a) strength of concrete, b) effective slenderness ratio,  $KL/r$ , c) width-thickness ratio,  $b/t$ , and d) presence of steel fibers in concrete.

The specimens employed in the experimental program are divided into two groups according to the size of the steel tubes.

### 1. Size 6x3" Tubes

Six specimens designated as T633H, T633C6, T633C4, T633C4F, T633C6F, and T633C8F were included in the first group, where T stands for "Tubular brace"; the first two numbers for width and depth of tube section in unit of inch; the third number for the thickness of tube wall in unit of 1/16 inch (1.6 mm); H for "Hollow"; C for "Concrete-filled"; the number following C for the strength of concrete in unit of ksi; and F for "Fibers". All of them had the same tube section of 6x3x3/16" (152x76x4.8 mm). Specimen T633H is hollow bracing member which was used for reference to study the general difference in behavior between hollow and concrete-filled bracing members. The rest five specimens were filled with different strengths of concrete with or without steel fibers. Therefore, these six specimens had identical properties except for different types of concrete. The details of these specimens are shown in Figures 3.1 to 3.6.

### 2. Size 4x2" Tubes

Three specimens designated as T424H, T424C6, and T422H were included in this group. Specimen T424H and specimen T424C6 had the same wall thickness of 4/16 inch (6.4 mm), the difference being that specimen T424C6 was filled with 6 ksi (4.1 KN/cm<sup>2</sup>) concrete while specimen T244H was hollow. Specimen T242H was hollow with wall thickness of 2/16 inch (3.2 mm). Specimens T424H, T424C6, and T422H are shown in Figures 3.7 to 3.9, respectively. The purpose of using specimens in this group was to investigate the effect of

concrete to members with different slenderness ratios and different width-thickness ratios by comparing with specimens in the first group. The geometrical and physical properties of all specimens are tabulated in Table 3-1.

All specimens were made of A500 Grade B cold-formed steel tubes, and A36 steel plates were used to for the gusset plates. The welds between gusset plates and end plates, and between tube and gusset plates were designed according to AISC Specification (3) and UBC (38) so that allowable strength of plates and welds would be thirty three percent higher than that of the tubes. The typical shape and size of gusset plates are shown in Figures 3.10 and 3.11 for size 6x3" (152x76 mm) and 4x2" (102x51 mm) tubes, respectively.

### 3.3 Material properties

#### 3.3.1 Steel Tube

All steel tubes were ordered as ASTM-A500, Grade B cold-formed structural tubes. The actual material properties were derived from two different types of tensile test. One was determined from yield force during initial tensioning. In addition, 3-inch (76 mm) gage-length coupon tests were performed to find stress-strain relationship and ultimate strength and elongation. Average values of coupon tests are listed in Table 3-2 for different parts of the tube sections and compared with nominal values. Typical stress-strain curves from coupon tests are shown in Figure 3.12.

Size 3x6" tubes were ordered at two different times. It was noted that even for the same specified tubes, significant

difference in ultimate strength and elongation was found. The difference was about 10% according to the coupon tests. The tube from which specimens T633H and T633C6 were made was more ductile and had low strength than the tubes which were ordered the second time and from which specimens T633C4, T633C4F, T633C6F, and T633C8F were fabricated. This explained why these four specimens cracked earlier than specimens T633H and T633C6 under the same load history. The same phenomenon was observed in stub columns in the preliminary tests.

Concrete-filled stub columns made from tubes ordered the first time did not show fracture. However, the columns made from the tubes ordered the second time had vertical fractures along the corner after local buckling on four sides formed a ring. Figure 3.13 shows the difference between stub columns made from tubes ordered the first and second time, respectively.

The material properties in the flat sides of structural tubes exhibited about 20% lower strength than in corner areas, which was also associated with a drastic decrease in fracture strain by a factor of 20 to 30% in corner areas. Whereas, the decreased strength in flat sides is only of minor consequence for tube section, the reduction in fracture strain in corner area has important implications for fatigue life of members. Such differences are typical for cold-formed shapes. This is one reason why tubes always show cracks at the corners first.

### 3.3.2 Concrete

The mixtures of different strengths of concrete were designed according to the method recommended by Portland Cement Association (25). Portland Type I cement was used for all specimens. Round coarse aggregate of 1/4 inch (6.4 mm) maximum size and sand of 1/10 inch (2.5 mm) maximum size were used. The mix proportions for different strengths of concrete are listed in Table 3-3.

The same percentage of steel fibers, which were 1.2 inches (30 mm) in length with two hooks at both ends as shown in Figure 3.14, was used in different batches of concrete. The initial purpose of using fibers was to increase the ductility of concrete. As recommended by Reference 22, fibers in the amount of 2.5% of mortar volume was used. Superplasticizer in the amount of 0.5% of cement weight was used during concrete mixing to improve workability. The volume of concrete in each batch was determined so that it was enough for one bracing specimen, one stub column, and two standard concrete cylinders.

The results of standard concrete cylinder tests showed that the final strength, except for 8 ksi strength concrete, was generally 10% above the design strength which is recommended by ACI Committee (1). The presence of fibers did not change the strength of concrete much, but it increased the ultimate strain of concrete quite substantially. The results of cylinder tests are shown in Figure 3.15, and the average strength of concrete is also listed in Table 3-3.

### 3.4 Fabrication Process

#### 3.4.1 Tubes filled with Concrete

The fabrication process for concrete-filled tubular bracing specimens can be summarized as follows:

1). After the tube was cut to required length, slots for gusset plates at both ends of the tube were cut by a band saw. Two pieces of wood were inserted into the slots and one end of the tube was sealed for concrete casting, Figure 3.16.

2). Concrete was mixed according to design proportions. While concrete was filled into the tube from the open end, a steel bar was used for compact. A vibrator was also used outside the tube at several areas along the length.

Concrete from the same batch was filled into two standard modules to make concrete cylinders. Procedure recommended by ACI was followed for making and testing cylinders.

3). After 24 hours the pieces of wood were removed from slots and the both ends of the tube were covered by plastic. Specimens were cured at room temperature for 28 days before testing. The same method was used to cure concrete cylinders.

4). Gusset plates were welded to the end plates by fillet welds (E7018 electrodes) of predetermined length and size as shown in Figures 3.10 and 3.11. Welding was done by an experienced welder under careful supervision to ensure adequate penetration of the weld and orthogonality and concentricity of the gusset-end plate junction.

5). The end and gusset plate assemblies were then placed in an assembly jig as shown in Figure 3.17. The jig has the same diagonal dimension as the test frame. Four 1 1/4 inch

(32 mm) HS bolts were used to hold the assemblies in the jig. Following that, the concrete-filled steel tube was put in place for welding to gusset plates. The tubes were welded to the gusset plates with fillet welds. Special attention was paid here to minimize any kind of distortion of the tube and concrete, and to prevent or reduce shrinkage. Short weld segments were used at strategic locations to hold the tube in place. Continuous welds were then placed between the short segments. This procedure is compatible with the Structural Welding Code Specification (33).

6). At certain predetermined locations along the specimen, the surface was cleaned and a number of strain gages were applied. Figures 3.1 to 3.9 show the location of these strain gages. Finally the specimen was hoisted from the jig and placed in the testing frame. Ten to eleven 1 1/4 inch (32 mm) HS bolts were used to connect the end plates to the testing frame.

7). The specimen then was wiped to remove dust and dirt. After mounting the instrumentation, the initial crookedness was measured. Then the specimen was coated with hydrated lime (white wash) for visual observation of the yield zones.

#### 3.4.2 Hollow Tubular Specimens

The fabrication method used for hollow tubular specimens essentially followed the same procedure as employed in the fabrication of the ones filled with concrete except omit steps 2) and 3) in which concrete was mixed, placed and cured.

### 3.5 Test Set-Up

#### 3.5.1 Loading System

The loading system is combination of a four-hinged testing frame, reaction wall, and a double-acting hydraulic actuator. Figure 3.18 shows the complete test-up and Figure 3.19 schematically shows the test frame and the reaction wall.

The four-hinged frame, in which the concrete-filled steel tubular specimen is diagonally mounted, consists of two horizontal beams of W14x153 and two vertical columns of W14x53. The horizontal beams and columns are connected by four 3-1/2 inch (182 mm) pins with additional reinforcement plates installed at the hinge locations. These connections yield to a null stiffness of the testing frame in response to the horizontal force. Thus, the behavior of bracing specimens can be studied in absence of any interaction with the surrounding frame.

The reaction wall provides a strong reaction support which is necessary for the hydraulic actuator and forces the vertical columns of the frame to rotate about their base hinges. The four large columns, two of which are braced together at each end of the testing frame, provide lateral support.

The push-pull double-acting hydraulic actuator is mounted horizontally on the top beam of the testing frame. The active end of the actuator is connected to a bracket attached to the upper beam of the four-hinged frame while the fixed end is connected to the reaction wall.

The actuator has a capacity of 250 kips (1110 KN) in

tension and 330 kips (1470 KN) in compression and a stroke of 16 inch (41 cm). The zero position of the piston is fixed so as to allow about 8 inches (20 cm) of stroke length to be utilized in each direction. The movement of the piston is controlled by a servovalve unit which, in turn, is controlled manually through the set point of a 406.11 model controller by MTS. The piston is powered by a 15 gallons per minute (57 liters/min.) Vickers pump.

The loading system performed well during the entire experimental program except for one problem. The hysteresis loops recorded on the X-Y Recorder showed a rigid (stiff) response (vertical drop) at each reversal. This phenomenon has been observed by previous investigators also who used this test set-up (4,5,8,13)

### 3.5.2 Instrumentation

The instrumentation consisted of linear potentiometer rods, a wire transducers, a load cell and EP series strain gages. These instruments were used to measure axial and mid point lateral deformations, actuator horizontal force and strains in specimens at predetermined hinge locations.

According to the available test set-up and instrumentation, the axial deformation of the specimens was defined by the average of the relative movement of the two moving parts of the telescope rods. The relative movement of each rod, equal to the axial deformation of the specimen, caused a change in voltage of the attached transducer. Significant difference between these two transducers existed

and average of these was used as the axial deformation. The lateral displacement at the mid point was measured by a wire position transducer, model 1850-SMM-50. Both wire and rod transducers were calibrated before and after each test.

The horizontal force of the actuator was measured by a load cell, Lebow Model 13129-122, and recorded on a data acquisition system (HP 3497A) and an X-Y Recorder. Assuming the beams and columns of the test frames are rigid and because they are hinged together, the force applied to the specimens is related to that of actuator as follows:

$$P_{al} = P_a / \text{Cos}\alpha \quad (3.1)$$

where,

$P_{al}$  = Axial load applied to the specimen

$P_a$  = Actuator force applied to the testing frame

$\alpha$  = The angle which the bracing specimen makes with the horizontal

Eight to twenty EP series strain gages were placed on each specimen at prescribed sections as shown in Figures 3.1 to 3.9. Their purpose was to measure the axial force carried by the steel tube and for hollow specimens to simultaneously cross-check the actuator force by using the above formula. It is also important to measure the strain levels at which local buckling occurred in the specimens. The output of strain gages was recorded and printed by the HP data

acquisition system mentioned above. The instrumentation performed well during testing except the wire position transducer, which sometime gave erroneous readings.

### 3.5.3 Data Acquisition System

The data acquisition system, Figure 3.20, mainly consisted of the following components:

1). X-Y Recorder: An HP X-Y Recorder, Model HP 7015B, was used to plot the hysteresis loops during testing. It served two basic functions: 1) to monitor the axial displacement and control the test, and 2) to facilitate visual observation regarding degradation of hysteresis loops, local buckling, yielding in the member and its connections, and checking the rod transducers performance.

2). Scanning of Data Channels: Hewlett Packard Data Acquisition System, Model HP 3497A, was used to scan the channels during testing. The data was stored on a cassette tape and portions of the data were also printed as desired.

3). Voltmeters: Several voltmeters were used mainly to calibrate the transducers and to control the voltage changes of the servovalve unit during testing.

## 3.6 Loading History

### 3.6.1 Consideration of Loading History

Different basic ideas might be employed as starting point for forming a loading history for concrete-filled steel tube bracing member tests. But a desirable pattern of deformation sequences should satisfy the following two main purposes.

First, it should enable study of repeatability of the hysteresis loops with respect to strength degradation. Second, it should allow comparisons to be made with previous investigators' results.

Since, no previous test results for concrete-filled steel tubular bracing members are available, it is helpful to compare test results in this study with the results of hollow tubular bracing member tests under the same loading history. This would provide opportunity to study the effects of concrete filling directly. Gugerli (13) used a loading history to test hollow tubular bracing members which had similar dimensions as the specimens in this study. After carefully reviewing his loading history it was found that it could also service the first purpose as stated above. Accordingly, his loading history shown in Figure 3.21 was used in this study. This loading history is discussed in more detail in the following two sections.

### 3.6.2 Definition of $\Delta y^*$

The loading sequence was devised to provide information regarding:

- 1). Hysteresis loops for cyclic loading between the same deformation limits during different sequences of the tests.
- 2). Maximum compressive and tensile forces throughout the test.
- 3). Number of cycles till fracture.

In most previous studies on bracing members the specimens

usually were initially tensioned to yield load to make them straight or to eliminate residual stresses. But cold-formed tubular members do not exhibit a sharp yield point and the difference between yield stress and ultimate stress is small as shown in Figure 3.12. In such case the yield stress is generally defined as the stress (read from the stress-strain curve) corresponding to a permanent strain of 0.2% as shown in Figure 3.22. Therefore, all specimens in this study were pulled to a strain offset approximately 0.2% in the first cycle.

For setting some reference point as well as for comparison with previous studies, it is convenient to normalize axial deformations rather than using absolute deformations. For this purpose, a basic normalizing yield deformation,  $\Delta y^*$ , is introduced. The maximum tension or contraction in the loading history is expressed in terms of this basic normalizing axial deformation.

In this study,  $\Delta y^*$  was defined corresponding to a nominal yield strength of 36 ksi (25 KN/cm<sup>2</sup>). The reasons of using a nominal yield value of 36 ksi (25 KN/cm<sup>2</sup>) rather than the measured one from coupon tests are the following. As discussed earlier, cold-formed tubes have relatively higher yield strength than the more commonly used steel for hot rolled shapes. If the actual yield stress is used to define the normalized deformation, this means that the tubes will be subjected to larger deformation. This may not be very realistic since bracing members with higher yield strength may

not necessarily be subjected to larger deformation during a strong ground motion. Also 36 ksi (25 KN/cm<sup>2</sup>) is nominal yield strength for most common grade of structural steel.

Based on the above thoughts, 36 ksi (25 KN/cm<sup>2</sup>) was used to define the basic normalizing axial deformation for tests in this study. At the same time it also prevented tubes from being subjected to large absolute deformations which could cause severe early cracking because the difference between yield stress and ultimate stress is small. If the measured yield strength from coupon tests was used to define  $\Delta_y^*$ , tubes might have fractured too early to study the effect of other parameters which would show their influence in later cycles. However, this was done at the expense of direct comparability of normalized hysteresis loops with members having yield strengths, and direct application of normalized hysteresis models as will be discussed later in Chapter V.

### 3.6.3 Deformation Sequences Used

The same basic pattern was repeated for maximum absolute contraction between  $-5\Delta_y^*$  up to  $-15\Delta_y^*$  in steps of  $5\Delta_y^*$ . If specimen did not fracture early, the repetitive nature of loading history allowed a meaningful interpretation of fracture of specimens. At each level of maximum compressive deformation, two different sequences were followed. In the first, the specimen was cycled between  $\Delta_y^*$  as a fixed limit and  $-5\Delta_y^*$  etc., until the maximum contraction for that sequence was reached. In the second part, the fixed point was

at the maximum contraction and the deformation amplitude was increased by  $5\Delta_y^*$  in each cycle until the yield force was reached.

The loops of the first of sequence are comparable and provided information regarding cycles between fixed deformation limits whereas the second part mapped out the compression envelope.

CHAPTER IV  
EXPERIMENTAL RESULTS OF MAIN TEST PROGRAM

4.1 Introduction

Nine full-scale hollow and concrete-filled tubular bracing specimens as mentioned in the previous chapter were tested. Overall behavior, such as hysteresis loops and overall buckling mode as well as local performance such as local buckling, cracking and fracture modes were carefully monitored and watched by either instruments or visual observations. All specimens, test set-up, and instruments were carefully fabricated, checked, or calibrated. The whole system performed well during the entire process of testing.

Significant differences were found between the performance of hollow and concrete-filled tubular bracing specimens with width-thickness ratio of 30. According to the test results local buckling was found to be the most important factor influencing strength and ductility of tubular bracing members. The presence of concrete can change the local buckling mode and reduce its severity. As a result, the strength of specimens increased and ductility improved.

While the design criteria, preparation of specimens, and test set-up were discussed in Chapter III, this chapter will focus on presenting experimental observations and discussing test results in detail.

#### 4.2 General Observations and Discussions

Concrete and steel are two major building materials. Generally speaking, steel has high strength both in compression and tension and is also ductile, while concrete is good in compression and lacks ductility. Although combination of these two materials is so commonly used in reinforced and prestressed concrete structures, this idea can be used in a number of other ways since each material has its unique characteristics depending on the way the loads are applied, and geometrical configuration.

As a new combination, concrete-filled tubular bracing members certainly have their own special properties. Usually, these members are slender and perform their function as bracing members by providing desired strength and absorbing energy mainly in post-buckling stage under severe cyclic deformation. The presence of concrete provides support to the tube walls in local buckling, thereby increasing fracture life, and also increasing energy dissipation through crushing of confined concrete.

An understanding and knowledge of general behavior and failure modes of the test specimens will help in discussion of their characteristics in detail. Therefore, the general observations and failure modes of all tested specimens are presented in the following two sections first. The detailed observations and discussion of hysteresis behavior will be given thereafter.

#### 4.2.1 General Observations

The general observations of tests in this program can be summarized in the following five points:

1). The presence of concrete can increase the number of cycles to failure, and dissipate more energy than the hollow counterpart under the same loading history except in tube specimens with rather small width-thickness ratio.

2). Concrete can change the local buckling mode, reduce its severity, and delay the occurrence of cracking. These are strong points for using concrete.

3). The effect of concrete depends on the slenderness ratio of a specimen. The less slender a specimen, the more benefit can be obtained from concrete. However, if a bracing member is stocky enough and becomes a tube-confining concrete column, it will behave like a stub column as discussed in Chapter II. In that case, it is concrete that receives confinement from steel tubes rather than providing help to the tubes.

4). The effect of concrete shows strong dependency on the width-thickness ratio. Specimens with large width-thick ratio display significant improvement when filled with concrete. On the other hand, if the walls of a tubular specimen are thick enough not to have severe local buckling, the effect of concrete becomes very small. Generally speaking, the contribution or effect of concrete may be considered as being inversely proportional to the width-thickness ratio.

5). Unlike tube-confining concrete stub columns where the steel provides confinement to concrete and makes it stronger

and more ductile, concrete-filled tubular bracing specimens work in an opposite way. It is concrete that provides lateral support against the inward local buckling. Because the main function of concrete in this case is to change the mode of local buckling, increase in the strength or ductility of concrete does not show any significant influence on the behavior of these composite bracing specimens.

#### 4.2.2 Failure Modes of Specimens

All specimens experienced essentially the same loading history as discussed in the previous chapter. The following is the summary of failure modes of all specimens as well as hysteresis loops and the number of cycles where the specimens crack and fail. Some brief cross comparisons are also made between these specimens.

Hollow specimen T633H is made from 6x3x3/16" (152x76x4.8 mm) tube ordered the first time having width-thickness ratio of 30 and effective slenderness ratio of about 60. This specimen began to crack at cycle 4 and failed at cycle 9 as shown in Figure 4.1.

Specimen T633C6 is the same as specimen T633H except this one is filled with 6 ksi (4.1 KN/cm<sup>2</sup>) concrete. The specimen began to crack at cycle 9 and failed at cycle 14 as shown in Figure 4.2.

Specimens T633C4, T633C4F, and T633C6F were all made from 6x3x3/16" (152x76x4.8 mm) tubes ordered the second time, but filled with 4 ksi (2.8 KN/cm<sup>2</sup>) concrete, 4 ksi (2.8 KN/cm<sup>2</sup>) concrete with steel fibers, and 6 ksi (4.1 KN/cm<sup>2</sup>) concrete

with steel fibers, respectively. The behavior of all these three specimens was very similar, cracking at cycle 8 and failure at cycle 9 as shown in Figure 4.3. Although these specimens behaved similar to specimen T633C6 before cracking, they cracked and failed much earlier than specimen T633C6. It is mainly caused by different properties of the tube material received in the two orders. According to coupon tests discussed in the previous chapter, the tube material ordered the second time had slightly higher strength but about 10% lower ultimate strain than tubes ordered the first time. This explains why specimens T633C4, T633C4F, and T633C6F cracked and failed earlier. But results of these three specimens show that the variation in types and strength of concrete does not change the behavior of specimens.

Specimen T633C8F is made from the same stock as specimens T633C4, T633C4F, and T633C6F, but filled with 8 ksi (5.5 KN/cm<sup>2</sup>) concrete with steel fibers and two 30 inch (76 cm) 1x1x1/10" (25x25x2.5 mm) angles welded on both broad sides in the middle of the span in the longitudinal direction as shown in Figure 3.6. The idea was to see how the angle stiffeners would check outward local buckling of the compression flange. The behavior of this specimen basically turned out similar to specimens T633C4, T633C4F, and T633C6F. But plastic hinge and local buckle formed at one end of the angles instead in the middle of the specimen as shown in Figure 4.4 since the middle part was stiffened by the two angles.

Specimens T424H and T424C6 were made from 4x2x4/16" (102x51x6.4 mm) tube ordered the first time with

width-thickness ratio of 14 and effective slenderness ratio of about 95. Specimen T424H is hollow, while specimen T424C6 is filled with 6 ksi (4.1 KN/cm<sup>2</sup>) concrete. These two exhibited very similar behavior. Both showed cracking at cycle 15, and failed at cycles 16 and 18, respectively, Figure 4.5.

Hollow specimen T422H is made from 4x2x2/16" (102x51x3.2 mm) tube ordered the first time with width-thickness ratio of 30 and effective slenderness ratio of about 90. It began to crack at cycle 4 and failed at cycle 9 as shown in Figure 4.6.

Based on the observation that increase in strength of concrete over 4 ksi (2.8 KN/cm<sup>2</sup>) and use of steel fibers do not change behavior of these composite bracing specimens, specimen T633C6 will be used in the following discussion to represent all 6x3x3/16" (152x76x4.8 mm) tubular specimens filled with concrete.

All of the above points will be further explored in the study of two pairs of specimens. The first pair consists of 4x2x4/16" (102x51x3.2 mm) section tubular bracing specimens with width-thickness ratio of 14 and effective slenderness ratio of about 95 - hollow specimen T424H and the same filled with 6 ksi (4.1 KN/cm<sup>2</sup>) concrete, specimen T424C6. The second pair consists of 6x3x3/16" (152x76x4.8 mm) tubular bracing specimens with width-thickness ratio of 30 and effective slenderness ratio of about 60 - hollow specimen T633H and the same filled with 6 ksi (4.1 KN/cm<sup>2</sup>) concrete, specimen T633C6. The purpose of using these two pairs of specimens is twofold:

(a) To study the differences in behavior between hollow and

concrete-filled specimens, and (b) To study the effect of concrete on specimens with different width-thickness ratio and effective slenderness ratio.

### 4.3 Buckling Modes

#### 4.3.1 Overall Buckling

Specimens made from rectangular tubular sections, either hollow or filled with concrete, have two axes of symmetry. Thus, these specimens may buckle in flexure in either principle direction, i.e., the in-plane or the out-of-plane. In this study all the tested specimens buckled in pure flexural mode over the entire length in the in-plane direction, either upward or downward. No torsional deformation was observed.

Although the end connections in the in-plane direction are much stiffer than in the out-of-plane direction, the moment of inertia of specimens in the in-plane direction is smaller than in the out-of-plane direction. According to the previous researchers and the buckling mode exhibited in tests in this study, effective length factor in in-plane direction,  $K_y$ , is taken 0.5 and the length of the specimens is taken as the distance between two center points of the end plates, Figure 4.7. Equivalent sections based on transformed area method as shown in the same figure are used to compute the radius of gyration,  $r_x$  and  $r_y$ . The computed  $K_y L / r_y$  is approximately 60 for 6x3x3/16" (152x76x4.8 mm) specimens and 95 for 4x2x4/16" (102x51x6.4 mm) specimens. Effective length

factor for out-of-plane direction,  $K_x$ , is dependent on the relative stiffness of tubes and gusset plates. For the specimens tested, the computed value of  $K_x$  ranged from 0.8 to 0.83 according to the method recommended by Jain (18). Thus, the value of  $K_x L/r_x$  is about 55 for 6x3x3/16" (152x76x4.8 mm) specimens and about 85 for 4x2x4/16" (102x51x6.4 mm) specimens. In each case,  $K_y L/r_y$  in the in-plane direction is larger than  $K_x L/r_x$  in the out-of-plane direction. This confirms the observed overall buckling in the in-plane direction for all specimens used in this study.

Test results show that there is no significant difference in overall buckling mode between hollow and concrete-filled bracing specimens before local buckling occurred or plastic hinges formed. However, after plastic hinges appear, some difference in overall buckling mode is exhibited between hollow and concrete-filled specimens, and among specimens with different width-thickness ratios. The main difference is that hollow specimen T633H with width-thickness ratio of 30 was divided into two almost straight segments by plastic hinges as shown in Figure 4.8(a), while hollow specimen T424H with width-thickness ratio of 14 and all concrete-filled specimens bent in a more curvilinear cosine shape after plastic hinges formed as shown in Figure 4.8(b). This is because that plastic hinge moment capacity in concrete-filled specimens and hollow specimens with thicker walls remain very stable without much reduction after plastification.

#### 4.3.2 Local Buckling

Bracing members usually have slenderness ratios large enough to cause overall buckling under compression force. At the same time, this is usually accompanied with local buckling in plastic hinge zones due to high compression stresses. How well a bracing member performs under these conditions determines its ductility and energy dissipation capacity. Mode and severity of local buckling play an important role in this issue. It is one of the main purposes of this study to find the difference in local buckling modes between the hollow and concrete-filled tubular bracing members. At the same time, the local buckling behavior among hollow tubular specimens with different width-thickness ratios is also studied.

All specimens tested in this study develop plastic hinges near the mid span and also at both ends after buckling. Therefore, local buckling tends to localize within these zones. In the hollow tubular bracing specimens, width-thickness ratio is the main factor governing the severity of local buckling as also discovered by previous researchers. Although slenderness ratio of the specimen is also a factor, no significant difference is found in specimens tested in this study because of limited range of slenderness ratios used.

##### 4.3.2.1 Hollow Specimens

For hollow rectangular tubular bracing specimens, test results show that all specimens follow similar local buckling

00287

pattern except for its severity and time of occurrence in the load history. After a specimen undergoes overall buckling in compression, the compression flange at plastic hinges begins to buckle inwards which is also accompanied by the webs bulging outwards. How late this happens depends on width-thickness ratio as well as slenderness ratio of the specimen. The local buckling is concentrated in narrow zones in the middle of the span and at each end of the specimen, Figure 4.9(a). As the number of cycles increases, the bulges at the corners grow, leading to opening of small cracks which spread very quickly into the flange and both webs. When 50 percent or more of the section has fractured the specimen is considered to have failed.

Although all hollow tubular specimens follow similar local buckling pattern as discussed above, the time when local buckling occurs and its severity depend mainly on width-thickness ratio of the walls. In this study, hollow specimens T424H and T422H have effective slenderness ratio of about 90, but different width-thickness ratio. The specimen T424H is made from 4x2x4/16" (102x51x6.4 mm) section with width-thickness ratio of 14, while specimen T422H is made from 4x2x2/16" (102x51x3.2 mm) tube with width-thickness ratio of 30, which is within the AISC Specification limit (3). When subjected to the same loading history the two specimens behaved differently with respect to local buckling. Local buckling occurred in specimen T422H with width-thickness ratio of 30 almost immediately after first overall buckling. At this stage, the strain level at the plastic hinge was about

0.008 which is the same strain level at which local buckling occurred in the stub column specimens C633H and C422H with width-thickness of 30. This specimen showed visible cracks at cycle 4. However, specimen T424H with width-thickness ratio of 14 did not experience any local buckling until cycle 15 when cracking also occurred rather suddenly, Figure 4.9(b).

Hollow specimens T633H and T422H have the same width-thickness ratio of 30, but different effective slenderness ratios. The effective slenderness ratio of T633H is about 60 and that of T422H is 90. Test results show that both have very similar local buckling behavior. These two specimens had local buckling and cracking almost at the same instant in the deformation history. This also shows that effect of width-thickness is more significant than that of the slenderness ratio.

#### 4.3.2.2 Concrete-Filled Specimens

For the concrete-filled specimens, the local buckling follows a different pattern. Although local buckling occurs in compression flange at the location of plastic hinges, there are two major differences from the hollow specimens:

- 1). Unlike hollow tubular bracing specimens the flange of concrete-filled specimens buckles outwards rather than inwards due to the presence of concrete.

- 2). The local buckling is not concentrated in a narrow band as in hollow specimens. It forms a rather flat dome whose length is close to the width of the tube as shown in Figure 4.10(b). As number of cycles increases, the webs near

the buckled flange begin to buckle inwards, although, quite restricted by concrete fill. Following this, cracks form at the corners and propagate along the flange and the webs until the specimen fails. Thus the concrete fill reduces the severity of local buckling and consequently delays cracking in the specimen.

The change in the local buckling mode and the reduction in severity due to the presence of concrete are beneficial for these bracing specimens in two ways. First, after local buckling the section modulus of the buckled sections does not decrease since the distance between the top and bottom flanges increases instead of decreasing as shown Figure 4.11. This holds the plastic hinge moment without too much reduction. Secondly, severe strain concentrations are avoided due to restrained local buckling, thereby increasing the fracture life of the specimen. In other words, a specimen can survive more cycles and have larger post-buckling strength in each cycle than the hollow counterpart.

#### 4.4 Behavior of Specimens under Tension

##### 4.4.1 First Yield Force

In the first half of the initial cycle, all specimens were pulled to a strain offset approximately 0.2% as discussed in the previous chapter. According to the results shown in Figure 4.12(a), it can be seen that for 4x2x4/16" (102x51x6.4 mm) specimens T424H and T424C6, the first peak tension force of hollow specimen T424H is close to the concrete-filled specimen T424C6. No recognizable difference is found. This

is probably due to small  $A_c/A_s$  ratio ( $A_c/A_s = 2.0$ ), where  $A_c$  is the cross section area of concrete and  $A_s$  of steel. On the other hand, for the 6x3x3/16" (152x76x4.8 mm) section specimens T633H and T633C6 which have relatively larger  $A_c/A_s$  value ( $A_c/A_s = 4.7$ ), about 15% increase in the first peak tension force is noticed when compared with the hollow specimen T633H, Figure 4.12(b). Precise mechanism for such increase in peak tension force due to the presence of concrete is not entirely clear. But it is considered that the increase in tension force is mainly the result of the following two effects.

- 1). After the strain in a specimen reaches the fracture strain of concrete under tension, the concrete begins to crack at certain sections. But the concrete segments between two adjacent cracked sections still have bond force with steel tube and share some portion of the total tension force. The specimen can be simplified into an unequal cross section tension member as shown in Figure 4.13.

Because the test is controlled by deformation, a larger force is needed for the same deformation in an unequal cross section specimen whose smallest section is equal to that of the hollow counterpart. But when the  $A_c/A_s$  is too small, the bond force in the interface between steel and concrete may not be that effective to transfer significant tension force to concrete such as in 4x2x4/16" (102x51x6.4 mm) specimen. As a result, the portion of force carried by concrete is negligible in this case.

2). Under tension force the steel tube has longitudinal positive strain,  $\epsilon_1$ . At the same time, it also develops negative strain,  $\epsilon_2$ , in the transverse direction due to Poisson's effect. Concrete inside the tube does not permit free negative lateral strain in the tube. Thus, the tube is restricted laterally by concrete and is subjected to biaxial stress condition as shown in Figure 4.14. In order to compute the net longitudinal deformation of the specimen, it is necessary to consider the effect of lateral restraint from concrete. For the stress state as shown in Figure 4.14, we have:

$$\epsilon_1 = \sigma_1/E - \mu \cdot \sigma_2/E \quad (4.1)$$

where,

$\epsilon_1$  = Strain in steel in longitudinal direction

$\sigma_1$  = Stress in steel in longitudinal direction

E = Modulus of elasticity of steel

$\mu$  = Poisson's ratio of steel

$\sigma_2$  = Stress in steel in lateral direction

For simplicity, let it be assumed that the volume of concrete remains constant. In other words, lateral strain in concrete is zero and so is the lateral strain in tube.

Therefore,  $\epsilon_2$  can be set to zero.

$$\epsilon_2 = \sigma_2/E - \mu \sigma_1/E = 0 \quad (4.2)$$

or

$$\sigma_2 = \mu \sigma_1 \quad (4.3)$$

Substituting Equation (4.3) into Equation (4.1), we have the following expression for  $\epsilon_1$ :

$$\epsilon_1 = \sigma_1/E - \mu \mu \sigma_1/E \quad (4.4)$$

or

$$\epsilon_1 = \sigma_1/[E/(1-\mu^2)] \quad (4.5)$$

Let  $E_e = E/(1-\mu^2)$  be an equivalent modulus for considering the effect of concrete. The following formula can be used to compute the axial tension force for concrete-filled steel tubes:

$$\sigma_1 = \epsilon_1 E_e \quad (4.6)$$

If  $\mu = 0.3$ ,  $E_e = E/(1-0.3^2) = 1.1 E$ . This means that the specimen is 10 percent stronger than the hollow one under tension. For the same reason as mentioned in point 1), the 10 percent extra force is required to have the same deformation as a hollow specimen when only considering the lateral

restriction effect from concrete.

It should be pointed out that Equation (4.2) gives an ideal situation in which the change in volume of concrete is assumed to be zero. In the real case the force should be smaller than the value given by Equation (4.6), since some lateral deformation exists in concrete. In other words,  $\epsilon_2$  is not really equal to zero. Particularly, when  $A_c/A_s$  is relatively small the stiffness of steel is much larger than that of concrete. This will cause concrete to have some lateral deformation. In this case the increase in tension force due to concrete will become negligible. If the above two effects are considered together, the maximum increase in tension force due to concrete is about 15%. Some previous researchers have also reported similar results (32).

In this study, bracing specimen T424C6 made of 4x2x4/16" (102x51x6.4 mm) tube belongs to the case where  $A_c/A_s$  is small. Large lateral stiffness of thick tube walls cause more deformation in the concrete inside the tube. Therefore, Equation (4.6) gives an upper limit on the increase in tension force due to lateral restraining effect of concrete.

As the number of cycle increases during testing, concrete inside the tube loses its integrity gradually in the plastic hinge zones. The increase in tension force due to the factors discussed above should remain effective at location away from the plastic hinges. This is confirmed by the test results in this study as will be discussed in the next section.

#### 4.4.2 Cyclic Peak Tension Forces

The peak tension forces in each cycle for specimens T633H and T633C6 are shown in Figure 4.15(a). The force for concrete-filled specimen T633C6 is about 15 percent larger than the hollow specimen T633H. This confirms the conclusion presented in the previous paragraph. It can also be noticed in this figure that, besides the difference in cyclic peak tension forces, the specimen T633C6 filled with concrete has much longer fracture life than the hollow specimen T633H. However, the difference in cyclic peak tension forces between specimens T424H and T424C6 with width-thickness ratio of 14 is very small as can be seen in Figure 4.15(b). The reasons for this were also discussed in the previous section.

#### 4.5 Behavior of Specimens under Compression Force

##### 4.5.1 First Buckling Load

There are several methods available to estimate the first buckling load for hollow tubular compression members such as the SSRC Basic Column Strength formulas used by AISC for allowable stress design. It has been shown in some previous studies that the test results agreed very well with the computed values from this procedure (13). In this study three hollow tubular bracing specimens are included. The computed forces from the procedure by AISC agree well with the forces from test results as shown in Figure 4.16. The effective length factor,  $K$ , is taken equal to 0.5 and  $L$  is equal to 142" (361 cm). This means that AISC procedure for allowable stress design (deleting the factor of safety) can be used to predict

the first buckling load for hollow tubular specimens.

No formula or procedure was available for computing buckling loads for composite bracing members until the first edition of "Load and Resistance Factor Design" (2) was published by AISC recently. A procedure is given to compute the capacity for concrete-filled tubular compression members. That procedure is based on test results and concrete is considered by modifying yield stress and modulus of elasticity of steel, thereafter the procedure for steel column design is followed (31). After studying this procedure and comparing the results with test results in this study it is found that this method is rather crude and gives results which are generally quite conservative. Therefore, it is necessary to develop more rational procedures to predict the first buckling load for concrete-filled tubular bracing members.

According to the test results, before compression force reaches the first buckling load, no local buckling was observed in concrete-filled specimens tested in this study. This means that the first buckling load is mainly controlled by overall buckling without any effect of local buckling. Test results also show that variation of concrete strength does not change the value of the first buckling load by significant amount. Specimen T633C4, T633C4F, T633C6F, and T633C8F, made from 6x3x3/16" (152x76x4.8 mm) section, have identical properties except for different types of concrete. First buckling loads for all these specimens are almost the same as seen in Figure 4.17. For specimens T424H and T424C6, made from 4x2x4/16" (102x51x6.4 mm) section, which are slender

and more compact than 6x3x3/16" (152x76x4.8 mm) specimens, the first buckling load for concrete-filled specimen T424C6 is only slightly larger than the hollow counterpart T424H.

Two procedures have been developed to compute the first buckling load for concrete-filled tubular bracing members in this study. The characteristics discussed above have been reflected in these two methods. The details of these two methods are given in the following sections.

#### 4.5.1.1 Tangent Modulus Method

According to the above discussion, the most rational starting point, therefore, will be to assume that the first buckling load is governed by overall stability. In this method to compute the first buckling load, Euler's theory is used with the some modifications to consider the contribution of concrete.

##### 1. Basic Assumptions

1). Members are assumed to be in axial compression only with pin supports at both ends. An effective length factor,  $K$ , can be introduced to consider different end conditions.

2). The moment of inertia of both steel and concrete is considered in computing the stiffness of the section,  $EI$ .

3). Tangent modulus is used in place of elastic modulus for both concrete and steel.

##### 2. Detailed Procedure

The detailed procedure and its verification by using test

results from this study are described in the following.

- 1). The Euler formula for a composite section gives,

$$P_b = \frac{\pi^2 ( E_{st} I_s + E_{ct} I_c )}{( KL/r )^2} \quad (4.7)$$

where,

$P_b$  = The first buckling load

$E_{st}$  = Tangent modulus of steel

$E_{ct}$  = Tangent modulus of concrete

$I_s$  = Moment of inertia of steel

$I_c$  = Moment of inertia of concrete

$K$  = Effective length factor for the member

$L$  = Length of the member.

2). According to coupon tests the following function is chosen to define the stress-strain relationship for A500 Grade steel. A comparison between a typical curve from coupon tests and the plot of Equation (4.8) is shown in Figure 4.18. Both agree with each other very well.

$$\epsilon_s = \sigma_s / E + 0.002 (\sigma_s / F_y)^{15} \quad (4.8)$$

and

$$E_{st} = d\sigma_s / d\epsilon_s$$

or

$$E_{st} = 1 / [ 1 / E + 0.03 \sigma_s^{14} / F_y^{15} ] \quad (4.9)$$

Where,

$E$  = Elastic modulus of steel

$\epsilon_s$  = Strain of steel

$\sigma_s$  = Stress of steel

$F_y$  = Yielding stress of steel

3). For concrete the following expression is commonly used to describe the stress-strain relationship. Figure 4.19 shows a typical curve from concrete cylinder tests and the plot of Equation (4.10).

$$\sigma_c = f'_c \left[ \frac{2 \epsilon_c}{0.002} - \left( \frac{\epsilon_c}{0.002} \right)^2 \right] \quad (4.10)$$

and

$$E_{ct} = d\sigma_c / d\epsilon_c$$

or

$$E_{ct} = f'_c \left[ \frac{2}{0.002} - \left( \frac{2 \epsilon_c}{0.002^2} \right) \right] \quad (4.11)$$

where,

$\sigma_c$  = Stress of concrete

$\epsilon_c$  = Strain of concrete

$f'_c$  is the strength of concrete. If it is larger than 6 ksi

(4.1 KN/cm<sup>2</sup>), it is taken to equal to 6 ksi (4.1 KN/cm<sup>2</sup>). The reason for this is that it is very difficult to control the quality of concrete above 6 ksi (4.1 KN/cm<sup>2</sup>) inside a slender tube. The strength above 6 ksi (4.1 KN/cm<sup>2</sup>) obtained in cylinder tests does not guarantee such high strength inside a tube, since, to produce concrete above 6 ksi (4.1 KN/cm<sup>2</sup>) more stringent quality control is essential according to some previous researchers (29).

4). We have compatibility condition,

$$\epsilon_s = \epsilon_c \quad (4.12)$$

and the equilibrium condition,

$$P_b = \sigma_s A_s + \sigma_c A_c \quad (4.13)$$

where,

$A_s$  = Area of steel

$A_c$  = Area of concrete

6). Solving Equations (4.7) to (4.13) gives the buckling load  $P_b$ .

The solution is obtained by a trial and error method using a computer. The flow chart for the solution algorithm and the computer program in BASIC Language is presented in Appendix A.

The above procedure is used to compute the first buckling load for specimens T633H, T633C6, T424C6, T424H, and T422H.

Figure 4.20 shows results from the tests and the computation. It is evident from this figure that this procedure can very well estimate the first buckling load for both hollow and concrete-filled tubular bracing specimens. When it is used for a hollow tubular specimen just set the area of concrete equal to zero. The limitations of this procedure are also discussed in Appendix A.

#### 4.5.1.2 Approximate Method

Although the above method gives satisfactory results which fit test results for concrete-filled tubular bracing members, it requires complex calculations and the use of a computer is essential. It is not very convenient for practical structural analysis and design. The second method presented herein attempts to combine the main characteristics of these composite bracing members with computational simplicity. The method is based on the following assumptions:

- 1). Steel tube and concrete work independently for the purpose of computing the first buckling load. Thus AISC (3) Formula (1.5-1) can be used to compute the force taken by steel.

- 2). The stress-strain relationship of steel is linear before the force reaches the buckling load.

- 3). The strain in concrete is the same as in steel so that the stress in concrete can be computed by Equation (4.10).

The following is the detailed procedure:

- 1). Use the AISC Formula (1.5-1) to compute the buckling

stress for steel without considering the presence of concrete and the factor of safety.

$$\sigma_s = [ 1 - 0.5 (KL/r)^2 / C_c^2 ] F_y \quad (4.14)$$

where,

$\sigma_s$  = Stress in steel

K = Effective length factor, assumed equal to 0.5

L = Length of member, taken equal 142" (361 cm)

r = The radius of gyration of tube section

$C_c$  = Slenderness ratio that separates elastic and inelastic buckling

$F_y$  = Nominal yield strength of steel tube

2). Compute strain and stress in concrete.

$$\epsilon_c = \epsilon_s = \sigma_s / E_s \quad (4.15)$$

and

$$\sigma_c = f_c' [ 2 \epsilon_c / 0.002 - ( \epsilon_c / 0.002 )^2 ] \quad (4.10)$$

Where,

$\epsilon_c$  = Strain in concrete

$\epsilon_s$  = Strain in steel

$\sigma_c$  = Stress in concrete

$f_c'$  is the strength of concrete, as discussed in the previous method it is taken no more than 6 ksi (4.1 KN/cm<sup>2</sup>).

3). The buckling force,  $P_b$ , can be computed by the following equation.

$$P_b = \sigma_s A_s + \sigma_c A_c \quad (4.16)$$

If  $KL/r$  of a member is larger than  $C_c$  the first buckling load may be computed by using the AISC procedure without considering the effect of concrete since the contribution from concrete is small. This method is used to compute the first buckling load for the five specimens mentioned in Tangent Method. The results are shown in Figure 4.20. It is clear from this figure that this Approximate Method can also predict the first buckling load very well.

The procedure given by AISC for load and resistance factor design is also used to compute the buckling loads. The results are also shown in Figure 4.20. It can be seen that this method generally underestimates the buckling loads and is on the conservative side.

#### 4.5.2 Cyclic Peak Compression Forces

Peak compression force in each cycle is an important factor in determining the energy absorption capacity of a bracing member. Past studies have shown that compression loads suffers steep reduction from the first cycle to the

second cycle, but become quite stable after about the third cycle (13,18). The test results of both hollow and concrete-filled tubular specimens in this study show similar trend. At the same time, some significant difference is also found between hollow and concrete-filled bracing specimens.

Generally speaking, the deterioration of cyclic peak forces in a deformation controlled testing is mainly due to the following reasons. The first is the residual deformation accumulated from previous cycles. The second is the severe local buckling which reduces the moment capacity in plastic hinge zones. There may be some other factors responsible for deterioration, but these two factors have been recognized quite widely. As discussed in Section 4.3.2 (Local Buckling Mode), the presence of concrete can change the mode of local buckling and reduce its severity. This helps to maintain the plastic hinge moments. Thus, the portion of deterioration of cyclic peak forces due to local buckling becomes very small or nearly zero. Test results in this study show that the cyclic peak forces in a concrete-filled specimen decrease at lower rate than hollow tubular specimens due to less severe local buckling.

Apart from the number of cycles to failure for a specimen, it is thought in this study that the rate of drop in cyclic peak forces is also important. For the purpose of evaluation, the slope of dashed line AB as shown in Figure 4.21 can be used to reflect the rate of drop in cyclic peak force.

During cyclic loading the specimens are usually pulled to

different levels of tensile deformation. While in most cycles a specimen is pulled to  $\Delta_y^*$ , in some cycles the specimen is only brought to zero deformation or is pulled to its yield force. This variation in tension deformation affects the compression force following the tension deformation in the same cycle, such as points "a" and "b" in Figure 4.21. The higher cyclic compression force at point "a" is due to over-elongation in the first half cycle, and force at point "b" is because the specimen is only pulled to zero deformation in the first half cycle. These points should not be considered when computing the rate of drop in cyclic peak force in order to apply this concept to different loading histories. A suggested loading history for obtaining the line AB is recommended as shown in Figure 4.22. The main purpose is to eliminate the influence of variable tension deformation. It is expected that if the specimens in this study had experienced the loading history shown in Figure 4.22 all points representing the cyclic peak compression forces would have fallen on line AB, Figure 4.23.

Figure 4.24 shows the measured compressive peak forces in each cycle for specimens T633H and T633C6, made from 6x3x3/16" (152x76x4.8 mm) tubes. Specimen T633H is hollow, while specimen T633C6 is filled with 6 ksi (4.1 KN/cm<sup>2</sup>) concrete. From the second cycle on, although the peak compression forces drop in both specimens, the rate of drop is different. For the hollow specimen T633H, not only does the cyclic peak force drop at a larger rate, but also it fails earlier due to the severe local buckling. The decrease in

cyclic peak forces for the concrete-filled specimen T633C6 is much slower and lasts longer. In terms of steady drop rate (slope of line AB in Figure 4.24) the value for hollow specimen T633H is about 7 kip/cycle and only 3.2 kip/cycle for its concrete-filled counterpart, specimen T633C6.

As discussed above, the deterioration of cyclic peak force is mainly due to severe local buckling, which in turn is the consequence of large width-thickness ratio. The presence of concrete can change local buckling mode and reduce its severity. Therefore, the presence of concrete can decrease the rate of drop in cyclic peak forces as seen in specimens T633H and T633C6.

On the other side, if the width-thickness of a specimen is small enough in itself to prevent severe local buckling, the merit of using concrete becomes negligible. Figure 4.25 shows the cyclic peak compression forces for hollow specimen T424H and concrete-filled specimen T424C6. Both specimens are made from 4x2x4/16" (102x51x6.4 mm) tube. Since the tube has small width-thickness ratio of 14, no visual local buckling occurred until just before failure even for hollow specimen as discussed earlier in Section 4.3.2. Therefore, the presence of concrete changed nothing since local buckling was not a problem to begin with. It can be seen from Figure 4.25 that the drop rate of cyclic peak compression forces in both specimens and the number of cycles to failure are very similar.

The cyclic peak compression forces for specimens T633H and T422H, made from 4x2x2/16" (102x51x3.2 mm) tube, are shown

in Figure 4.26. Both specimens are hollow and have the same width-thickness ratio of 30, but different slenderness ratio. It can be seen that both bracing specimens have almost the same drop rate in cyclic peak forces and the same number of cycles to failure under the same loading history. On the other hand, Figure 4.27 shows the result for specimens T424H and T422H which are very similar excepts for width-thickness ratio. Two points of difference between the two can be noticed in this figure. The first is the slope of line AB, and the second is the number of cycles to failure. The comparison of the two sets of specimens, T633H - T422H, and T424H - T422H, shows that width-thickness ratio is more important than slenderness ratio in determining the rate of drop in cyclic peak compression force and the number of cycles to failure.

It is also interesting to note the difference in compression forces at reversal points in each cycle for specimens T633H and T633C6 as shown in Figure 4.28. Upto the reversal point from maximum contraction in each cycle all specimens had experienced significant overall buckling and the local buckling reached its maximum level in the cycle. The measured compression forces at reversal points for the concrete-filled is larger than the hollow one. The difference is mainly due to differences in local buckling mode and its severity as discussed earlier. On the other hand, Figure 4.29 shows the cyclic compression force at reversal point from maximum contraction for specimens T424H and T424C6 with width-thickness ratio of 14. As expected, the difference

between the two is small.

#### 4.6 Hysteresis Behavior

In earthquake resistance structures the energy dissipated by bracing members is a very important factor. It is the area enclosed by hysteresis loops in each cycle. Figures 4.30 to 4.34 show the hysteresis loops for hollow specimen T633H and concrete-filled counterpart, specimen T633C6, in cycle 1,2,4 and 7. The energy dissipated in these cycles as well as the total by each specimen is listed in Table 4-1. It is clear from these figures and the table that the two specimens dissipate a significant amount of energy during the first cycle. But in subsequent cycles the area under the hysteresis loops began to drop rapidly. On other hand, in each cycle the composite bracing specimen absorbs much more energy than the hollow one. Furthermore, the former has longer fracture life and also absorbs a lot of energy in cycles beyond cycle 9, where the hollow specimen T633H had failed.

It is easy to expect that the difference in hysteresis loops between hollow specimen T424H and concrete-filled specimen T424C6 with width-thickness ratio of 14 would be very small. This is because both have very similar behavior and concrete does not provide any noticeable help to a tube with small width-thickness ratio. More detailed discussion of hysteresis behavior will be presented in the next chapter where the hysteresis loops are studied in more detail and an empirical hysteresis model is proposed.

## CHAPTER V

### MODELING THE HYSTERESIS LOOPS

#### 5.1 Introduction

A quantitative knowledge of hysteresis behavior of bracing members is essential in order to compute the seismic response of steel frames braced with concrete-filled tubular bracing members. This requires a quantitative model to describe the real hysteresis loops as closely as possible. Several types of analytical models have been developed in the past to represent the cyclic buckling behavior of steel bracing members (13,16,17,26,30). Reference 16 gives a very good summary of these different types of models.

The first type is a finite element model. This type of models generally subdivides a bracing member longitudinally into a series of segments which are further subdivided into a number of smaller units as shown in Figure 5.1(a). While providing the most realistic representation of the behavior of a bracing member, this type of models usually demands computations which are too costly to be applied to practical analyses of large-scale braced structures.

The second type is physical theory models. This type of models applies simplified theoretical formulations based on physical considerations that permit the cyclic inelastic behavior to be computed by use of the model as shown in Figure

5.1(b). Although these models attempt to combine the realism of finite element approaches with the computational simplicity, they still require material property and geometric property inputs and a lot of calculation work and interpretation for the input data. This would be even more difficult for this new type of composite bracing members since the interaction between concrete and steel is not yet quite fully understood on a micro level.

Phenomenological models (Empirical models) are the third type of models. Models of this type are based on a set of simplified hysteresis rules as shown in Figure 5.1(c) which mimic the observed axial force - axial deformation curves of a bracing member. Currently, empirical models are most commonly used for analysis of large-scale braced structures. Users of such models only need to specify some simple input data. Models in this group require minimum computations, and have no complex processing of section and material property inputs as in the previous two types of models. This is particularly suitable for composite bracing members whose properties at micro level have not been fully explored yet.

After reviewing and comparing of these three different types of model, it is considered to formulate an empirical model for concrete-filled tubular bracing members based on limited test results obtained in this study. Among available empirical models for steel bracing members, Jain's model (18) has been used quite extensively by numerous researchers in the past. Jain's model is a modified version of Singh's model

(30). Comparing hysteresis loops from Jain's model and the test results of tubular bracing specimens shows that Jain's model generally follows the hysteresis loops measured from tests except for the effect of local buckling. This should not be much of a problem for concrete-filled tubular bracing members since severe local buckling is prevented due to the presence of concrete. However, Jain's model needs to be adjusted to fit the test results.

This chapter will first introduce Jain's model and study the discrepancies between hysteresis loops obtained from his model and the test results. This will help identify the areas which need to be modified to consider the effect of concrete. Finally, an empirical model is proposed and verified by the test results in this study.

## 5.2 Review of Jain's Model

A brief review of Jain's model is given in this section. His model is basically a refined version of Singh's hysteresis model (30). These two models essentially share the same basic assumptions and detailed procedure. The main difference is the force values at control points. Therefore, in the following sections, the basic assumptions are given first. Then the detailed procedure of this empirical model is described, which includes the modifications made by Jain.

### 5.2.1 Basic Assumptions

Jain's model is modified Singh's model which originally was based on Prathuangsit's semi-empirical model (26) which

required some assumptions and calculations similar to those in a physical model. Therefore, while most of assumptions made by Prathuangsit are common to these three models, some may not be necessary for either Jain's or Singh's model which belongs to empirical type of models. A brief summary of basic assumptions made by Prathuangsit are given in the following. Points which do not apply to Jain's model are also indicated.

1). Bracing members have an elastic-perfectly plastic stress-strain relationship.

2). Both, members and connections have elastic-perfectly plastic moment-curvature relationship with the fully plastic moment modified due to the presence of axial force.

3). The member is of uniform cross-section and supported laterally along its length such that no out-of-plane deformation can occur.

4). End rotations of the rigidly connected columns and girders in braced frames may be neglected as compared to the rotations at the connections of the bracing members.

5). The magnitude of initial plastic rotation,  $\theta_p'$  was selected on the basis of the agreement of theoretical maximum compressive load carried by the member with the load capacity of the same member as computed by using the column axial strength formula in Part 2 of AISC Specification (3).

This assumption may not be necessary in an empirical model since it is assumed that members are perfectly straight initially. Furthermore, maximum compression loads are usually computed by empirical formulas such as AISC equations rather than by theoretical analyses.

6). An approximate expression for curvature ( $\phi = d^2y/dx^2$ ) was used to obtain the force deformation relation in a closed form. This solution was used to generate hysteresis curves for bracing members. This assumption is only necessary for physical models since empirical models in most cases do not need the expression for curvature.

### 5.2.2 Detailed Procedure

A brief description of this model in non-dimensional form (i.e.  $P/P_y$  vs.  $\Delta/\Delta_y$  plot) is given in the following,  $P_y$  and  $\Delta_y$  being the tensile yield force and yield displacement, respectively.

Assuming that an initially straight member is loaded first in tension the member will elongate elastically along the branch OE as shown in Figure 5.2 until yield load  $P_y$  is reached. If the load is further increased the member will follow the yield path EF and an elastic unloading along FM.

On compression the initial elastic curve can be plotted at a slope,  $\delta$ , equal to  $AE/L$  from point O as shown by segment OA in Figure 5.3, where A (in  $AE/L$ ) is the area of cross-section and E is the modulus of elasticity. The member will buckle at a maximum compression load, point A, which is obtained by using AISI or AISC equations in the first cycle. Continued compression results in path ABC, where point B is the compression load at  $5\Delta_y$  and point C is the compressive load at  $12\Delta_y$ . Control points B and C are given by  $18/(KL/r)$

$P_y$  and  $12/(KL/r) P_y$ , respectively, for all cycles.

If the direction of axial displacement is reversed at point C it results in compression load decreasing to zero followed by an increasing tensile load along the path CDEF. Based on the maximum compressive displacement as given by point C and the effective slenderness ratio of the member, residual strain  $\epsilon$  can be computed from the following equation:

$$\epsilon = 0.0175 [0.55 (\Delta/\Delta_y)/(KL/r) + 0.0002 (\Delta/\Delta_y)^2] \quad (5.1)$$

Coordinates of point E are given by  $(P/P_y, \Delta/\Delta_y)$  where  $P/P_y$  is equal to 1.0 and  $\Delta/\Delta_y$  is equal to  $(1 + \epsilon L/\Delta_y)$ .  $L$  is the length of the member. To locate the point D, a line OD' is drawn from the origin at a slope of 1/3 times the initial elastic slope,  $\delta$ , which intersects the line CE at point D'. Intercept OD is taken as  $60/(KL/r)$  times the distance OD'.

A line DH is drawn parallel to the initial elastic slope to distinguish the loading history in the region CDH from that in AHDE. If the direction of axial displacement is reversed anywhere along CG, member retraces the same path. If reversal occurs from the branch GD, the member unloads elastically along KL and further reversal occurs either along LK or L'K. Similarly, if reversal occurs from the branch DE, the member unloads elastically along IJ. If reversal occurs before H, the member follows the path JI or J'I, otherwise the return is along J"D.

A new hysteresis loop is assumed to have begun when the member starts unloading from point E or F or the member exceeds the previous maximum compressive displacement, point C. The maximum compression load in the second hysteresis loop is given by  $30/(KL/r) P_y$  and in the third and subsequent loops by  $25/(KL/r) P_y$ . A new hysteresis loop is established by selecting new points A, B, C, D and E.

### 5.2.3 Comparison of Test Results with Jain's Model

Experimental hysteresis loops for hollow specimen T633H of effective slenderness ratio of about 60, specimen T422H of effective slenderness ratio of about 88, and specimen T424H of effective slenderness ratio of about 92 are shown in Figures 5.4 to 5.13 respectively. These hysteresis loops are from deformation sequence cycles 1,2,5 and 10 (for specimen T424H only). Theoretical loops were obtained using Jain's model and also plotted in the same figures.

Figures 5.4 to 5.13 show that Jain's model follows the general shape of experimental curves. But significant discrepancies exist for specimens T633H and T422H with width-thickness ratio of 30 between measured hysteresis loops and Jain's model. These discrepancies are in the following three aspects:

The first is the difference in compression forces at reversal point (maximum contraction) in the first cycle. The load obtained from Jain's model is overestimating the measured one from tests as shown in Figures 5.4 and 5.7. This is due

to the fact that Jain's model does not consider the decrease in hinge moment due to severe local buckling. As discussed in Chapter IV regarding local buckling behavior, severe local buckling in specimens T633H and T422H with width-thickness ratio of 30, which is within the AISC Specification Limit (3), caused drop in compression forces.

On the other hand, Figure 5.10 shows the first hysteresis cycle for specimen T424H with width-thickness ratio of 14. According to this figure, both measured and computed hysteresis loops in first cycle agree very well and no significant difference exists between the forces at reversal point. This is confirmed by the tests that no visible local buckling was observed in specimen T424H till failure, and no force drop occurred due to local buckling.

The second discrepancy lies in general overestimation of compression forces for members in which severe local buckling occurs. Figures 5.6 and 5.9 show hysteresis loops in cycle 5 for specimens T633H and T422H, respectively, with width-thickness ratio of 30. From the second hysteresis loop on the measured compression forces from tests in both specimens are generally lower than the forces given by Jain's model. It is believed that this difference in compression forces is also caused by severe local buckling which occurred in the first cycle.

On the other hand, Figures 5.12 and 5.13 show very good agreement between forces from tests and the model in cycles 5 and 10 for specimen T424H with width-thickness ratio of 14. This confirms that while the forces computed from the model

are quite reasonable for a member in which no severe local buckling occurs, it overestimates the compression forces for members with large width-thickness ratios which is likely to cause severe local buckling.

The fact that this model does not consider the decrease in hinge moments due to local buckling limits its use only to members with small width-thickness ratios. It is suggested that in order to make this model more generally applicable width-thickness ratio would need to be considered.

The third discrepancy between Jain's model and test results lies in the compression loads in intermediate cycles as shown in Figures 5.5, 5.8 and 5.11 for specimens T633H, T424H and T422H, respectively. It can be seen from these figures that compression loads in intermediate cycles are much smaller than those predicted by Jain's model. Specimen T424H with width-thickness ratio of 14 did not exhibit any local buckling during test, yet it shows the same discrepancy between the model and test results as specimens T633H and T422H. Therefore, local buckling can not be responsible for this difference between the model and test results. Jain's model overestimates the compression loads in intermediate cycles by big margins.

### 5.3 Proposed Model

#### 5.3.1 Modifications in Jain's Model

Width-thickness ratio is not too critical for concrete-filled bracing members since severity of local buckling is reduced due to the presence of concrete.

Therefore, Jain's model can serve as the basis of the proposed model for composite bracing members. Study of hysteresis loops from the tests and Jain's model showed that the following factors in Jain's model may need to be modified to include the effect of concrete:

1. Maximum Tension force

Cyclic tension forces obtained from test results and the discussion presented in Section 4.4 (Behavior of Specimens under Tension Forces) showed that the first yield force and cyclic tension forces increase in comparison to their hollow counterparts due to the presence of concrete. The first yield force vs. different  $A_c/A_s$  ratios for specimens T633C6 and T424C6 and their hollow counterparts are plotted in Figure 5.14, where  $A_c$  is the area of concrete and  $A_s$  that of steel. The increases in tension force in specimens T633C6 with  $A_c/A_s$  ratio of 4.7 is about 15%. Tension force in specimen T424C6 with  $A_c/A_s$  ratio of 2.0 is nearly the same as for hollow specimen T424H. As per the discussion presented in Section 4.4.1 (First Yield Force), it is believed that the increase in tension force due to concrete will not be larger than 15%. Therefore, these two specimens give two extreme cases.

Although no test results of increase in tension force for intermediate  $A_c/A_s$  ratio between 2.0 and 4.7 are available in this study, it is assumed that the increase in tension force due to concrete varies linearly with  $A_c/A_s$  ratio between

2.0 and 4.7 as shown in Figure 5.15. When  $A_c/A_s$  is smaller than 2.0, the increase is taken equal to zero, and the increase in tension forces is 15% when  $A_c/A_s$  ratio is larger than 4.7. The following is the mathematical expression to compute the increase in tension force due to concrete:

$$\text{Increase } \beta = \begin{cases} 0. & A_c/A_s \leq 2.0 \\ \frac{0.15}{2.7} [ A_c/A_s - 2 ] & 2.0 < A_c/A_s < 4.7 \\ 0.15 & 4.7 \leq A_c/A_s \end{cases} \quad (5.2)$$

Therefore, the yield force of a member filled with concrete,  $P_{yc}$ , can be computed by expression  $(1+\beta) P_y$ , where  $P_y$  is the yield force of steel tube. The force,  $P_{yc}$ , will be used instead  $P_y$  to locate points E and F in this model as shown in Figure 5.16.

## 2. Maximum Compressive Loads

Figure 5.17 shows the measured first buckling loads for specimens T633C6 and T424C6 as well as their hollow counterparts, specimens T633H and T424H. The curves from SSRC Formulas by AISC are also shown in the same figure. The figure shows that direct use of AISC equations does not give good estimate of the first buckling load for specimens filled with concrete. On the other hand, the procedures developed in Section 4.5.1 (First Buckling Load) can predict the first buckling loads,  $P_b$ , very well.

Maximum compression load in the second and subsequent hysteresis loops can be calculated as  $35/(KL/r_t) P_y$ , where  $r_t$  is the radius of gyration of transformed section. Comparison of the second and third hysteresis loops from test results with the computed loads indicated that these are reasonable approximations.

### 3. Compression Envelope

The initial elastic branch can be approximately plotted at a slope,  $\delta$ , equal to  $A_s E/L$  where  $A_s$  is the area of cross-section of steel and  $E$  is the modulus of elasticity of steel as obtained from the tension tests. This is shown by segment OA in Figure 5.16. Compression envelope is represented by segment OABC, where point B is the compression load at  $5\Delta_y$  and point C is the compression load at  $12\Delta_y$ . Control points B and C are given by  $22/(KL/r_t) P_y$  and  $15/(KL/r_t) P_y$ , respectively. These values were obtained by empirical fit with the test results.

### 4. Tension Envelope

The tension envelope is represented by segment CDE in Figure 5.16. Based on the maximum compressive displacement as given by point C and effective slenderness ratio of the member residual strain  $\epsilon$  can be computed from Equation (5.1) which is the same as in Jain's model. The increase in tension force,  $\beta$ , can be calculated based on  $A_c/A_s$  ratio from Equation (5.2). Coordinates of point E are given by  $(P/P_y, \Delta/\Delta_y)$  where  $P/P_y$  is

equal to  $(1 + \beta)$  and  $\Delta/\Delta_y$  is equal to  $(1 + \epsilon L/\Delta_y)$ .  $P_y$  is the yield force of tube and  $L$  is the length of the member. To locate point  $D$ , the slope of line  $OD'$  is taken  $1/9$  times the initial elastic slope,  $\delta$ , instead of  $1/3 \delta$  in Jain's model. At the same time, intercept  $OD$  is taken as  $80/(KL/r_t)$ , instead  $60/(KL/r)$  in Jain's model, times the distance  $OD'$  for first two new cycles. The reason for these two modifications is to reflect the less "pinched" shape of tension envelope curves in concrete-filled bracing members. However, from the third new cycle on, intercept  $OD$  is taken as  $60/(KL/r_t)$  times the distance  $OD'$  to consider the reduction of hinge moment capacity due to local buckling in web areas and crushing of concrete which occur in later cycles.

#### 5. Subsequent Hysteresis Loops and Cycles

The definition of a new hysteresis loop is the same as in Jain's model discussed earlier in Section 5.2.2. But the maximum compression load in the second and subsequent hysteresis loops is given by  $35/(KL/r_t) P_y$ . This is based on the fact that no significant difference was found in tests between maximum compression forces from the second new cycle on.

Intermediate cycles essentially follow the same rules as discussed earlier in Section 5.2.2. But one modification is made. Line  $I'C$  is introduced which is parallel to the  $\Delta/\Delta_y$  axis and passes through the maximum compression displacement in the previous hysteresis loop, point  $C$ , as shown in Figure

5.18. If reversal occurs from the branch GD, the member unloads elastically along KK'. Further reversal occurs either along K'K or L"K. Similarly, if reversal occurs from the branch DE, the member follows the path I'I or I"I, otherwise the return is along ND.

### 5.3.2 Verification of Proposed Model

The proposed hysteresis model is compared with the hysteresis loops obtained for specimens T633C6 and T424C6. Effective slenderness ratio of these specimens are about 65 and 100, respectively, and width-thickness ratios are 30 and 14, respectively. These comparisons are presented in Figures 5.18 to 5.23. It can be seen that this model gives reasonable agreement.

It should be noted that since load history in tests in this study was controlled by deformation in terms of a nominal axial yield deformation  $\Delta_y^*$  corresponding to a nominal yield strength of 36 ksi (25 KN/cm<sup>2</sup>) rather than the measured one from coupon tests. The reason for this was discussed in section 3.6.2 in detail. On the other hand, the yield deformation  $\Delta_y$  in this empirical model is based on the real yield stress. This is approximately 54 ksi (37 KN/cm<sup>2</sup>) from coupon tests, being 1.5 times the nominal yield stress of 36 ksi (25 KN/cm<sup>2</sup>) used in controlling the tests. Therefore, before comparing with hysteresis loops from the model, the deformations in terms of  $\Delta_y^*$  from the test results need to be transformed into the deformations in terms of  $\Delta_y$ . This can be

done by multiplying the  $\Delta/\Delta_y^*$  value by 1/1.5, or 2/3 in order to get  $\Delta/\Delta_y$  values for the model.

### 5.3.3 Limitations of Proposed Model

This model is based on the test results mainly on two pairs of specimens, T633C6 and T424C6 and their hollow counterparts, whose effective slenderness ratio are not too far apart. Test results show that the effect of concrete strongly depends on width-thickness ratio, slenderness ratio as well as  $A_c/A_g$  ratio. Therefore, It is felt that there is need for more test results on specimens with wider variation of these parameters. It is believed that such data will help in obtaining more precise control points than what has been proposed in this study.

### 5.4 Summary

Hysteresis loops for hollow specimens were compared with those obtained from Jain's model. It was observed that Jain's model does not consider the decreases in cyclic forces due to severe local buckling. But this is not a problem in concrete-filled bracing members since severe local buckling is prevented due to the presence of concrete. However, it is still necessary to make some modification in Jain's model to include the effect of concrete.

Based on limited test results of concrete-filled bracing members and review of Jain's model, an empirical hysteresis model is proposed in this study. It is suggested that more

tests on specimens with wider range of parameters are needed in order to better define the control points for this model.

CHAPTER VI  
SUMMARY AND CONCLUSION

6.1 Introduction

This study was concerned with finding a suitable solution to premature fracture problem of cold-formed rectangular tubular bracing members. Previous studies have shown that rectangular tubular bracing members are likely to crack early at corners of tube caused by severe local buckling and stress concentrations at plastic hinge locations. Width-thickness ratio as well as slenderness ratio of members are cited as two key factors. On the other hand, test results of concrete-filled tubular beams and stub columns show that the presence of concrete not only increases the strength of members, but also changes the local buckling mode and reduces its severity. This gives a clue that filling concrete in tubular bracing members might have similar improvement since bracing members combine the characteristics of both beams and columns under bending and axial deformations.

A series of hollow and concrete-filled tubular beams, stub columns, and full-scale bracing specimens were tested in this study to understand how concrete and steel work together in these composite bracing members.

Significant differences and improvement in behavior were

observed in concrete-filled bracing specimens compared to hollow counterparts. The most significant finding is that concrete filling can change the local buckling mode, thereby, reducing its severity, delay cracking, and elongate the fracture life particularly for specimens with large width-thickness ratio. At the same time, different types and strength of concrete did not have significant influence on the behavior of such composite bracing members.

This chapter will first summarize the various phases of this study. Conclusions from tests and analyses as well as suggested further studies are given thereafter.

## 6.2 Summary

This investigation began with studying the behavior of hollow tubular bracing members and concrete-filled steel tubular beams and stub columns. The concept of concrete filling is introduced from beams and columns into bracing members. The major difference between these two types of composite members lies in that concrete in tubular bracing members prevents severe inward local buckling of tube walls rather than receiving confinement from steel tube as in columns. It is believed that filling concrete in tubular bracing members should have similar improvement as for beams and columns. The overall concept, the purpose and objective of this study were presented in Chapter I.

This study is divided into two phases. The first is preliminary tests, in which hollow and concrete-filled beams and stub columns were tested to obtain some basic information

as to how concrete changes local buckling mode in these members. The second is the main tests, in which full-scale hollow and concrete-filled tubular bracing specimens were tested. The test results were used to formulate an empirical model to simulate the hysteresis behavior of these composite bracing members.

The preliminary tests consisted of 12 hollow and concrete-filled beams and stub columns. The main parameter for beam tests is the strength of concrete with and without steel fibers. The main parameters for stub column tests are different types and strength of concrete and different width-thickness ratio under monotonic loading. Special attention is paid here to local buckling behavior of these specimens at various stages of loading. Test results showed that in both beams and stub columns the presence of concrete changed the local buckling mode and reduced its severity. Strength of concrete and steel fibers did not show significant effect to improve the ductility in both types of specimens.

Chapter II presented the detailed program of preliminary tests on beam and stub column specimens. This included the test procedures and discussion of results.

There are nine full-scale hollow and concrete-filled tubular bracing specimens in the main tests. The main parameters are different types of concrete and width-thickness ratio as well as slenderness ratio of specimens. For the purpose of comparison, all specimens were tested under the same loading history. Significant differences between hollow and concrete-filled tubular bracing specimens with

09307

width-thickness of 30 were found. The main role of concrete is to change local buckling mode, prevent premature fractures, and increase the number of cycles to failure.

For inelastic dynamic analysis of structures with such compose bracing members, it is required to have a quantitative model to describe their hysteresis behavior. After reviewing several available empirical models it was found that Jain's model could be adapted for concrete-filled tubular bracing members with some changes. The proposed model is verified by the results of tests in this study.

The main test program was presented in Chapters III, IV, and V. In Chapter III, test procedures was described in detail, which included preparation of specimens, introduction of loading system and data acquisition system, and explanation of loading history. Chapter IV presented the test results and discussion. Review of Jain's model and the proposed model were presented in Chapter V.

### 6.3 Conclusions

The major findings and conclusions from this study can be summarized as follows:

- 1). Hollow rectangular tubular bracing members are structurally efficient. However, some measures are needed to prevent these members particularly with large width-thickness ratios from premature fractures.

- 2). Width-thickness ratio is a key factor to determine the fracture life of a hollow tubular bracing member. Specimens in which the width-thickness ratios met the

requirement of even Part 2 of the AISC Specification (Plastic Design) suffered severe local buckling resulting in deterioration of hysteresis loops and early fractures. Filling the tubes with concrete is an efficient way to improve behavior of these members.

3). The effect of concrete in a concrete-filled tubular bracing member varies according to the width-thickness ratio as well as slenderness ratio. The larger the width-thickness and the less slender a member, the more prominent is the influence of concrete. *lower  $KL$ ?*

4). Higher strength of concrete does not seem to show significant effect on the behavior of such composite bracing members, nor does the addition of steel fibers.

5). Concrete filling increases the compression strength and slightly the tension strength depending on  $A_s/A_c$  and slenderness ratio of the member. A modified tangent modulus theory can be used to estimate the first buckling load. A simple approximate method is also suggested. The increase in tensile force due to the presence of concrete compared to the hollow section ranges from zero to about 15 percent depending on the ratio of area of concrete to steel.

6). The presence of concrete can change the local buckling mode. In the concrete-filled bracing members tested the local buckling forms in the following order: flange buckles outwards first, then webs buckle inwards. This is different from the hollow specimens in which the flange buckles inwards and the webs buckle outwards. The change in

the mode of local buckling increases strength and improves ductility in the plastic hinge zones.

7). Apart from the change in local buckling mode, the presence of concrete also reduces its severity. In a hollow tubular bracing member, local buckling concentrates itself within a very narrow strip. However, in a concrete-filled tubular bracing member, the local buckling is spread over larger area to form a flat dome. This decreases the stress concentration, especially at the corners, thus increasing the fatigue life.

8). Since concrete filling changes the mode of local buckling and reduces its severity, the behavior of bracing members is improved in the following two aspects. The first is that the hysteresis loops are more "full" than those of the hollow ones, and the second is that the member can take more cycles before failure. This means that a concrete-filled tubular bracing member absorbs more energy than the hollow counterpart.

9). Jain's empirical hysteresis model can be used for a concrete-filled tubular bracing member after some modifications to account for the presence of concrete. The proposed modifications were presented in Chapter V. The main changes were that several key points were adjusted to reflect less "pinched" shape of hysteresis loops in concrete-filled bracing members.

#### 6.4 Suggestion for Further Studies

Since concrete-filled tubular bracing specimens tested in

this study do not cover a wide enough range of parameters related to such composite members, more studies and tests are needed in the future to gain better understanding of the behavior of these members. In the following paragraphs, some suggestions are given which are based on the knowledge gained from this study.

Test results from this study and some previous studies have shown that severe premature local buckling adversely affects the fracture life of a bracing member under cyclic loading, and width-thickness ratio is the key factor to influence the occurrence and severity of local buckling. Therefore, further research should be carried out to find possible ways to decrease the effective width-thickness ratio and to provide stiffening of the tube walls to reduce the severity of local buckling.

Since this study mainly focussed on the effects of different types and strength of concrete, tests are needed to find influence of other parameters such as width-thickness ratio and slenderness ratio over broader range.

Test results from this study showed that the strength of concrete does not exhibit significant effect on the behavior of these composite bracing members. This suggests that low strength or light weight concrete may be enough for preventing severe local buckling while cost and weight of members are reduced.

TABLES

Table 2-1 Geometrical Properties of Beam Specimens

Group	1		2			
Specimen	BH	BHA	BC6	BC6F	BC8F	BC6A
Section	2.5 x 2.5 x 0.105"					
Length (inch)	34					
Span (inch)	30					
Annealed	No	Yes	No	No	No	Yes
Concrete (ksi)			6	6	8	6
Steel Fiber			No	Yes	Yes	No

Table 2-2 Ultimate Moments of Beam Specimens

Group	1		2			
Specimen	BH	BHA	BC6	BC6F	BC8F	BC6A
Moment ("k) (measured)	42.3	30.0	52.5	52.5	55.0	40.0
$F_y$ (ksi)	46	35	46	46	46	35
$f_c'$ (ksi)			6	6	8	6
$x^\dagger$	1.15	1.15	0.67	0.67	0.59	0.59
Moment ("k) (Computed)	41.6	31.6	46.9	46.9	47.8	36.3

†  $x$  is the compression depth of concrete.

Table 2-3 Energy Absorbed by Beam Specimens

Specimen Deformation		BH	BHA	BC6	BNC6F	BC8F	BC6A
		1"	Area	23.16	20.16	30.84	31.97
	Number of Cycle	2	2	2	2	2	2
2"	Area	20.06	21.56	47.91	49.88	49.22	41.63
	Number of Cycle	2	2	2	2	2	2
3"	Area	19.69	23.44	63.19	59.51	63.47	57.00
	Number of Cycle	2.75	3.5	3.5	2	6.5	5
Total Energy ("K)		105.85	165.48	378.67	282.72	574.76	418.52

Table 2-4 Geometrical Properties of Stub Columns

		1				2			
Specimens		C633HS	C424H	C633H	C422H	CC4	CC4F	CC6F	CC8F
Section		6x3x3/16 " + Angle	4x2x4/16 "	6x3x3/16 "	4x2x2/16 "	3x6x3/16"			
Area	Steel	3.50	2.59	3.14	1.32	3.14			
	Concrete					16.74			
Width-Thickness Ratio (b/t)		14	14	30	30	30			
Strength of Concrete (ksi)						4	4	6	8
Steel Fibers						No	Yes	Yes	Yes

Table 3-1 Geometrical Properties of Bracing Specimens

Group		1					2			
Specimen		T633H	T633C	T633C4	T633C4E	T633C6E	T633C8E	T424H	T424C6	T422H
Section		6x3x3/16"					4x2x4/16"		4x2x1/8"	
Area (in <sup>2</sup> )	Steel	3.14					2.59		1.40	
	Concrete		14.8					5.2		
Yield Strength (ksi)		54		60			54			
Slenderness Ratio	KL/r	58					92		88	
	KL/r <sub>t</sub>		65					100		
Width-Thickness Ratio (b/t)		30					14		30	
Strength of Concrete (ksi)			6	4	4	6	8		6	
Steel Fibers			No		Yes				No	

Table 3-2 Results of Coupon Tests of Steel Tubes

Tube	Specimen	Location	Yield Strength (ksi)	Ultimate Strength (ksi)	Fracture Elongation (%)
Ordered First Time	T633H T633C6 T424H T424C6 T422H	Flat	54	62	27
		Measured Corner	64	74	19
Ordered Second Time	T633C4 T633C4F T633C6F T633C8F	Flat	60	69	23
		Measured Corner	71	82	16
Nominal (ASTM - A500B)			Min 46	Min 58	Min 23

Table 3-3 Mix Proportion and Strength of Concrete

Material	Design Strength (ksi)		
	4	6	8
Cement	1	1	1
Water	0.6	0.45	0.35
Sand	3.0	1.7	1.0
Aggregate	3.0	2	1.56
Superplasticizer	0.005	0.005	0.007
Steel Fibers (if applicable)	0.3	0.26	0.22
Measured Strength (ksi)	4.56	6.78	7.78

Table 4-1 Energy Absorbed by Specimens  
T633H and T633C6

Cycle	Energy Absorbed ("K)		Difference ("K)
	T633C6	T633H	
1	230	145	85
2	110	75	35
4	70	50	20
7	180	75	105
Total for All Cycles	1950	700	1250

FIGURES

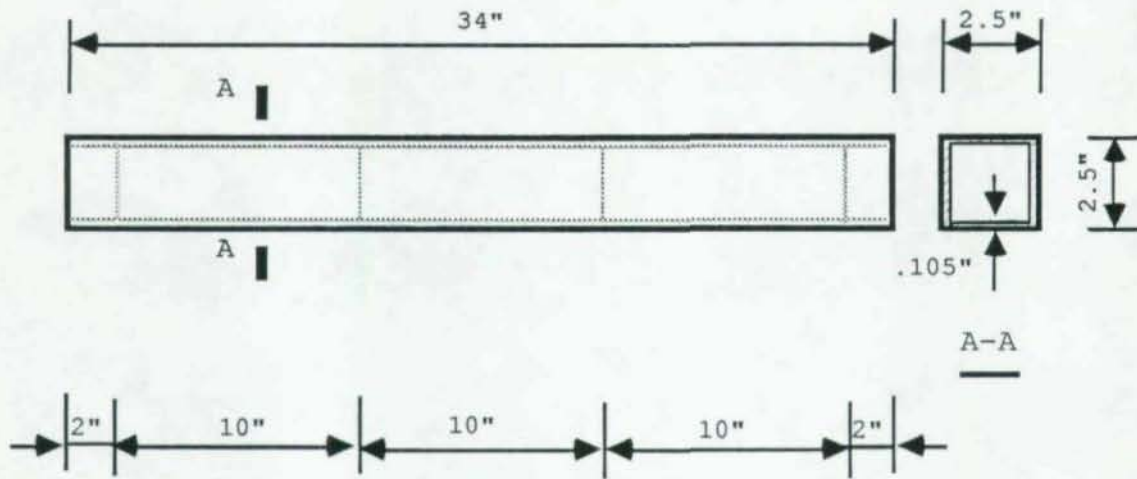


Figure 2.1 Typical Specimen for Beams

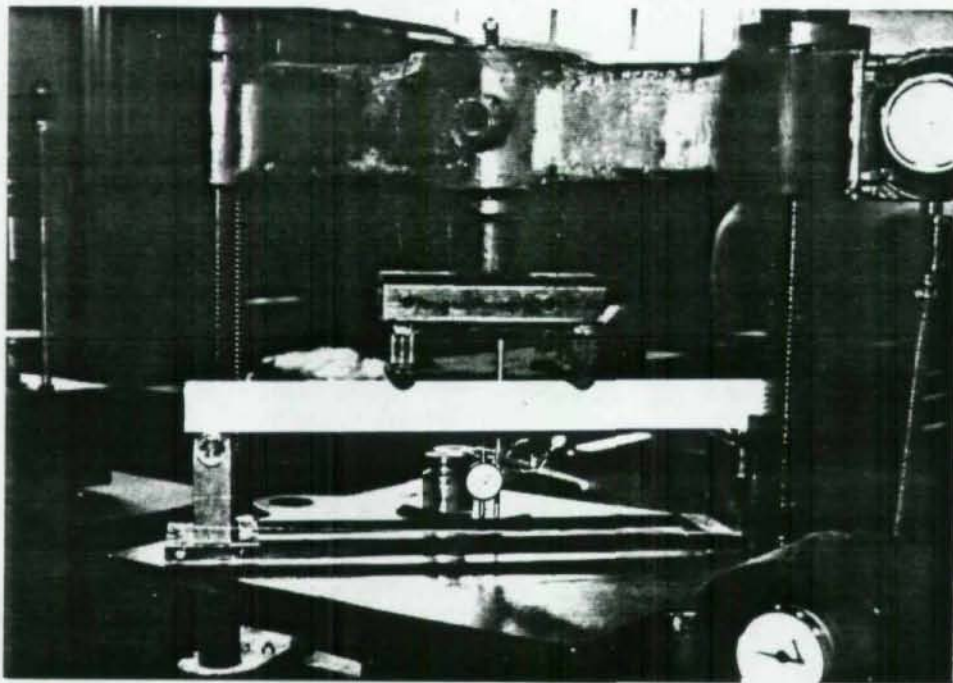


Figure 2.2 Test Set-Up for Beam Testing

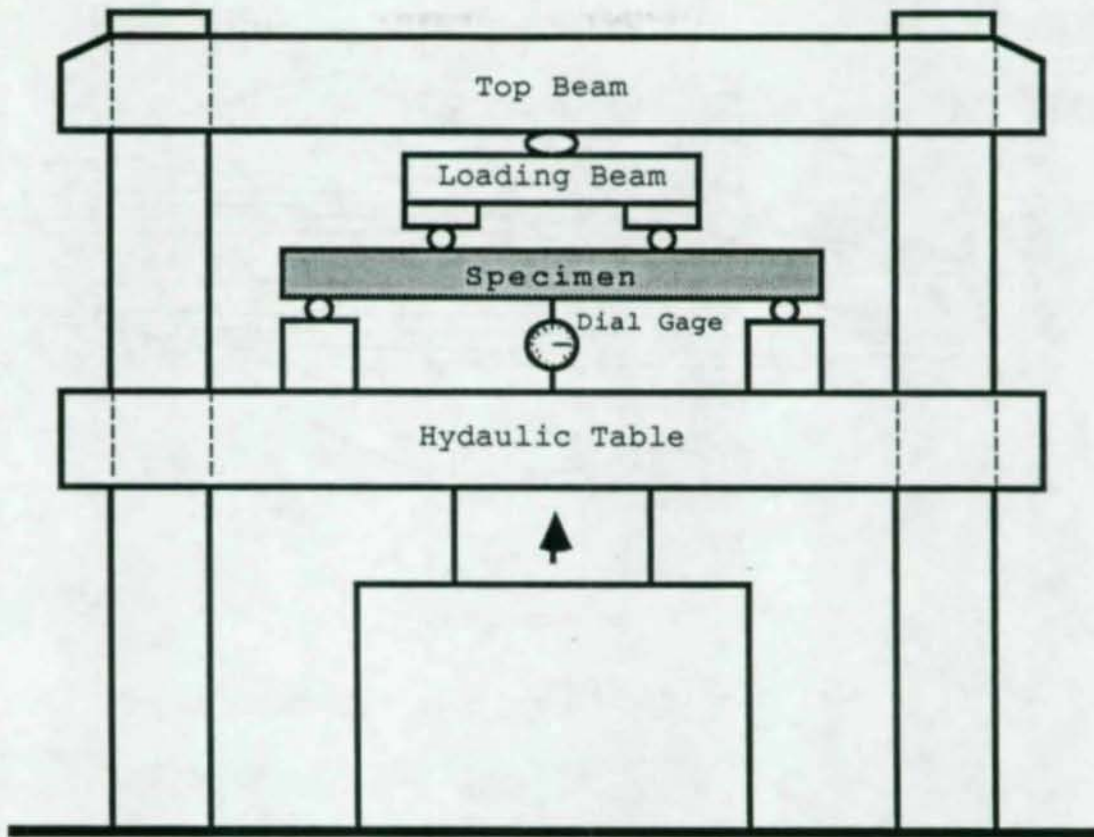
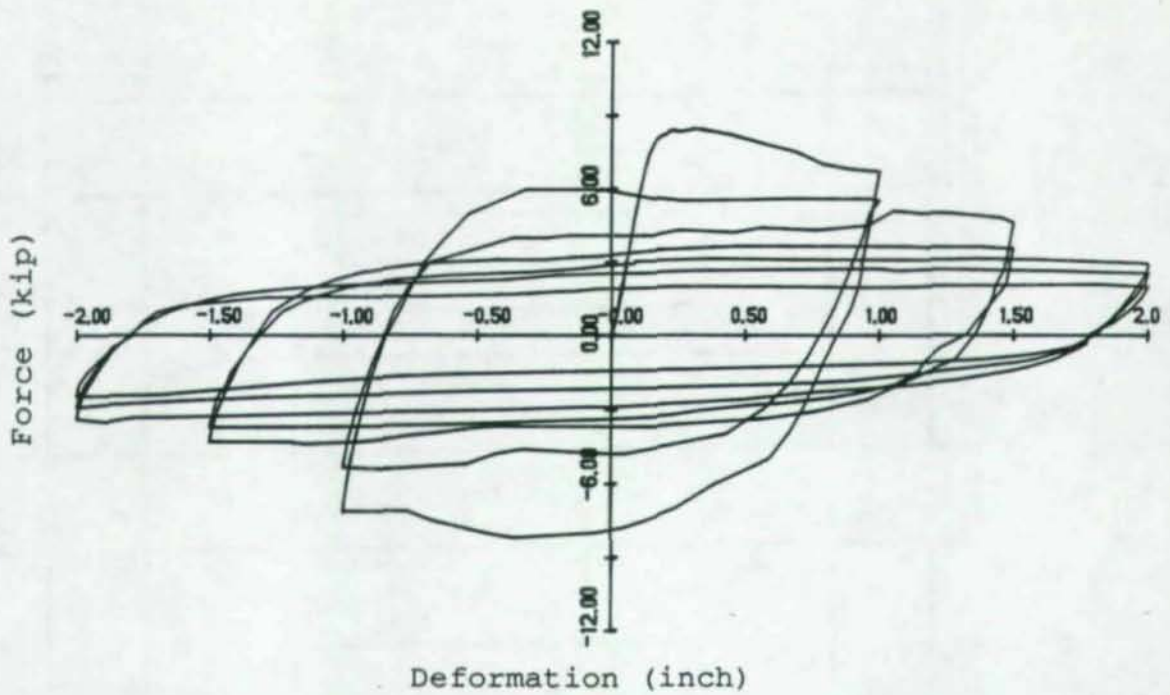


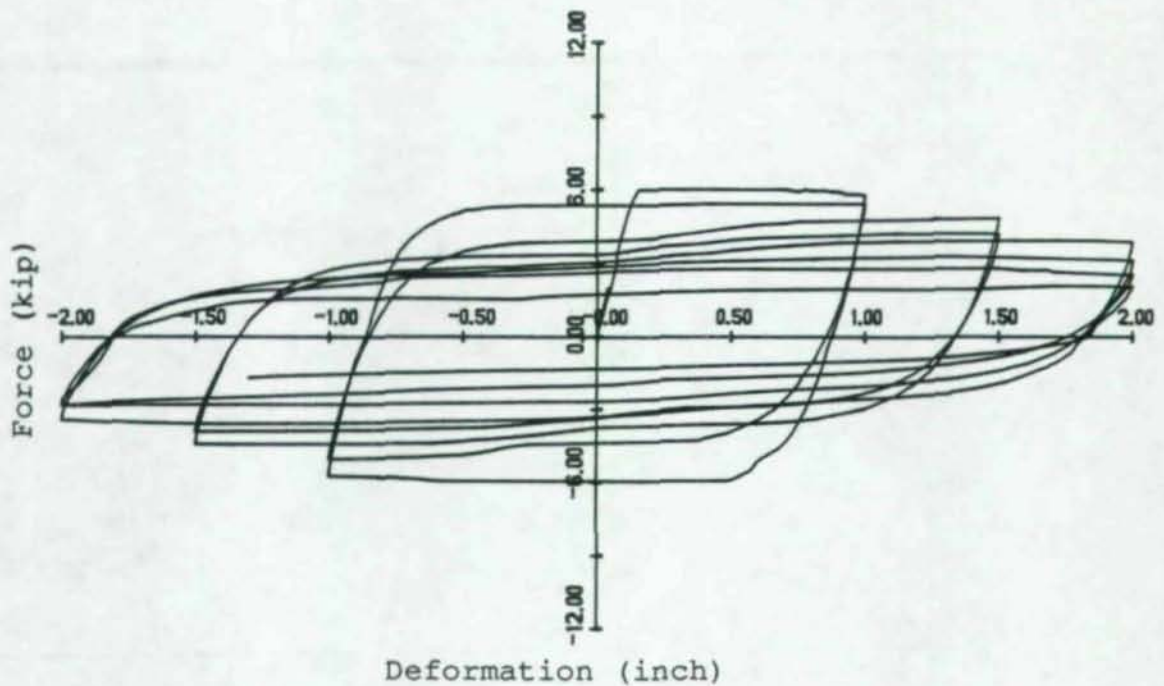
Figure 2.3 Schematic Drawing of the Test Set-Up for Beam Testing



Figure 2.4 Loading History for Beam Testing

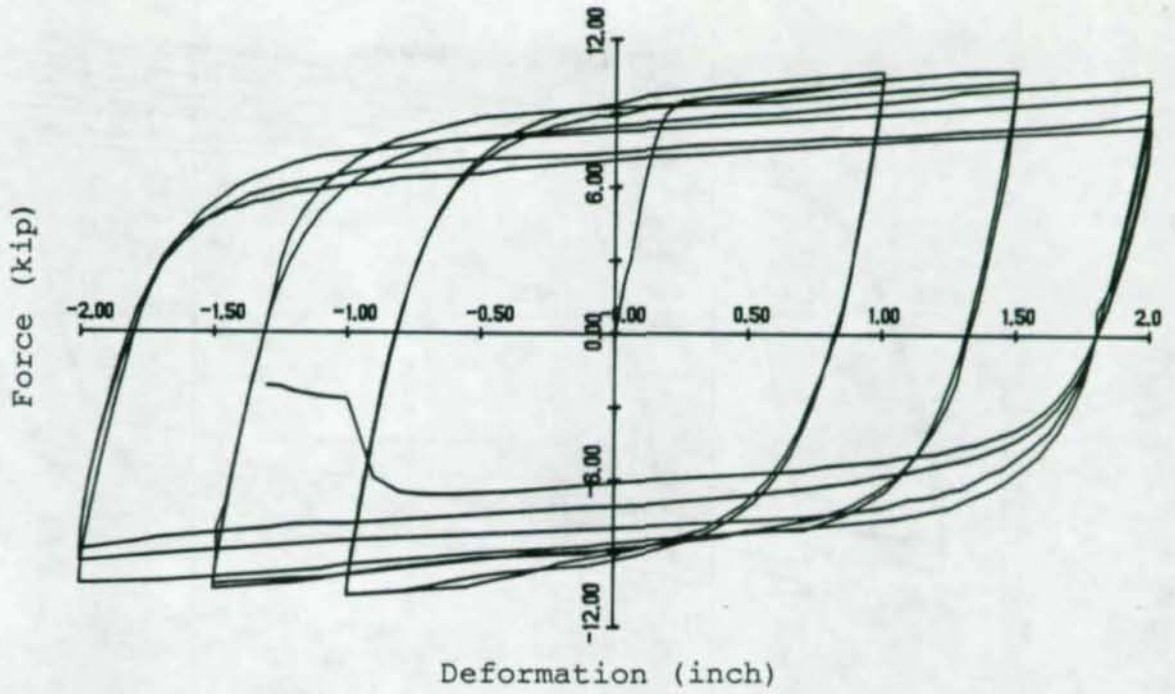


(a) Specimen BH -- Hollow Tubular Beam

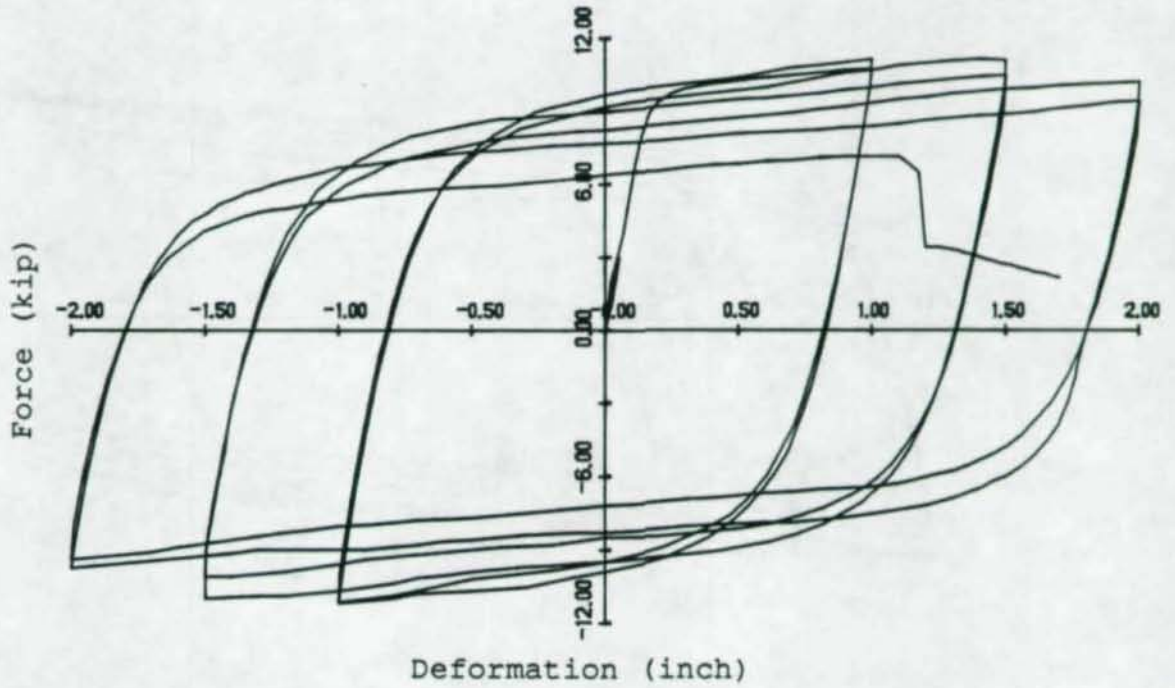


(b) Specimen BHA -- Annealed Hollow Tubular Beam

Figure 2.5 Hysteresis Loops of Group 1 Beam Specimens

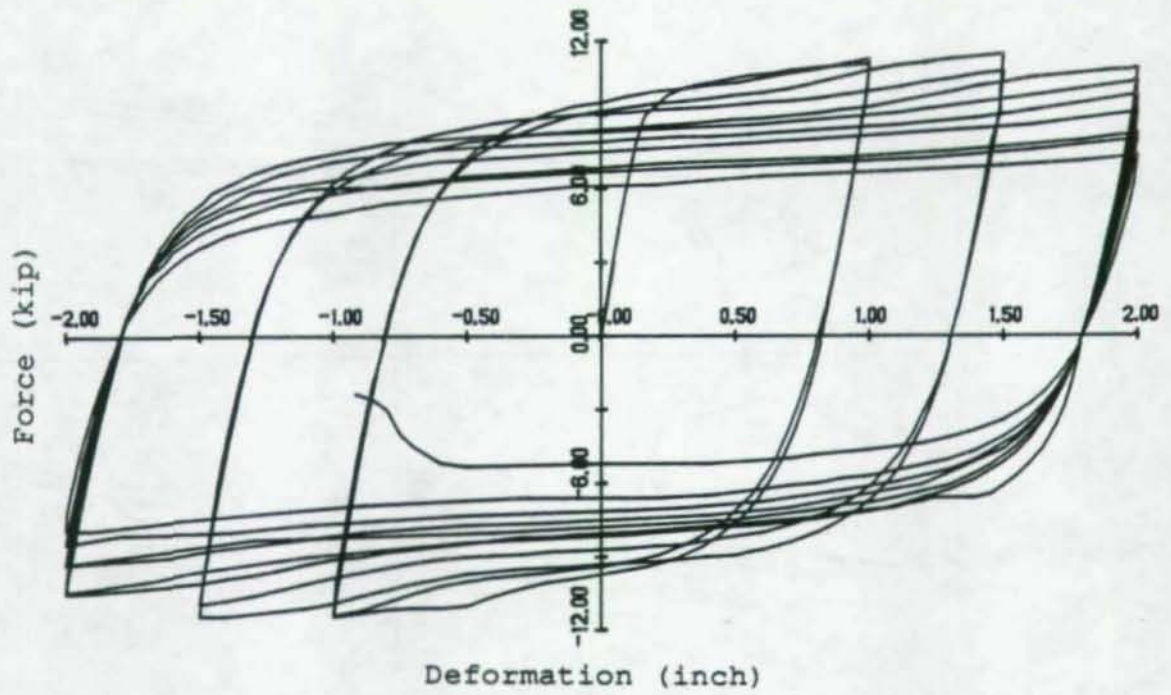


(a) Specimen BC6 -- Beam Filled with 6 ksi Concrete

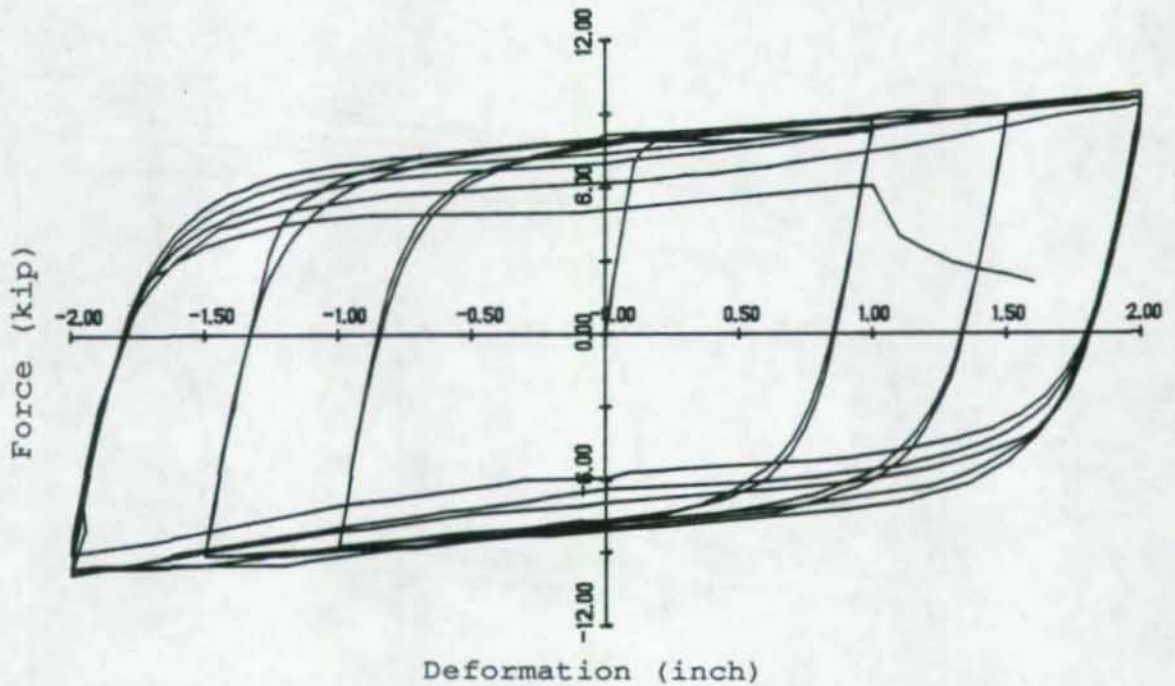


(b) Specimen BC6F -- Beam Filled with 6 ksi Concrete with Steel Fibers

Figure 2.6 Hysteresis Loops of Group 2 Beam Specimens (1)



(a) Specimen BC8F -- Beam Filled with 8 ksi Concrete with Steel Fibers



(b) Specimen BC6A -- Annealed Beam Filled with 6 ksi Concrete

Figure 2.7 Hysteresis Loops of Group 2 Beam Specimens (2)

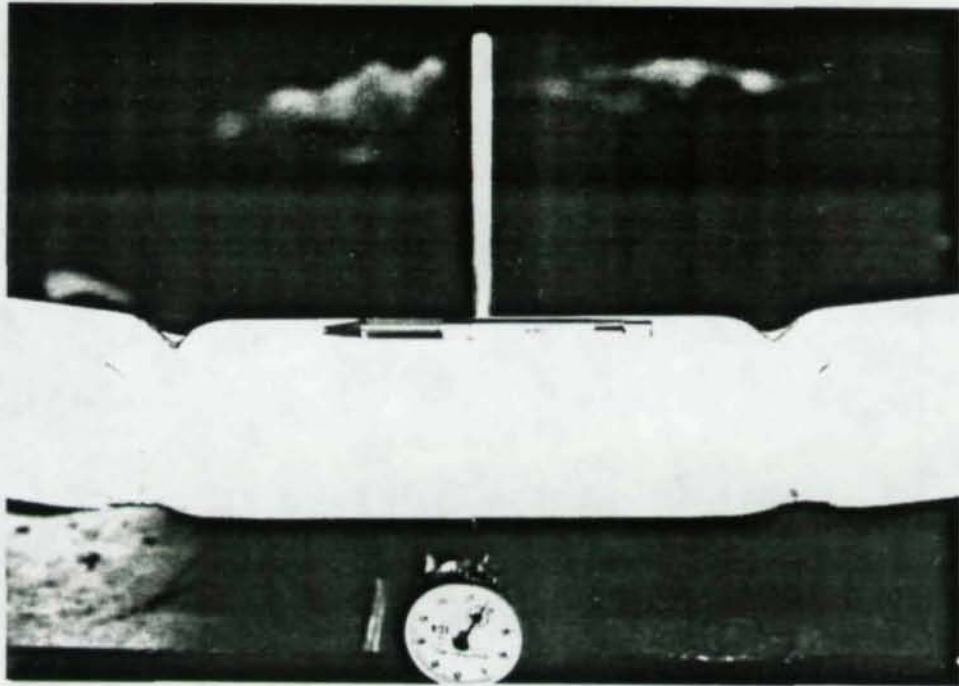


Figure 2.8 Local Buckling Mode of Hollow Beams

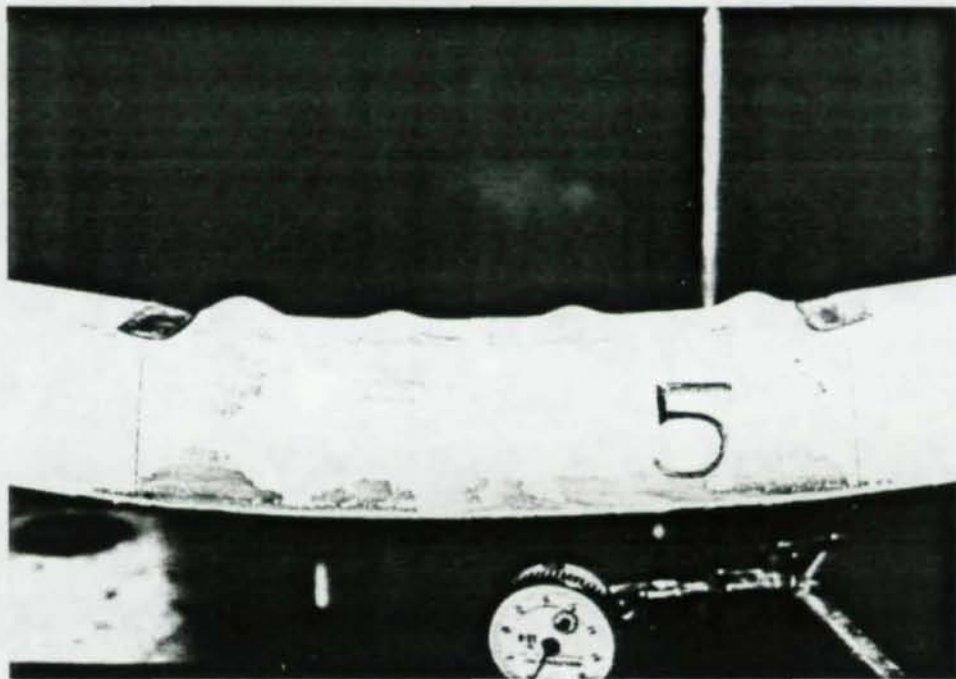
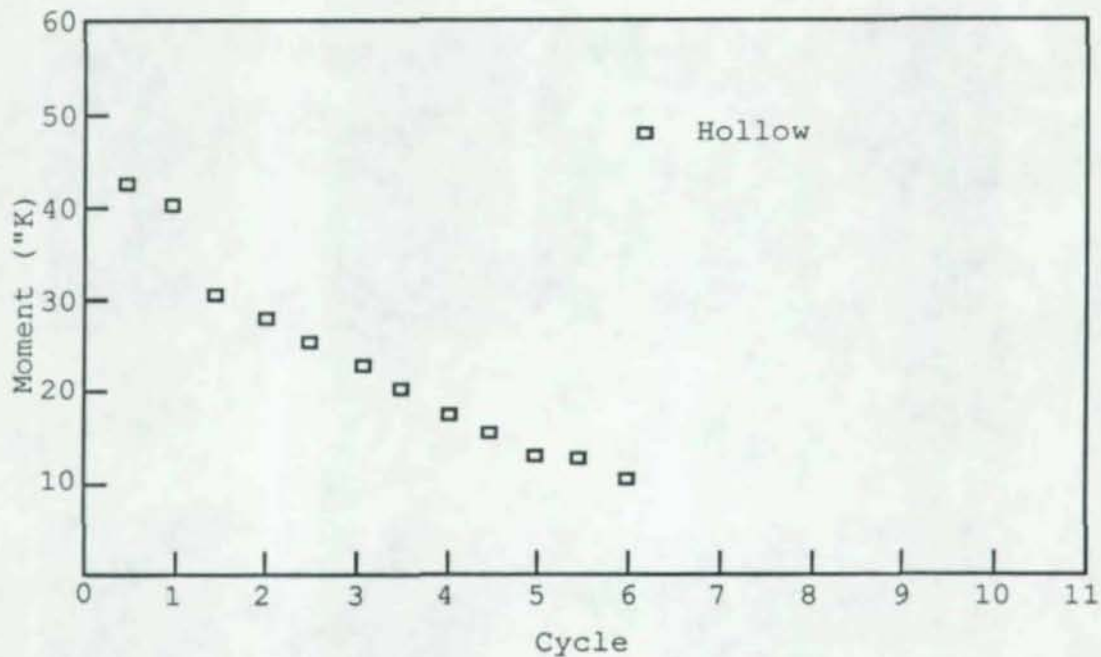
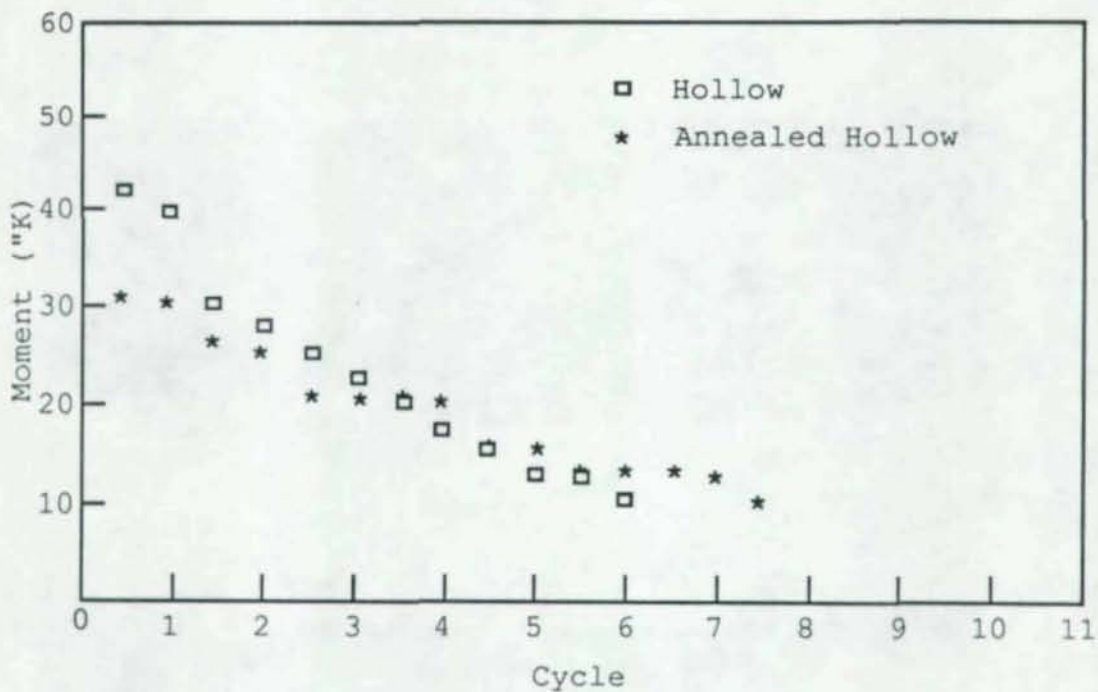


Figure 2.9 Local buckling Mode of Beams Filled with Concrete

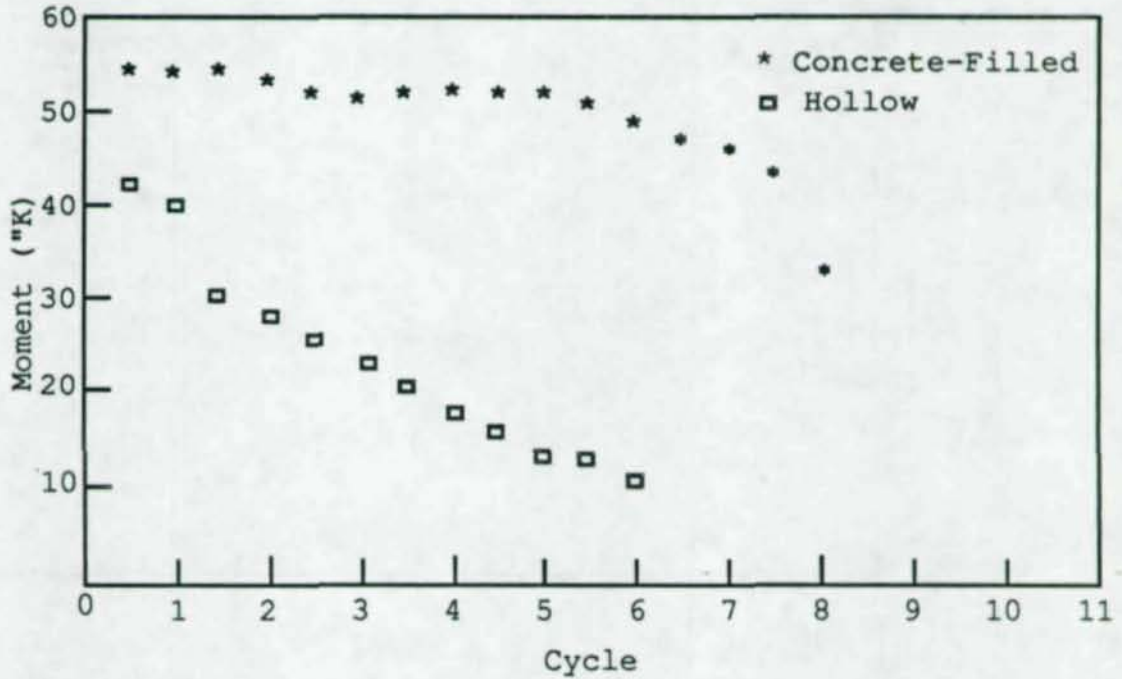


(a) Specimen BH -- Hollow Tubular Beam

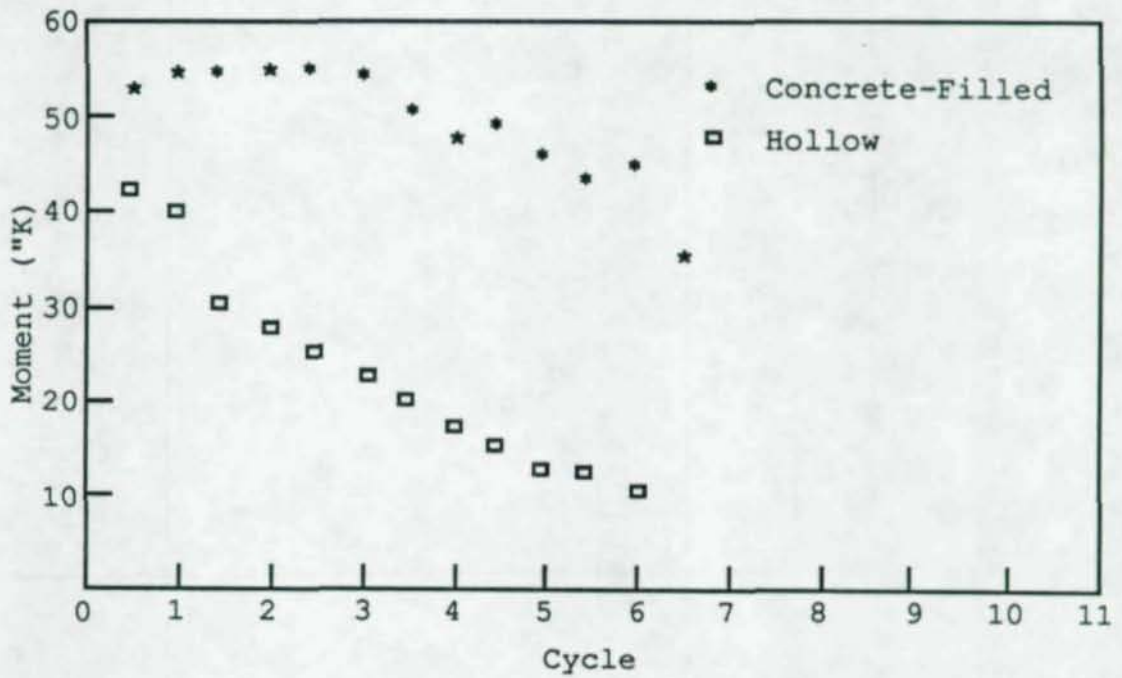


(b) Specimen BHA -- Annealed Hollow Tubular Beam

Figure 2.10 Maximum Cyclic Moments of Group 1 Beam Specimens

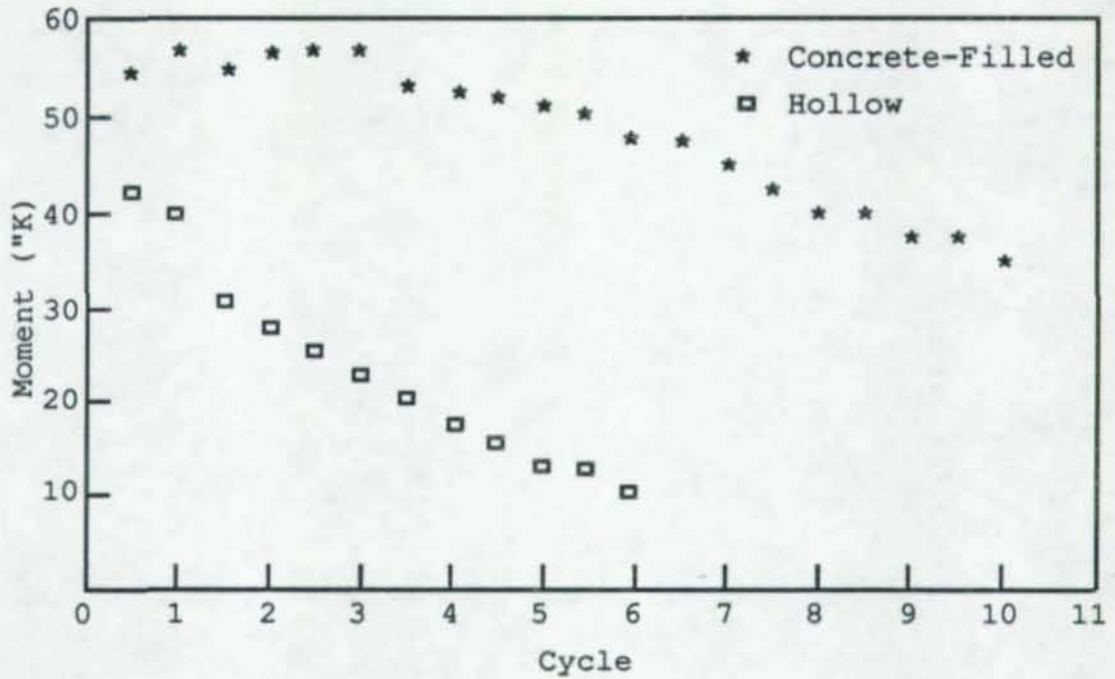


(a) Specimen BC6 -- Beam Filled with 6 ksi Concrete

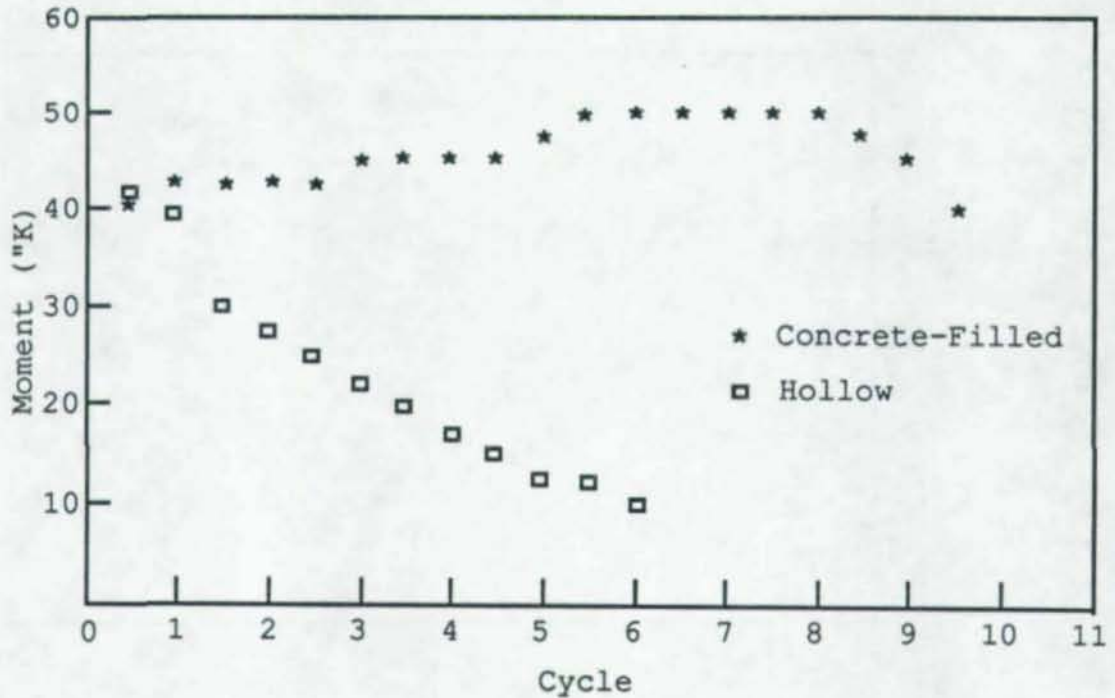


(b) Specimen BC6F -- Beam Filled with 6 ksi Concrete with Steel Fibers

Figure 2.11 Maximum Cyclic Moments of Group 2 Beam Specimens (1)



(a) Specimen BC8F -- Beam Filled with 8 ksi Concrete with Steel Fibers



(b) Specimen BC6A -- Annealed Beam Filled with 6 ksi Concrete

Figure 2.12 Maximum Cyclic Moments of Group 2 Beam Specimens (2)

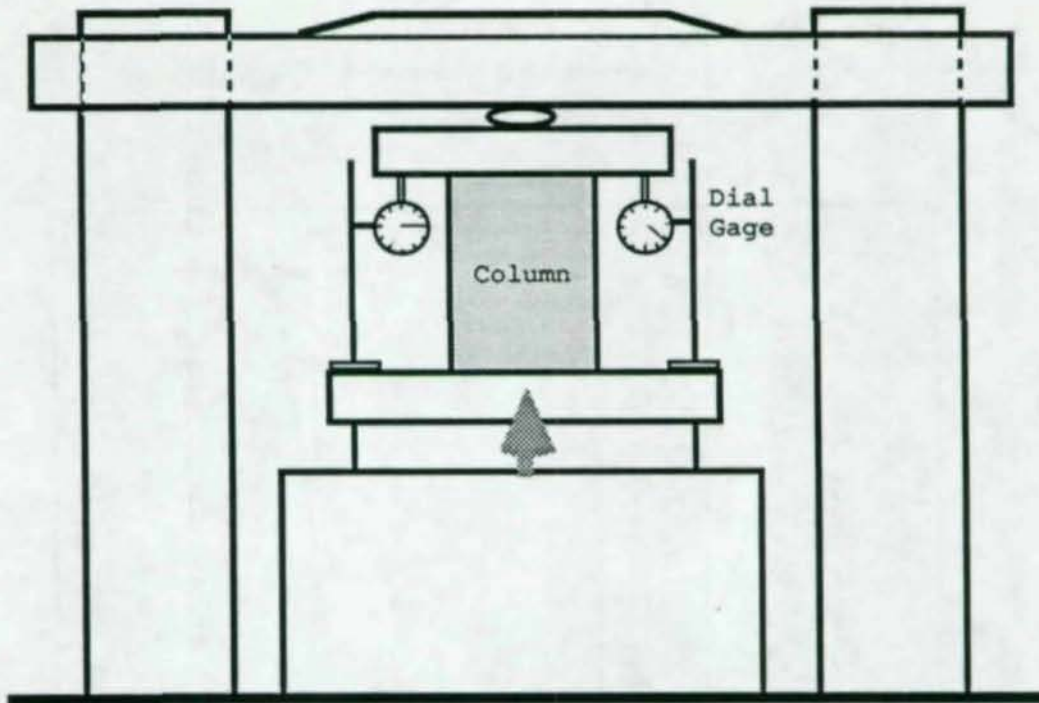
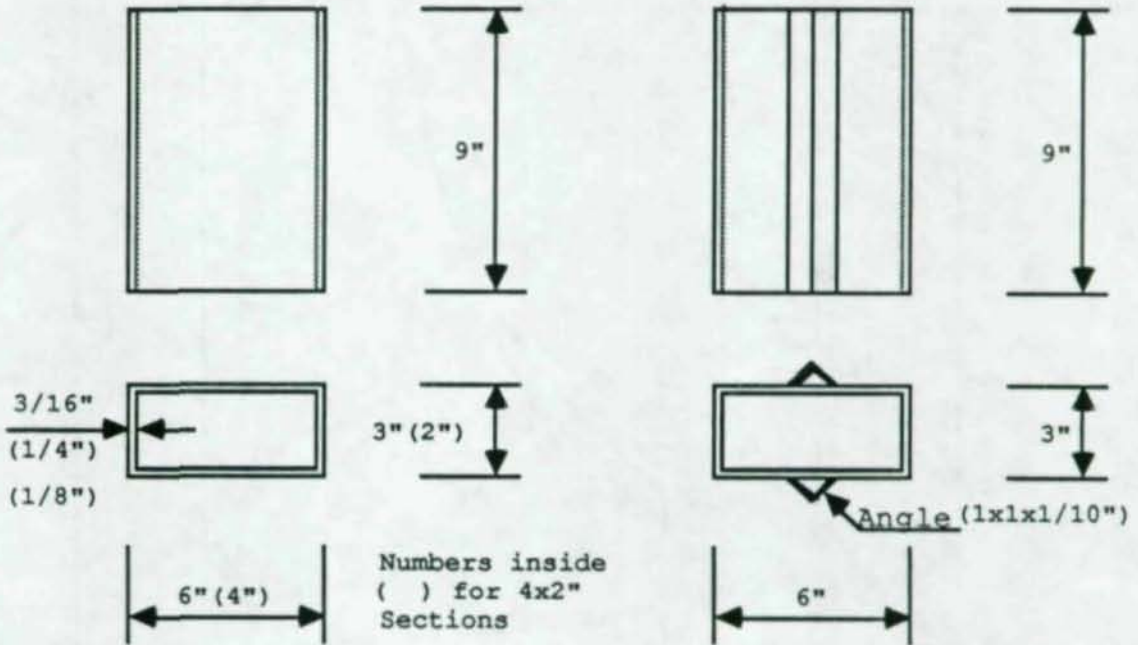


Figure 2.13 Test Set-Up for Column Test



(a) Typical Specimen

(b) Specimen C633HS

Figure 2.14 Typical Stub Column Specimen and Specimen C633HS

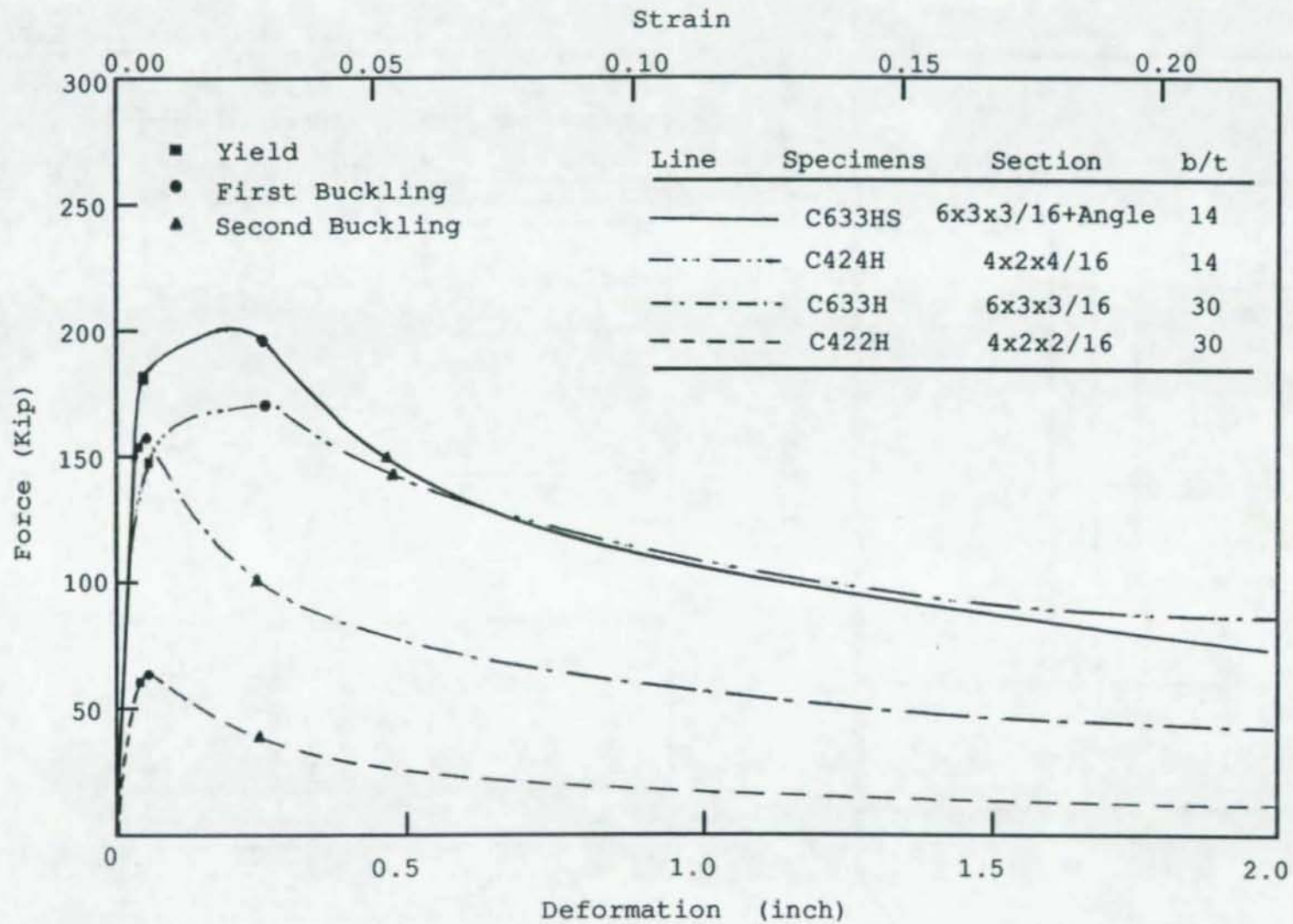


Figure 2.15 Force-Deformation Curves for Group 1 Stub Column Specimens

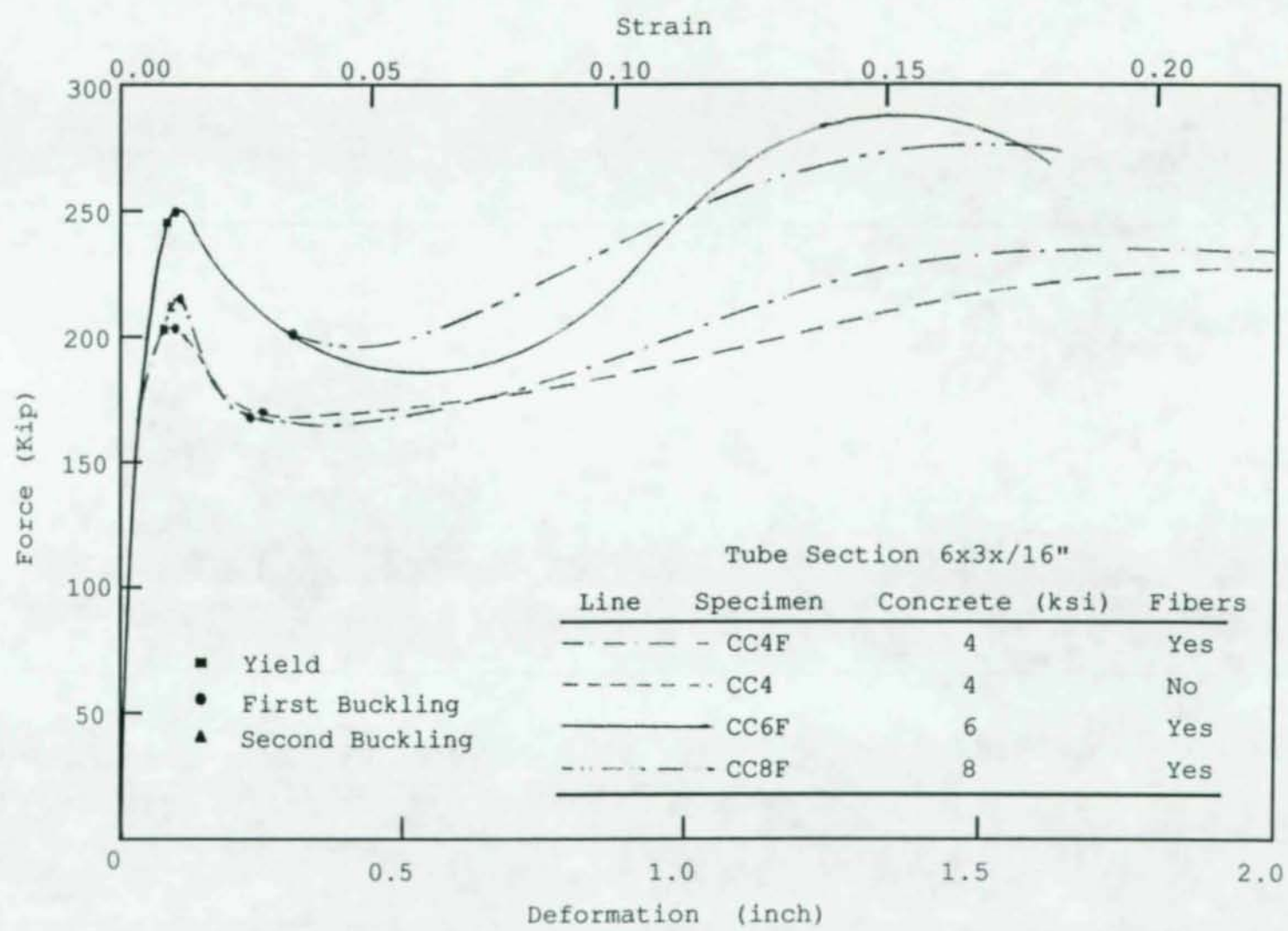


Figure 2.16 Force-Deformation Curves for Group 2 Stub Column Specimens

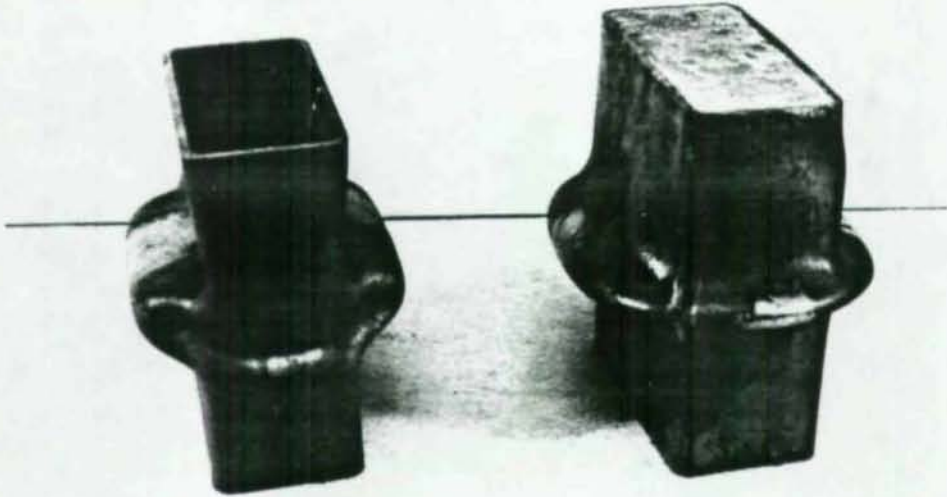


Figure 2.17 Different Local Buckling Modes Between Hollow and Concrete-Filled Stub Columns

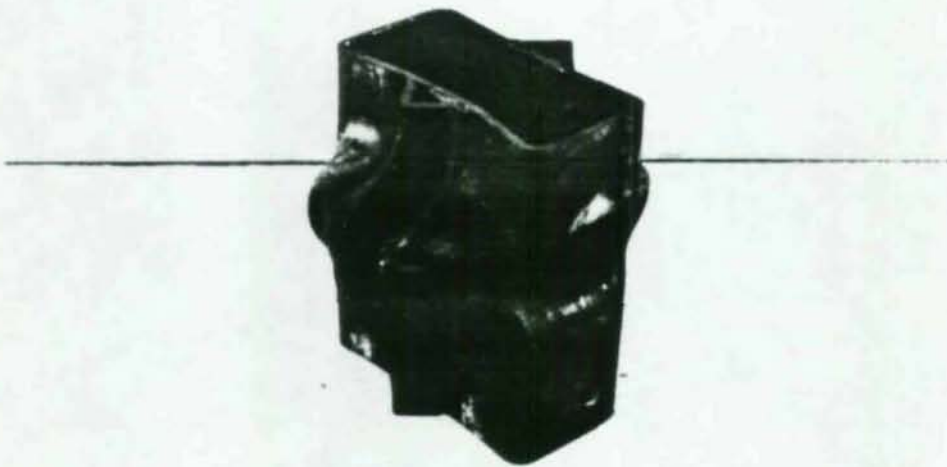
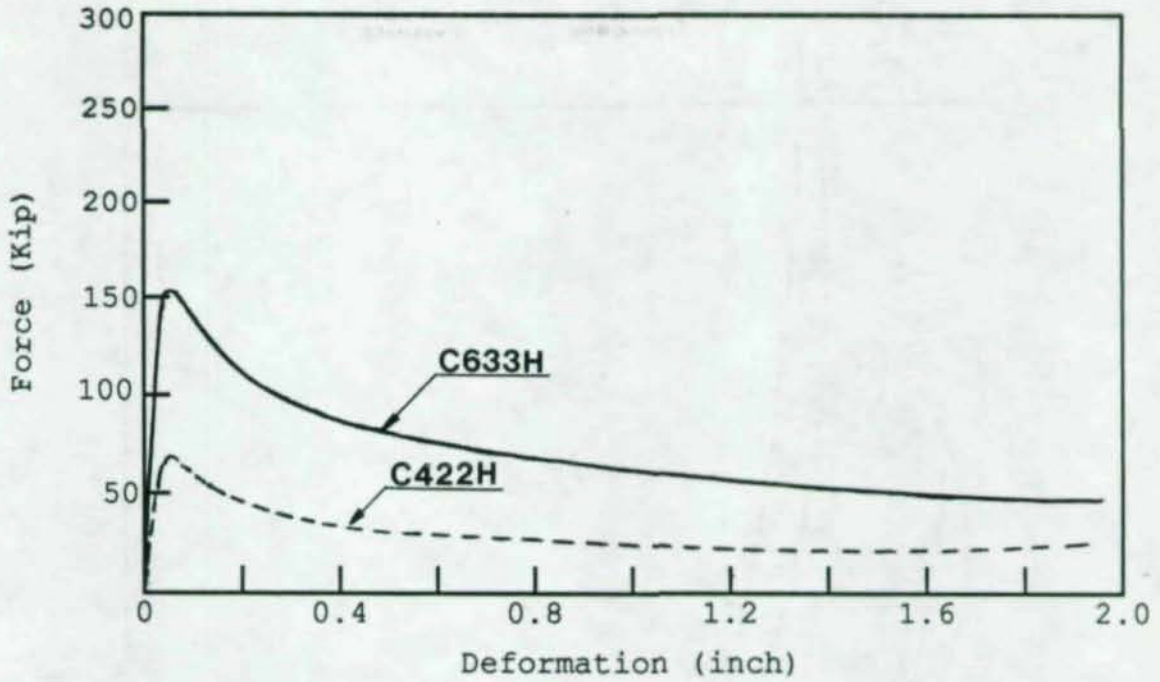
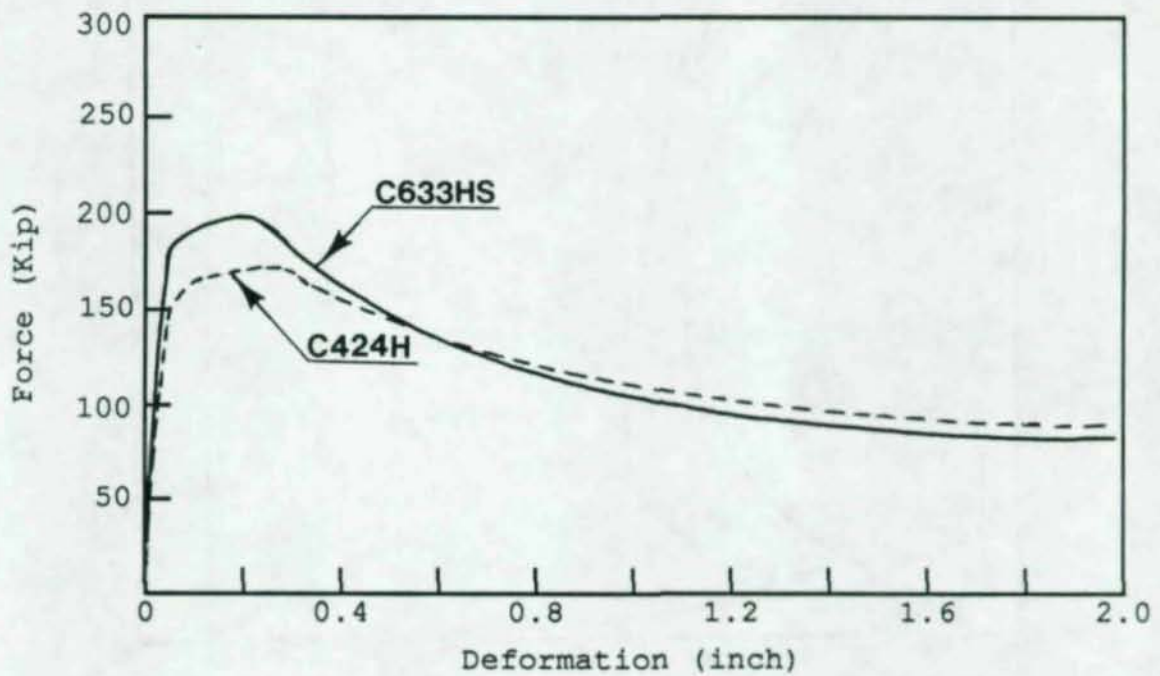


Figure 2.18 Local Buckling Mode For Column Specimen C633HS



(a) Specimens with Width-Thickness Ratio of 30



(b) Specimens with Width-Thickness Ratio of 14

Figure 2.19 The Difference in Stability of the Peak Force between Column Specimens with Different Width-Thickness Ratios

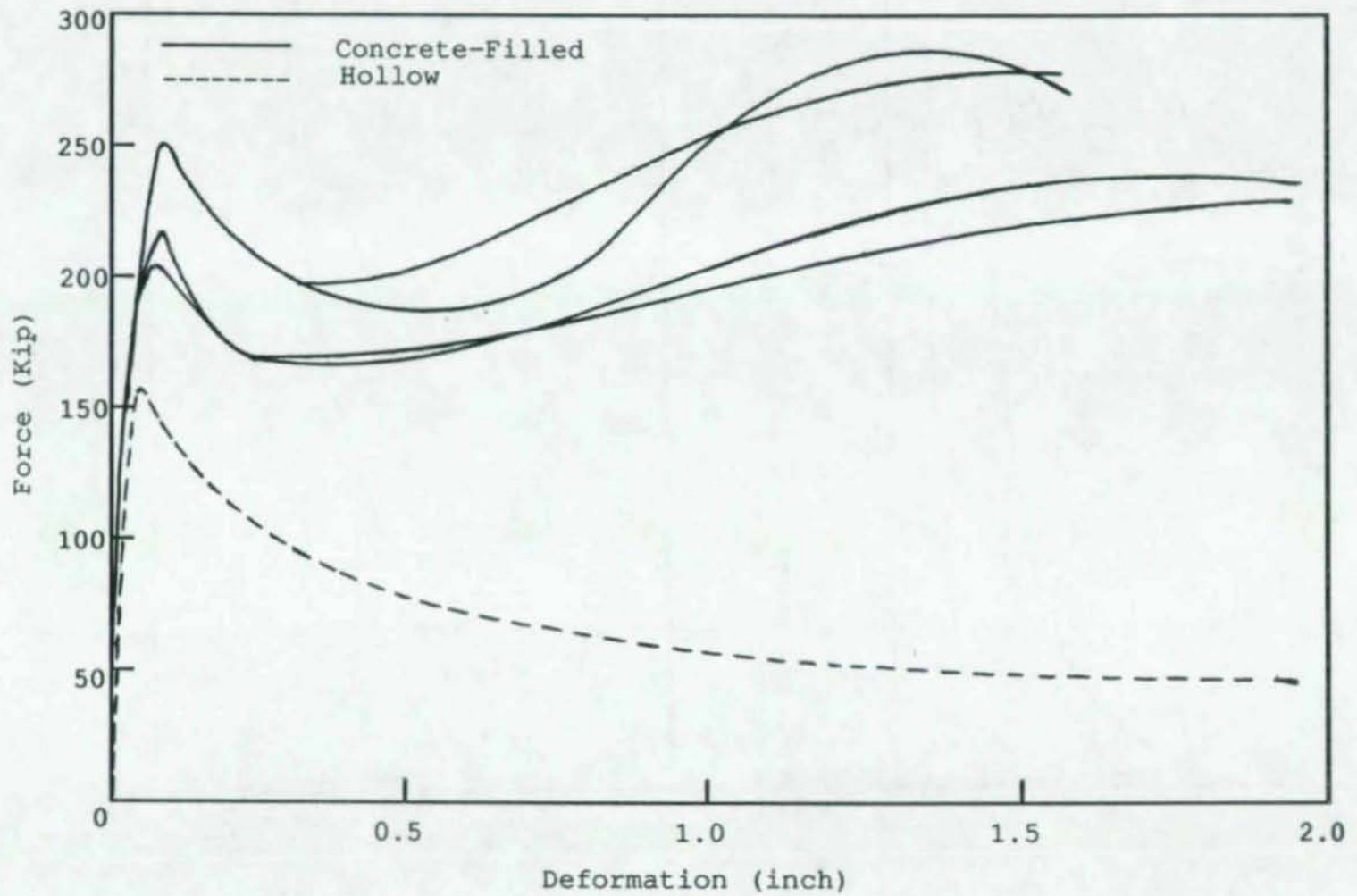


Figure 2.20 Difference in Stability of Peak Force between Hollow and Concrete-Filled Stub Columns

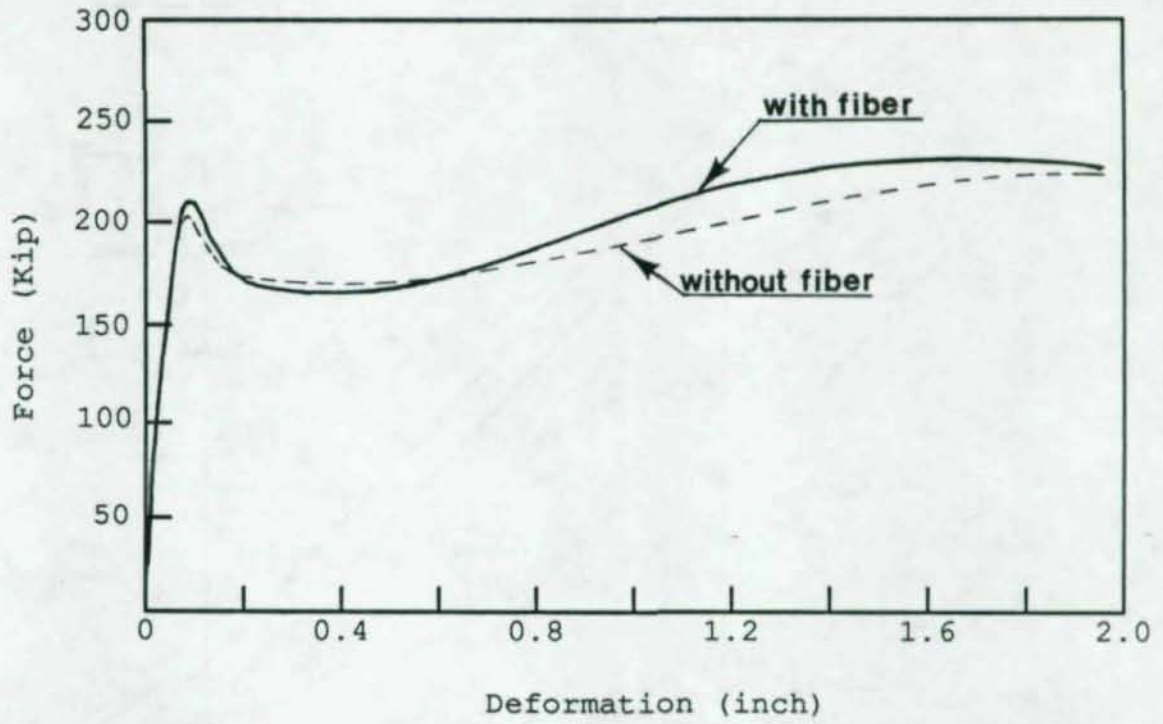
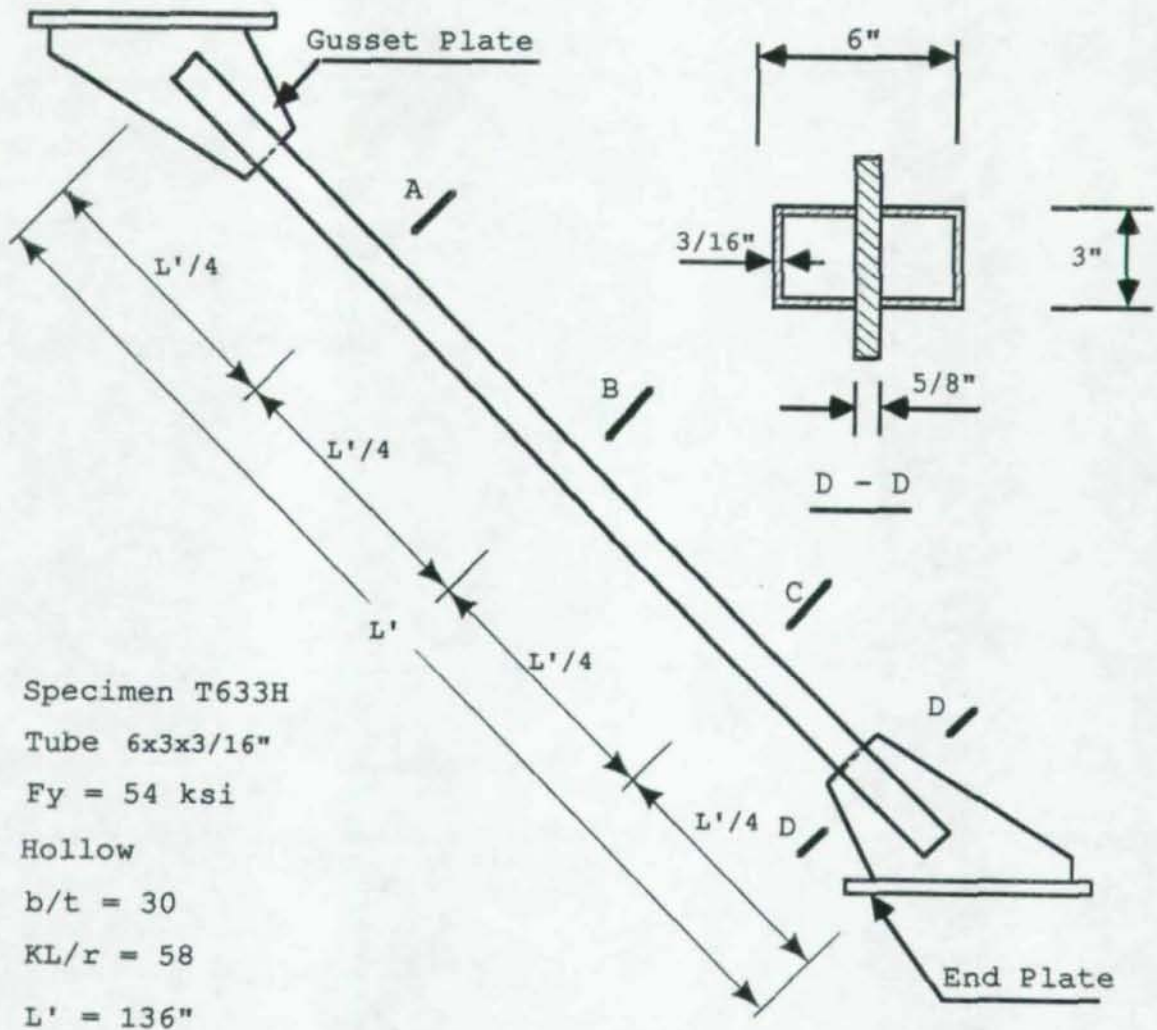


Figure 2.21 Comparison between Columns with and without Steel Fibers



Specimen T633H  
 Tube 6x3x3/16"  
 $F_y = 54$  ksi  
 Hollow  
 $b/t = 30$   
 $KL/r = 58$   
 $L' = 136"$

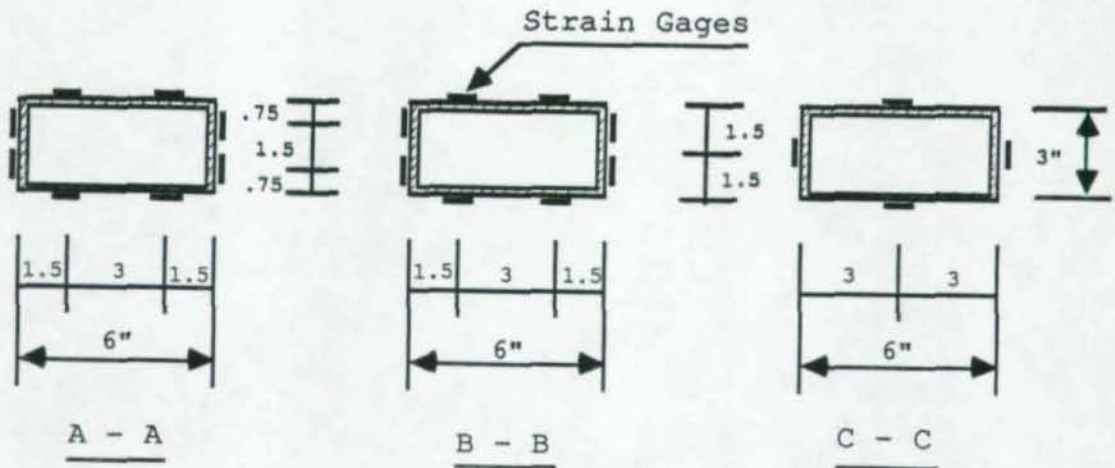
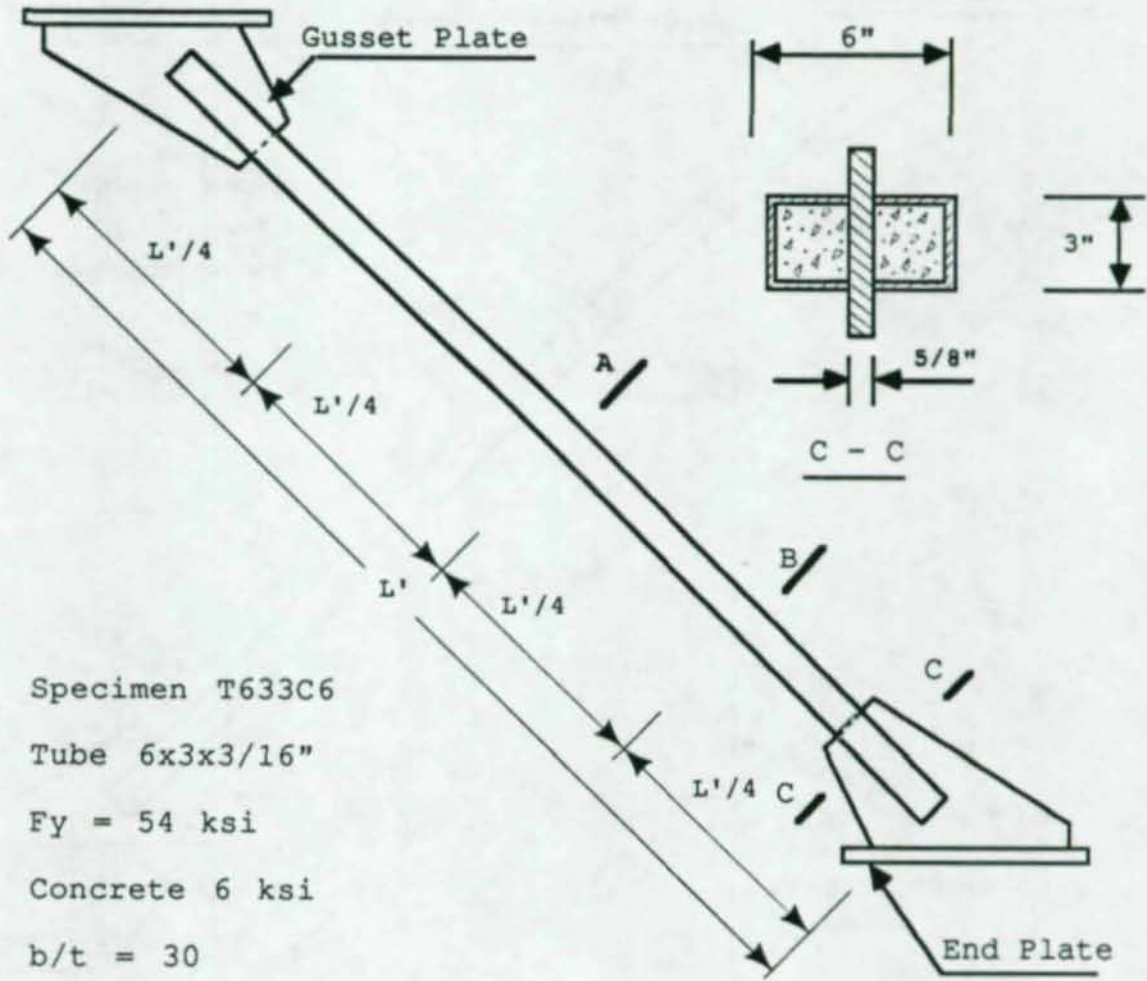


Figure 3.1 Hollow Bracing Specimen T633H



Specimen T633C6

Tube 6x3x3/16"

Fy = 54 ksi

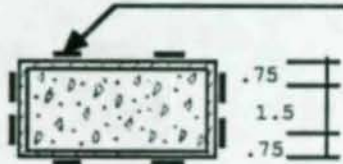
Concrete 6 ksi

b/t = 30

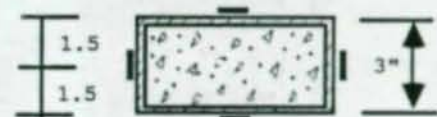
KL/r<sub>t</sub> = 65

L' = 136"

Strain Gages



A - A



B - B

Figure 3.2 Concrete-Filled Bracing Specimen T633C6

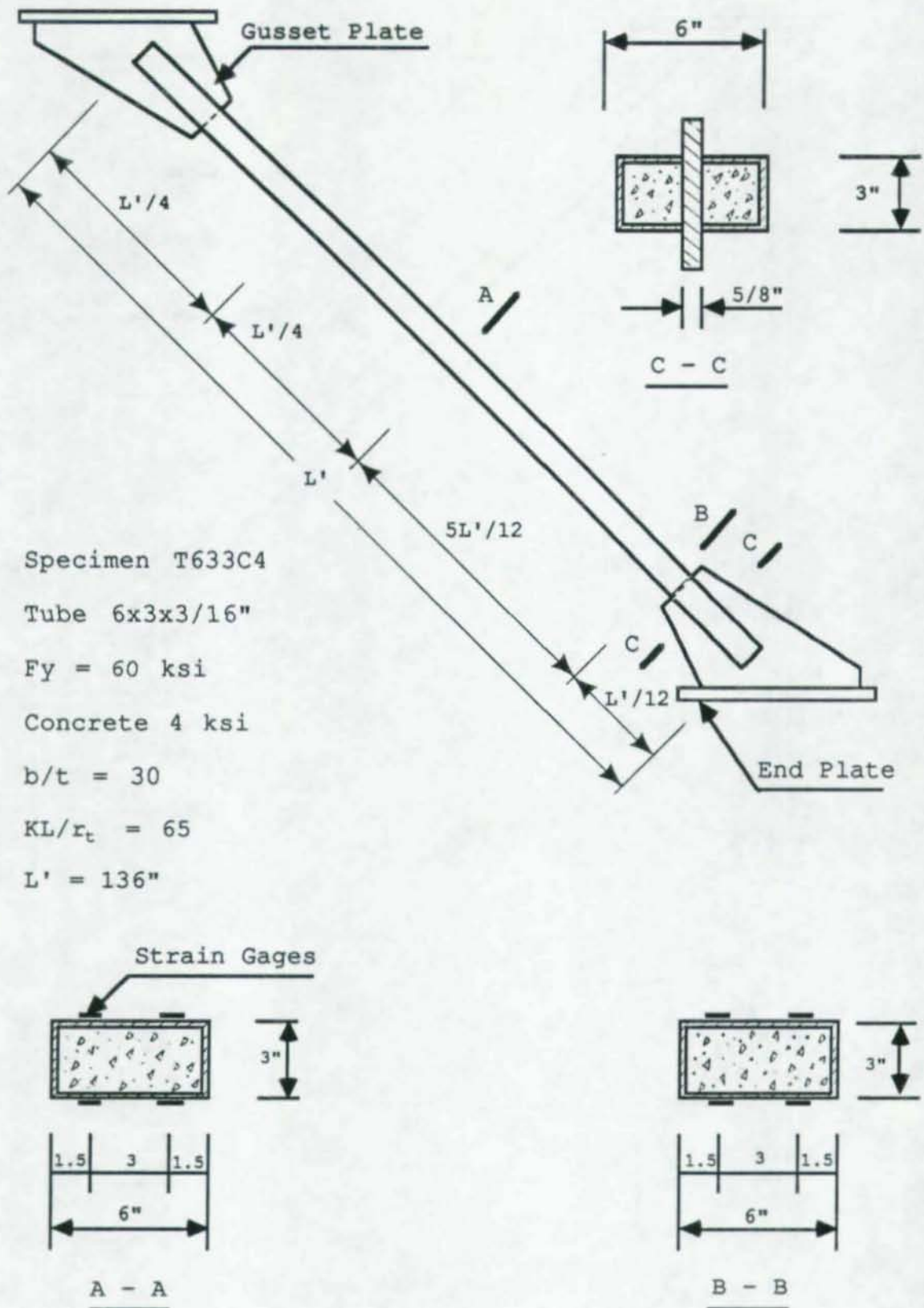
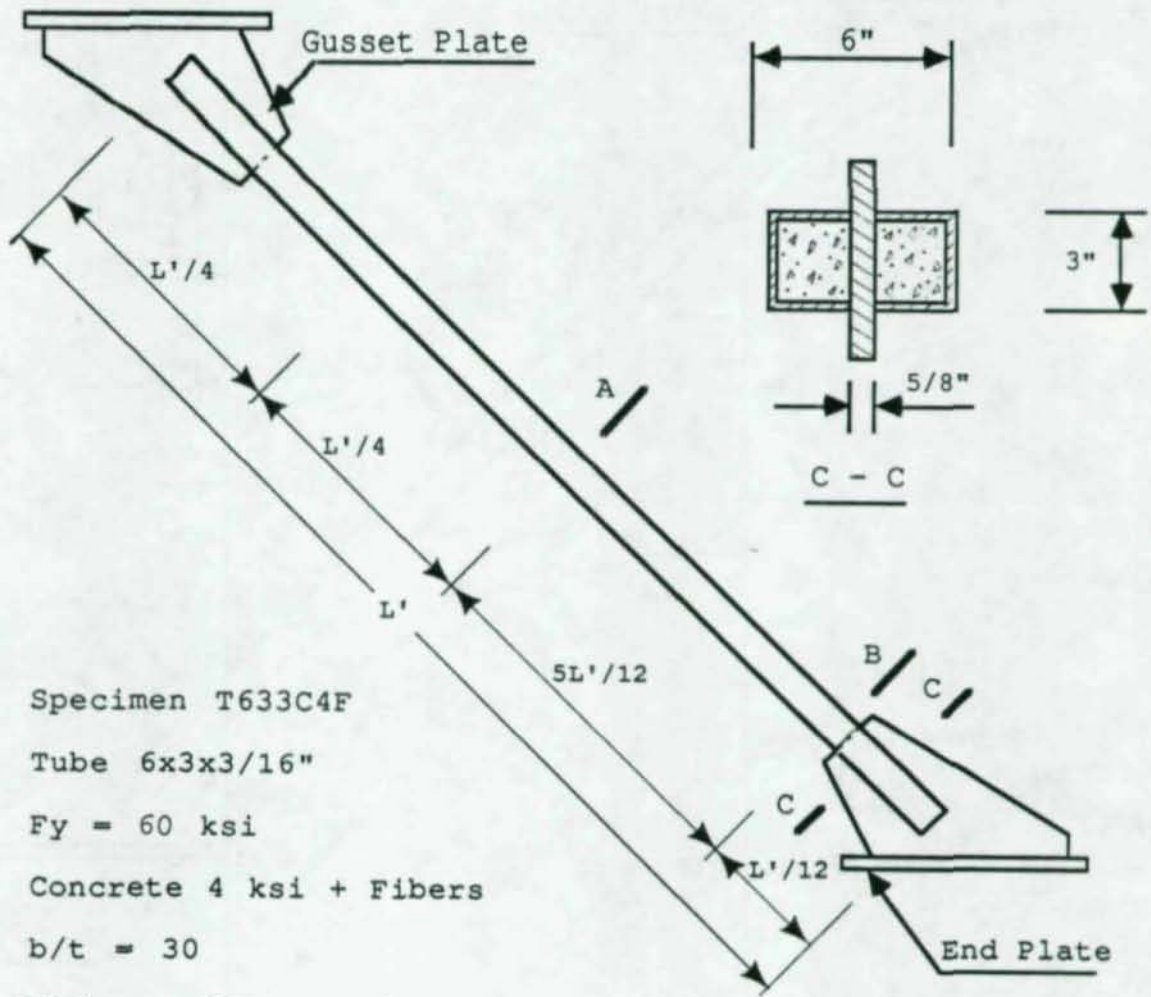


Figure 3.3 Concrete-Filled Bracing Specimen T633C4



Specimen T633C4F  
 Tube 6x3x3/16"  
 $F_y = 60$  ksi  
 Concrete 4 ksi + Fibers  
 $b/t = 30$   
 $KL/r_c = 65$   
 $L' = 136"$

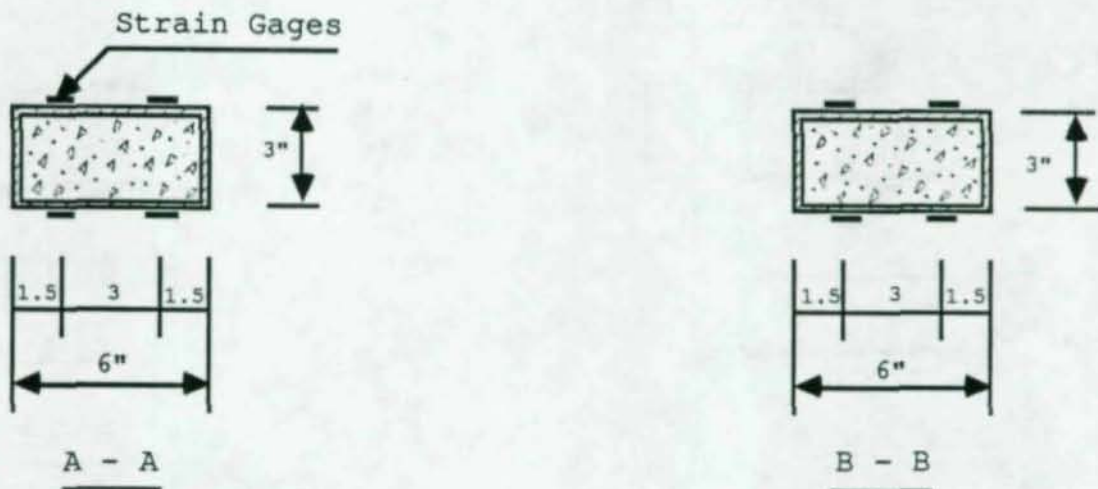
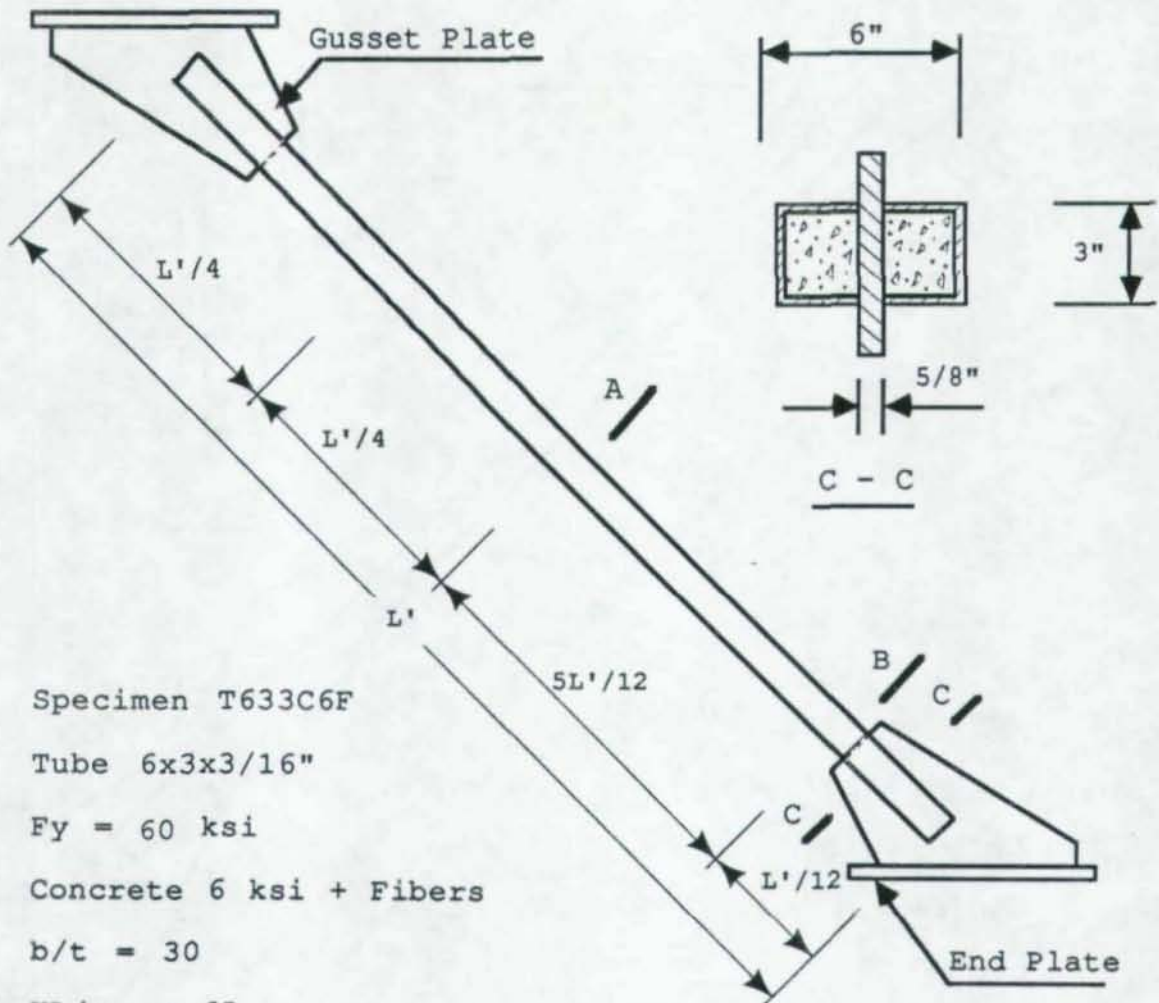


Figure 3.4 Concrete-Filled Bracing Specimen T633C4F



Specimen T633C6F

Tube 6x3x3/16"

$F_y = 60$  ksi

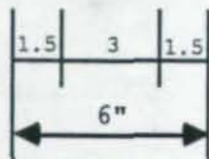
Concrete 6 ksi + Fibers

$b/t = 30$

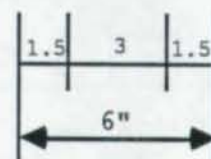
$KL/r_t = 65$

$L' = 136$ "

Strain Gages

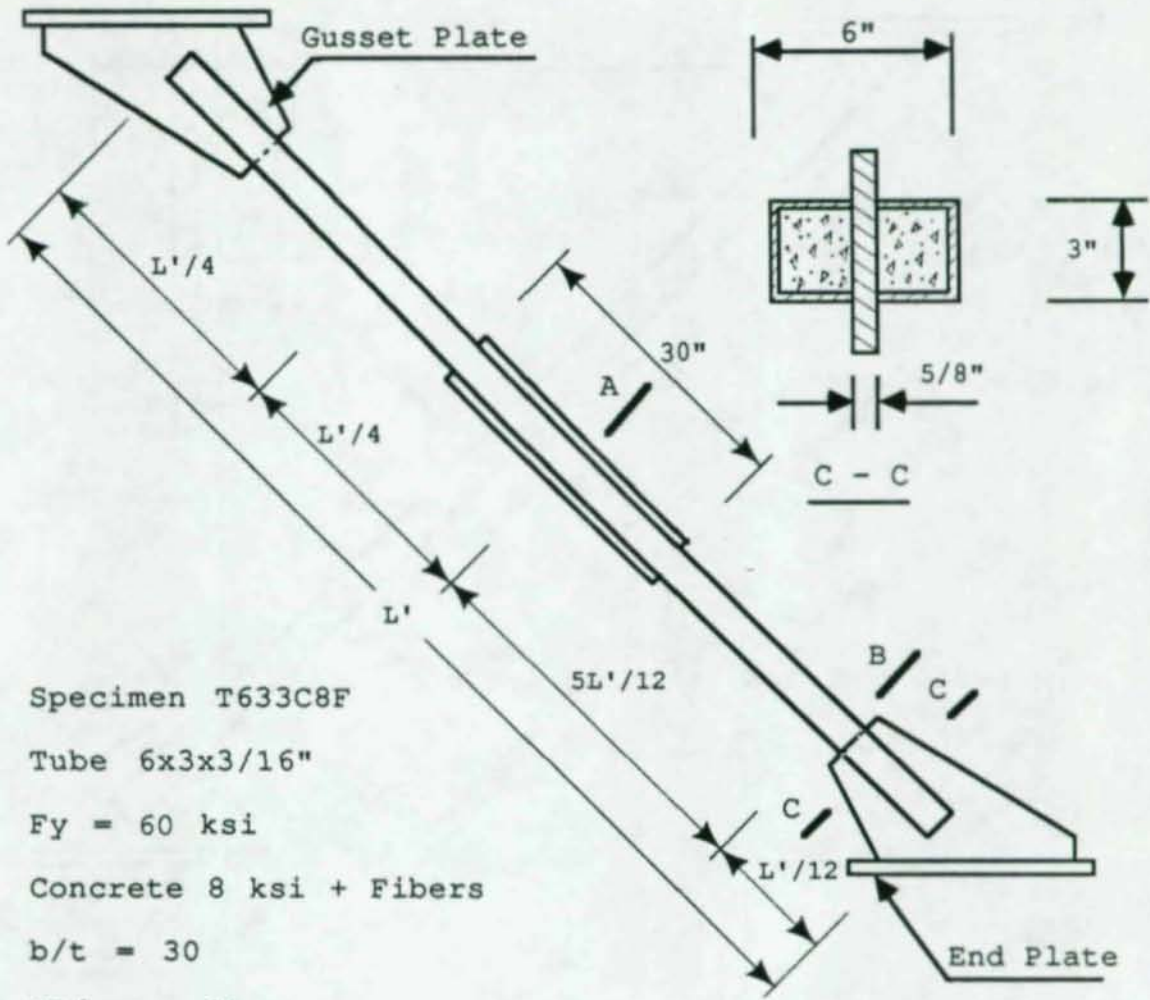


A - A



B - B

Figure 3.5 Concrete-Filled Bracing Specimen T633C6F



Specimen T633C8F  
 Tube 6x3x3/16"  
 $F_y = 60$  ksi  
 Concrete 8 ksi + Fibers  
 $b/t = 30$   
 $KL/r_t = 65$   
 $L' = 136"$

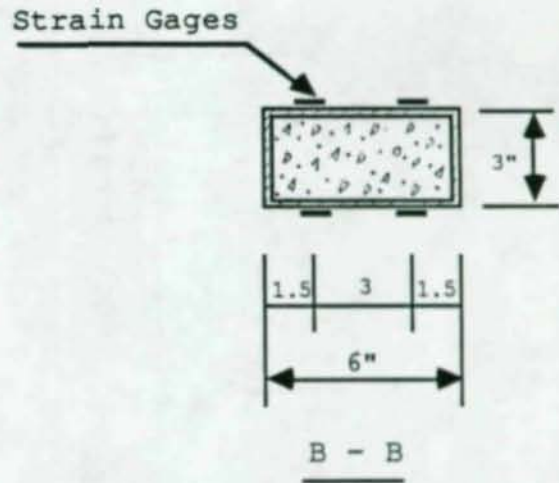
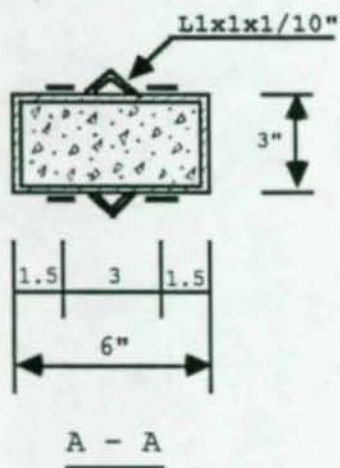
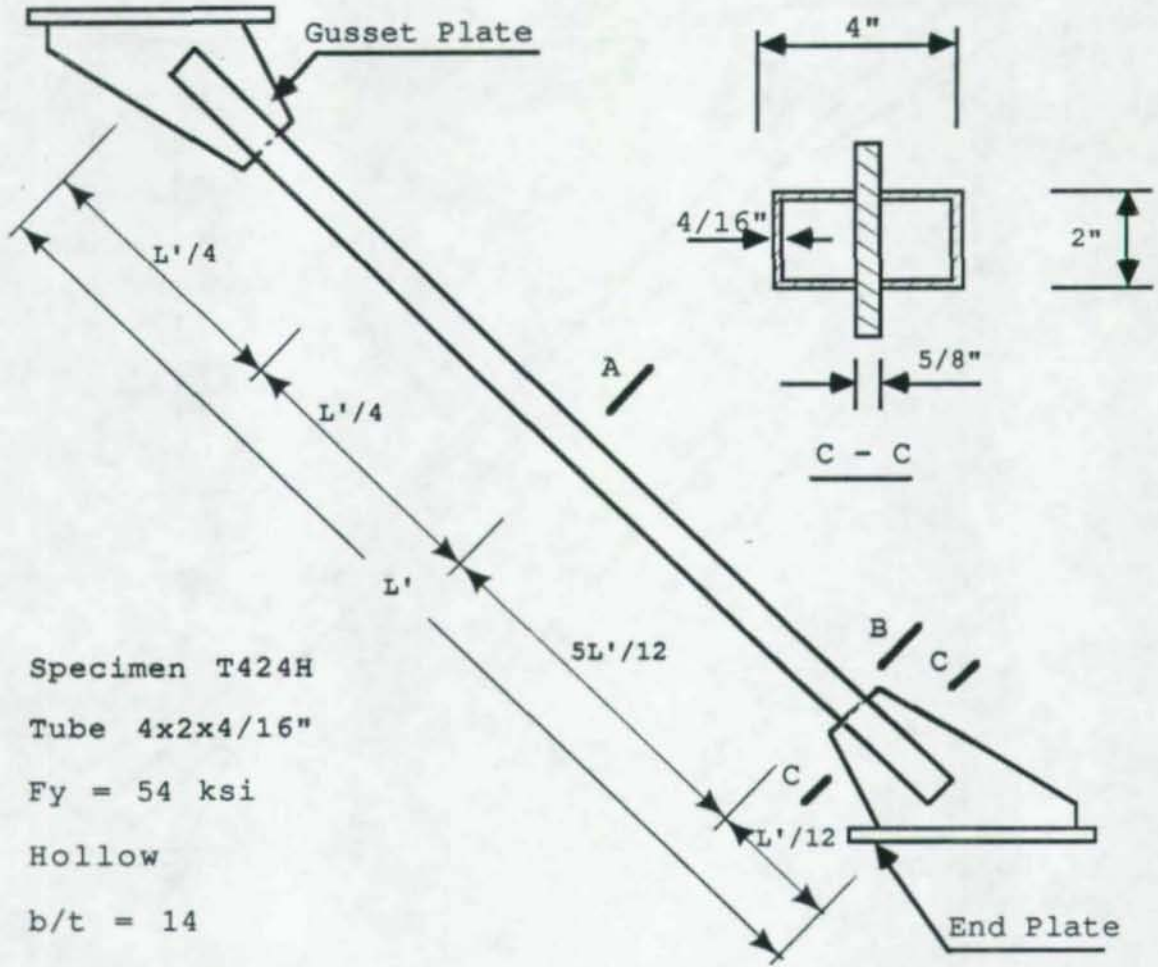


Figure 3.6 Concrete-Filled Bracing Specimen T633C8F



Specimen T424H

Tube 4x2x4/16"

Fy = 54 ksi

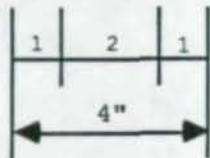
Hollow

b/t = 14

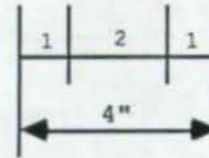
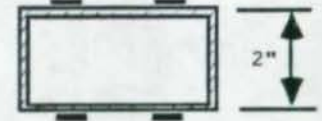
KL/r = 92

$L' = 137"$

Strain Gages

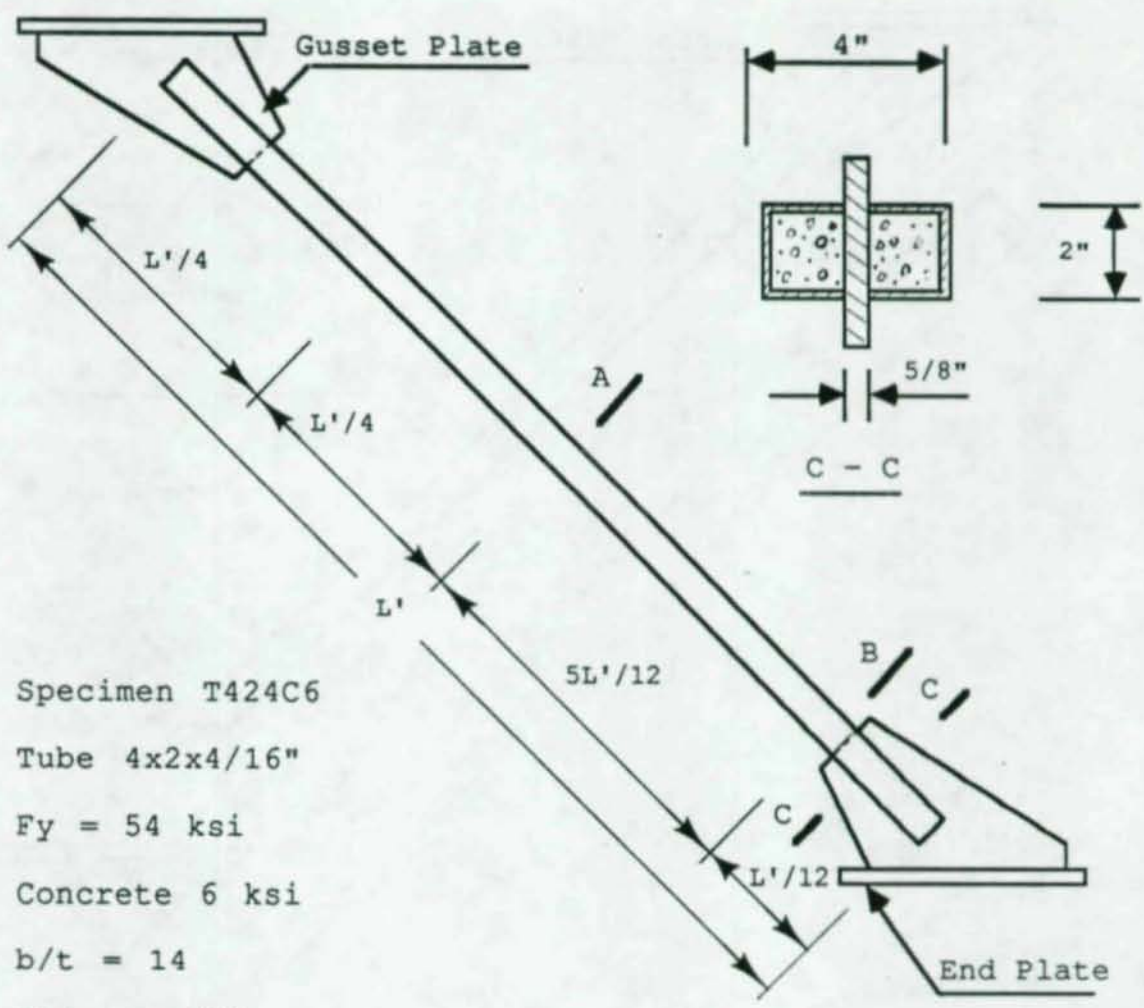


A - A



B - B

Figure 3.7 Hollow Bracing Specimen T424H



Specimen T424C6  
 Tube 4x2x4/16"  
 $F_y = 54$  ksi  
 Concrete 6 ksi  
 $b/t = 14$   
 $KL/r_t = 100$   
 $L' = 137$ "

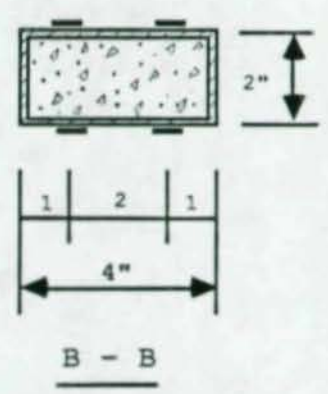
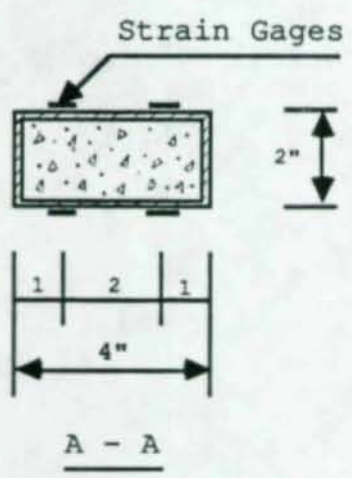
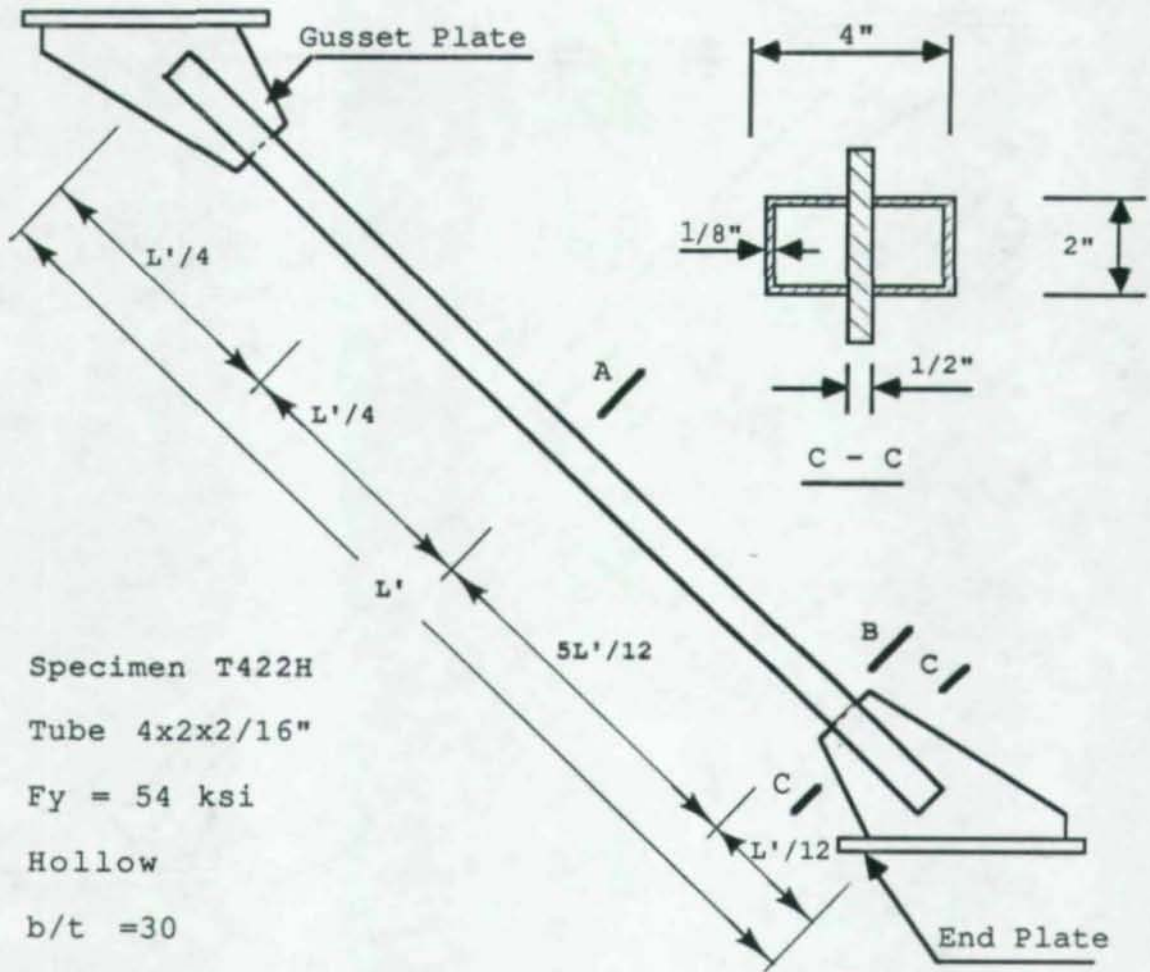


Figure 3.8 Concrete-Filled Bracing Specimen T424C6



Specimen T422H

Tube 4x2x2/16"

Fy = 54 ksi

Hollow

b/t = 30

KL/r = 88

L' = 137"

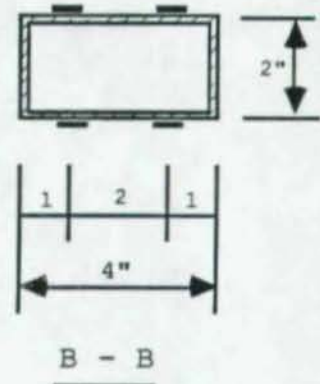
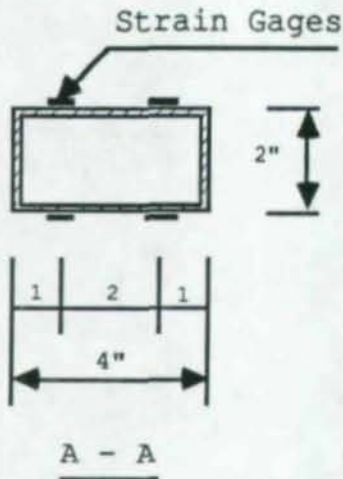


Figure 3.9 Hollow Bracing Specimen T422H

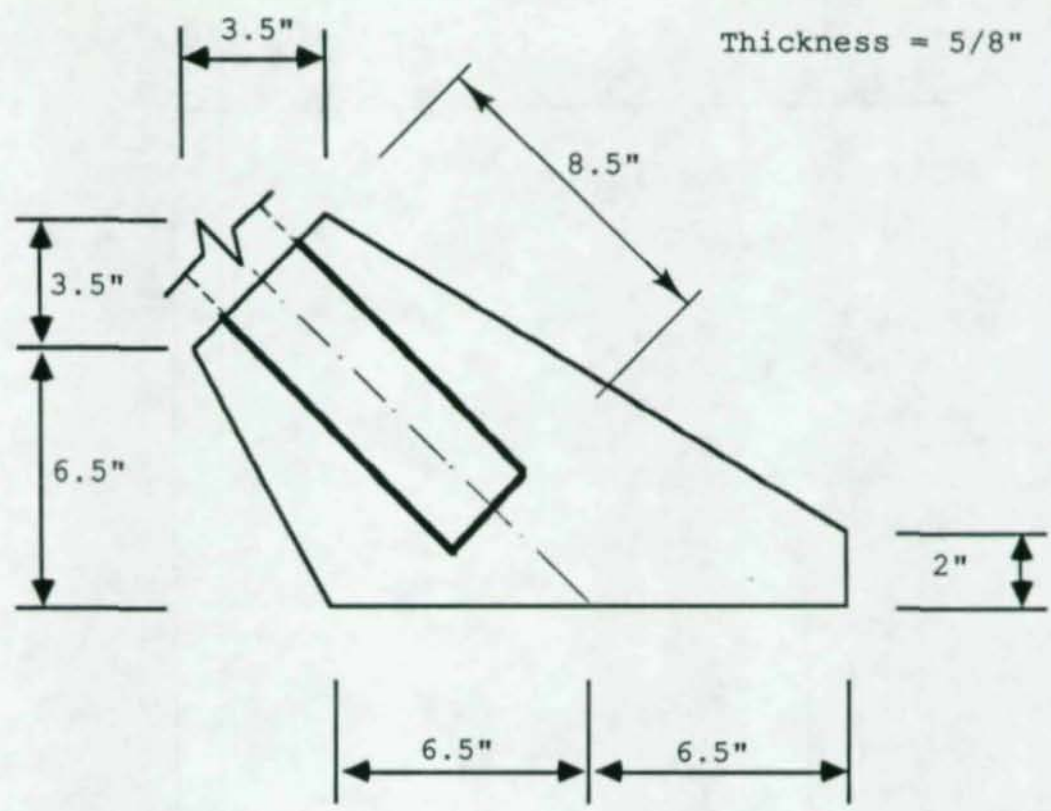


Figure 3.10 Gusset Plate for 6x3" Bracing Specimens

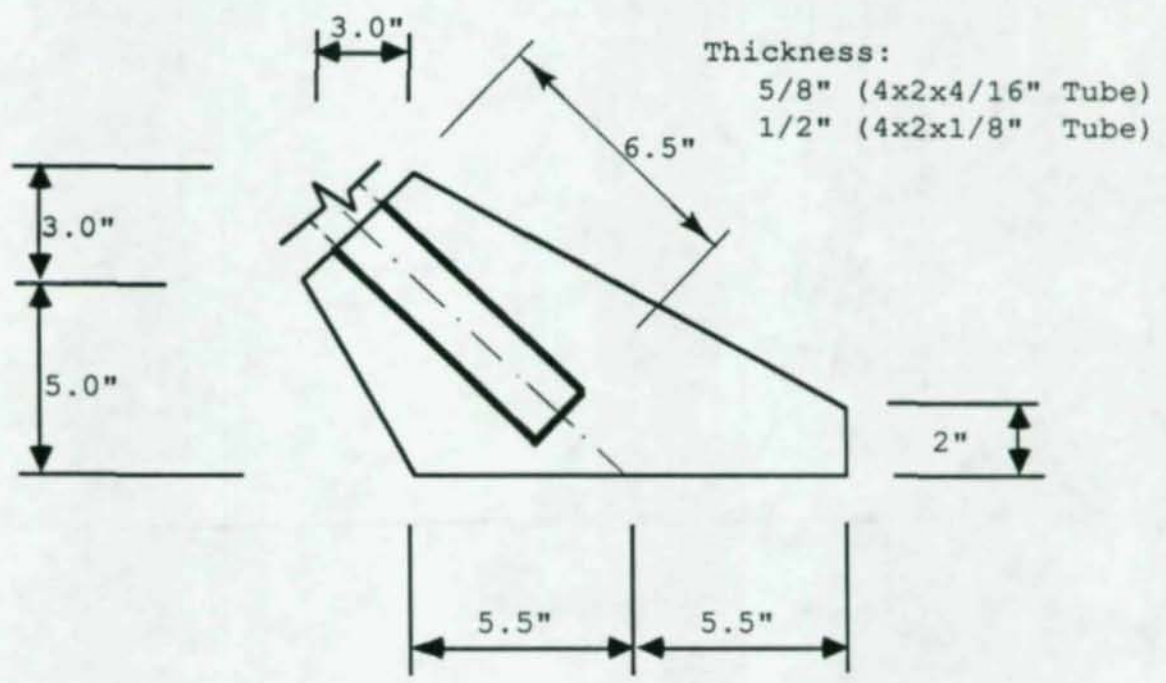


Figure 3.11 Gusset Plate for 4x2" Bracing Specimens

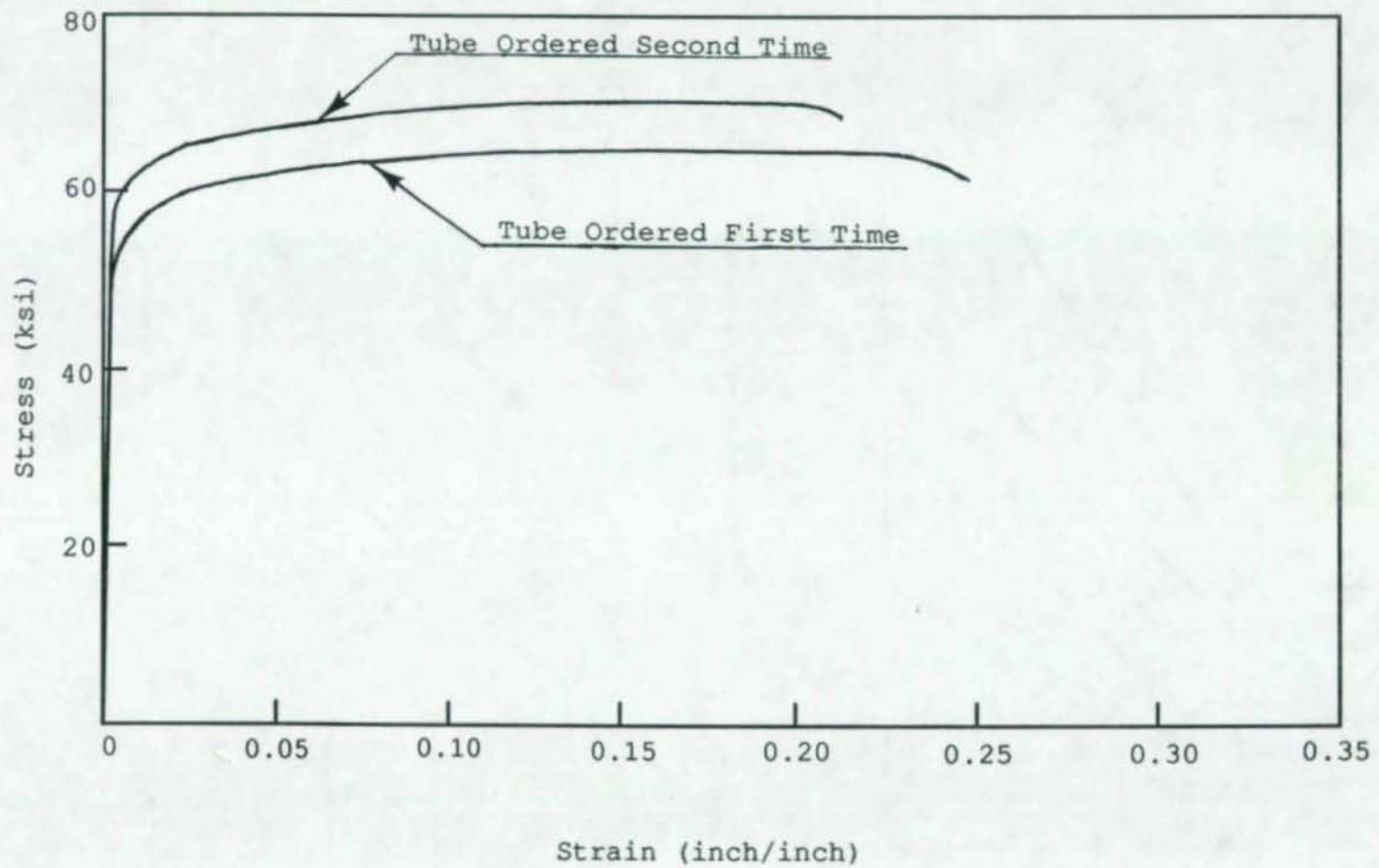


Figure 3.12 Stress-Strain Curves for Tube Material from Coupon Test

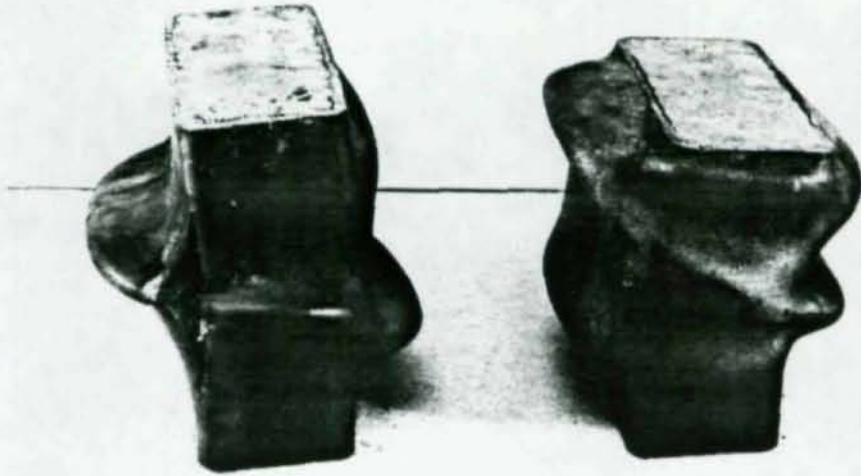


Figure 3.13 Cracking in Concrete-Filled Columns  
Made from Different Tubes

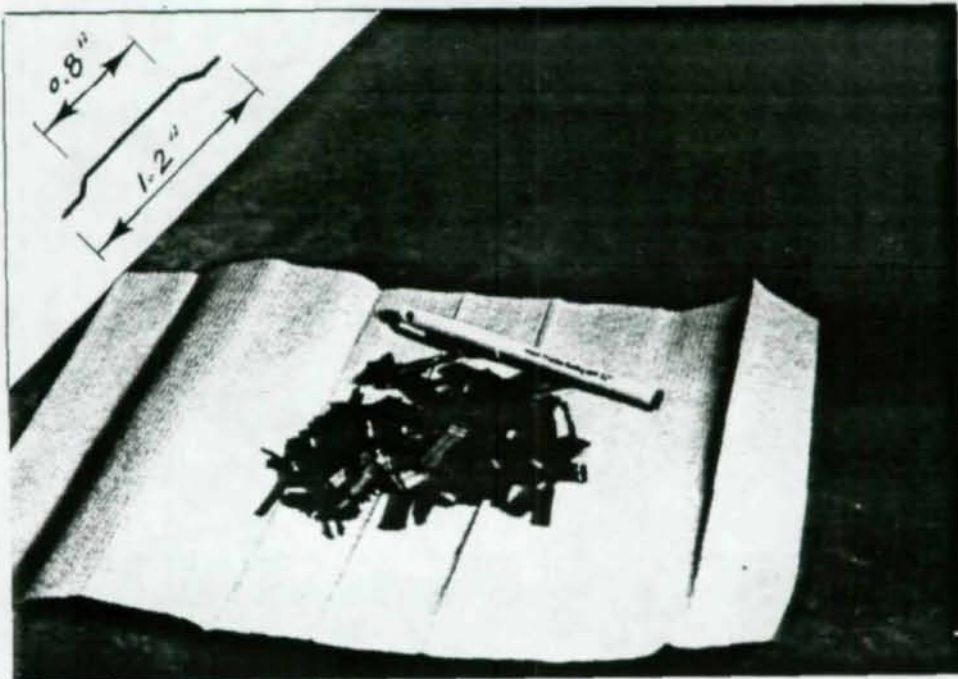


Figure 3.14 Steel Fibers

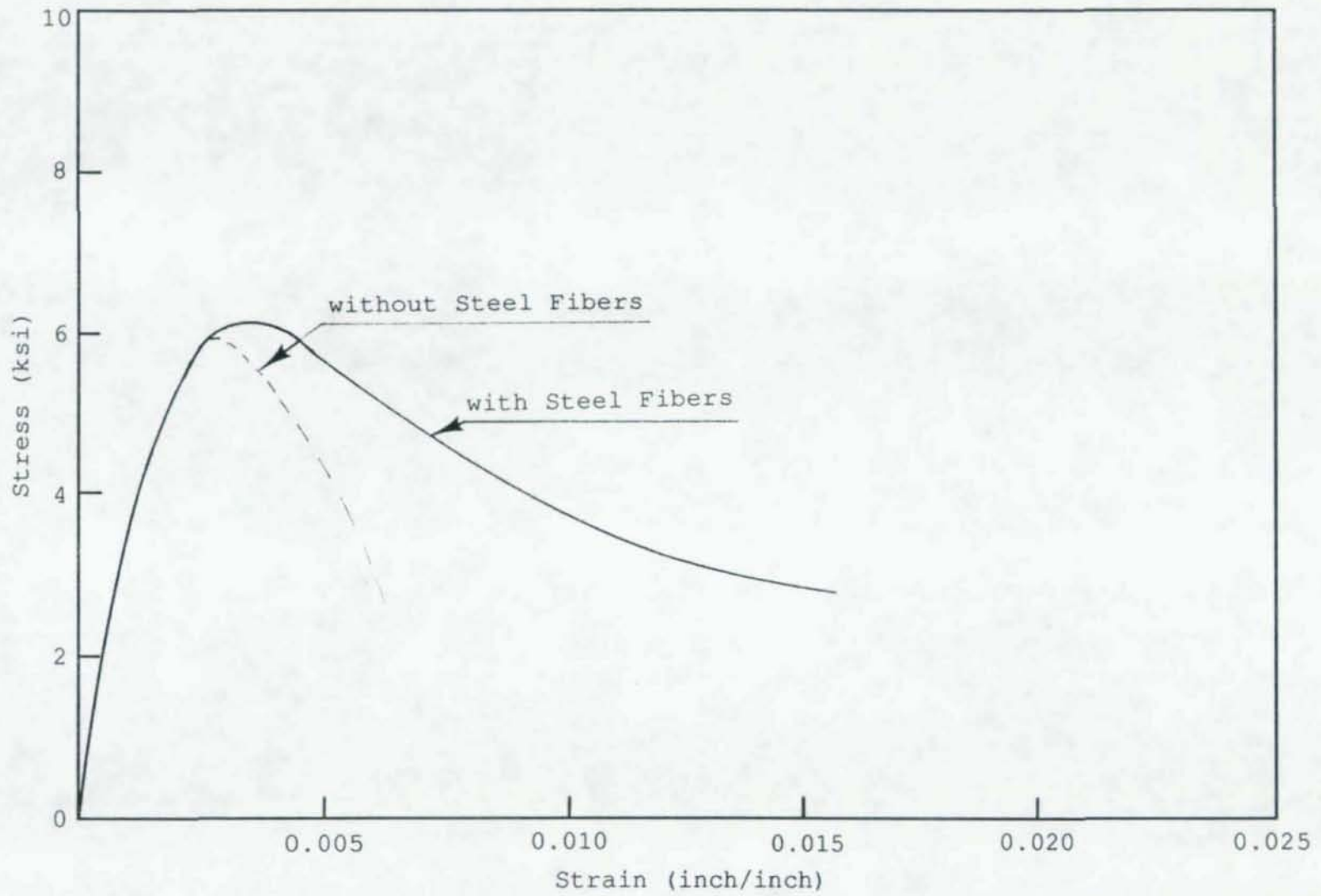


Figure 3.15 Concrete Cylinder Test Results

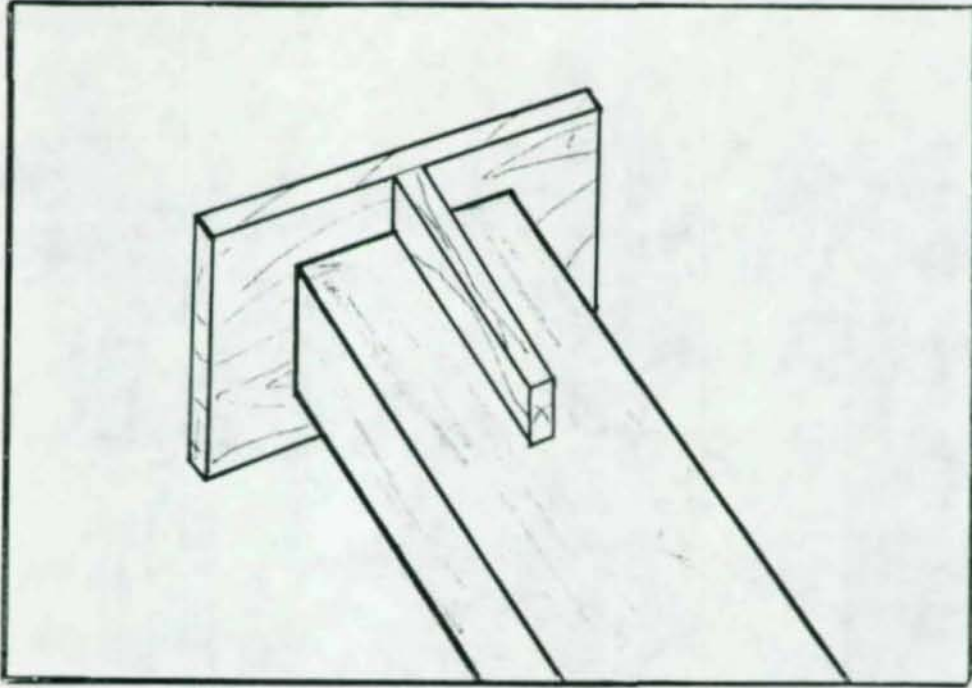


Figure 3.16 Tube End Treatment for Filling Concrete



Figure 3.17 Assembly Jig for Bracing Specimens

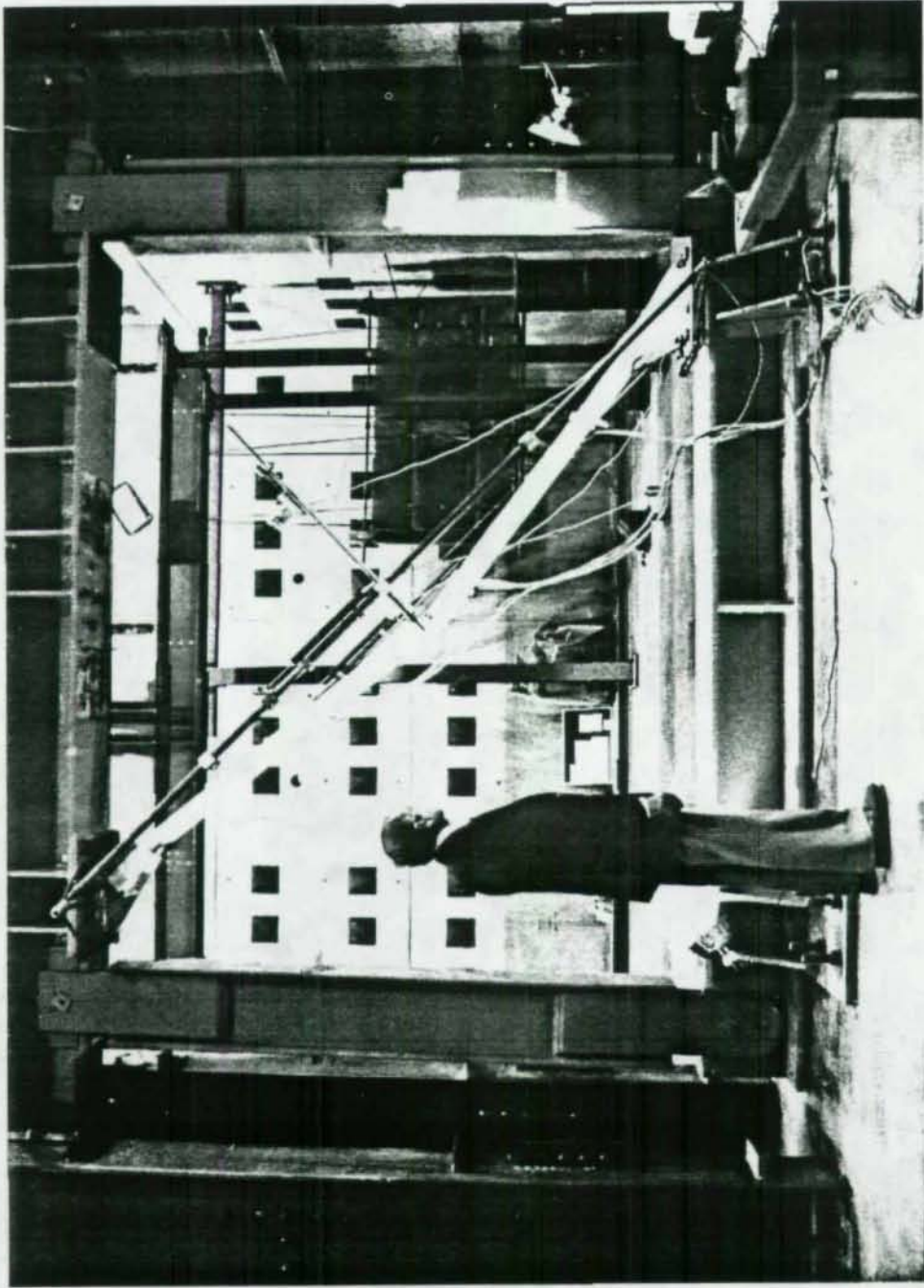


Figure 3.18 Test Frame for Bracing Specimens

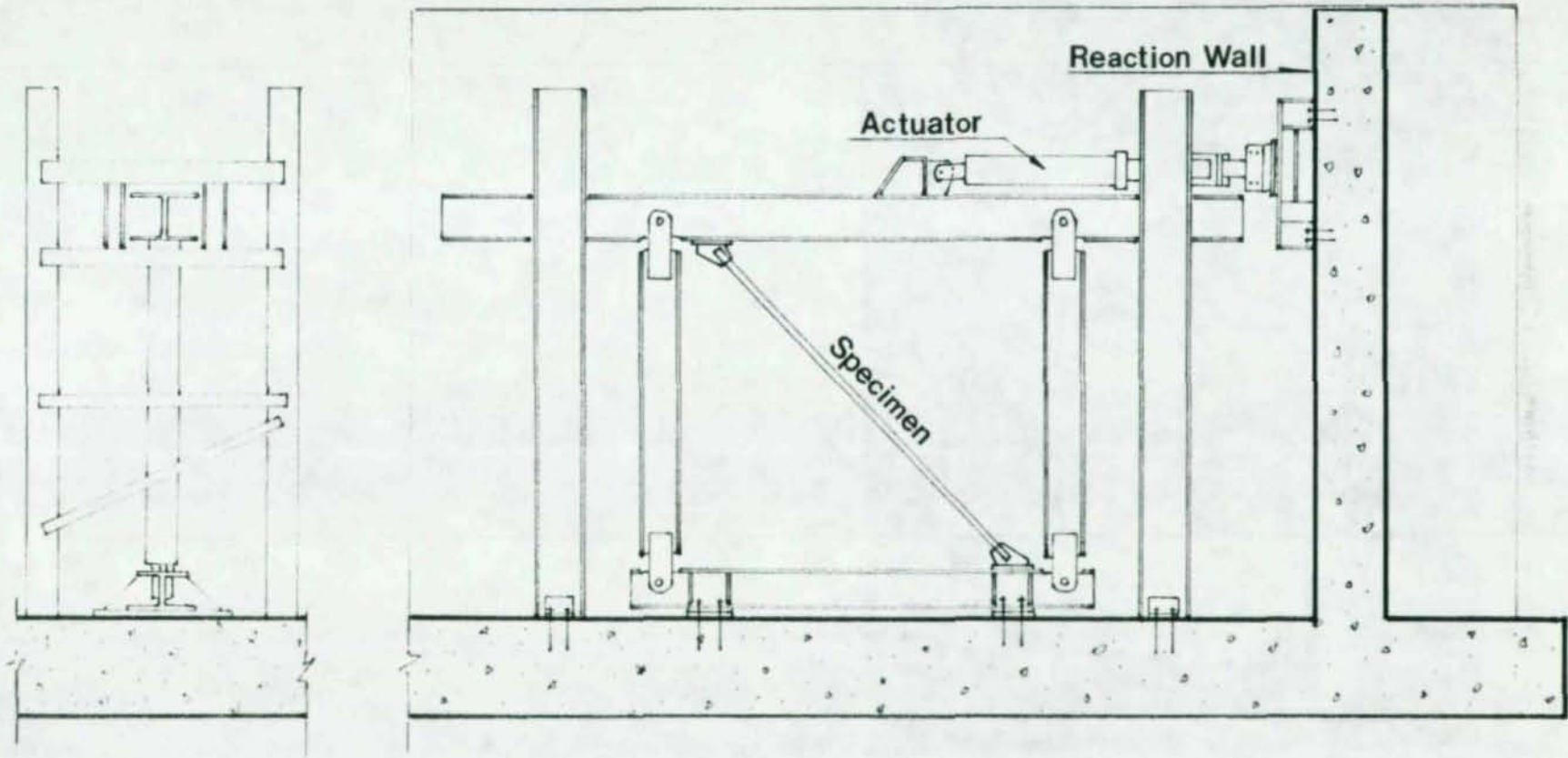


Figure 3.19 Schematic Drawing of the Testing Frame

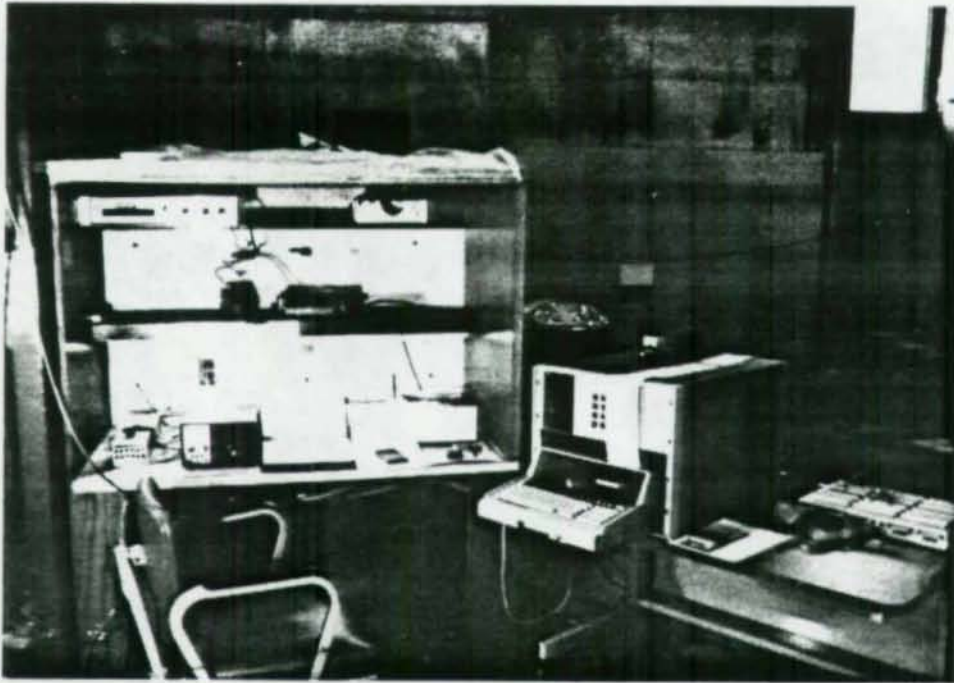


Figure 3.20 Data Acquisition System of Main Testing

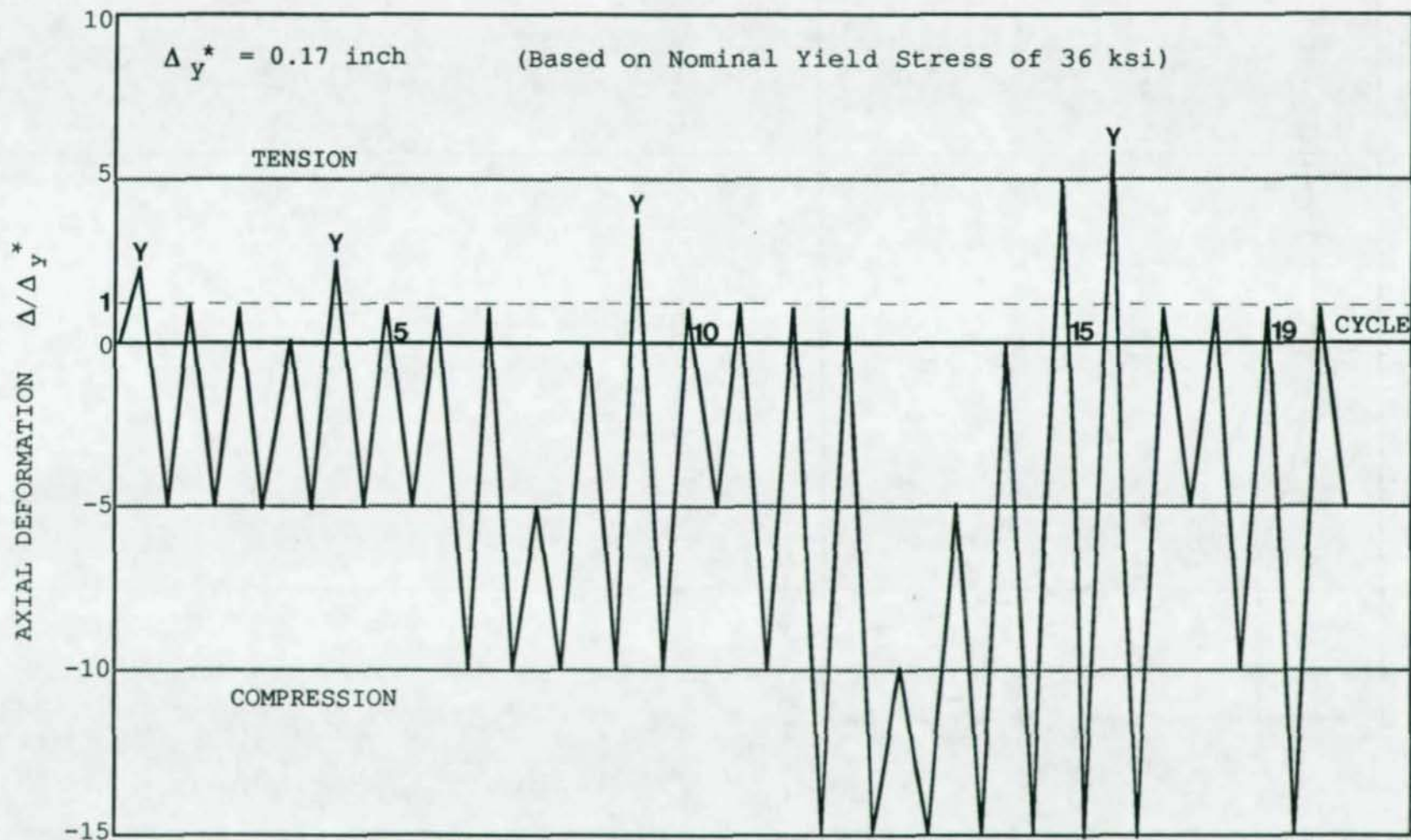


Figure 3.21 Loading History of Bracing Specimens

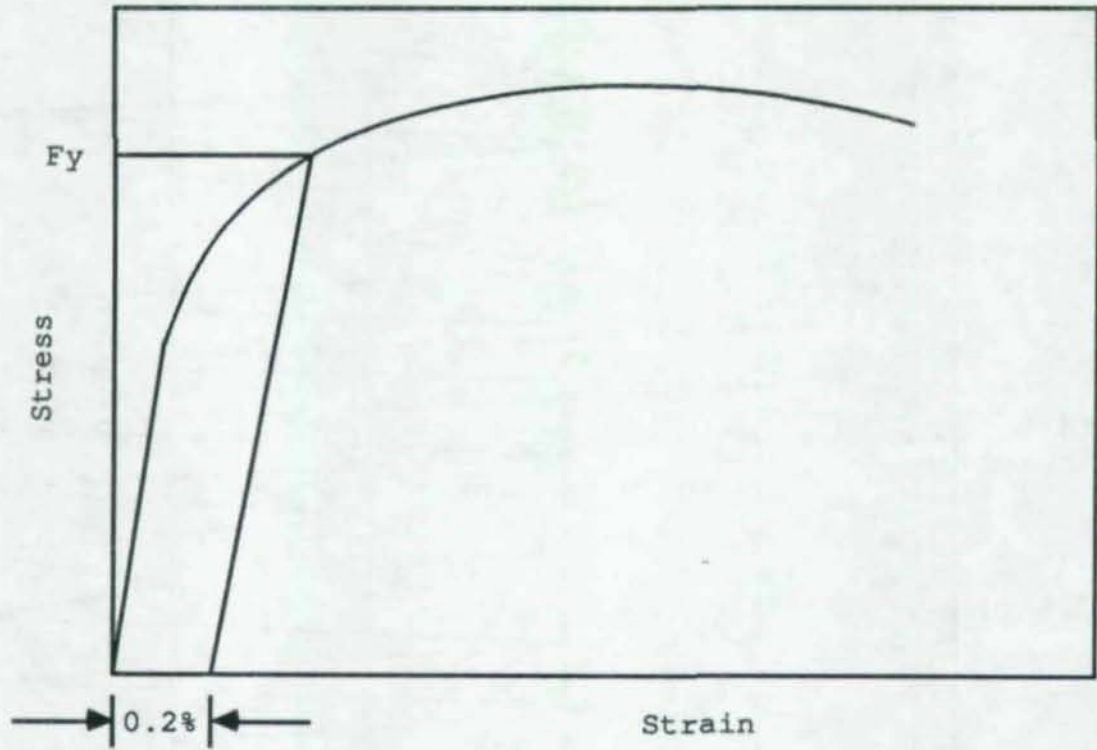
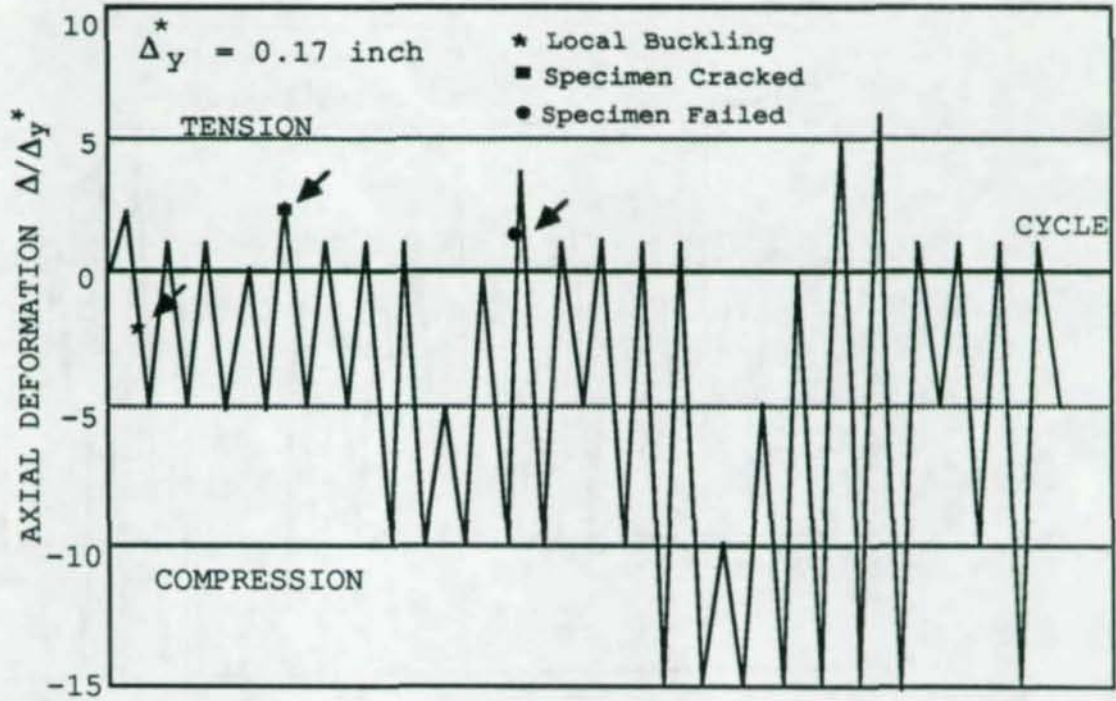
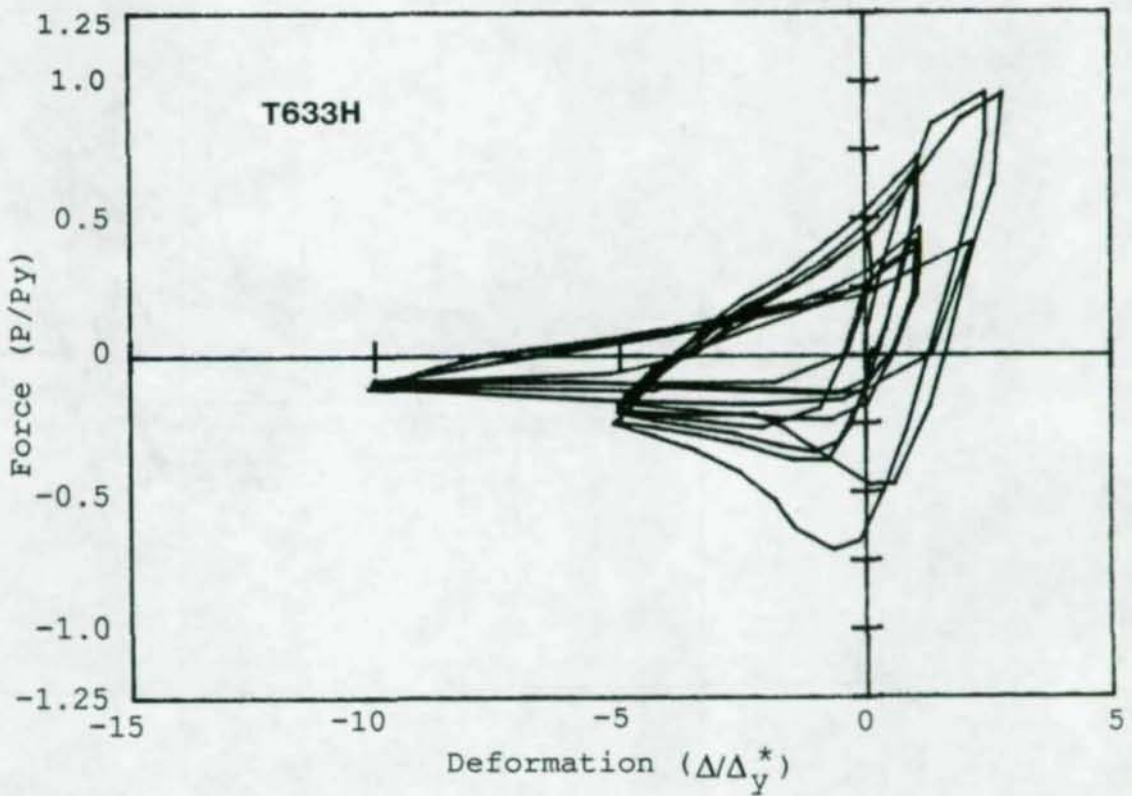


Figure 3.22 Definition of Yield Stress for Steel

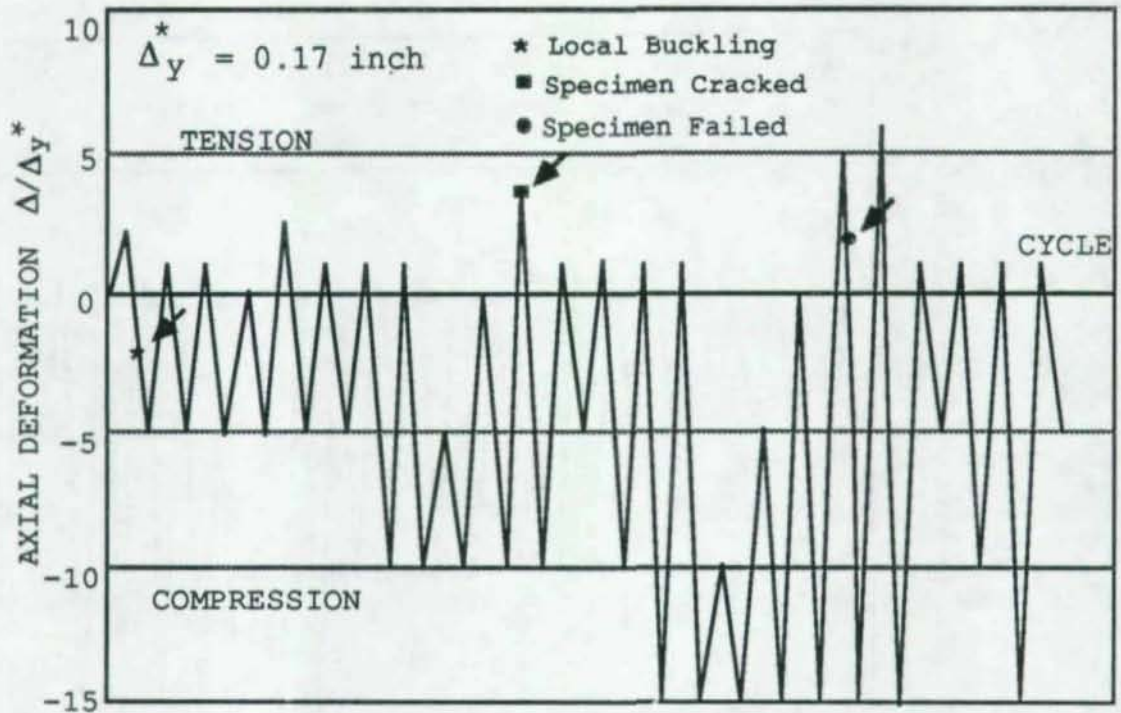


(a) Cycles When Specimen Cracked and Failed

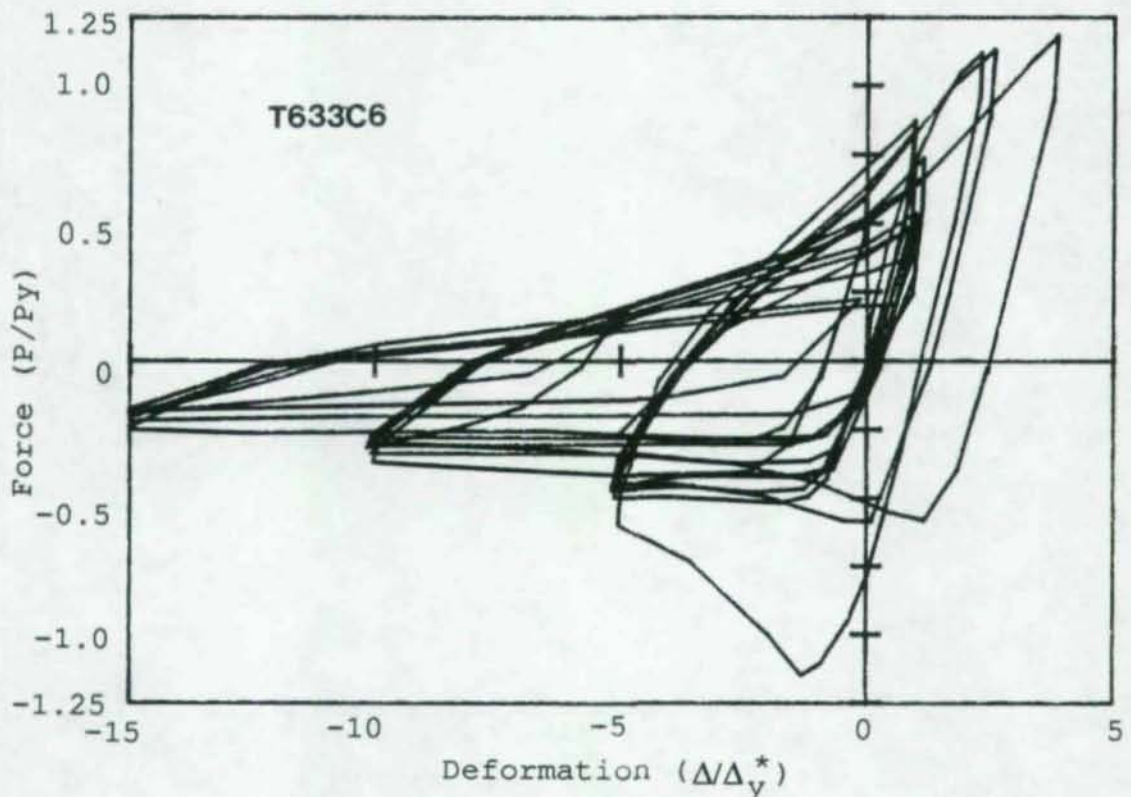


(b) Hysteresis Loops

Figure 4.1 Failure Mode and Hysteresis Loops of T633H

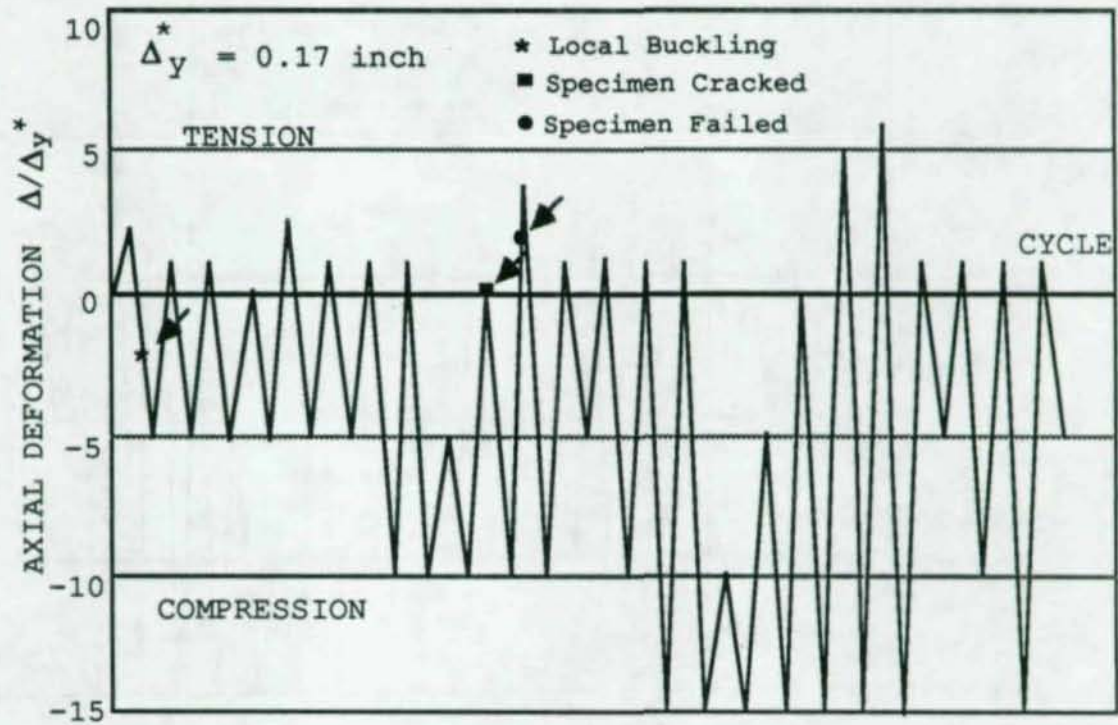


(a) Cycles When Specimen Cracked and Failed

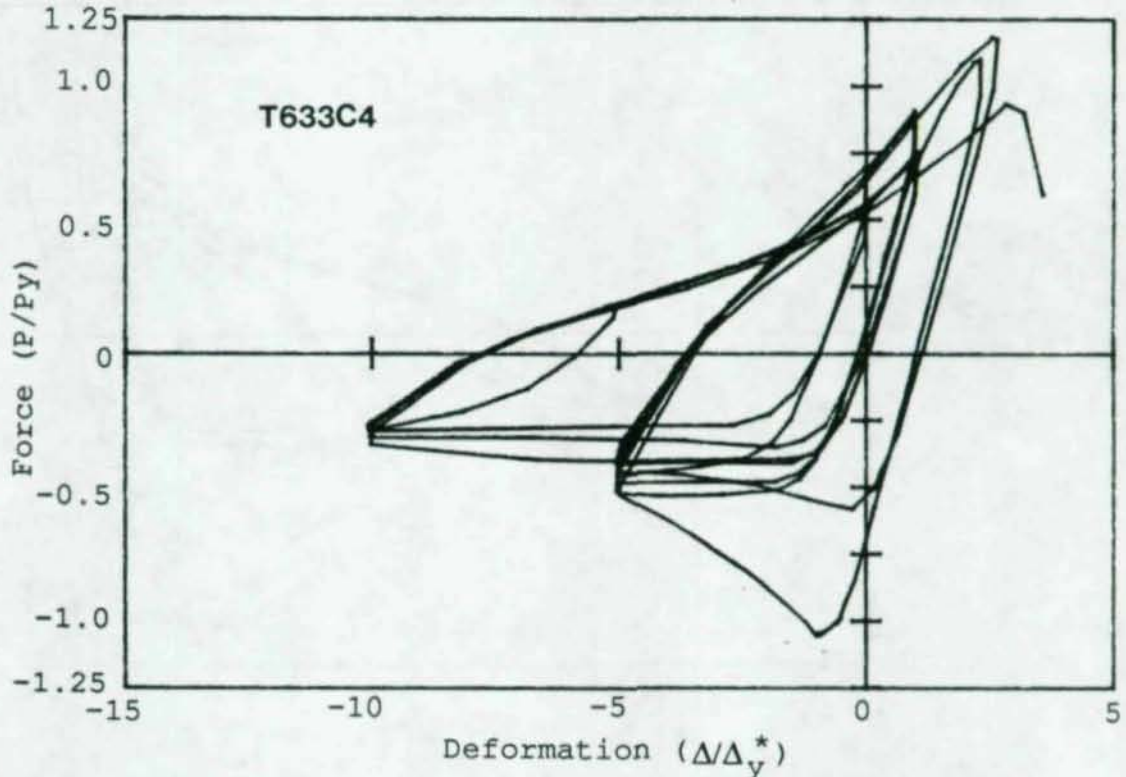


(b) Hysteresis Loops

Figure 4.2 Failure Mode and Hysteresis Loops of T633C6

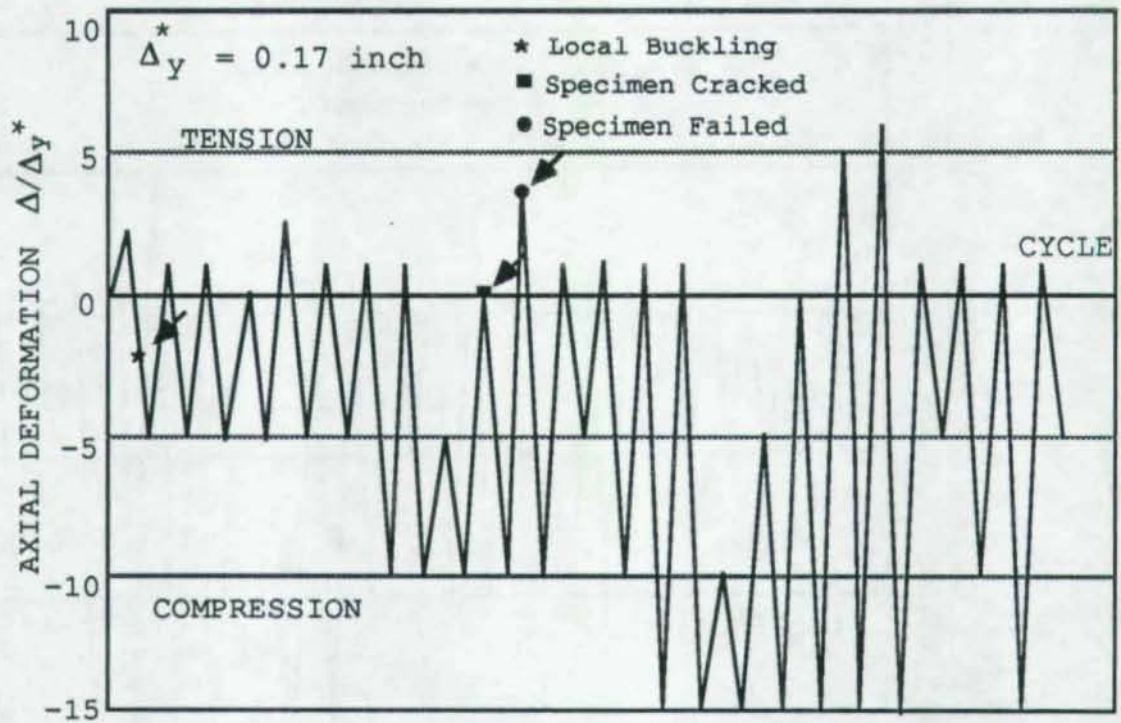


(a) Cycles When Specimen Cracked and Failed

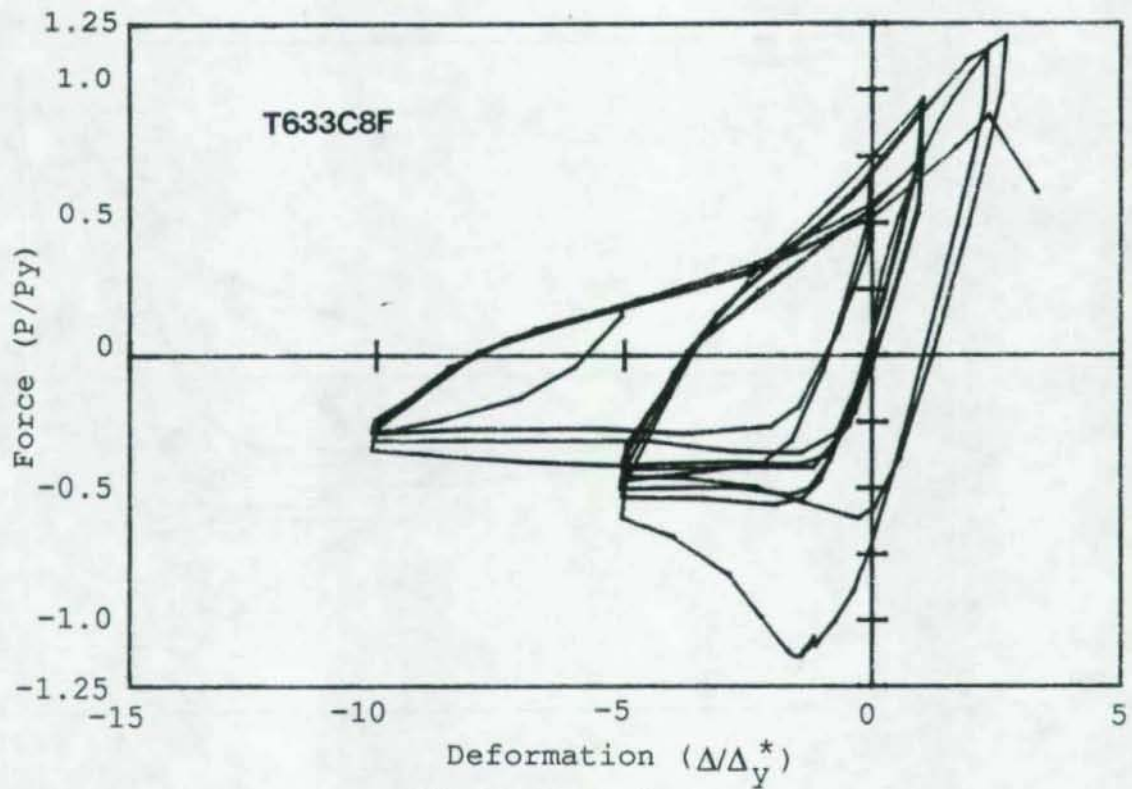


(b) Hysteresis Loops

Figure 4.3 Failure Mode and Hysteresis Loops of T633C4

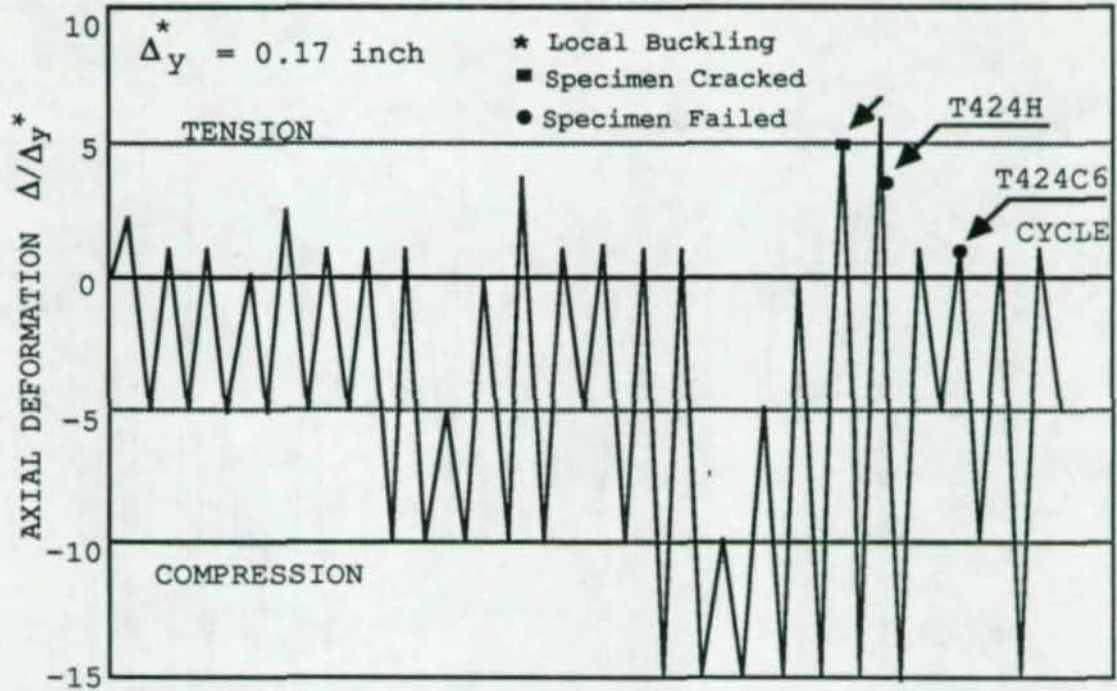


(a) Cycles When Specimen Cracked and Failed

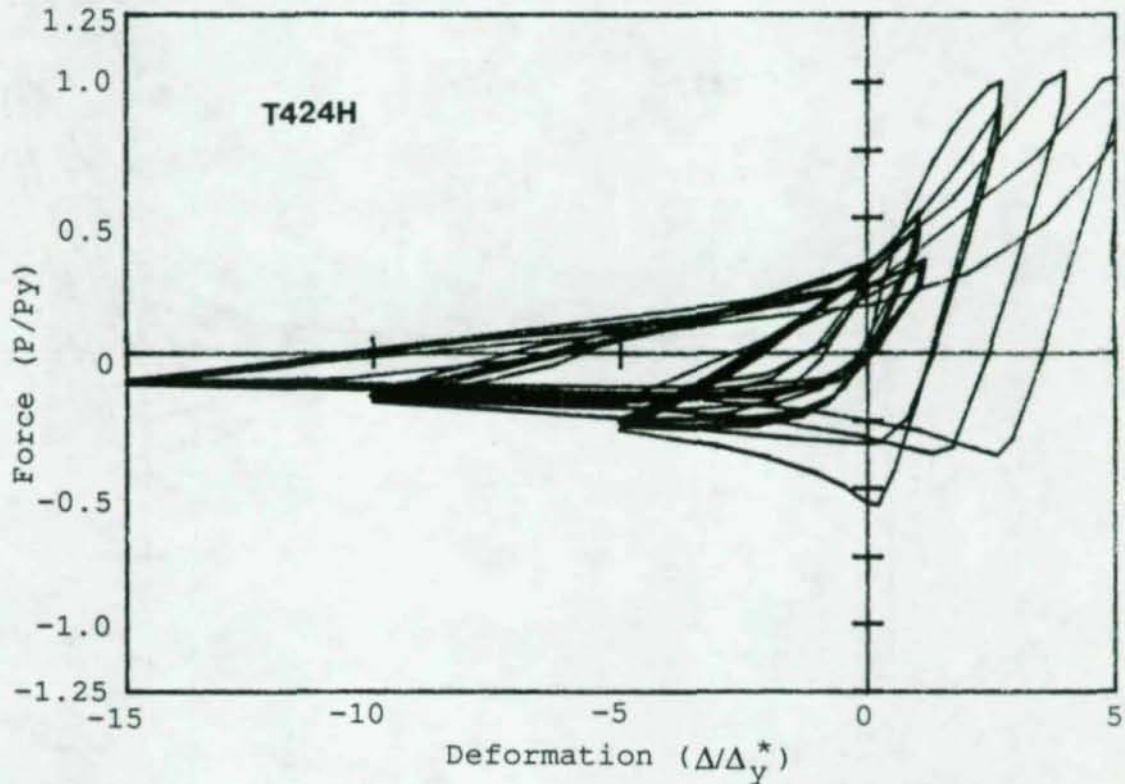


(b) Hysteresis Loops

Figure 4.4 Failure Mode and Hysteresis Loops of T633C8F

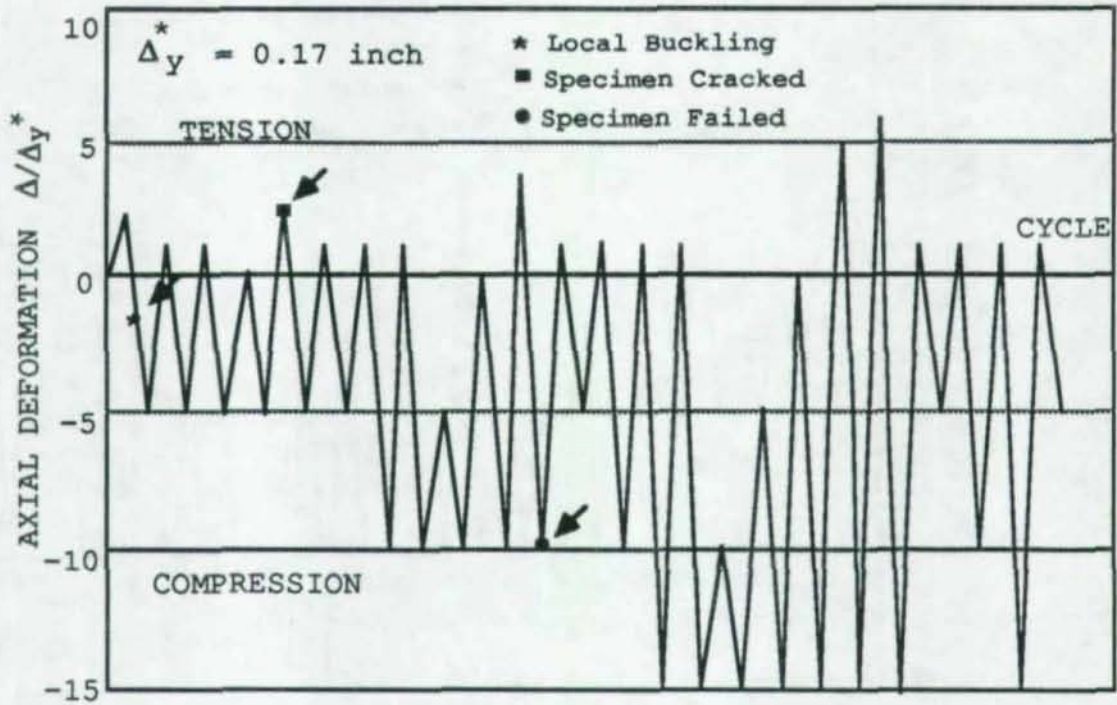


(a) Cycles When Specimen Cracked and Failed

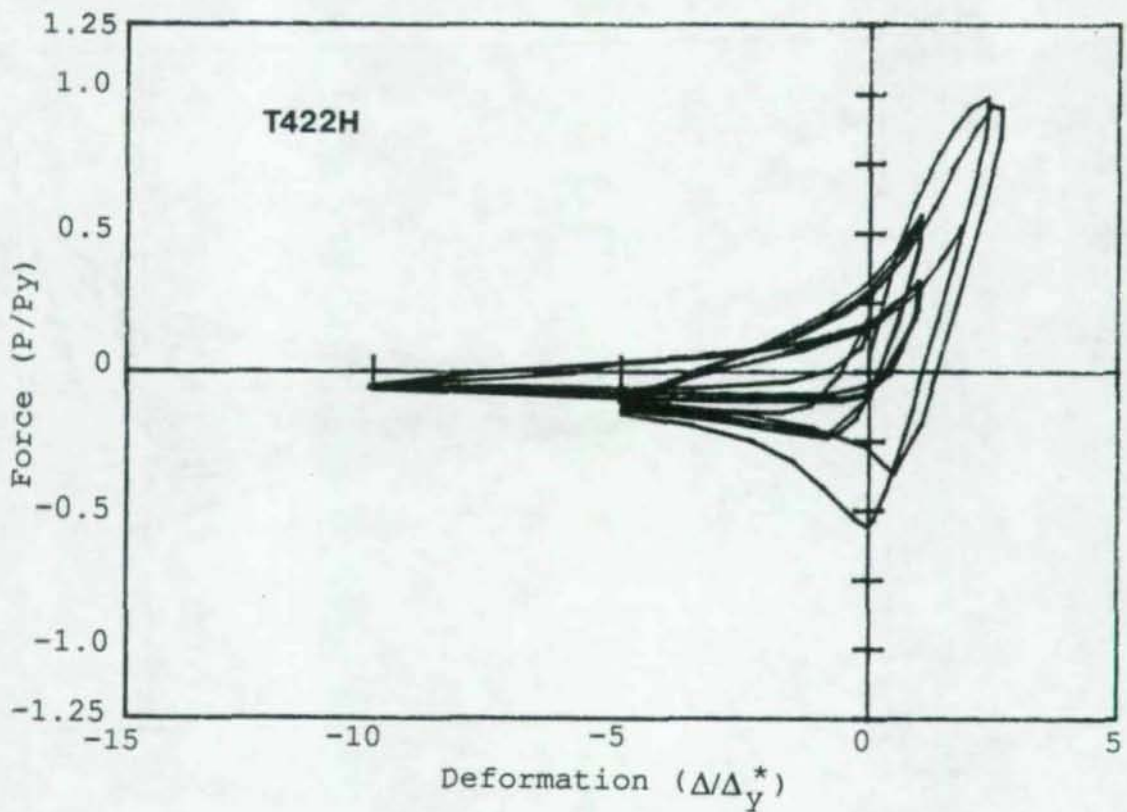


(b) Hysteresis Loops

Figure 4.5 Failure Mode and Hysteresis Loops of T424H



(a) Cycles When Specimen Cracked and Failed



(b) Hysteresis Loops

Figure 4.6 Failure Mode and Hysteresis Loops of T422H

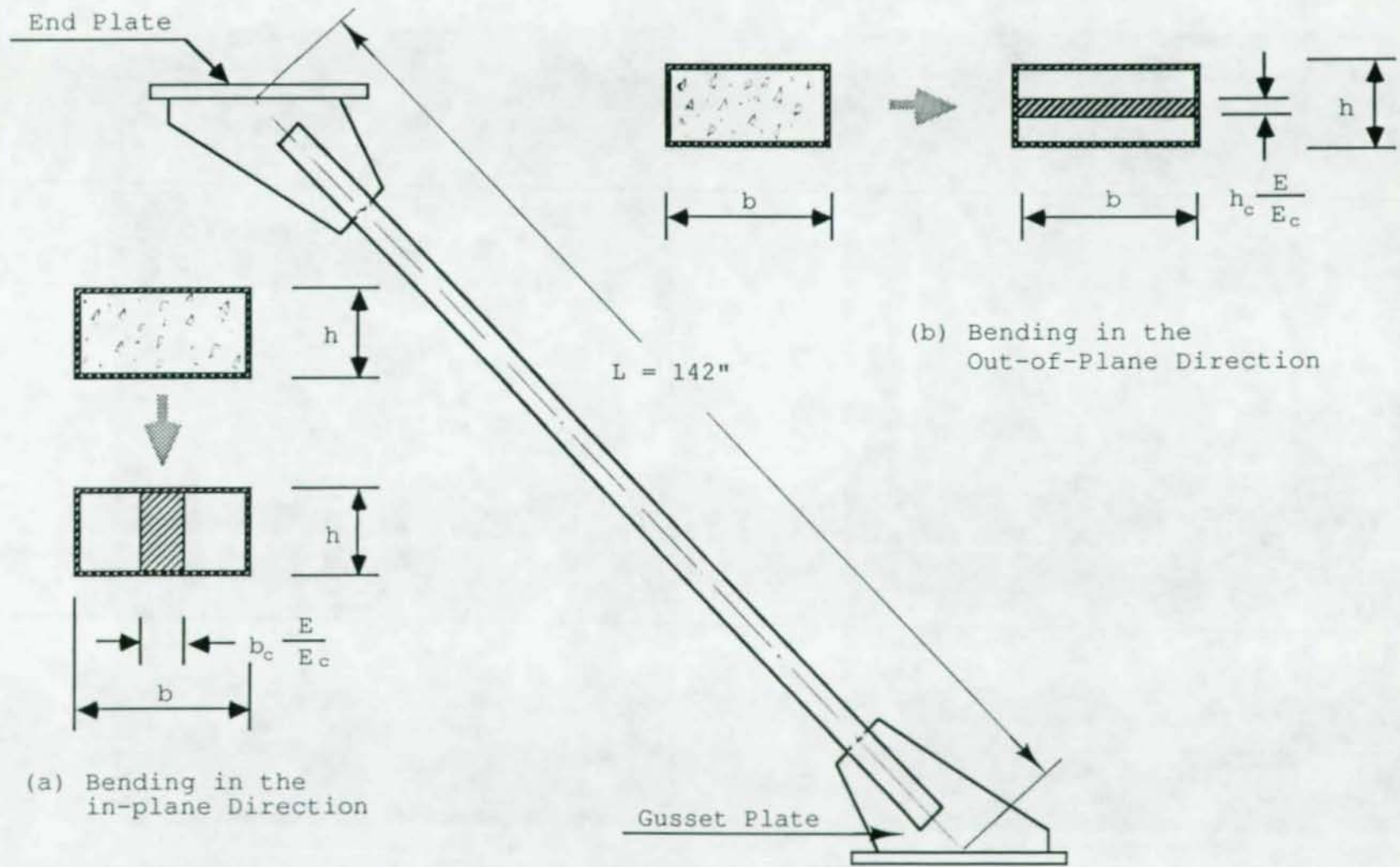
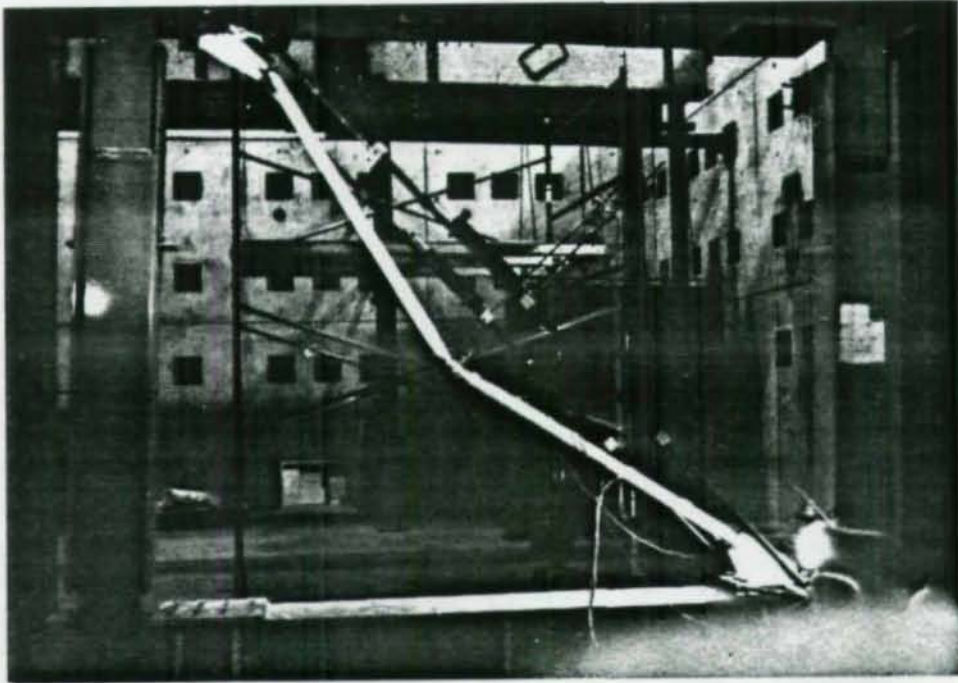
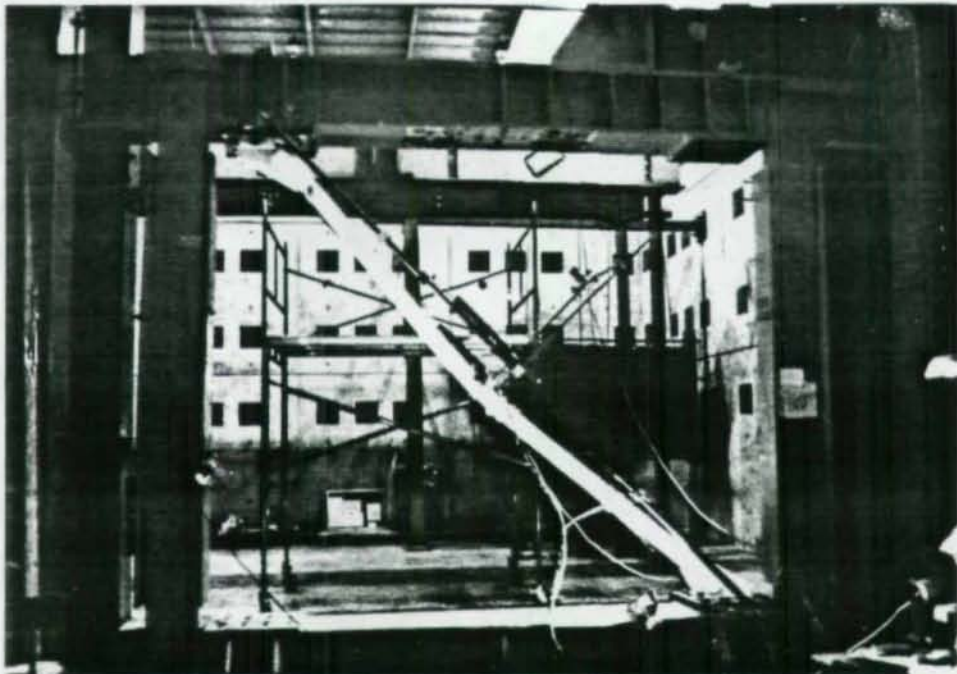


Figure 4.7 Computing Length of Specimen and Equivalent Sections

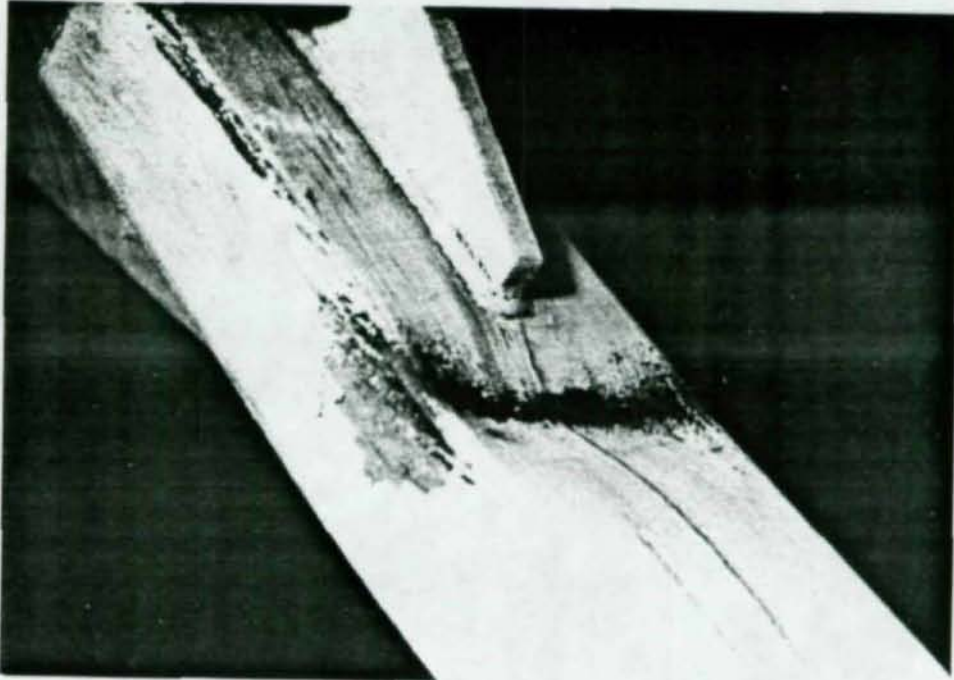


(a) Hollow Specimen T633H

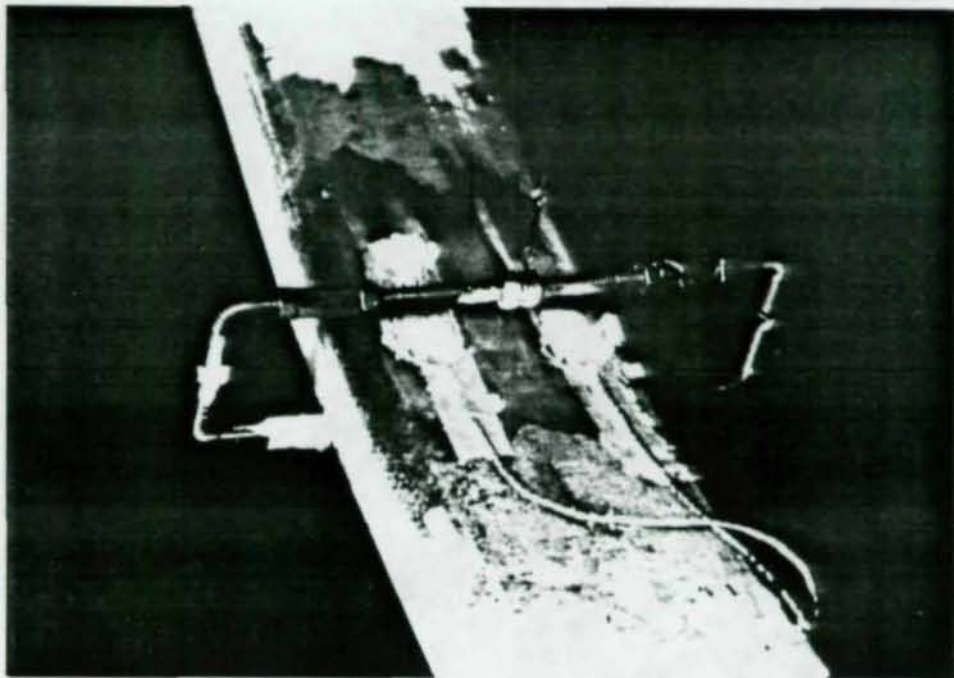


(b) Concrete-Filled Specimen T633C6

Figure 4.8 Overall Buckling Modes after Formation of Plastic Hinges

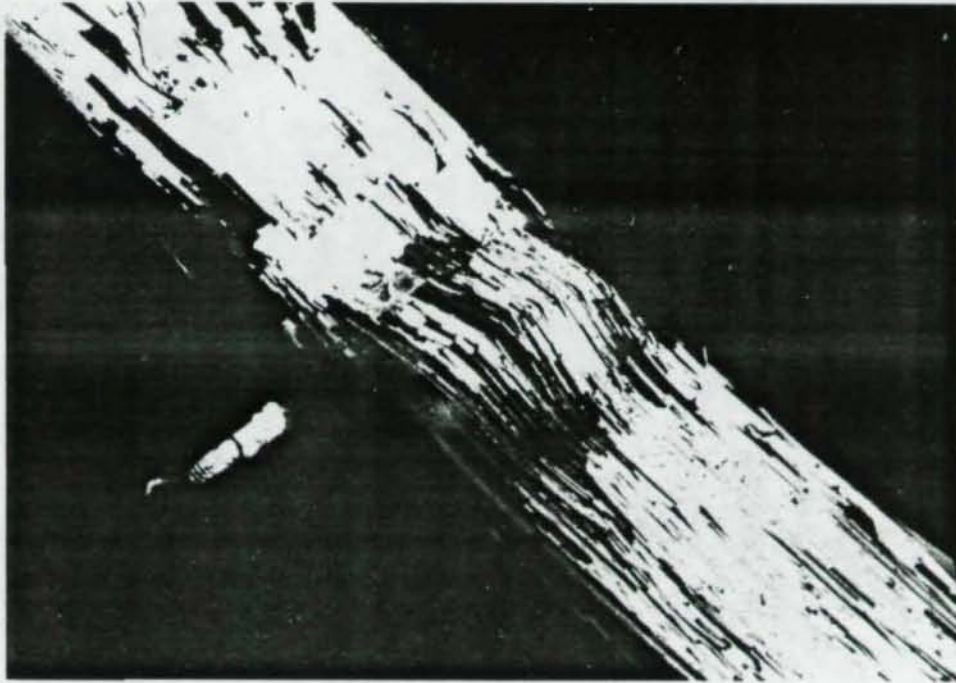


(a) Specimen T633H with  $b/t$  of 30

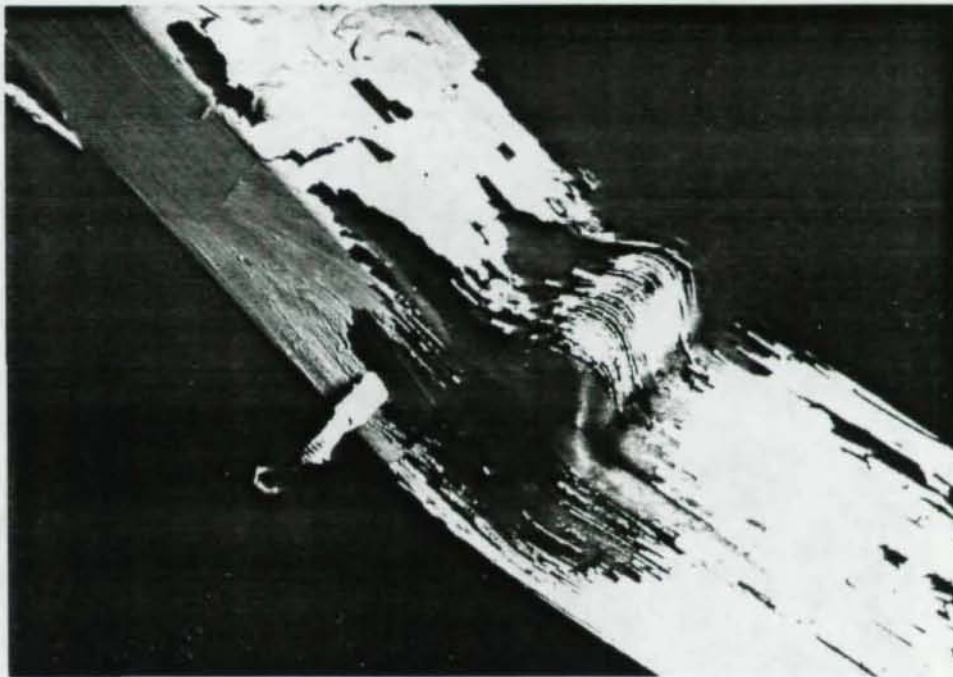


(b) Specimen T424H with  $b/t$  of 14

Figure 4.9 Local Buckling Modes for Hollow Specimens

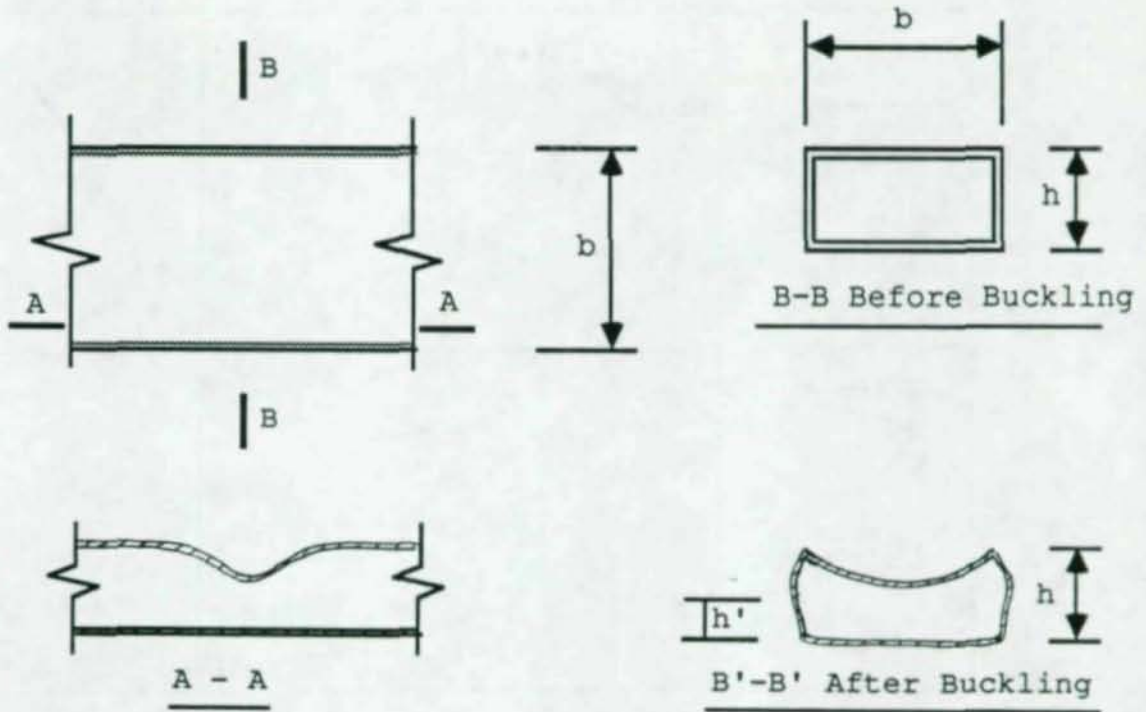


(a) First Local Buckling on Broad Sides

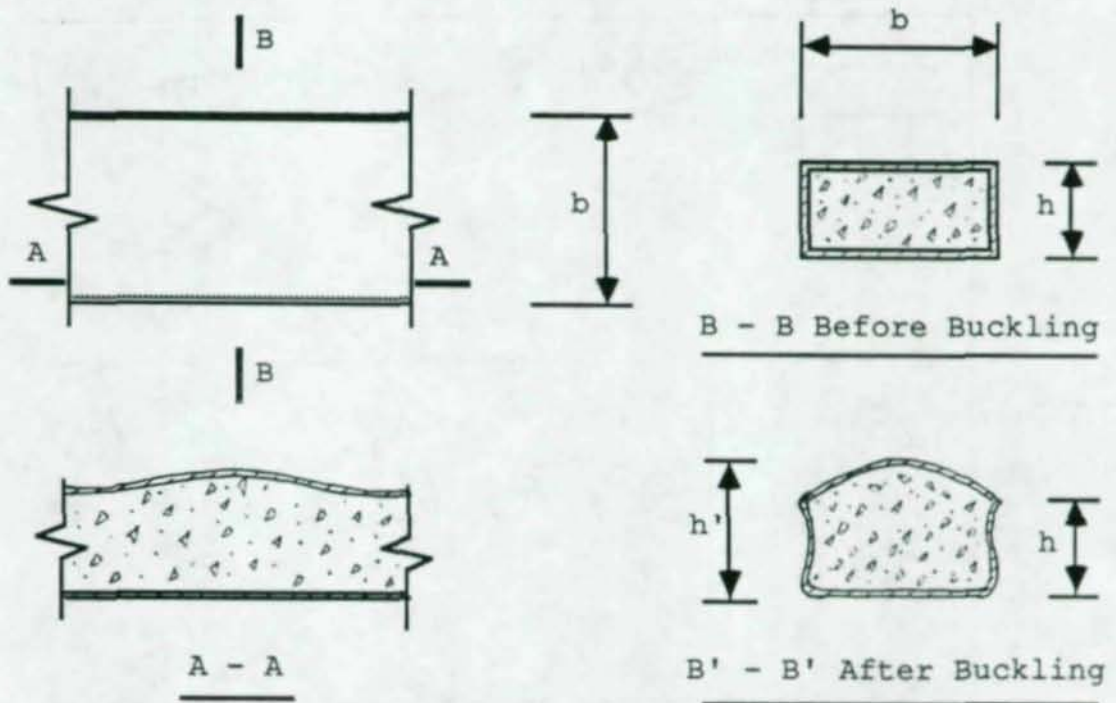


(b) Second Local Buckling on Narrow Sides

Figure 4.10 Local Buckling in Concrete-Filled Specimen T633C6

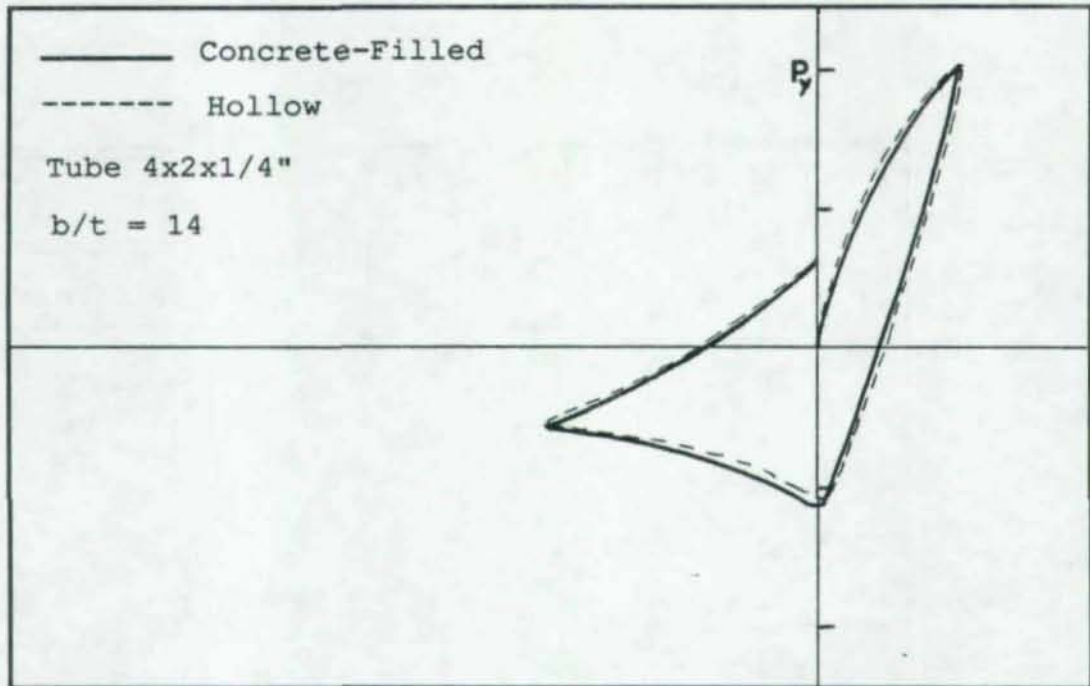


(a) Hollow Specimens

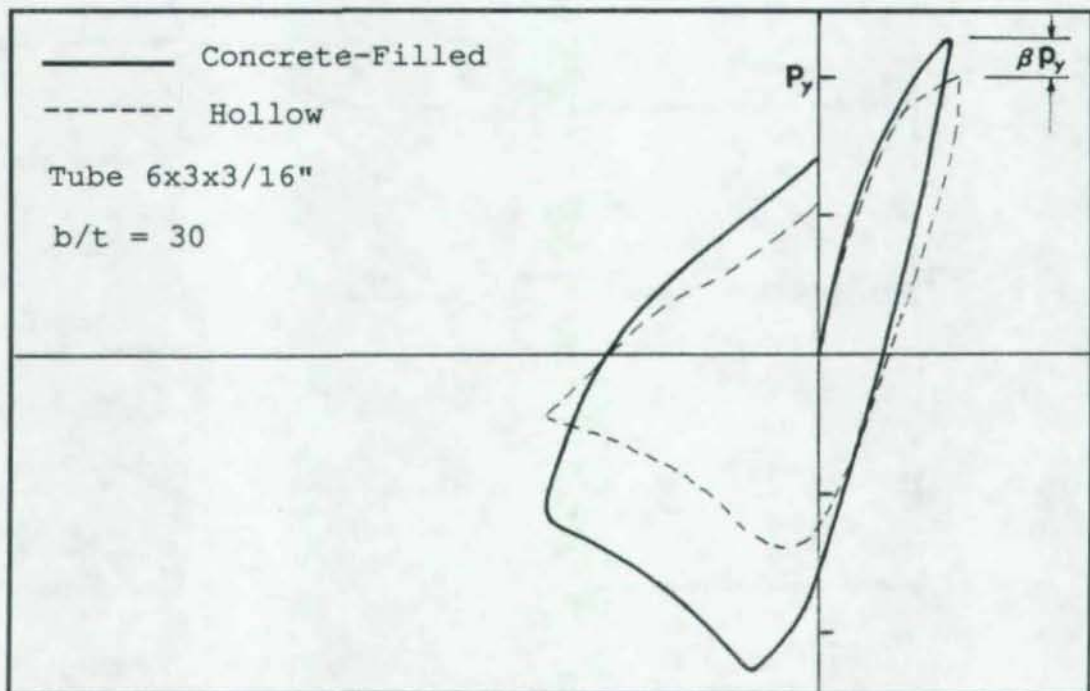


(b) Concrete-Filled Specimens

Figure 4.11 Buckled Sections Of Bracing Members



(a) Specimens T424H and T424C6



(b) Specimens T633H and T633C6

Figur 4.12 First Yield Force for Hollow and Concrete-Filled Specimens

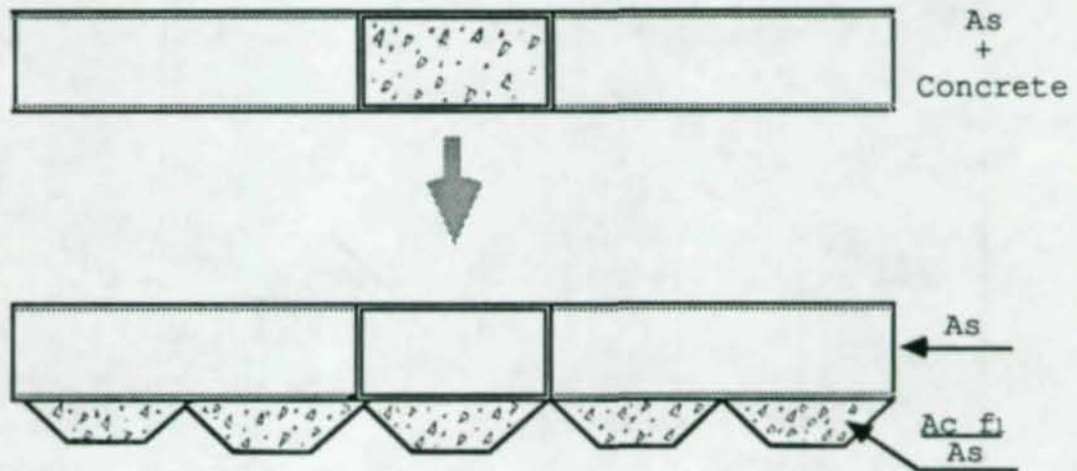


Figure 4.13 Equivalent Section of Concrete-Filled Specimen for Tension

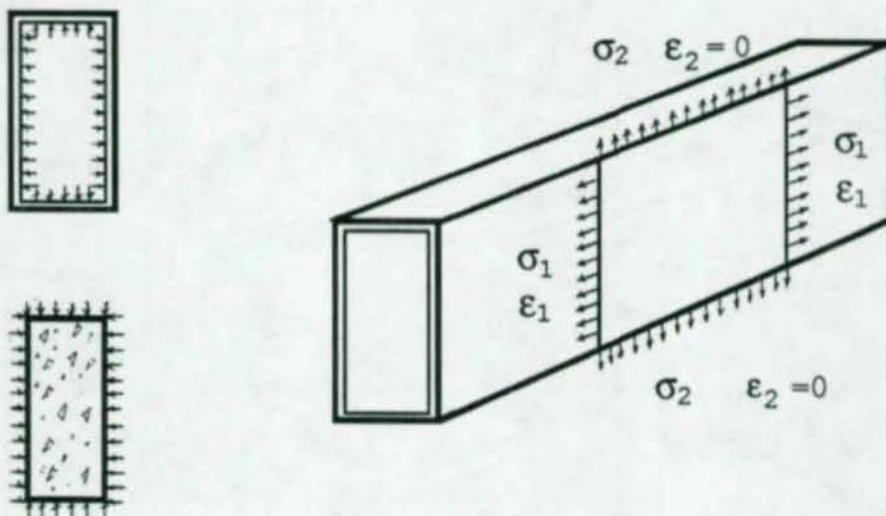


Figure 4.14 Stress State of One Side of Tube Wall Subjected to Lateral Restraint from Concrete under Tension

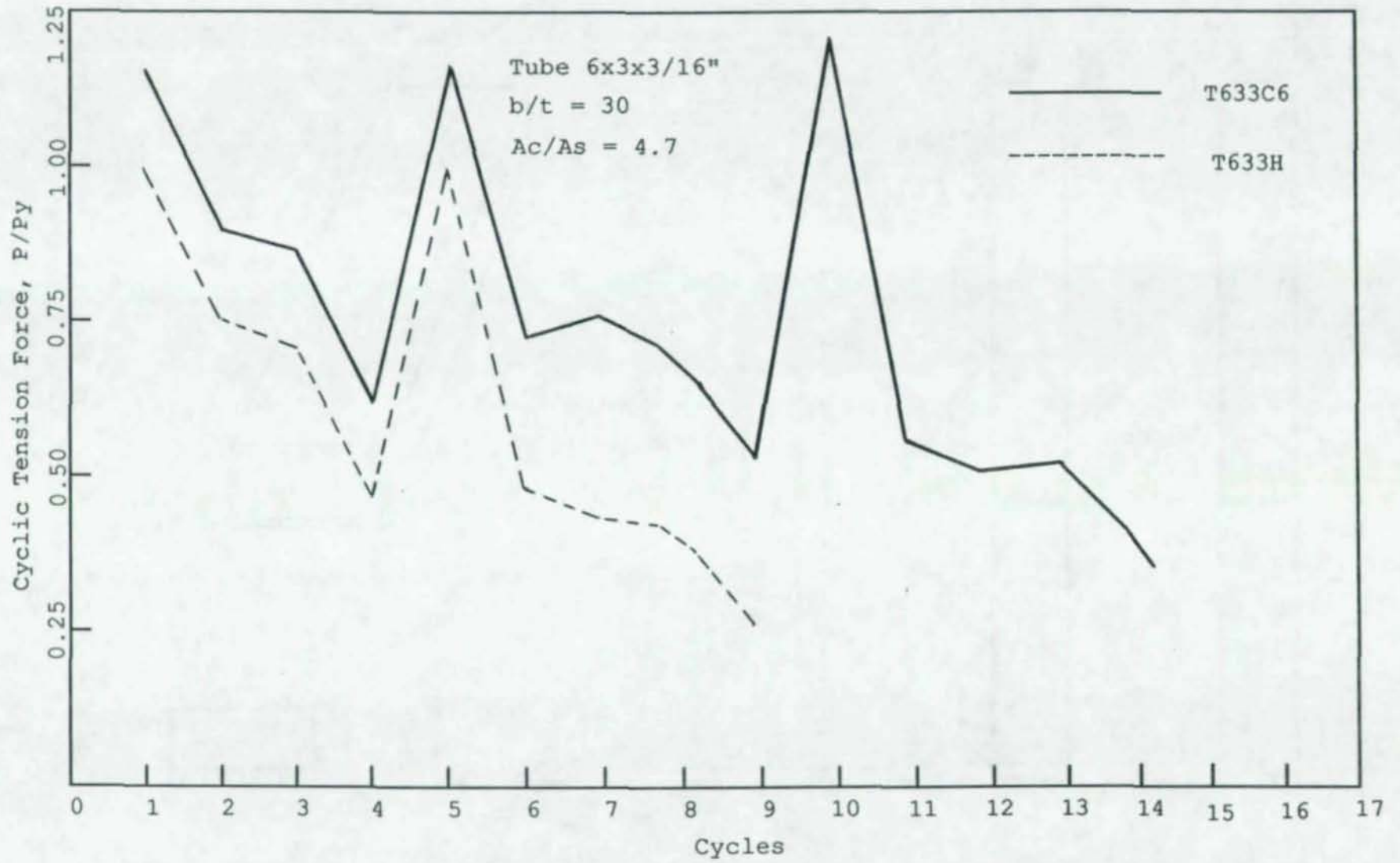


Figure 4.15(a) Cyclic Tension Forces for Specimens T633H and T633C6

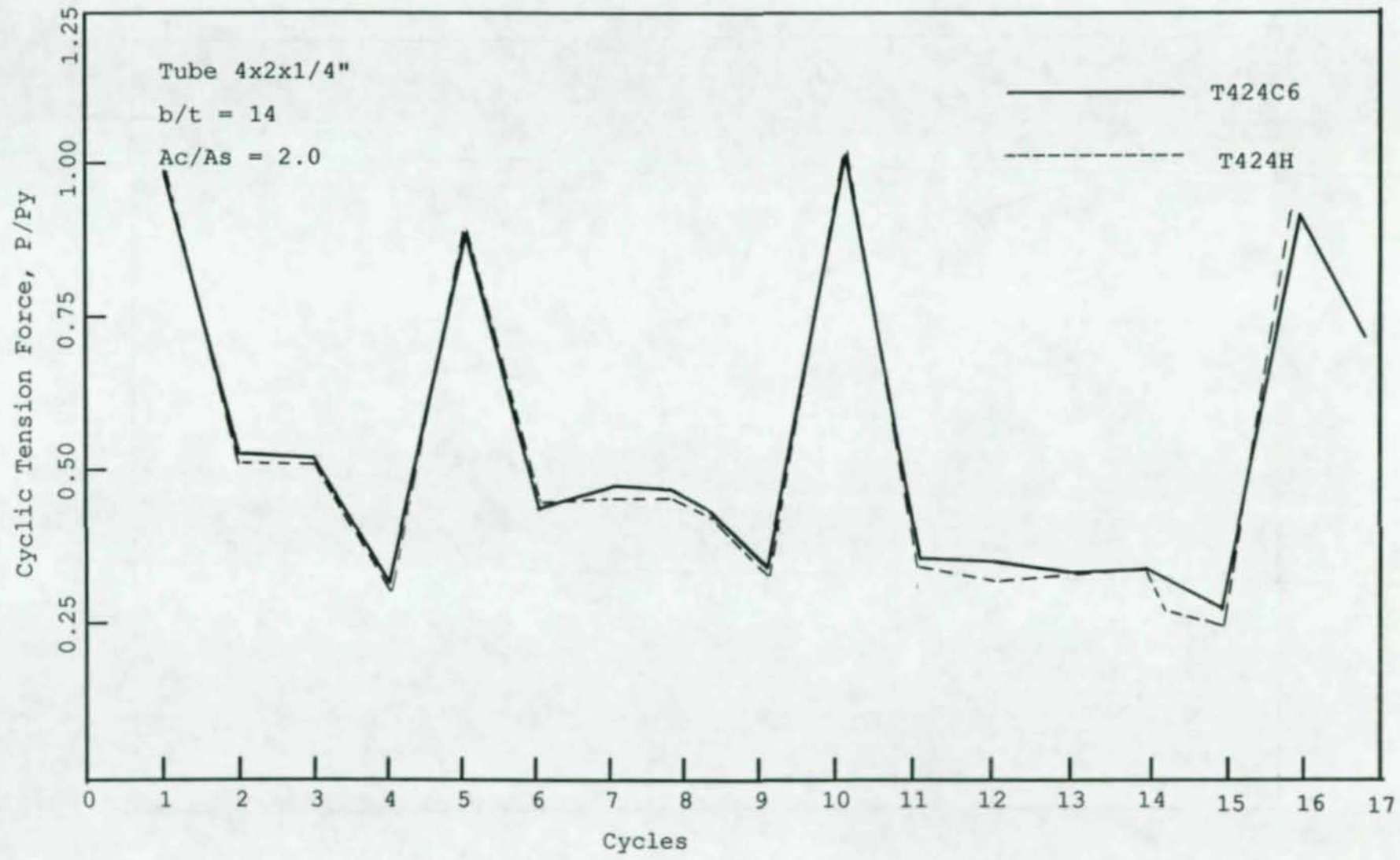


Figure 4.15(b) Cyclic Tension Forces for Specimens T424H and T424C6

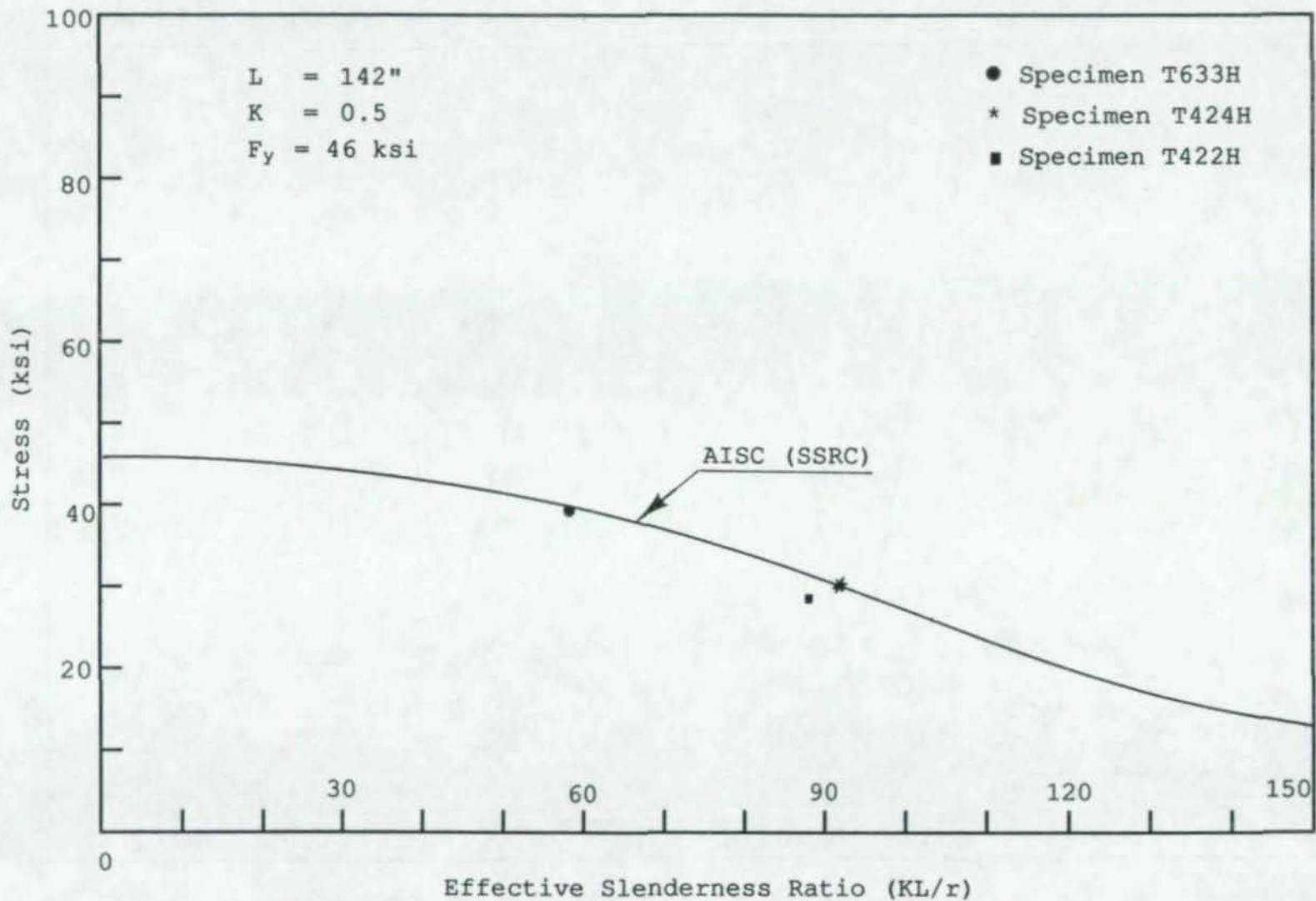


Figure 4.16 Measured Buckling Stress in the First Cycle for Hollow Specimens

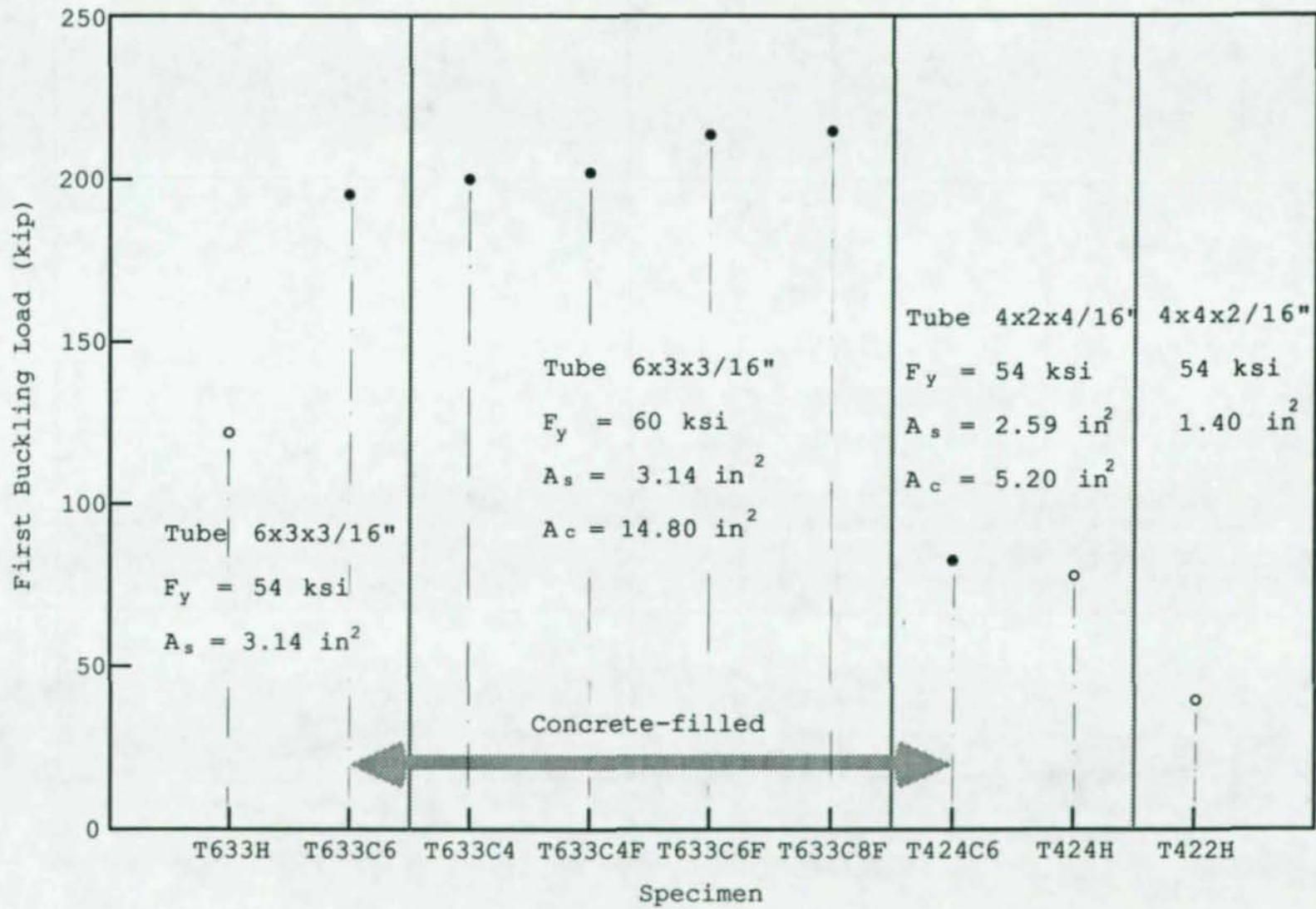


Figure 4.17 First Buckling Load from Tests for all Specimens

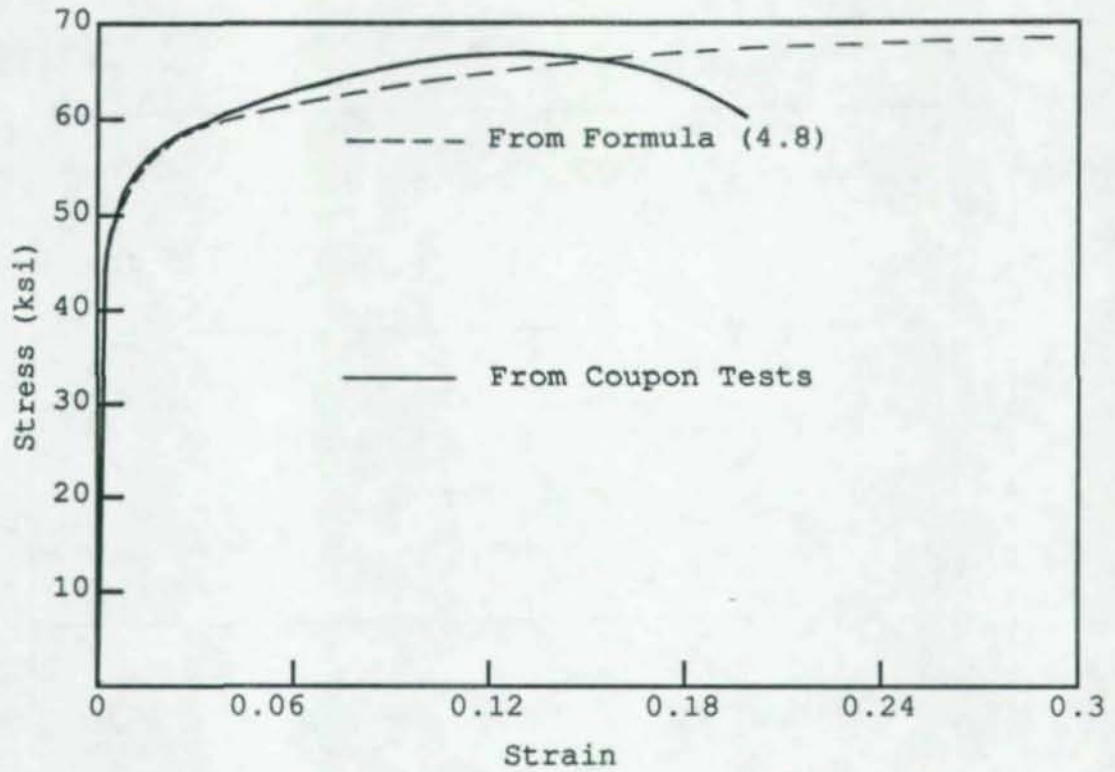


Figure 4.18 Typical Stress-Strain Relationship for Tubes

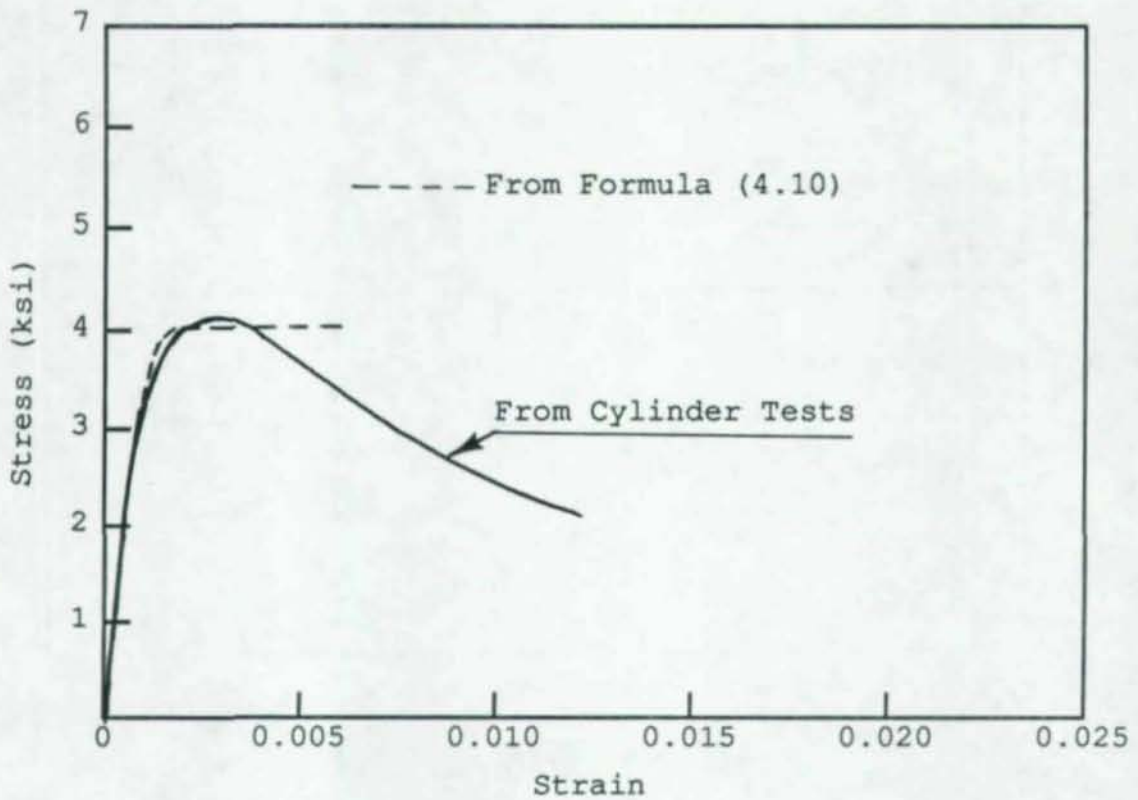


Figure 4.19 Typical Stress-Strain Relationship for Concrete

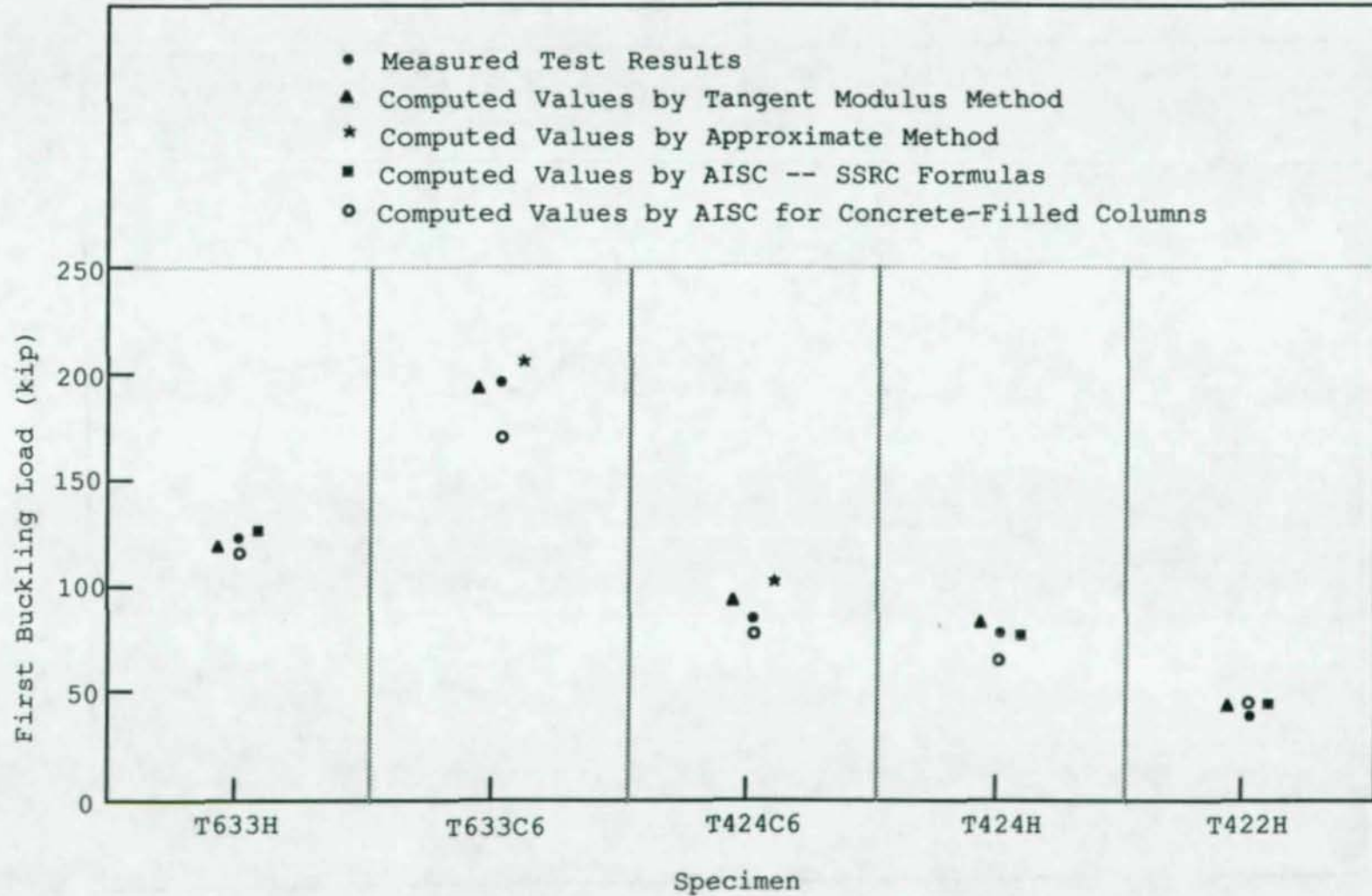
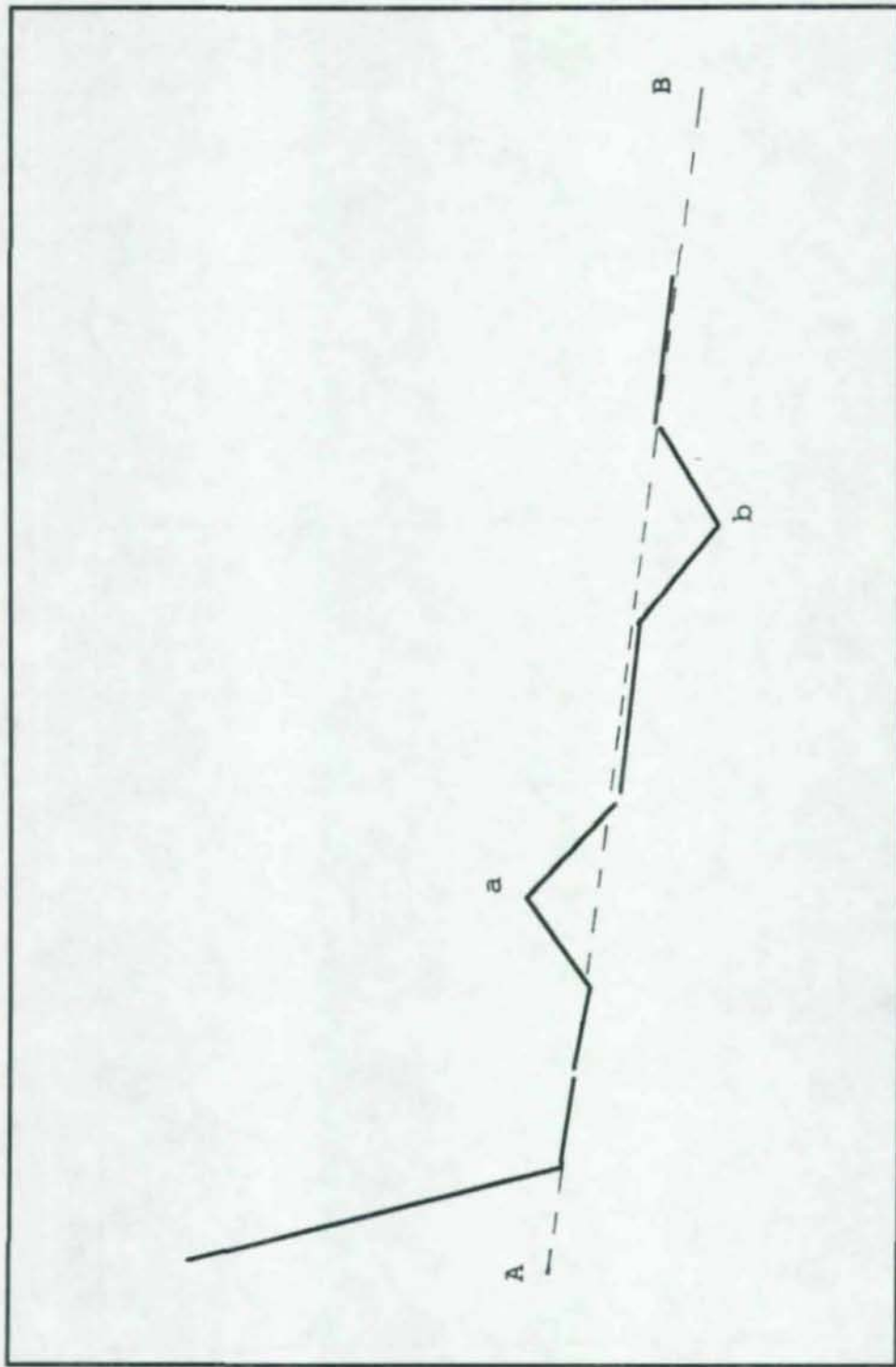


Figure 4.20 First Buckling Load Comparison between Computed values and Test Results



Cyclic Compression Force

Cycle

Figure 4.21 Definition of Drop of Cyclic Compression Force

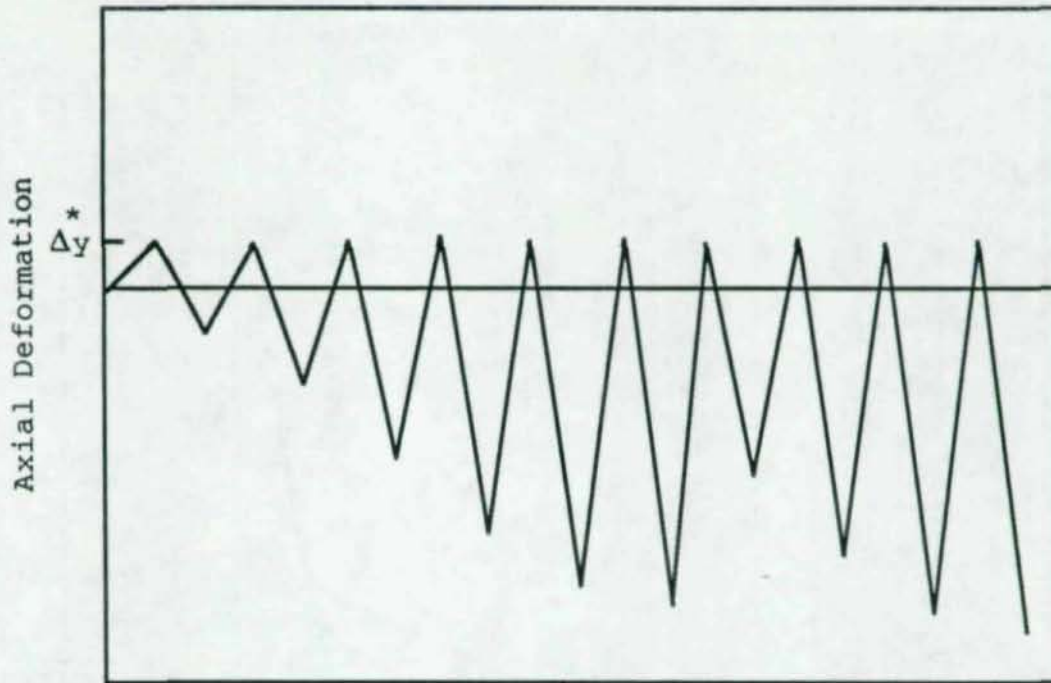


Figure 4.22 Suggested Loading History for Producing Steady Drop of Cyclic Compression Force

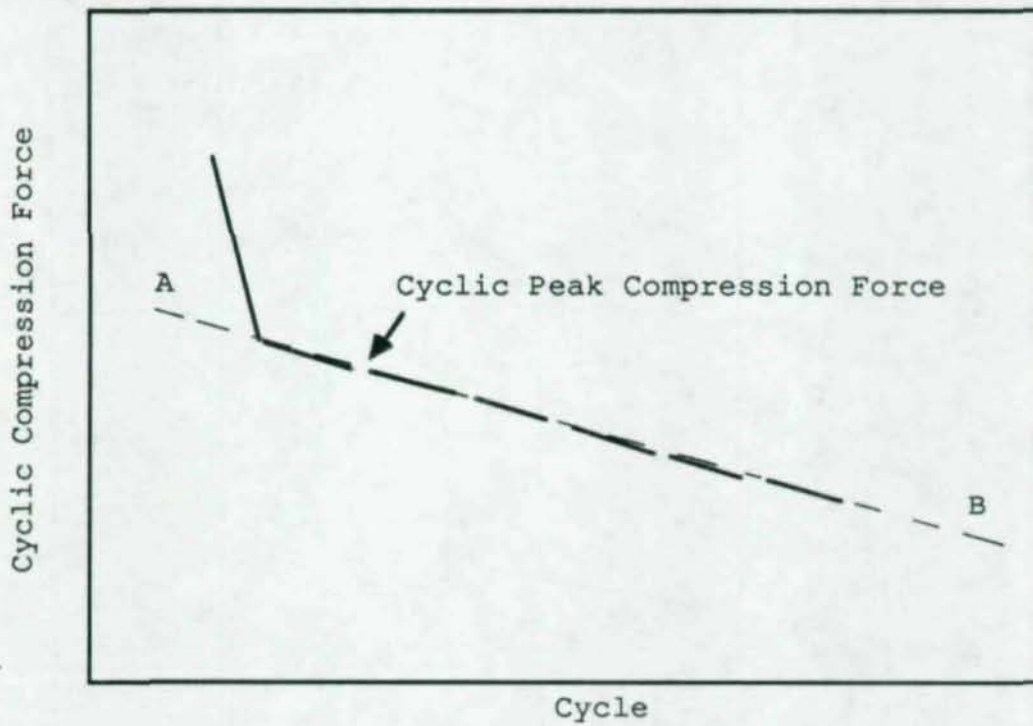


Figure 4.23 Expected Cyclic Peak Compression Force Drop Line

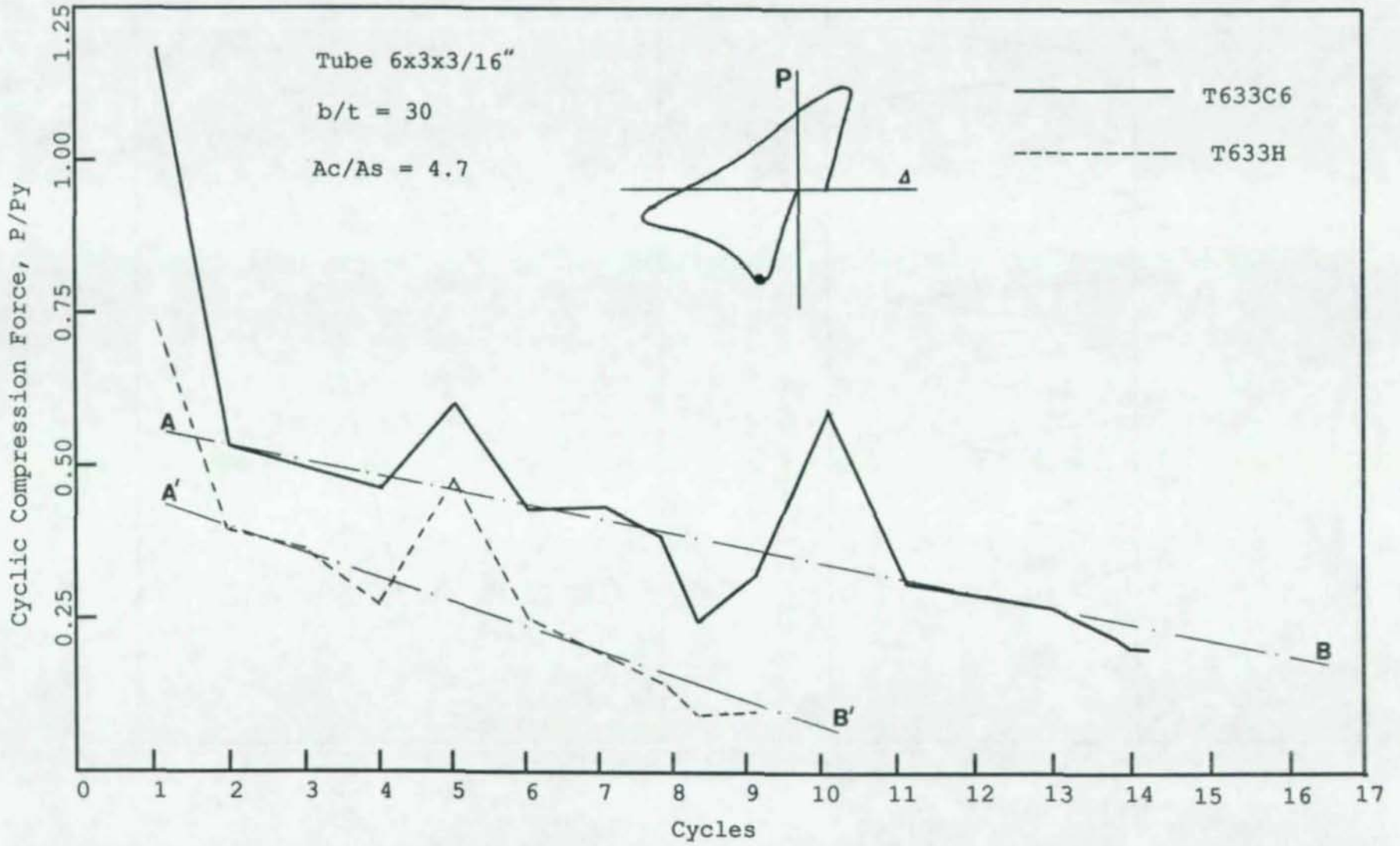


Figure 4.24 Cyclic Compression Force for Specimens T633H and T633C6

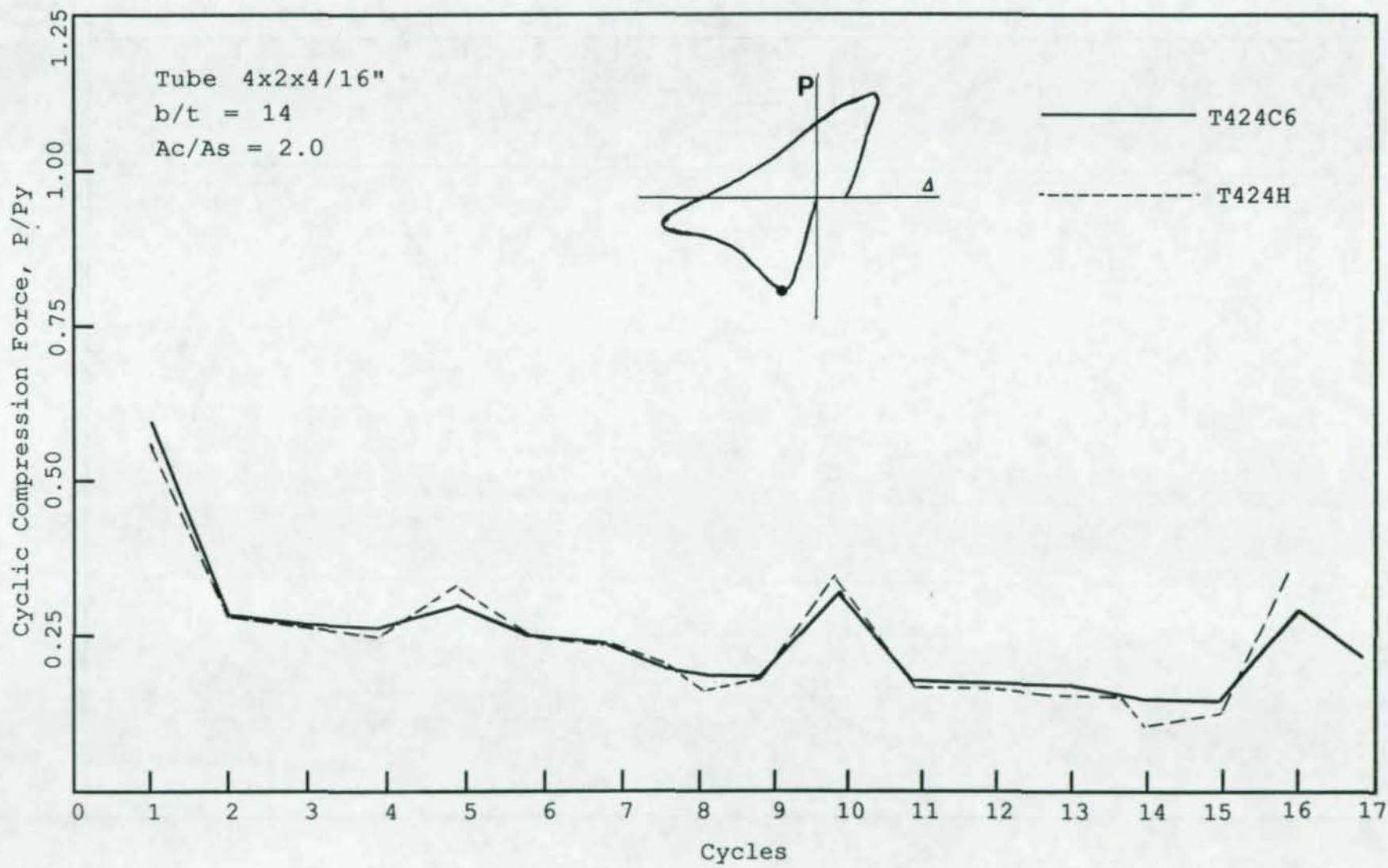


Figure 4.25 Cyclic Compression Force for Specimens T424H and T424C6

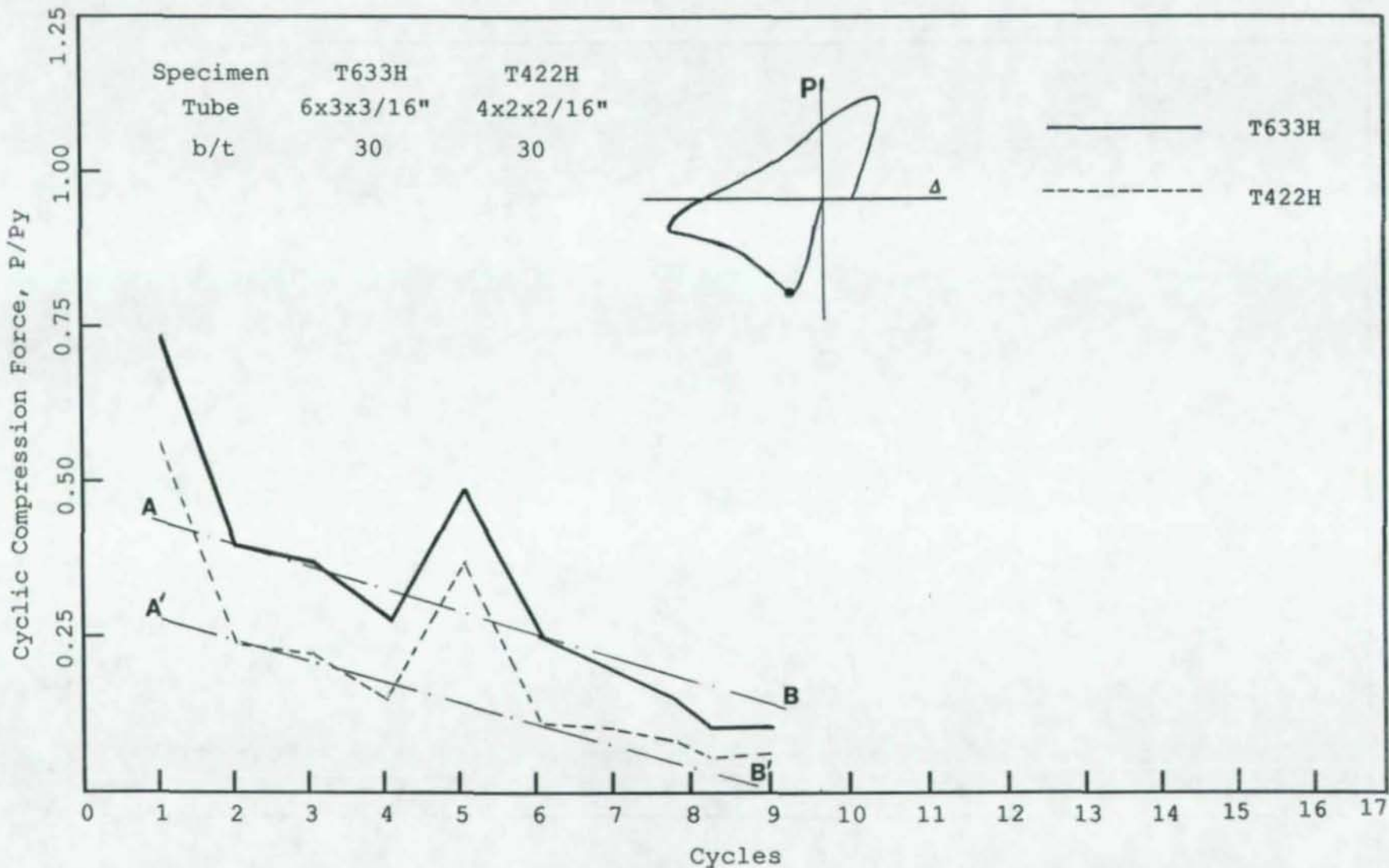


Figure 4.26 Cyclic Compression Force for Specimens T633H and T422H

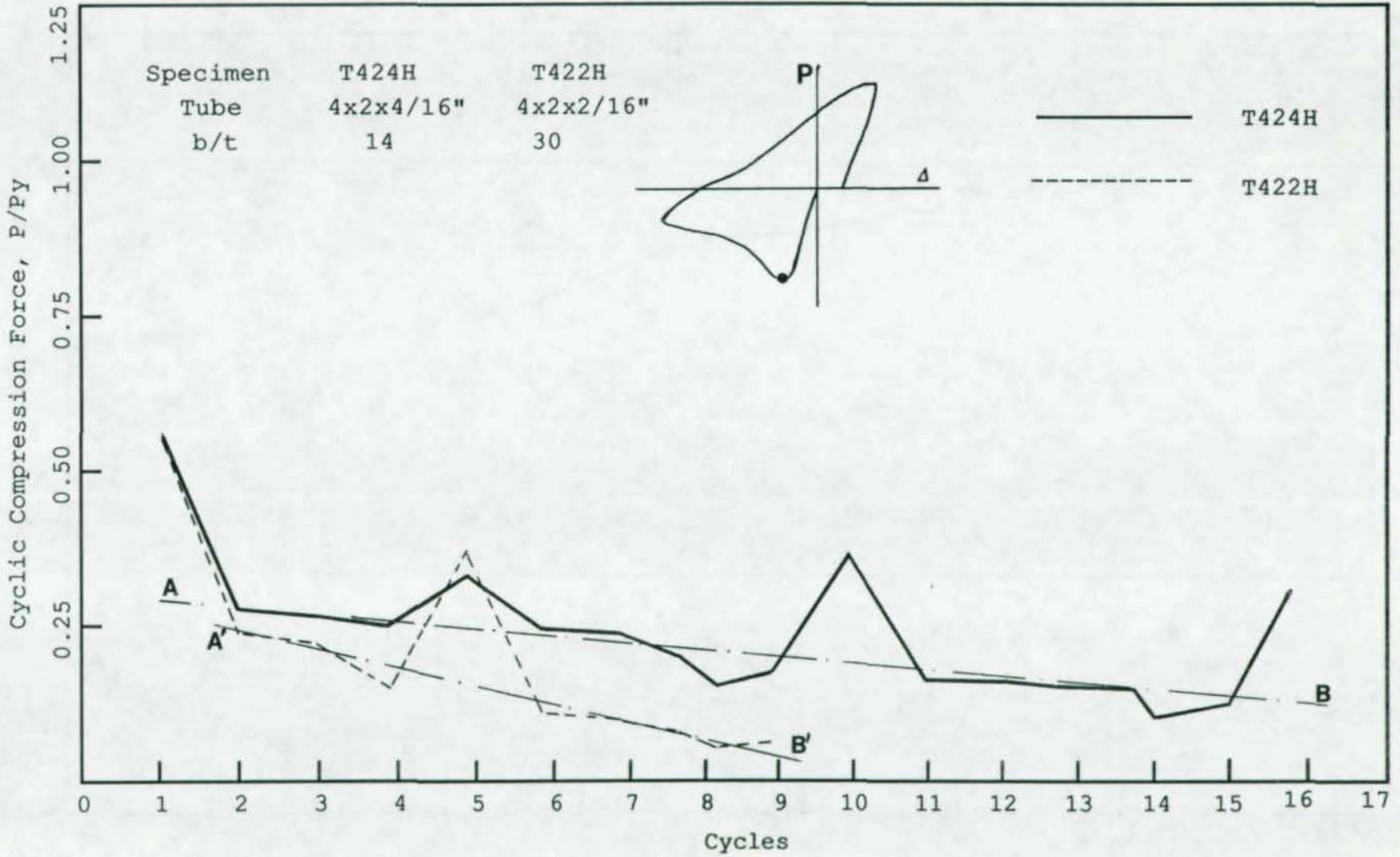


Figure 4.27 Cyclic Compression Force for Specimens T424H and T422H

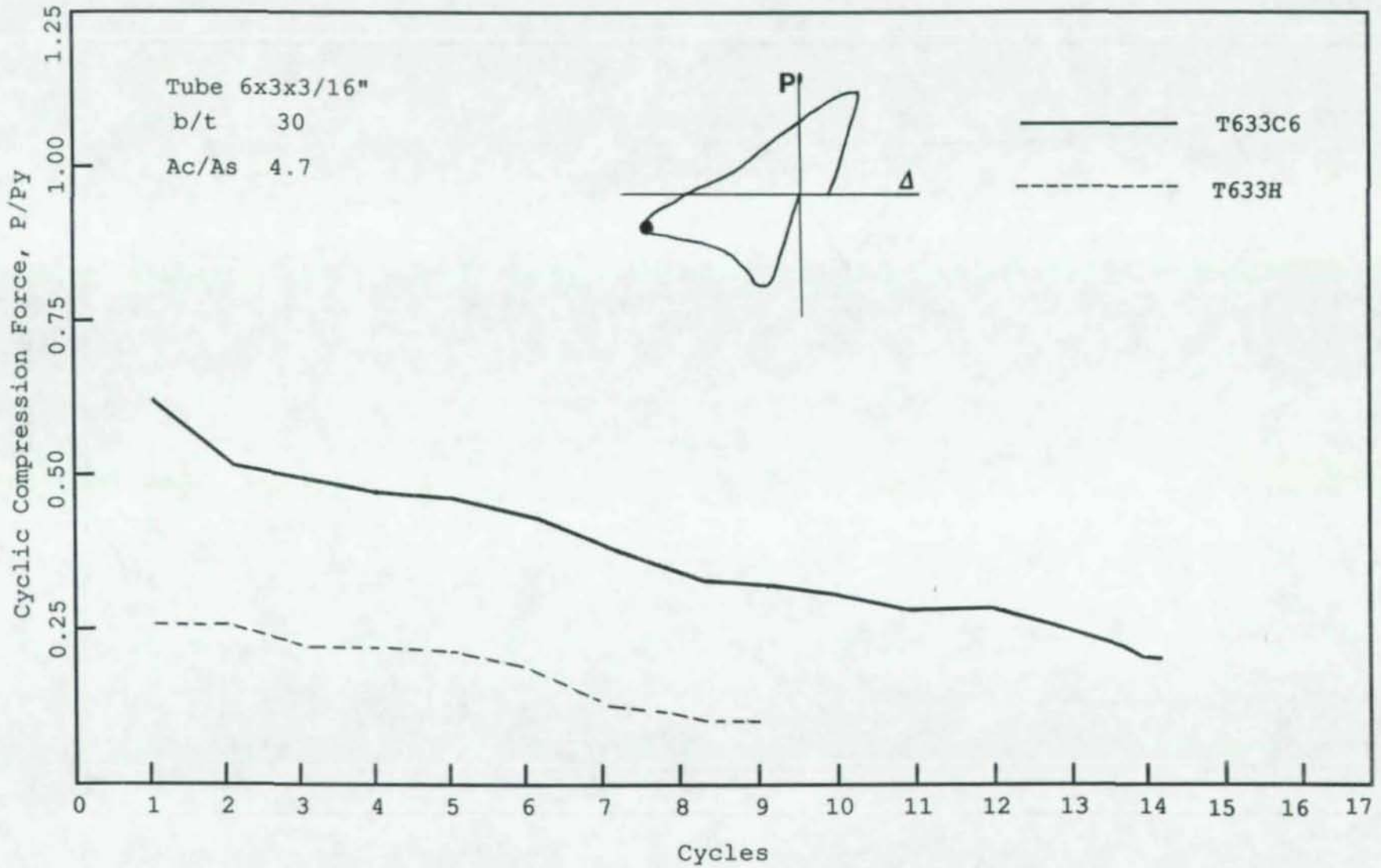


Figure 4.28 Cyclic Compression Force at Reversal Point for Specimens T633C6 and T633H

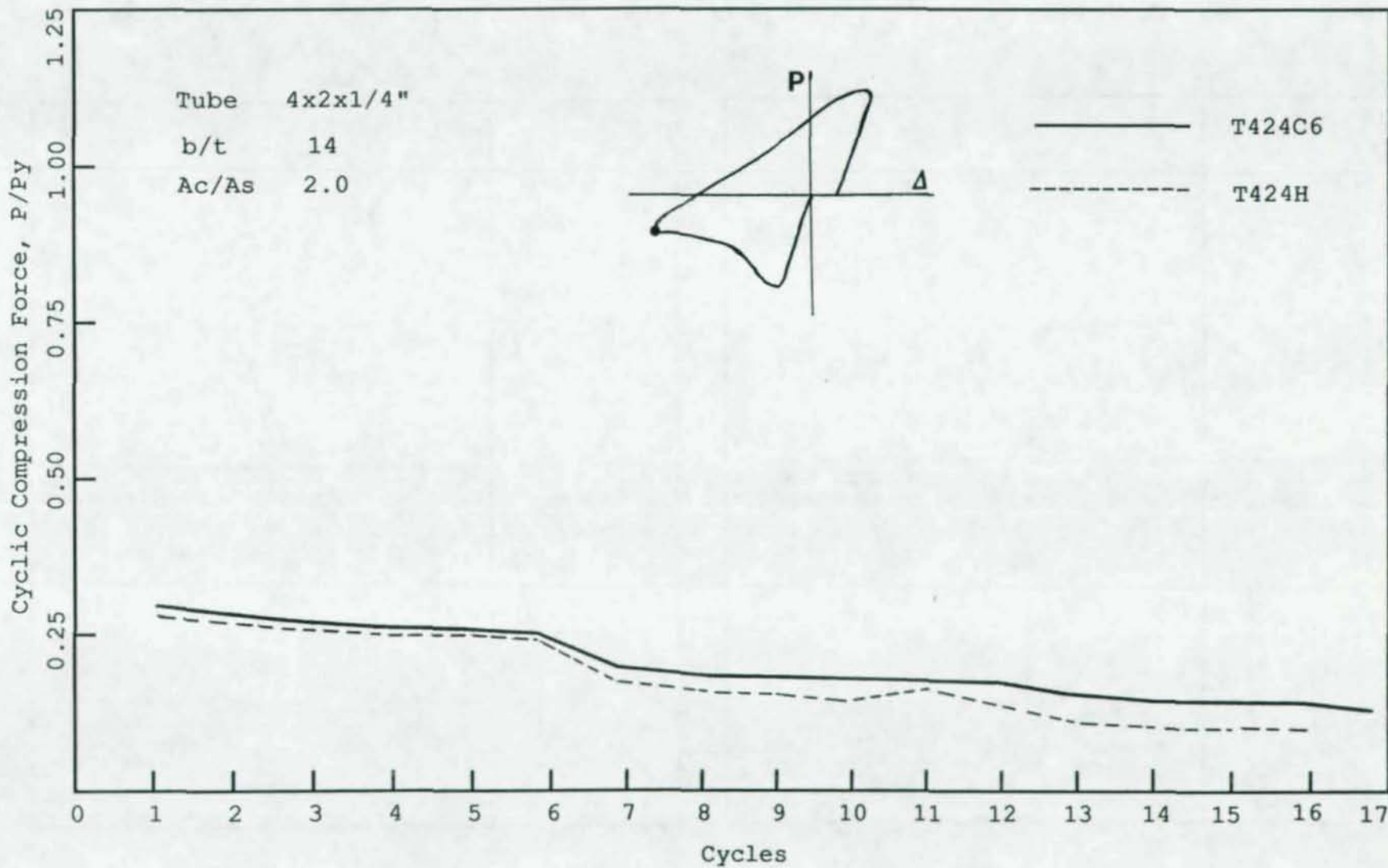


Figure 4.29 Cyclic Compression Force at Reversal Point for Specimens T424C6 and T424H

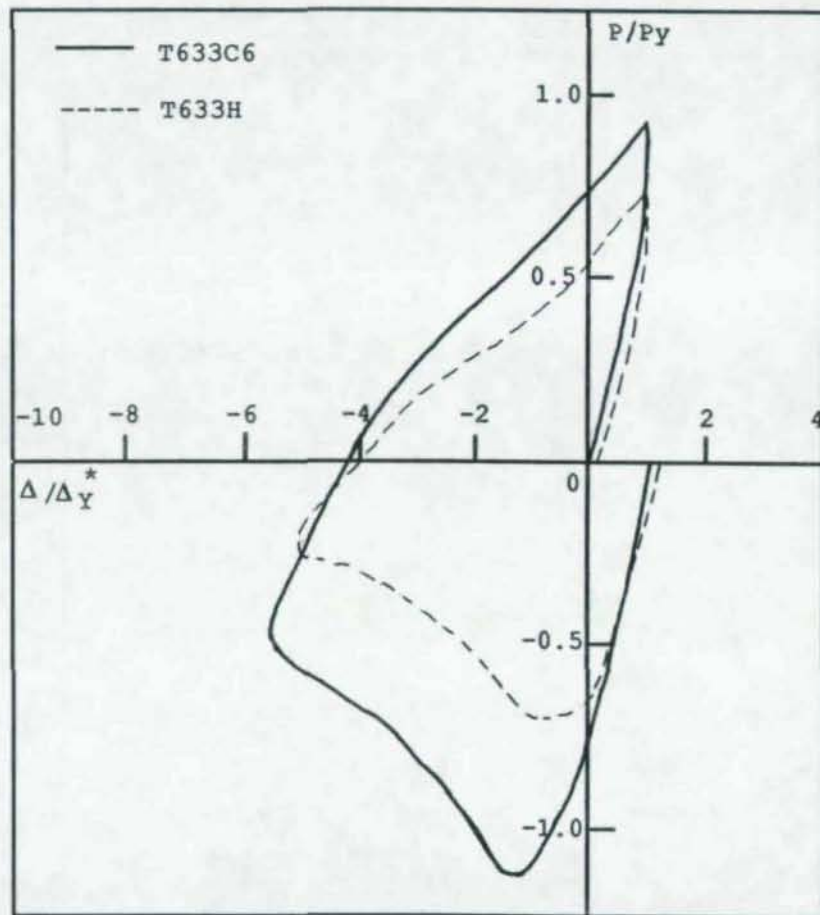


Figure 4.30 Hysteresis Loops for Specimens T633H and T633C6 in Cycle 1

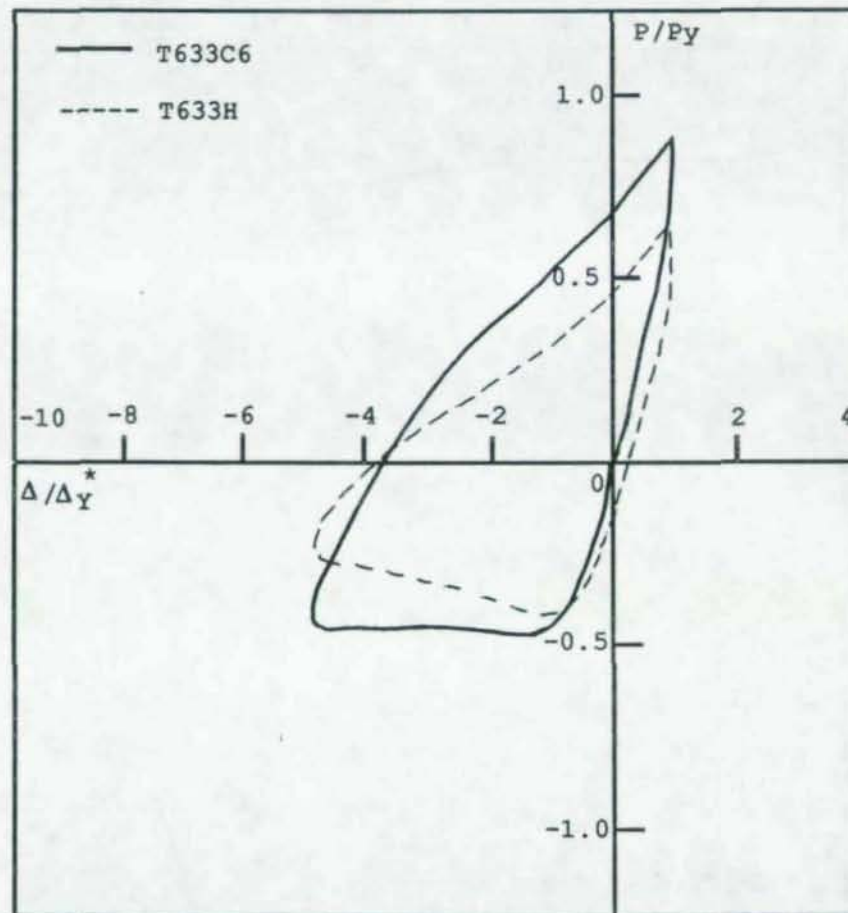


Figure 4.31 Hysteresis Loops for Specimens T633H and T633C6 in Cycle 2

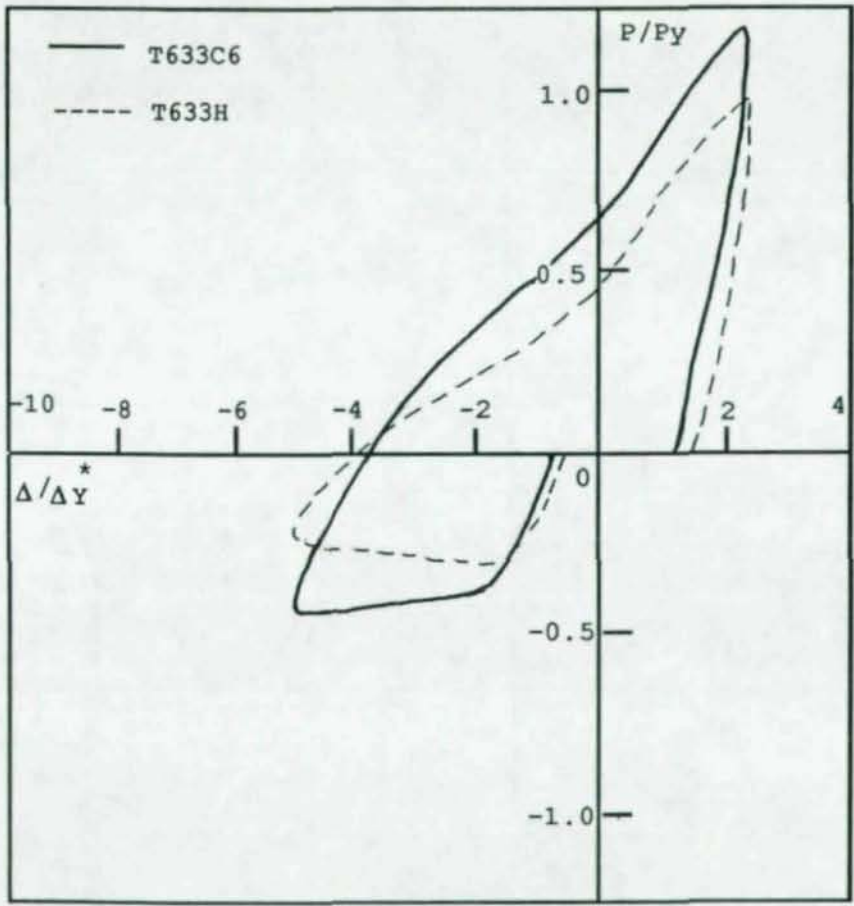


Figure 4.32 Hysteresis Loops for Specimens T633H and T633C6 in Cycle 4

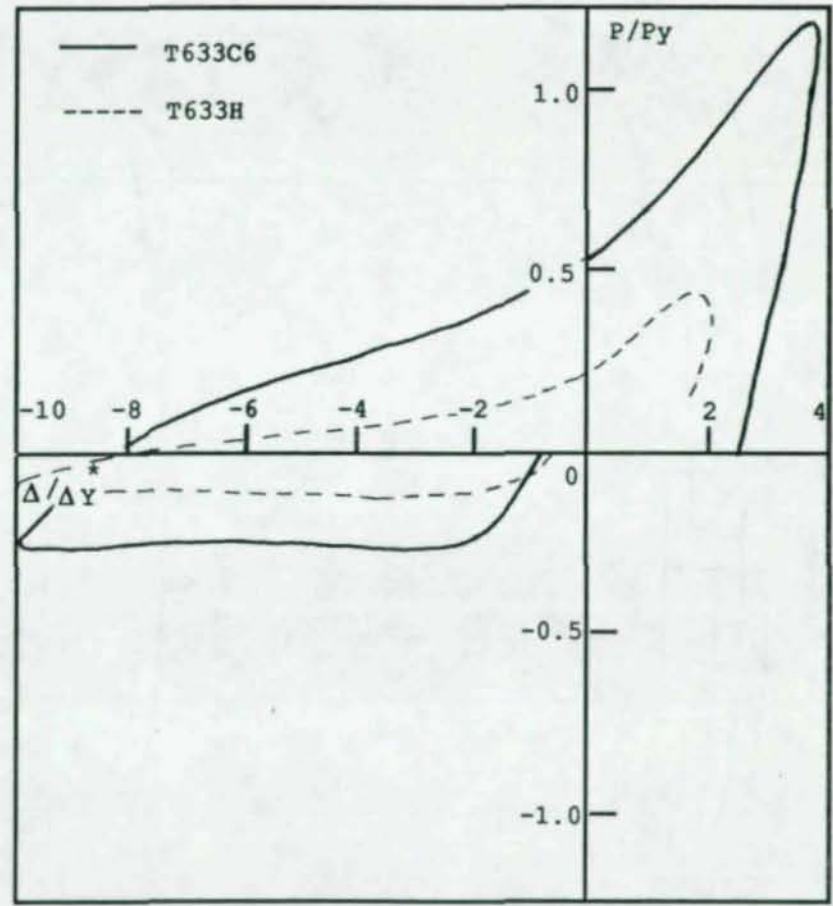


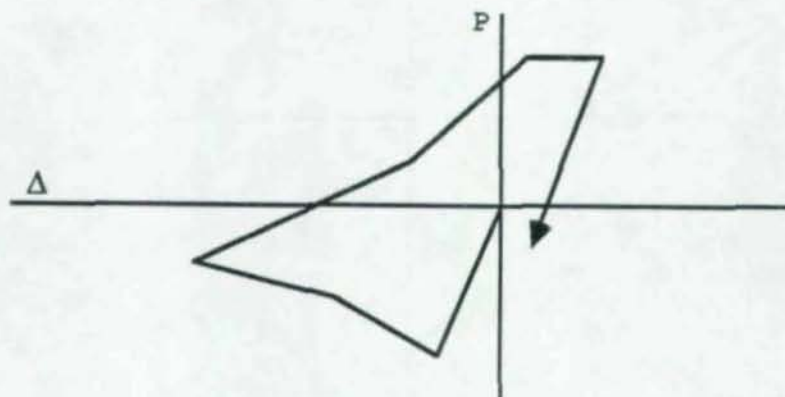
Figure 4.33 Hysteresis Loops for Specimens T633H and T633C6 in Cycle 9



(a) Finite Element Method



(b) Physical Theory Model



(c) Phenomenological Model

Figure 5.1 Different Types of Analytical models for Steel Bracing Members

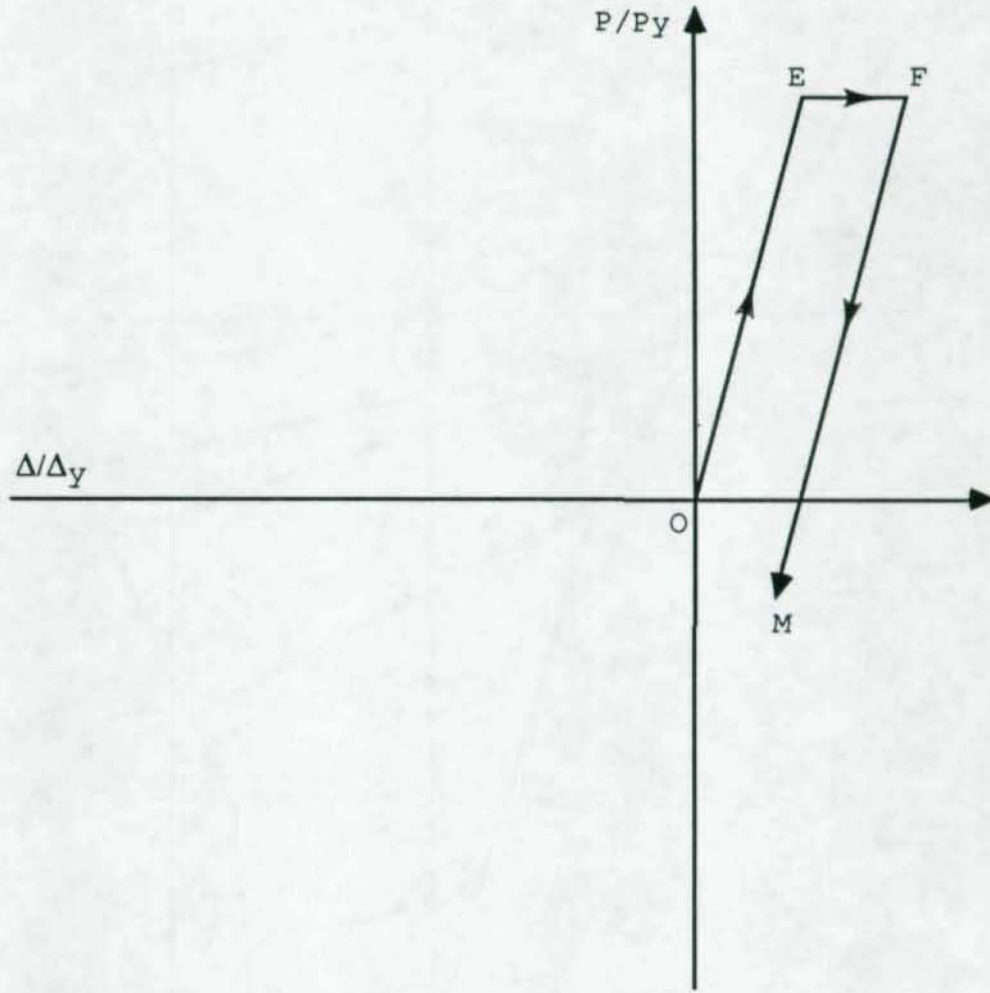


Figure 5.2 Initial Tensile Loading and Unloading Path

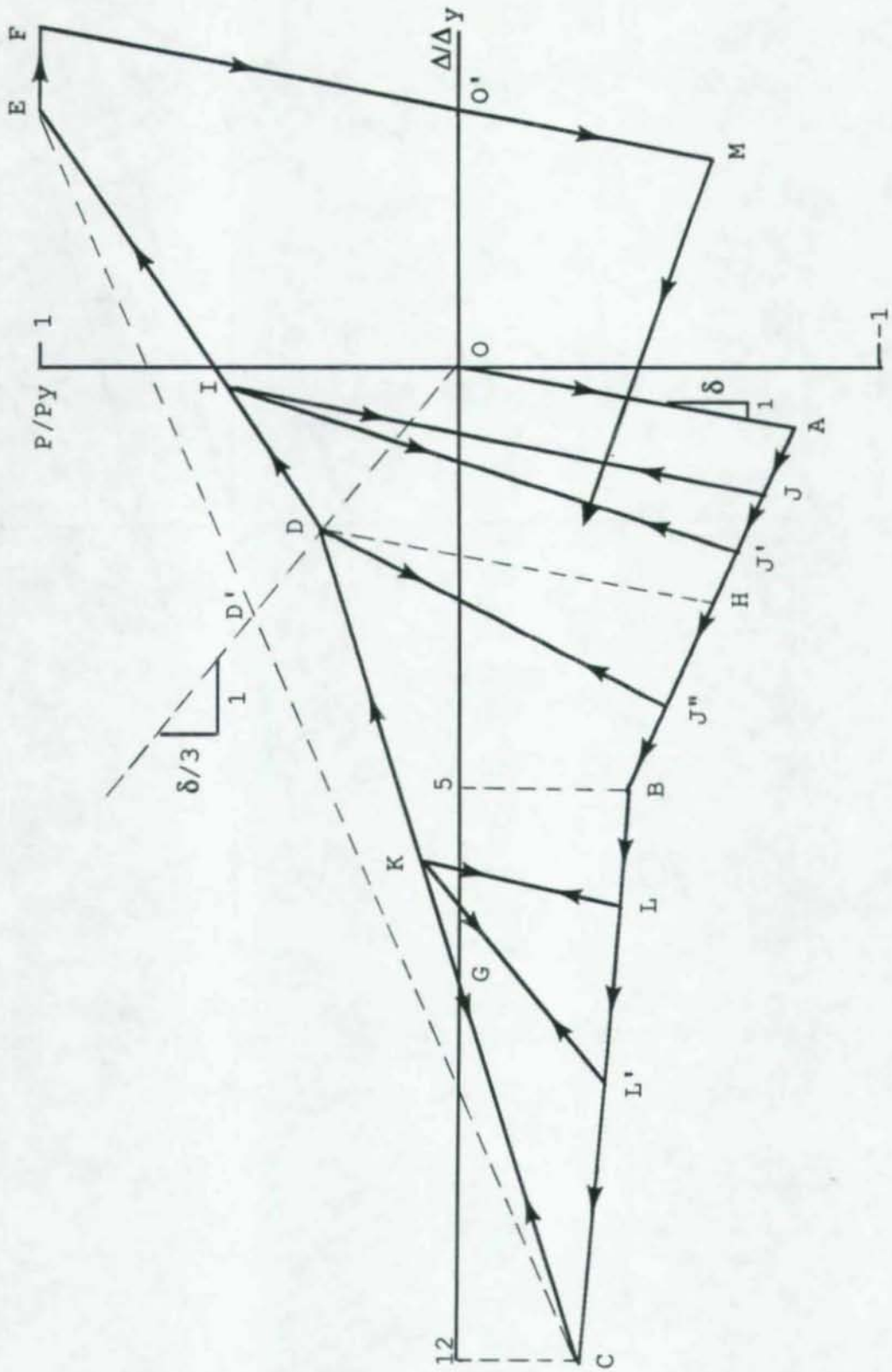


Figure 5.3 Jain's Hysteresis Model for Steel Bracing Members

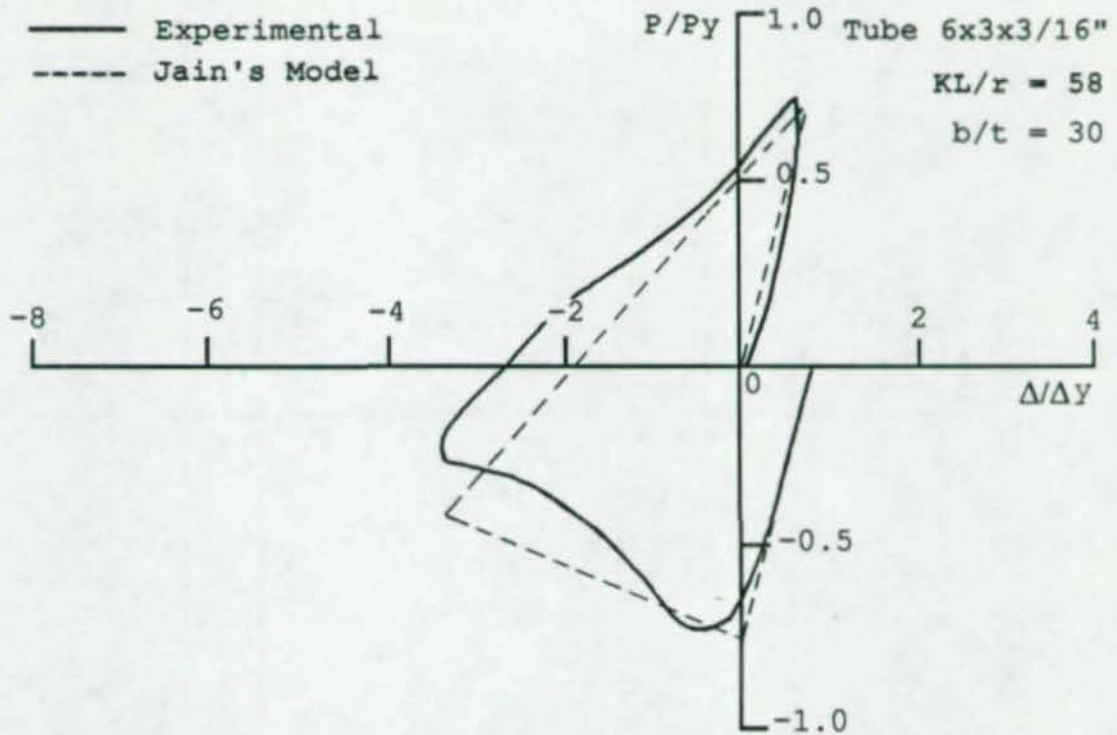


Figure 5.4 Comparison with Jain's Hysteresis Model for Specimen T633H, Cycle 1

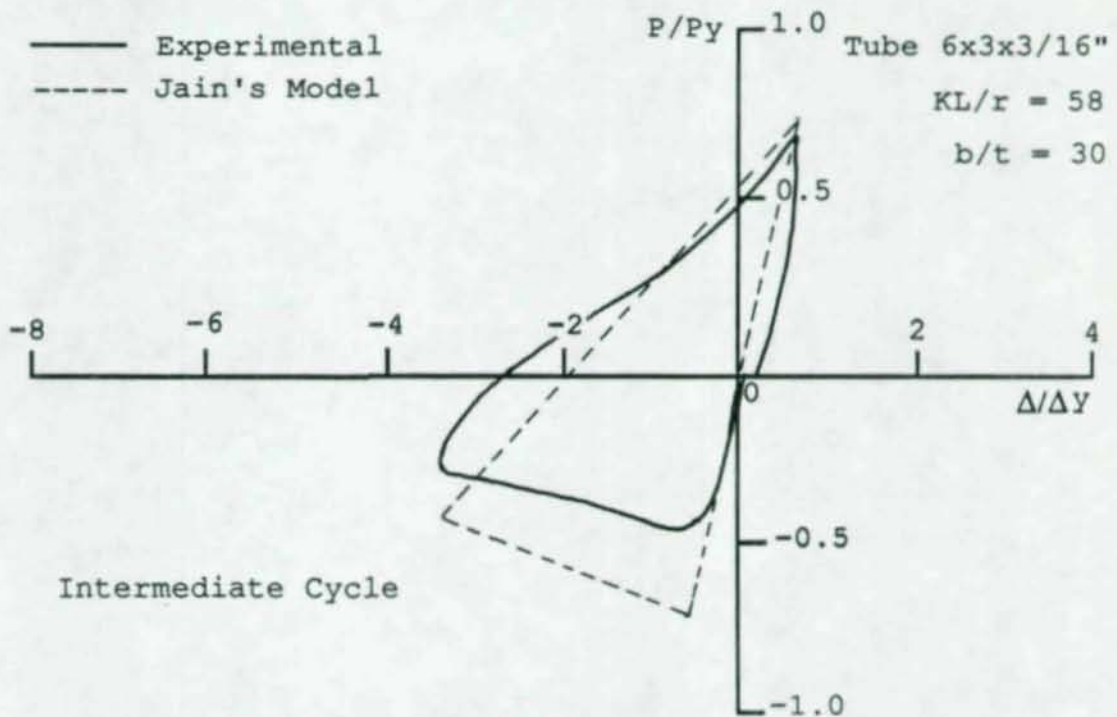


Figure 5.5 Comparison with Jain's Hysteresis Model for Specimen T633H, Cycle 2

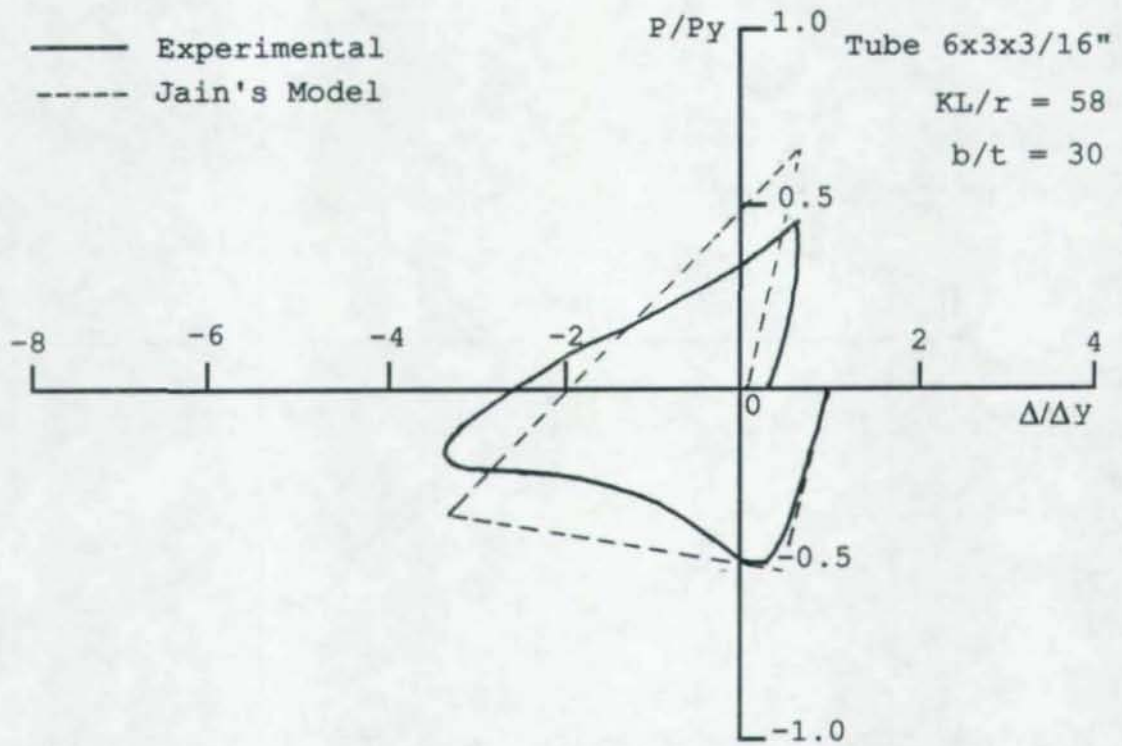


Figure 5.6 Comparison with Jain's Hysteresis Model for Specimen T633H, Cycle 5

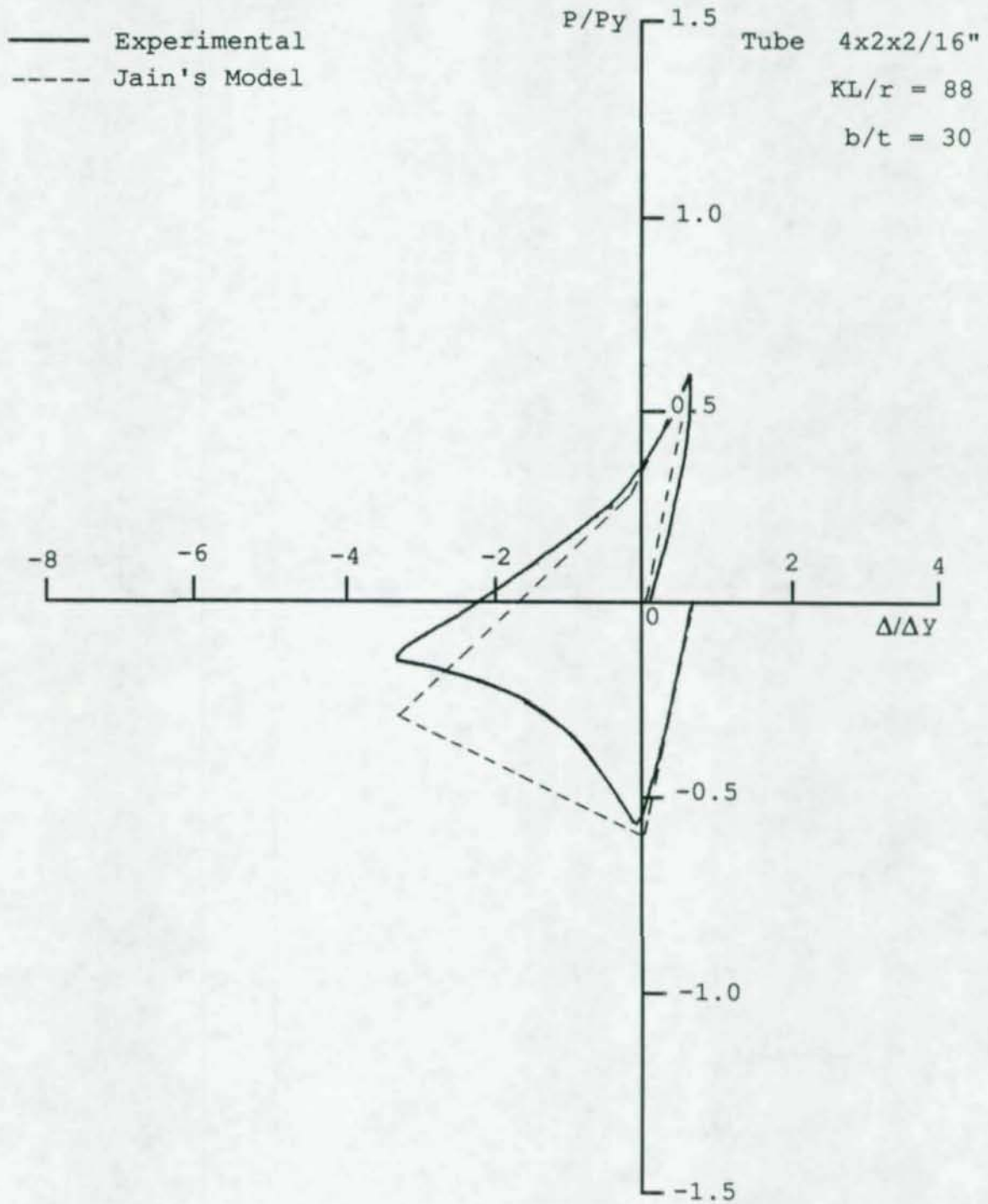


Figure 5.7 Comparison with Jain's Hysteresis Model  
for Specimen T422H, Cycle 1

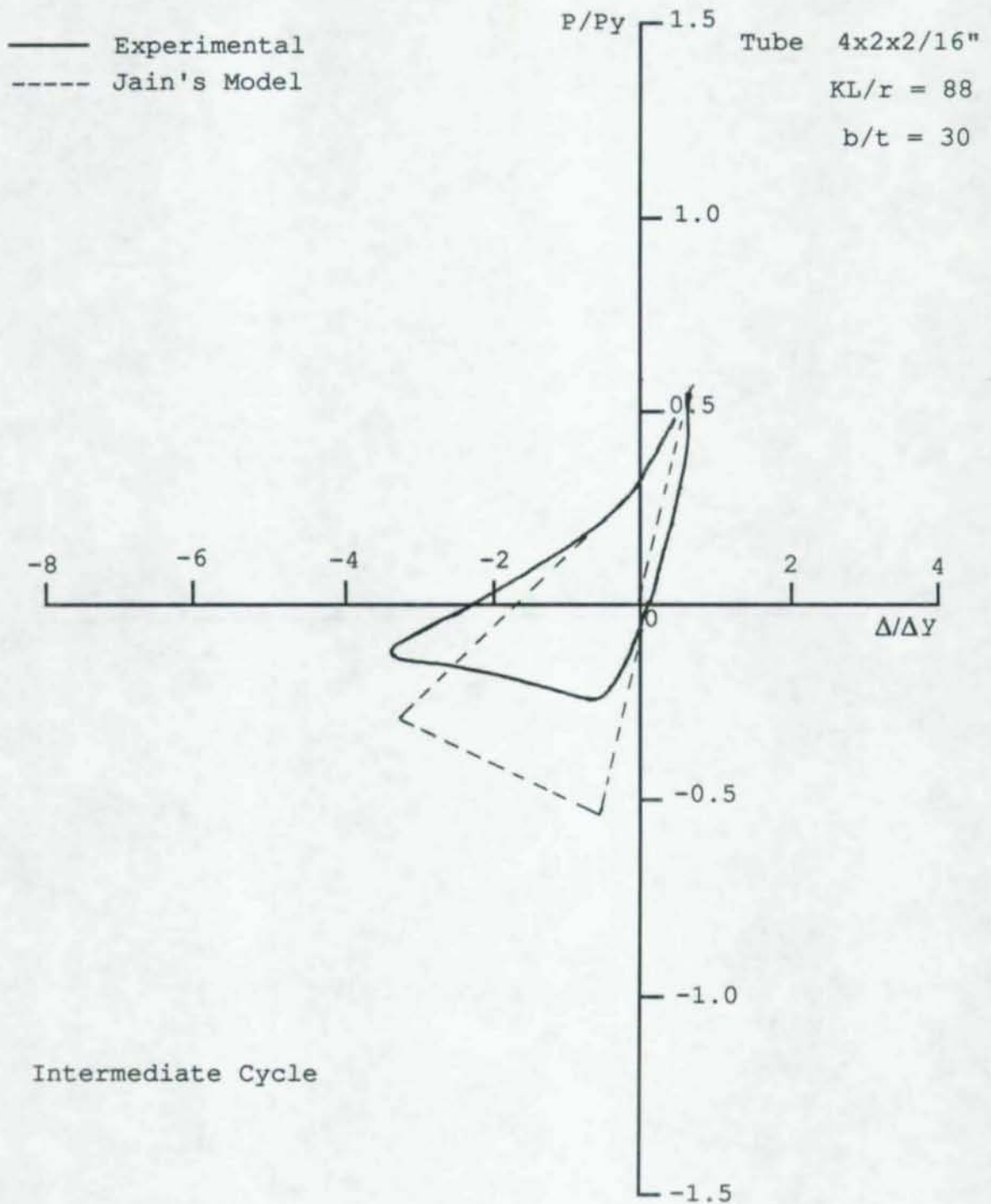


Figure 5.8 Comparison with Jain's Hysteresis Model for Specimen T422H, Cycle 2

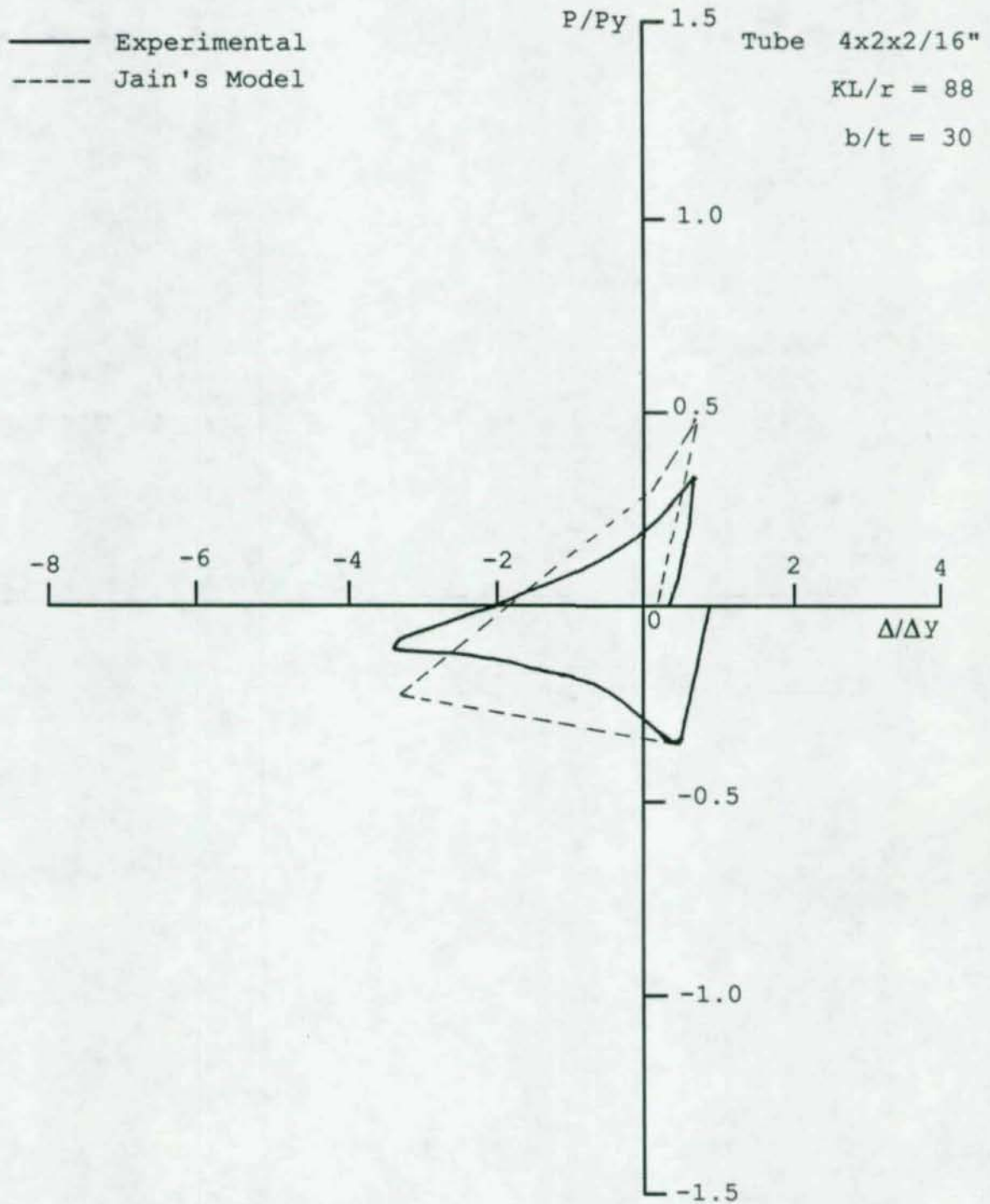


Figure 5.9 Comparison with Jain's Hysteresis Model for Specimen T422H, Cycle 5

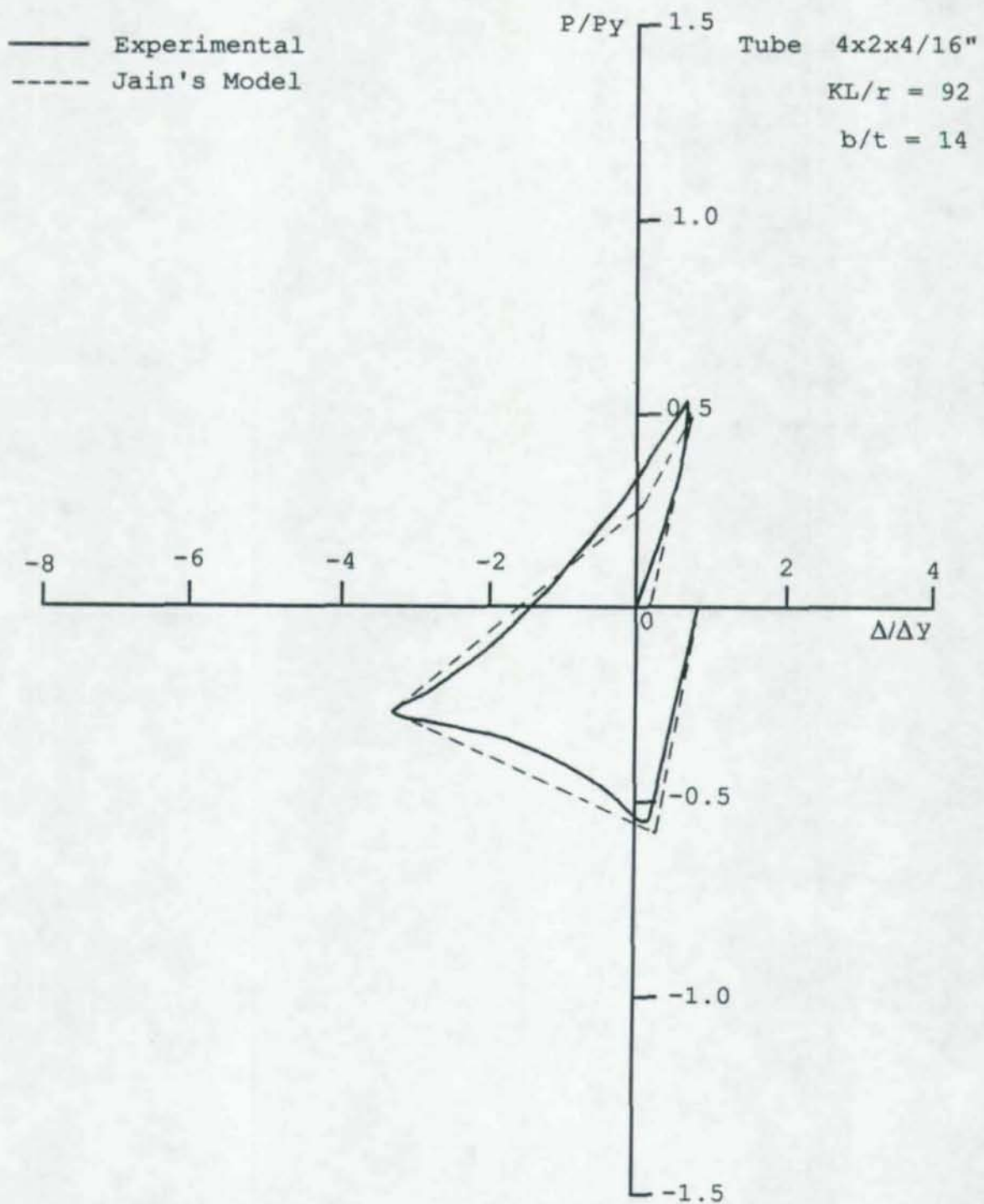


Figure 5.10 Comparison with Jain's Hysteresis Model for Specimen T424H, Cycle 1

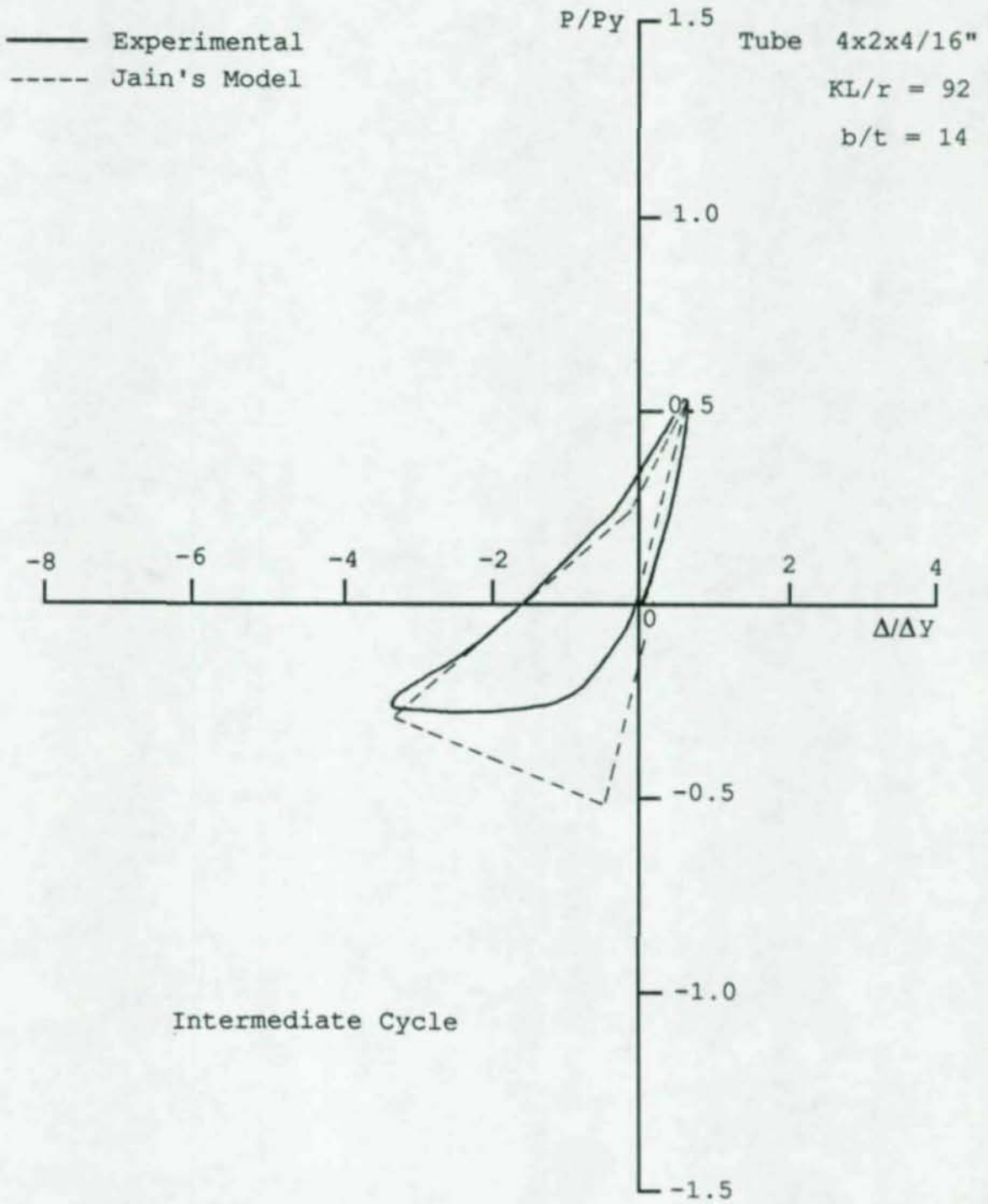


Figure 5.11 Comparison with Jain's Hysteresis Model for Specimen T424H, Cycle 2

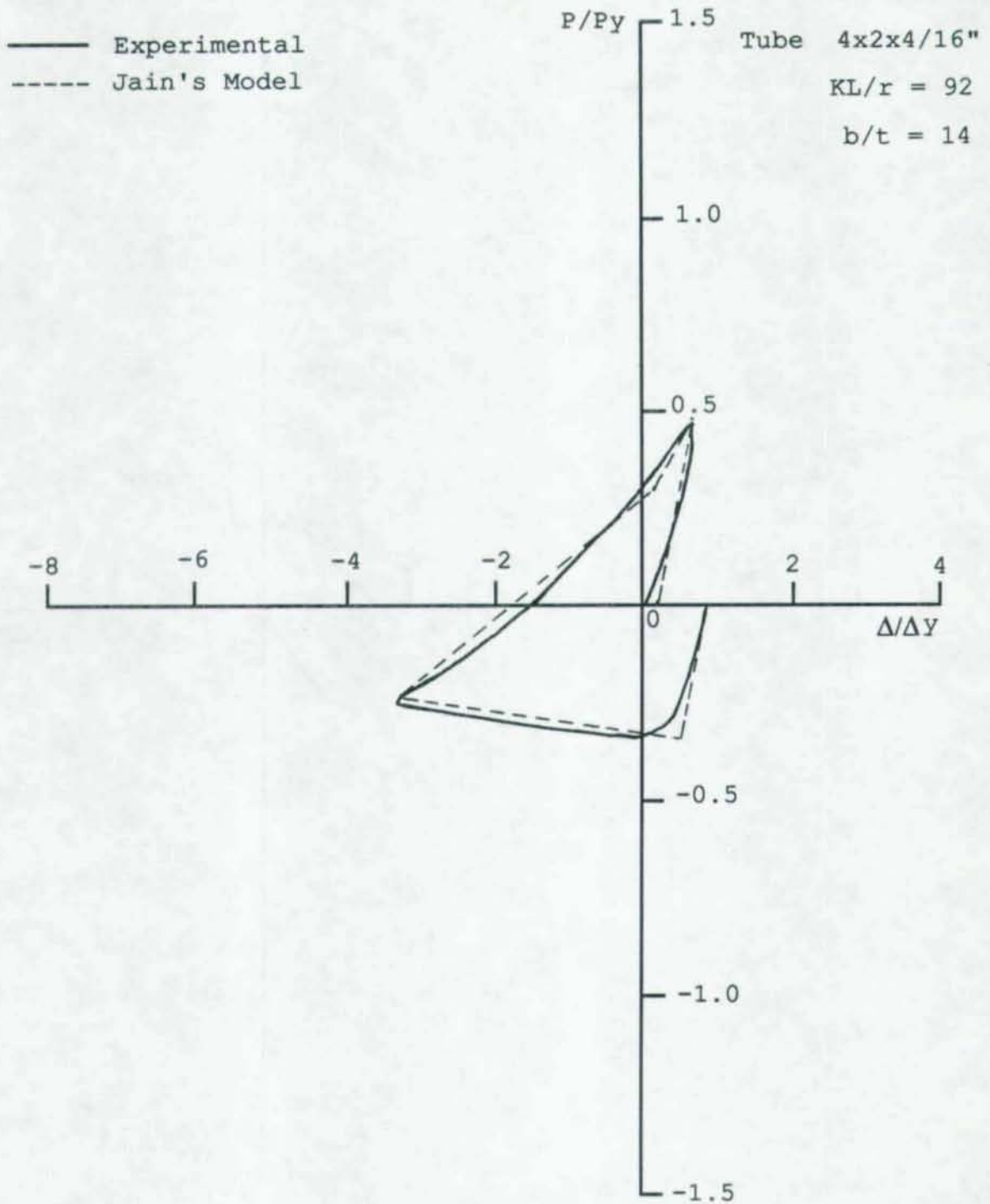


Figure 5.12 Comparison with Jain's Hysteresis Model for Specimen T424H, Cycle 5

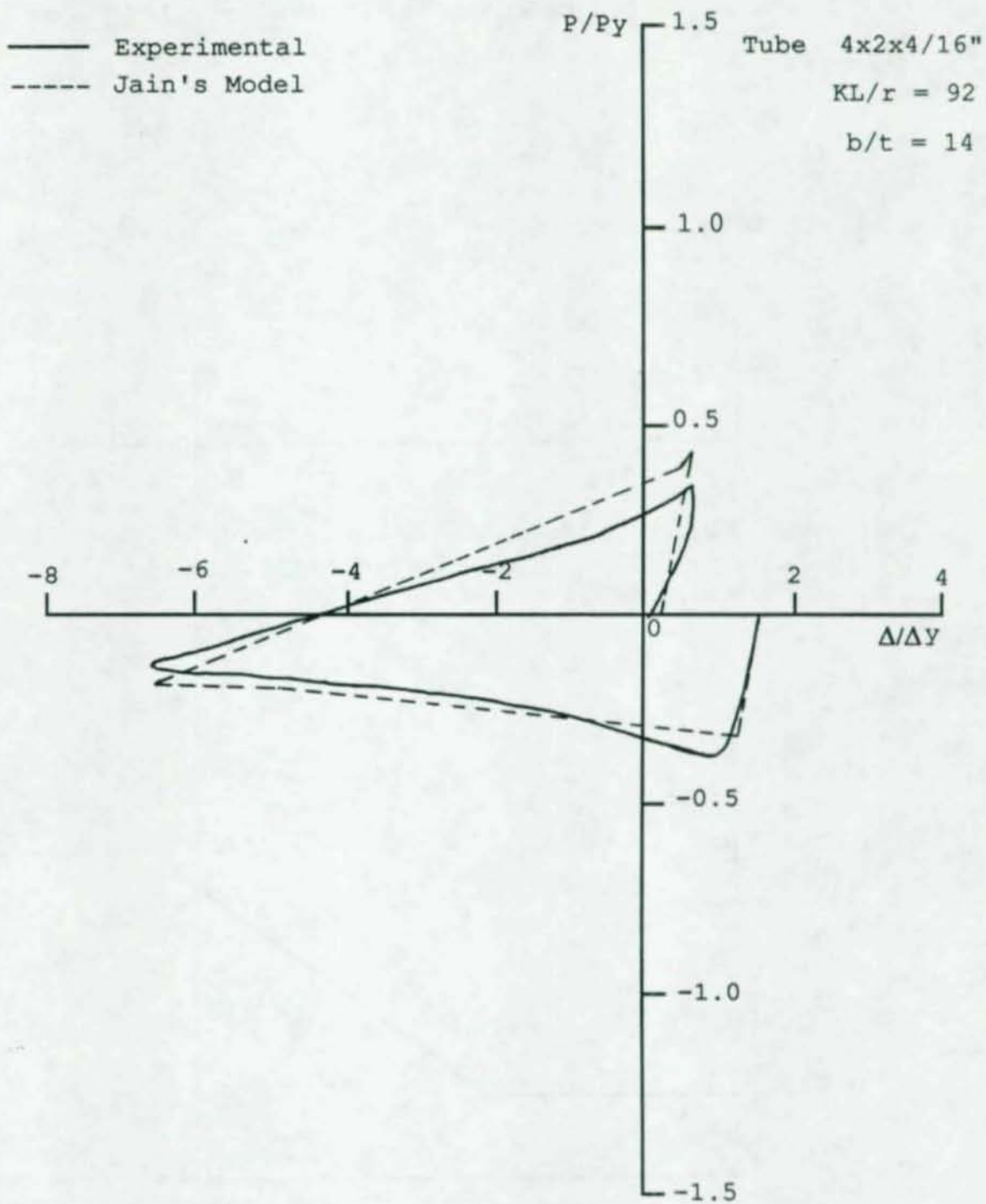


Figure 5.13 Comparison with Jain's Hysteresis Model for Specimen T424H, Cycle 10

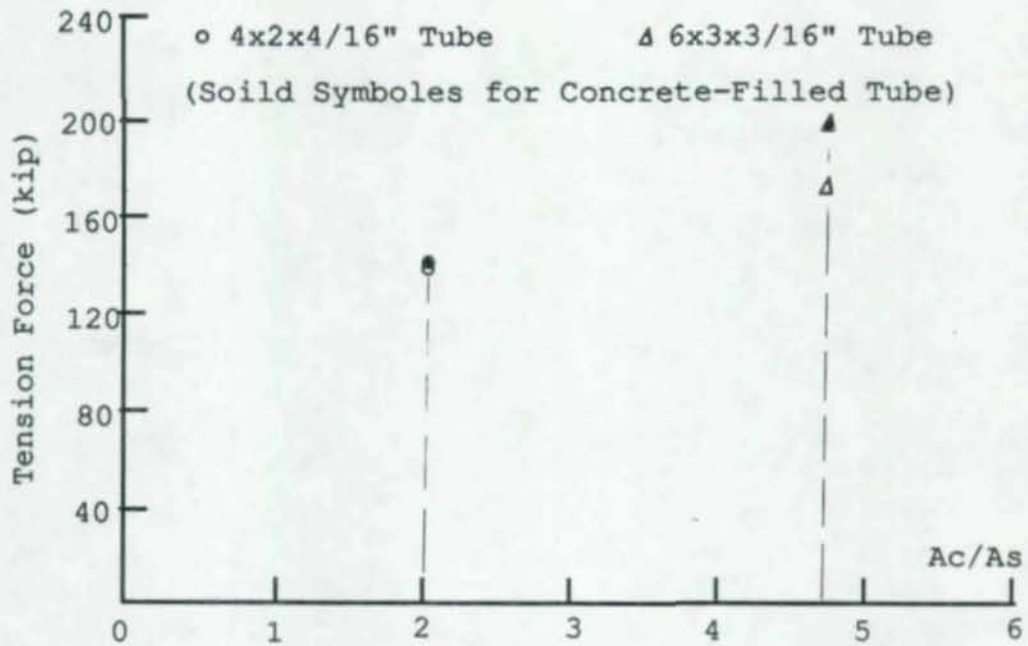


Figure 5.14 Relationship between Tension Force Increase vs. Ac/As Ratio

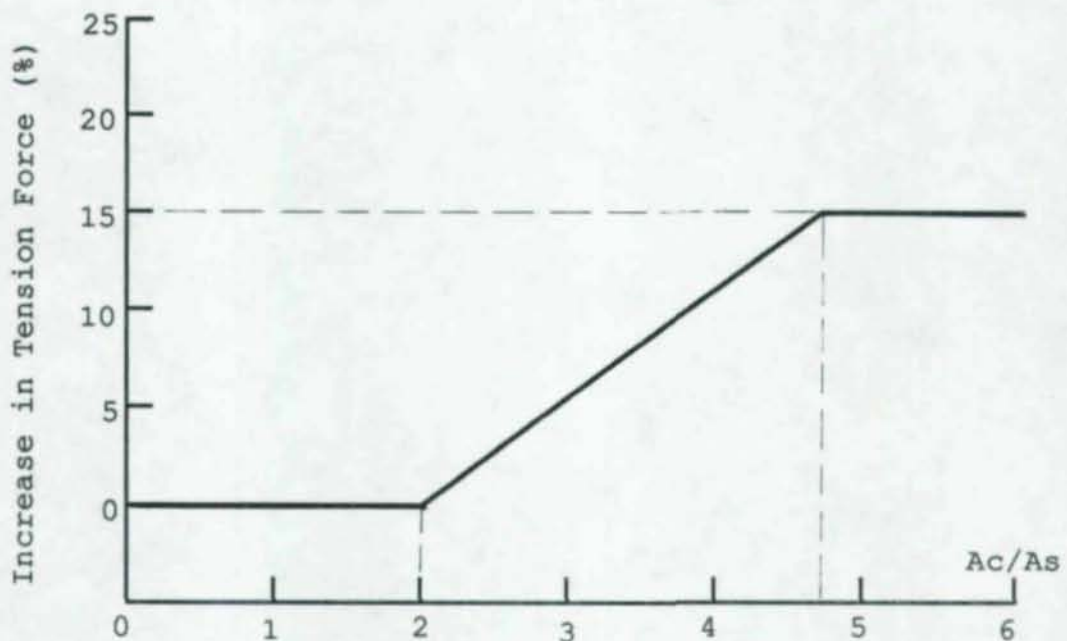


Figure 5.15 Assumed Relationship between Tension Force Increase vs. Ac/As Ratio

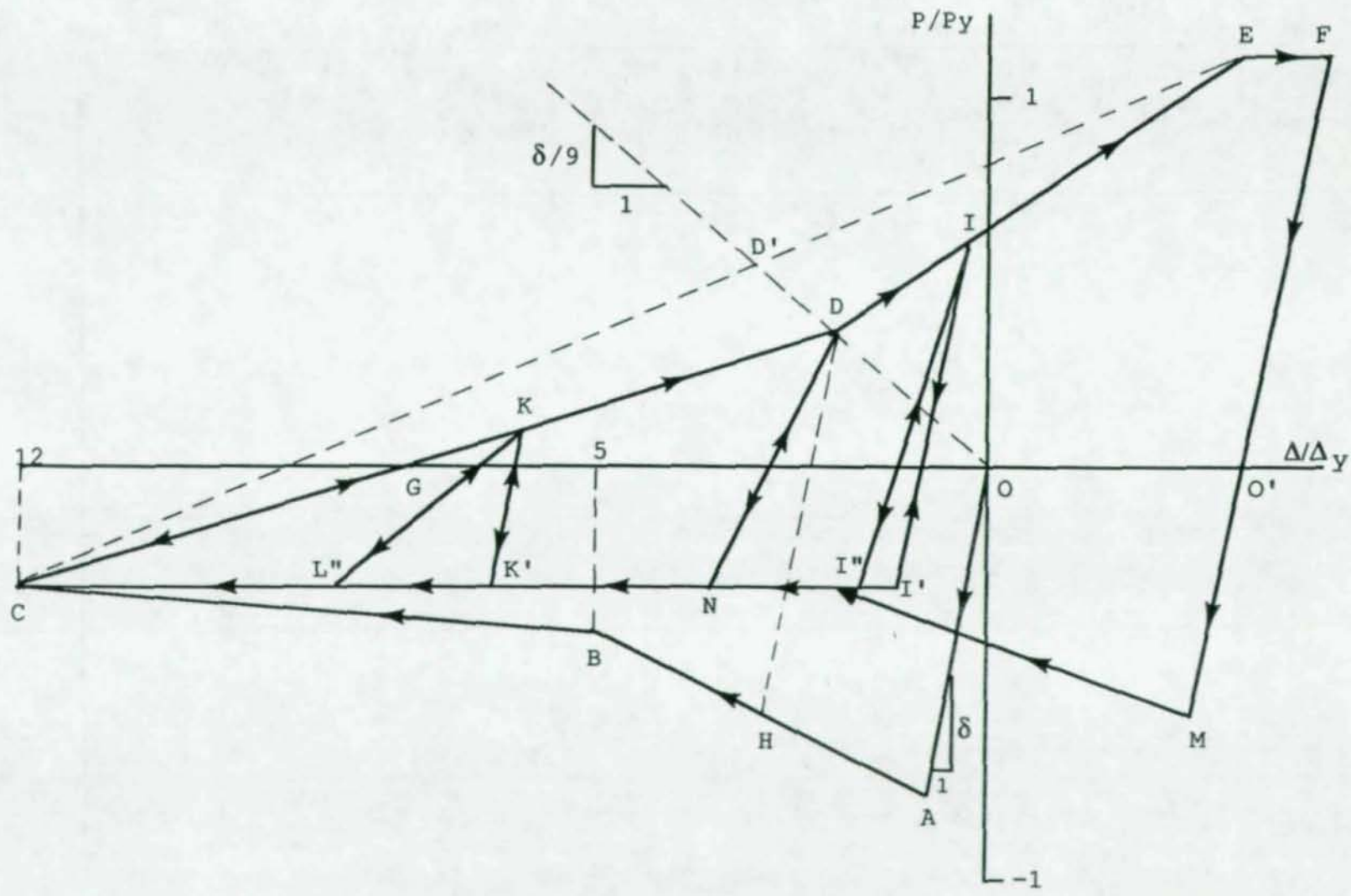


Figure 5.16 Proposed Hysteresis Model for Concrete-Filled Bracing Members

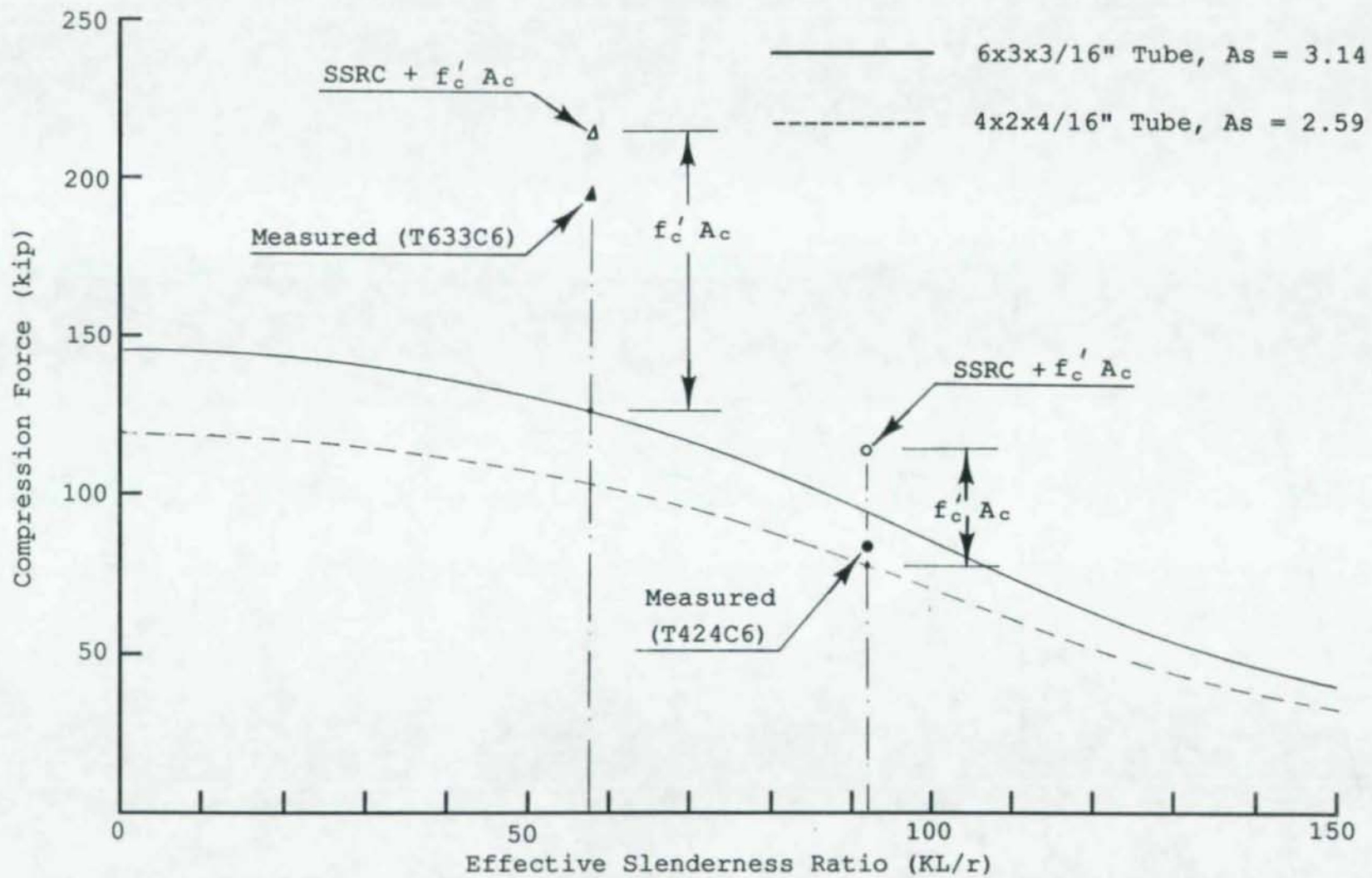


Figure 5.17 First Buckling Load from Tests and SSRC Formulas

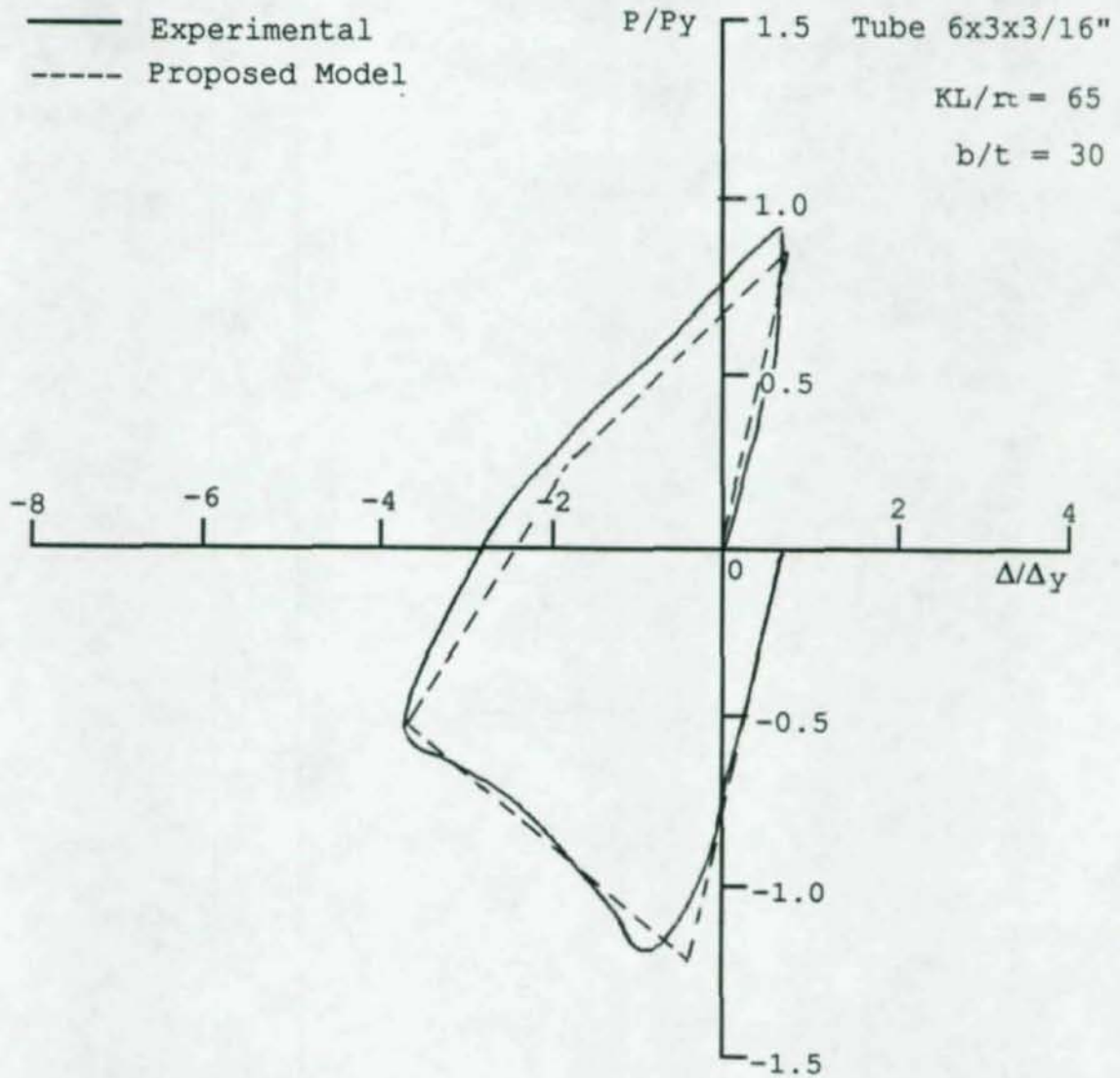


Figure 5.18 Comparison with Proposed Hysteresis Model  
for Specimen T633C6, Cycle 1

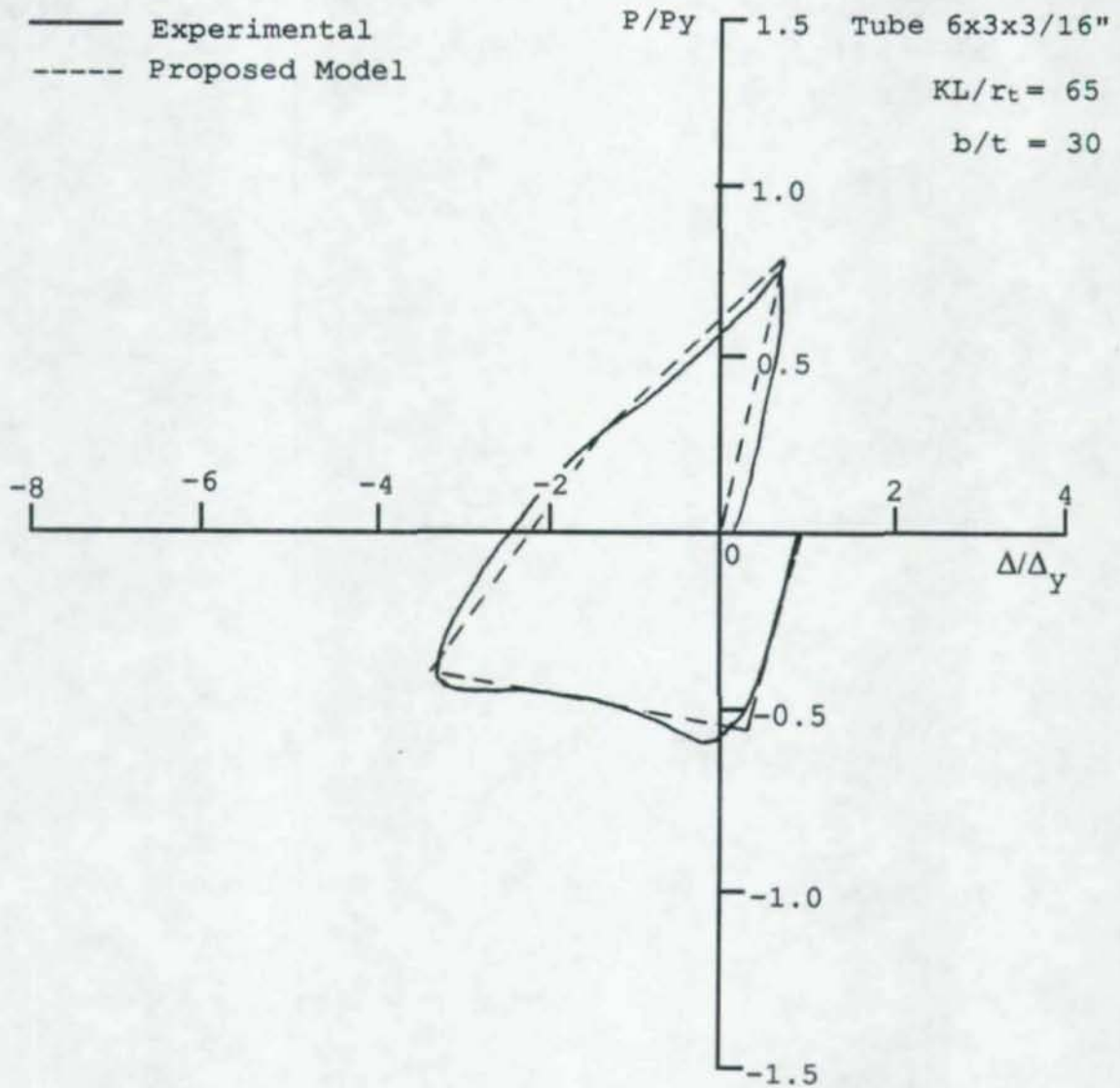


Figure 5.19 Comparison with Proposed Hysteresis Model  
for Specimen T633C6, Cycle 5

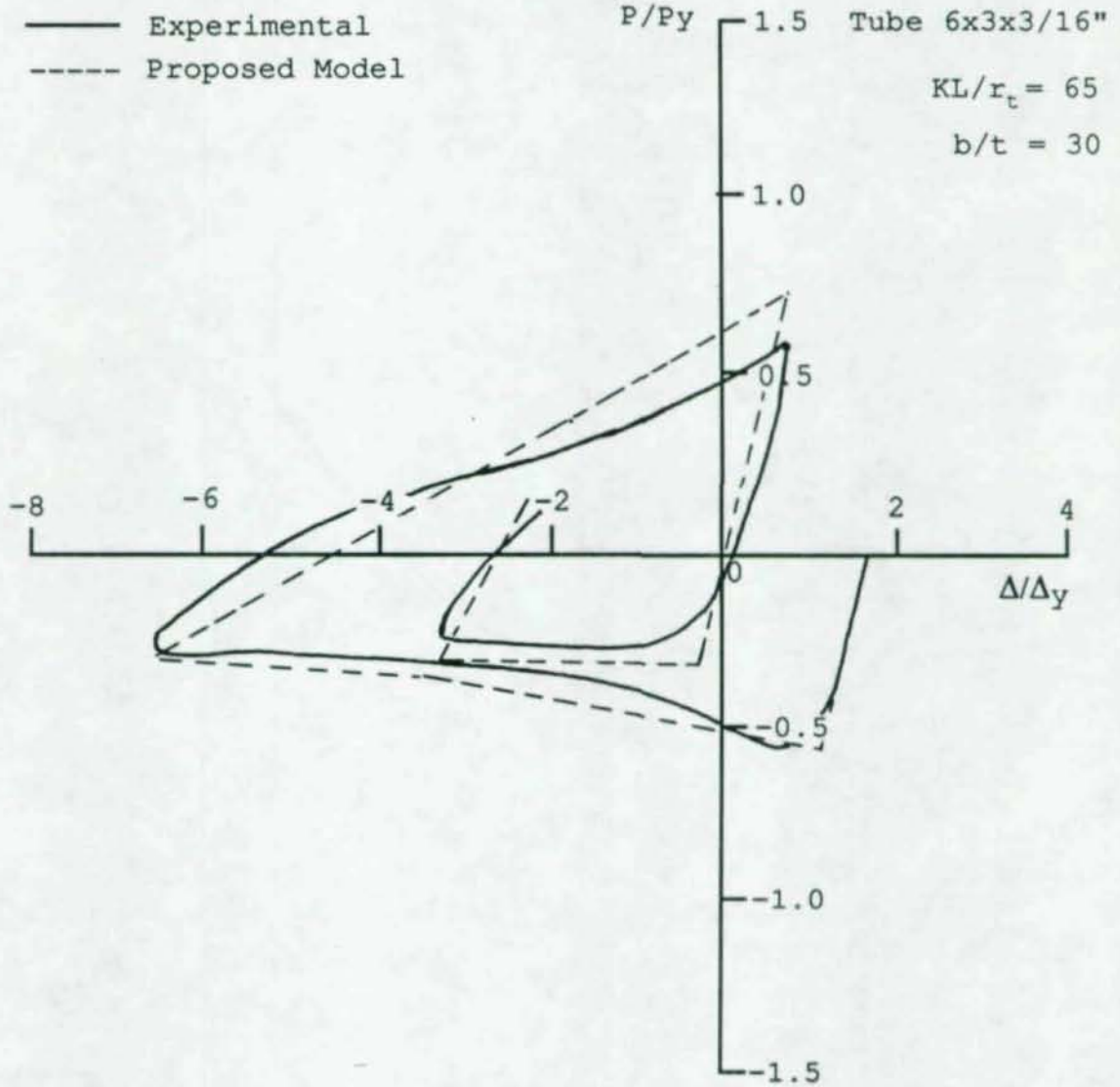


Figure 5.20 Comparison with Proposed Hysteresis Model for Specimen T633C6, Cycle 10

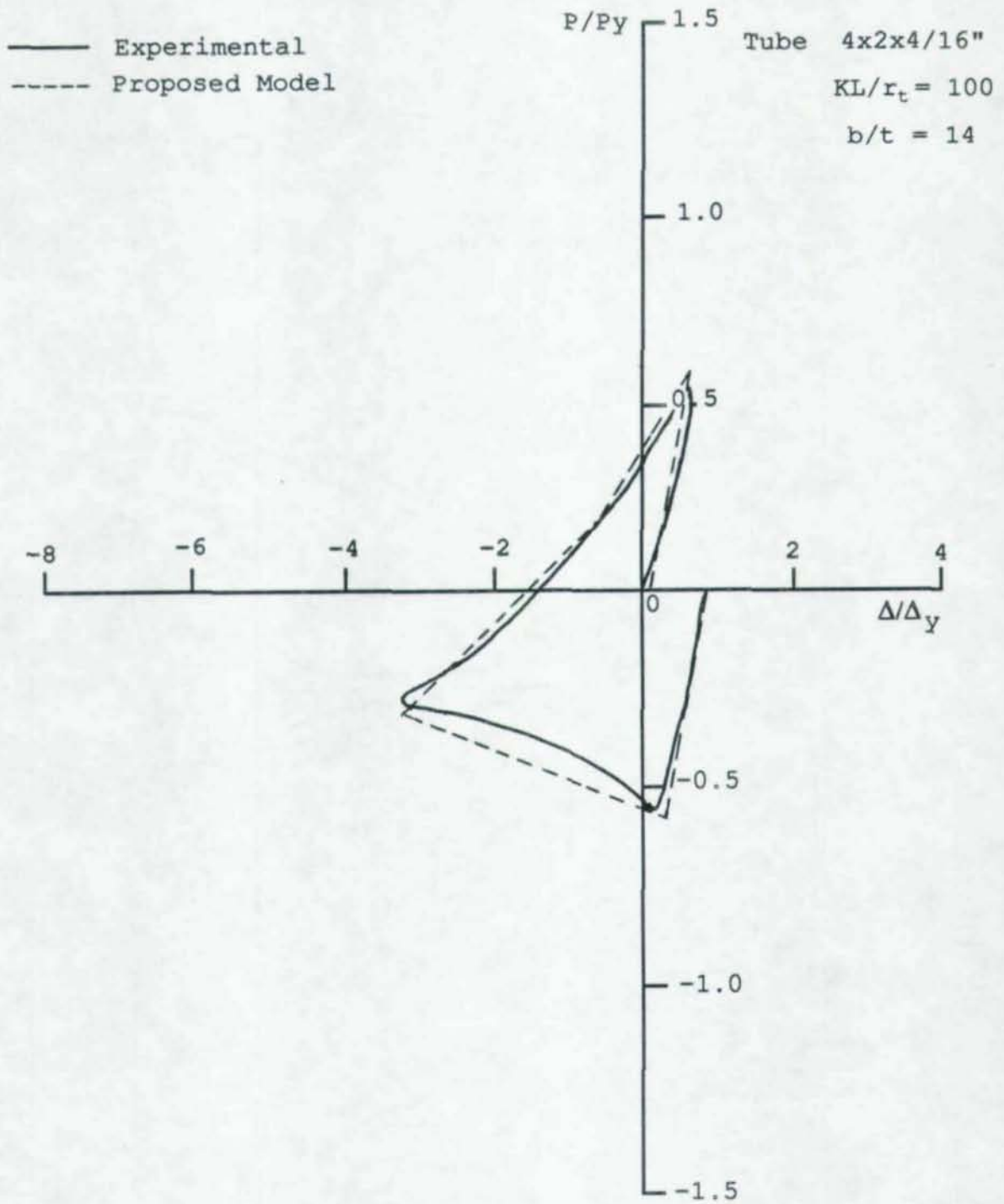


Figure 5.21 Comparison with Proposed Hysteresis Model for Specimen T424C6, Cycle 1

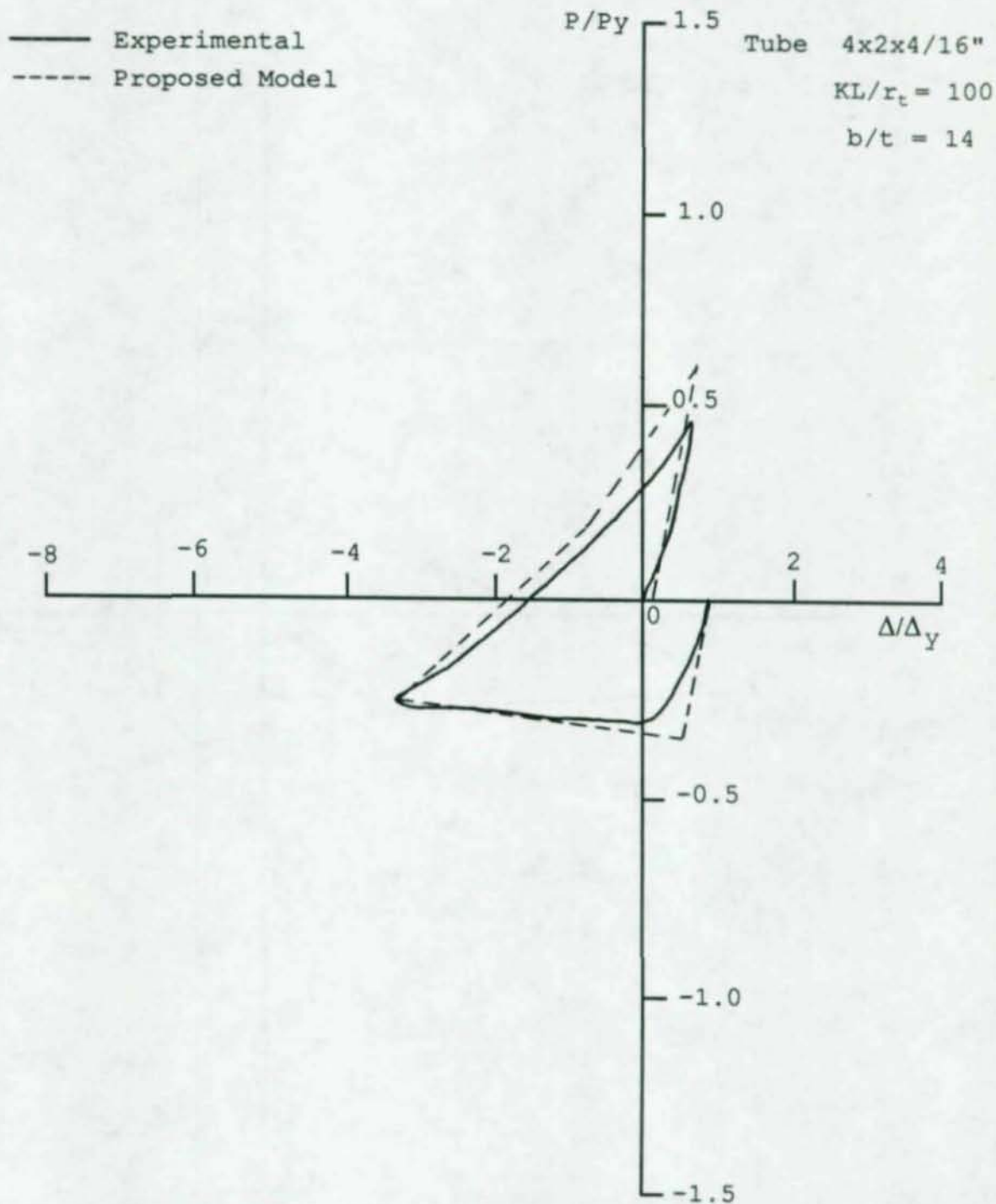


Figure 5.22 Comparison with Proposed Hysteresis Model for Specimen T424C6, Cycle 5

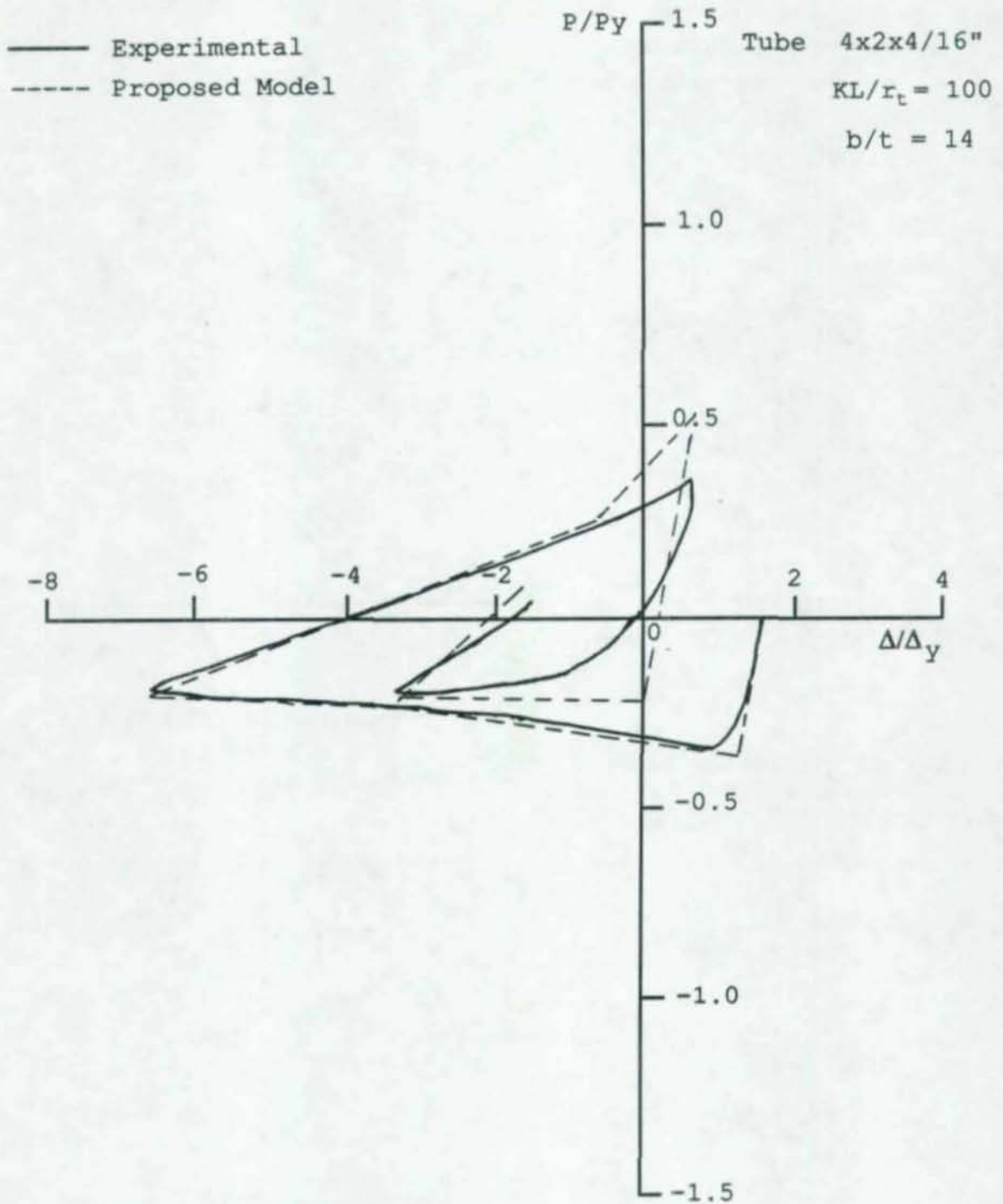


Figure 5.23 Comparison with Proposed Hysteresis Model for Specimen T424C6, Cycle 10

APPENDICES

APPENDIX A  
FIRST BUCKLING LOAD CALCULATION

The detailed procedure and equations to calculate the first buckling load for concrete-filled tubular bracing members by Method 1 were discussed and summarized in Chapter IV. This appendix will focus on discussing the limiting slenderness ratios within which this procedure can be used, and also on presenting the flow chart for solution algorithm and computer program which was written in BASIC Language.

A.1 Limiting Slenderness Ratios

The basic assumption in the procedure is that the buckling load is governed by overall stability. Before the force reaches buckling load, a member does not develop local buckling. Also the stresses in both concrete and steel lie in non-elastic but before plastification stage. If stress in either concrete or steel lies out this range, this procedure is not applicable. The following is the detailed discussion about these limits.

1. Plastification Limit (Lower Limit)

If a concrete-filled tubular bracing member is very stocky, it is possible that while stress in steel is within non-linear range, point "b" in Figure A.1(a), stress in

concrete has reached  $f_c'$ , point "b'" in Figure A.1(b), where the tangent modulus of concrete is equal to zero. For a given section there is a point where, under the application of the buckling load calculated from the procedure corresponding to a certain slenderness ratio of the member, the stress in concrete just reaches its ultimate compressive strength,  $f_c'$ . This particular slenderness ratio is the lower limit below which the member is too stock to apply this procedure. The following is the way to determine the lower limit of slenderness ratio,  $(KL/r)_1$ .

When stress in concrete reaches its strength,  $f_c'$ , the strain in both concrete and steel is 0.002. The tangent modulus of concrete is equal to zero. The stress and tangent modulus of steel at this point can be calculated by the following two equations which actually are Equations (4.8) and (4.9), respectively.

$$\epsilon_s = \sigma_s / E + 0.002 (\sigma_s / f_y)^{15} \quad (A.1)$$

and

$$E_{st} = 1 / [ 1 / E + 0.03 \sigma_s^{15} / F_y^{14} ] \quad (A.2)$$

If these stress and tangent modulus values of steel are substituted into Equation (4.7), we have the following equation according to the definition of lower limit:

$$A_c f_c' + A_s \sigma_s = \pi^2 I_s E_{st} / (KL)^2 \quad (A.3)$$

Let  $n$  be the ratio of area of concrete to steel,  $A_c/A_s$ .  
The above equation can be simplified in the following form:

$$(KL)^2 = \pi I_s E_{st} / [n A_c f_c' + A_s \sigma_s] \quad (A.4)$$

or

$$(KL/r)_1^2 = \pi^2 E_{st} / [n f_c' + \sigma_s] \quad (A.5)$$

Thus, Equations (A.1), (A.2), and (A.5) can be used to compute the lower limit of slenderness ratio in terms of radius of gyration of tube section.

## 2. Proportional Limit (Upper Limit)

If a concrete-filled bracing member is very slender, the stress in steel is relatively small. Then it would be reasonable to assume that the relationship between stress and strain of steel is linear. In other words, the tangent modulus of steel is constant and equal to elastic modulus,  $E$ . Therefore, there is an upper limit of slenderness ratio for a given section above which Euler formula can be used to estimate the buckling load.

Usually, it can be assumed that when stress in steel tube

is smaller than  $0.5F_y$ , the relationship between stress and strain is linear. This value may vary, but procedure presented below remains the same.

When the stress of steel is  $0.5F_y$ , the strain for the member may be given by  $0.5F_y/E$ . By similar procedure as for plastification limit, the following equation can be obtained:

$$A_c \sigma_c + 0.5 F_y A_s = \pi^2 (E I_s + E_{ct} I_c) / (KL)^2 \quad (A.6)$$

where,  $\sigma_c$  and  $E_{ct}$  can be computed by using the following two equations, respectively, which are actually Equations (4.10) and (4.11).

$$\sigma_c = f_c' [ 2 \epsilon_c / 0.002 - \epsilon_c^2 / 0.002^2 ] \quad (A.7)$$

and

$$E_{ct} = f_c' [ 2 / 0.002 - 2 \epsilon_c / 0.002^2 ] \quad (A.8)$$

Letting  $A_c/A_s$  be  $n$  and  $I_c/I_s$  be  $m$ , Equation (A.6) can be expressed as the following equation to compute the upper limit of slenderness ratio of the member in terms of radius of gyration of steel tube section:

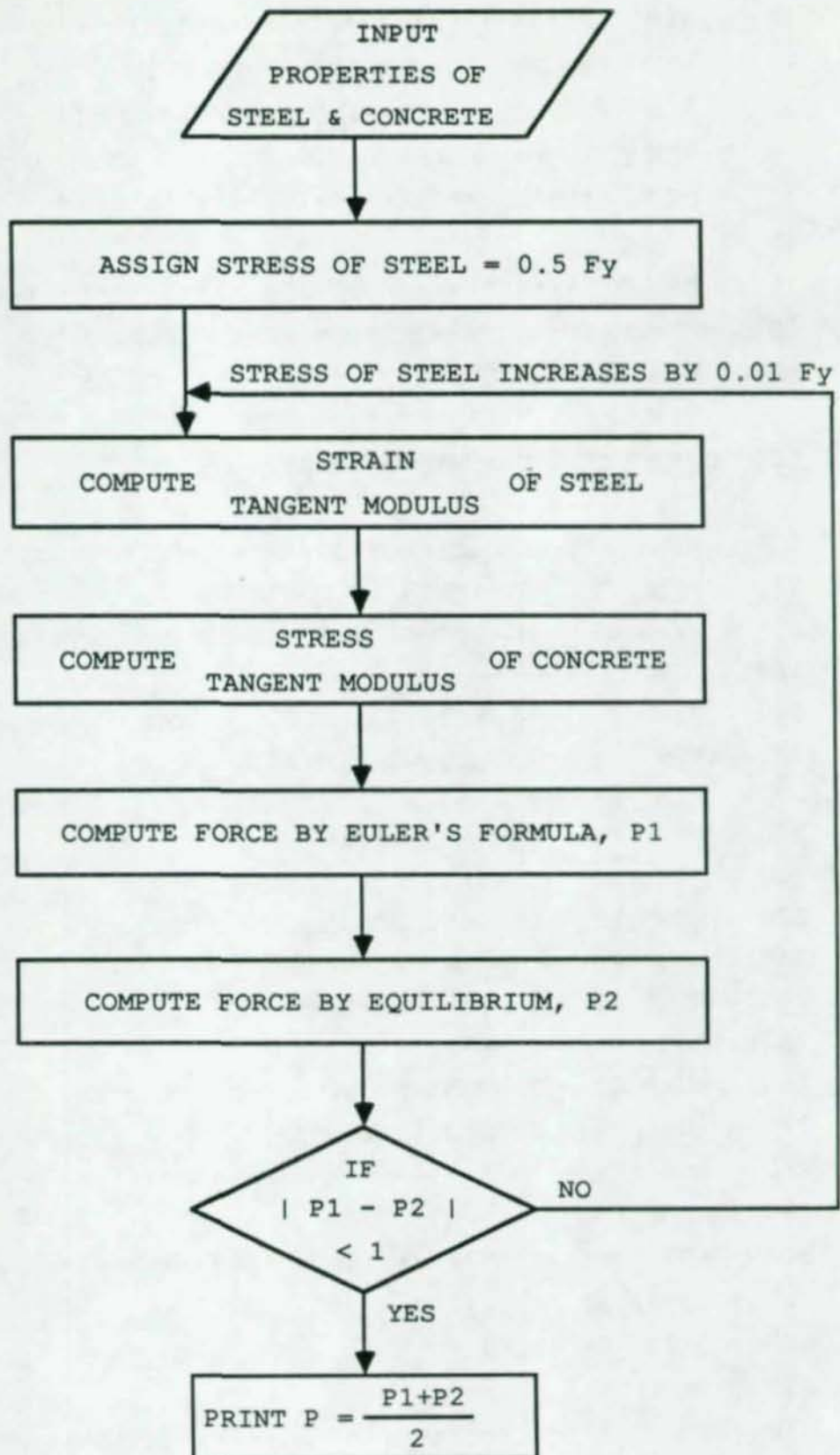
$$(KL/r)_u^2 = \pi^2 [ E + m E_{ct} ] / [ n \sigma_c + 0.5 F_y ] \quad (A.9)$$

For the sections used in this study, the lower and upper limits for 4x2x1/4" tube with 6 ksi (4.1 KN/cm<sup>2</sup>) concrete are 34 and 95, respectively. The limits for 6x3x3/16" tubes filled with different strength of concrete are shown in Figure A.2.

#### A.2 Flow Chart and Computer Program

The first buckling load for a concrete-filled member is obtained by a trial and error method. The first step is to set a relatively small value of stress for steel,  $\sigma_s$ , then compute tangent modulus for both concrete and steel and the stress in concrete. These values are substituted into Euler's formula for a composite section, Equation (4.7), and equilibrium condition, Equation (4.13). If the difference in the forces from these two equations is acceptable, procedure is terminated and their average value gives the buckling load. If the difference is too large, set a new value for stress of steel and repeat these steps until the difference is acceptable. This section consists of two parts. The first is the flow chart for the algorithm and the second is a listing of the computer program.

## 1. Flow Chart



## 2. Listing of Computer Program

```

10  REM *****
20  REM PROGRAM FOR COMPUTING BUCKLING LOAD
30  REM   OF CONCRETE-FILLED STEEL TUBES
40  REM           APRIL, 1987
50  REM *****
60  REM
70  REM ***** NOTATION *****
80  REM A1:  CROSS-SECTION AREA OF STEEL
90  REM E1:  MODULUS OF ELASTICITY OF STEEL
100 REM F1:  YIELD STRENGTH OF STEEL
110 REM I1:  MOMENT OF INERTIA OF STEEL
120 REM -----
130 REM A2:  CROSS-SECTION AREA OF CONCRETE
140 REM F2:  STRENGTH OF CONCRETE
150 REM I2:  MOMENT OF INERTIA OF CONCRETE
160 REM -----
170 REM K:   EFFECTIVE LENGTH FACTOR
180 REM L:   LENGTH OF MEMBER
190 REM -----
200 REM F0:  GIVEN INITIAL STRESS OF STEEL
210 REM S0:  INCREASE OF STEEL STRESS
220 REM E3:  TANGENT MODULUS OF STEEL
230 REM F3:  STRESS OF STEEL
240 REM S3:  STRAIN OF MEMBER
250 REM -----
260 REM E4:  TANGENT MODULUS OF CONCRETE
270 REM F4:  STRESS OF CONCRETE
280 REM *****
290 REM
300 REM ***** INPUT *****
310 INPUT A1,F1,I1,E1
320 INPUT A2,F2,I2
330 INPUT K,L
340 REM *****
350 REM

```

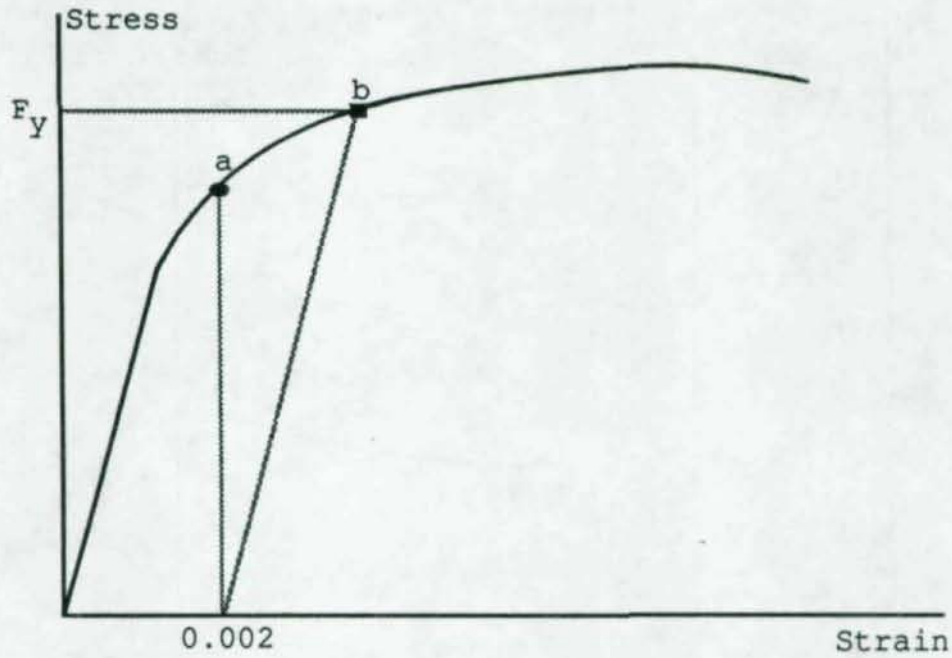
```
360  REM ***** COMPUTING *****
370  F0=0.5*F1
380  S0=0.01*F1
390  REM -----
400  FOR F3=F0 TO F1 STEP S0
410  S3=F3/E1+0.002*(F3/F1)^15
420  E3=1/(1/E1+0.03*F3^14/F1^15)
430  F4=F2*(2*S3/0.002-(S3/0.002)^2)
440  E4=F2*(2/0.002-(2*S3/0.002^2))
450  P1=3.14^2*(E3*I1+E4*I2)/(KL)^2
460  P2=F3*A1+F4*A2
470  P=P1-P2
480  P=ABS(P)
490  IF P < 1 THEN 520
500  NEXT F3
510  REM -----
520  P=(P1+P2)/2
530  PRINT "BUCKLING LOAD =";P
540  REM *****
550  STOP
560  END
570  REM *****
```

APPENDIX B  
EXPERIMENTAL HYSTERESIS LOOPS

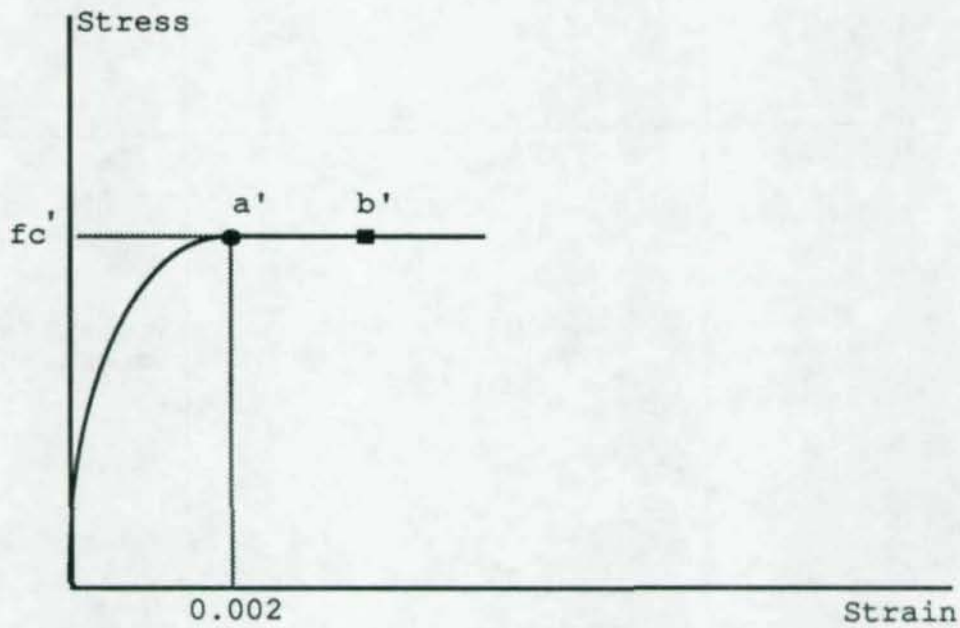
In this appendix the recorded hysteresis loops of concrete-filled specimens T633C6 and T424C6 and their hollow counterparts, specimens T633H and T424H, as well as hollow specimen T422H are presented in Figure B.1 to B.37. Specimens T633C4, T633C4F, T633C6F and T633C8F had the same tube section as specimen T633C6 and each was filled with different types of concrete. Since hysteresis behavior of these four specimens are similar to specimen T633C6 as discussed in Chapter IV, their hysteresis loops are not presented here.

The axial deformation was normalized corresponding to a nominal yield strength of 36 ksi (25 KN/cm<sup>2</sup>) as discussed in Chapter III. The yield strength of steel for the specimens whose hysteresis loops are presented here is about 54 ksi (37 KN/cm<sup>2</sup>) according coupon tests.

For concrete-filled specimens T633C6 and T424C6, loops of concrete-filled specimen and its hollow counterpart for each cycle are presented in the same figure for comparison. The loops for hollow specimen T422H are presented in the order of cycles.



(a) Stress in Steel lies in Non-Linear Stage, Point a, But below the Yield Point



(b) Stress in Concrete Just Reaches  $f_c'$ , Point a'

Figure A.1 Stress at Plastification Limiting

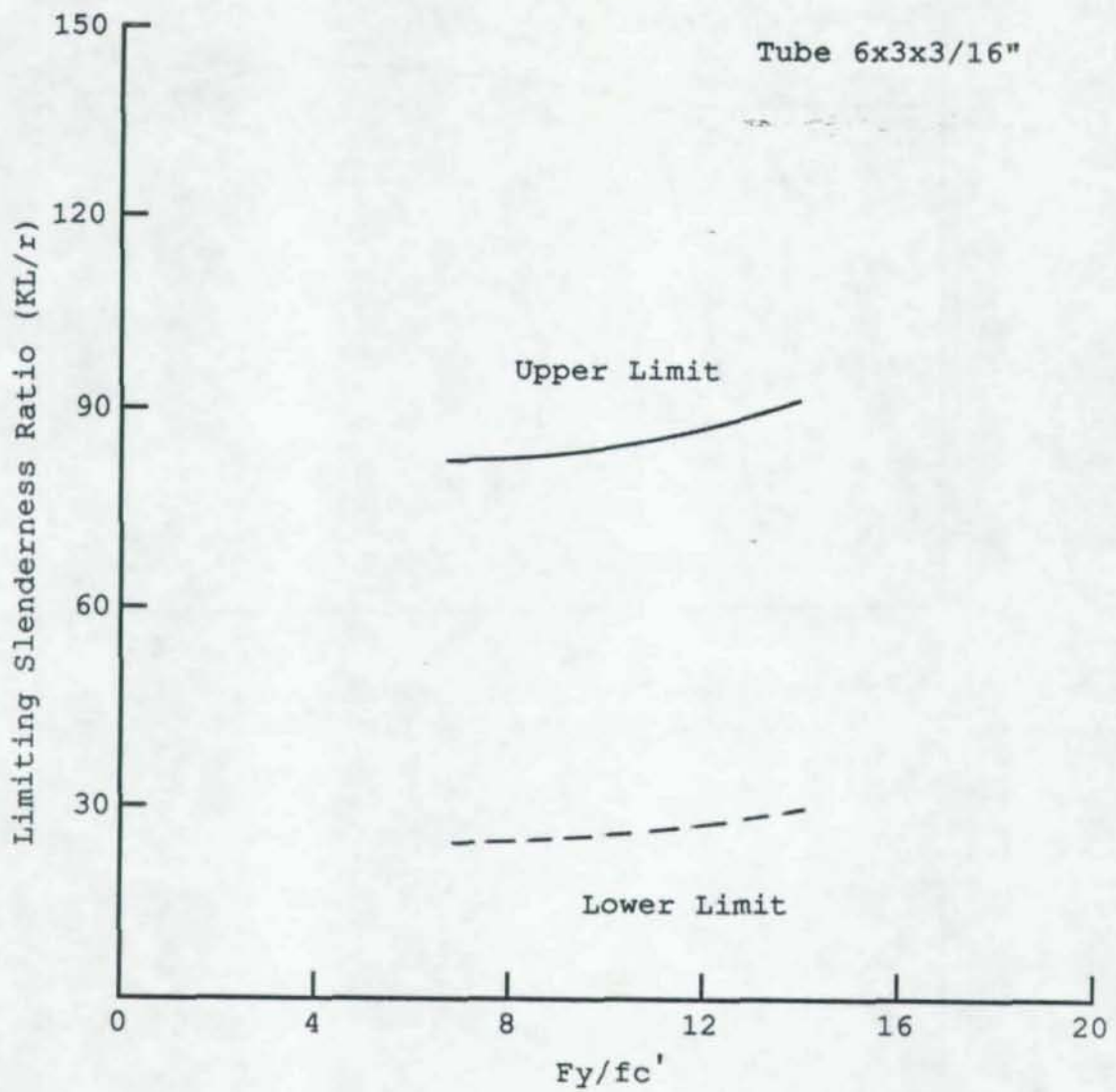


Figure A.2 Limiting Slenderness Ratios of 6x3x3/16" Tubes Filled with Different Strengths of Concrete

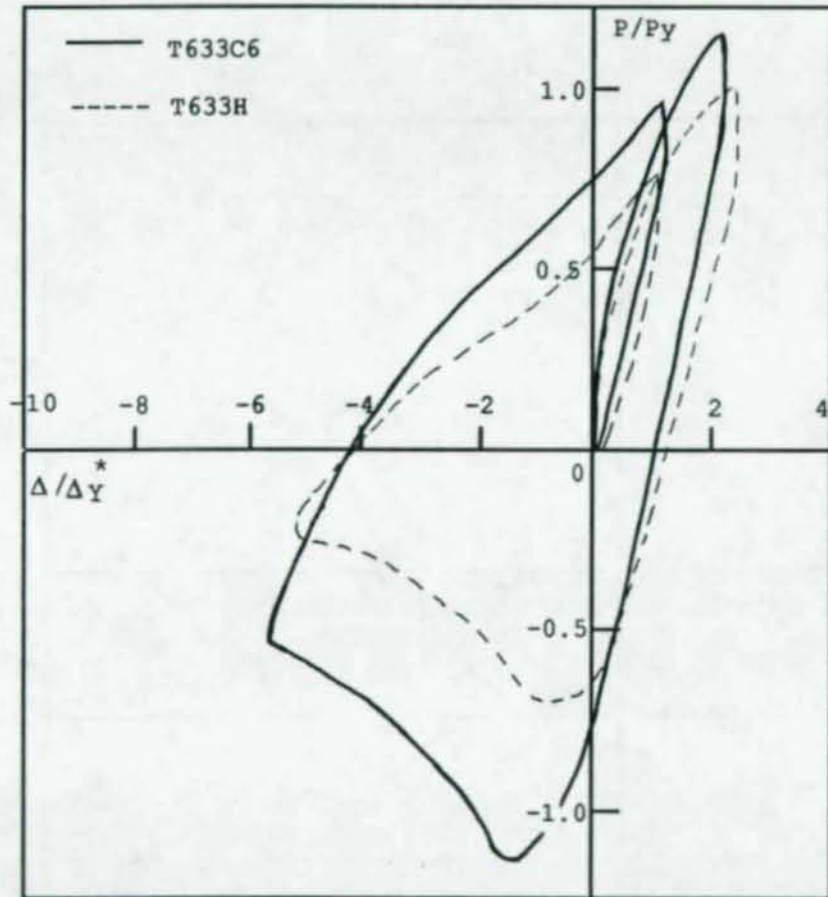


Figure B.1 Hysteresis Loops for Specimens T633H and T633C6 in Cycle 1

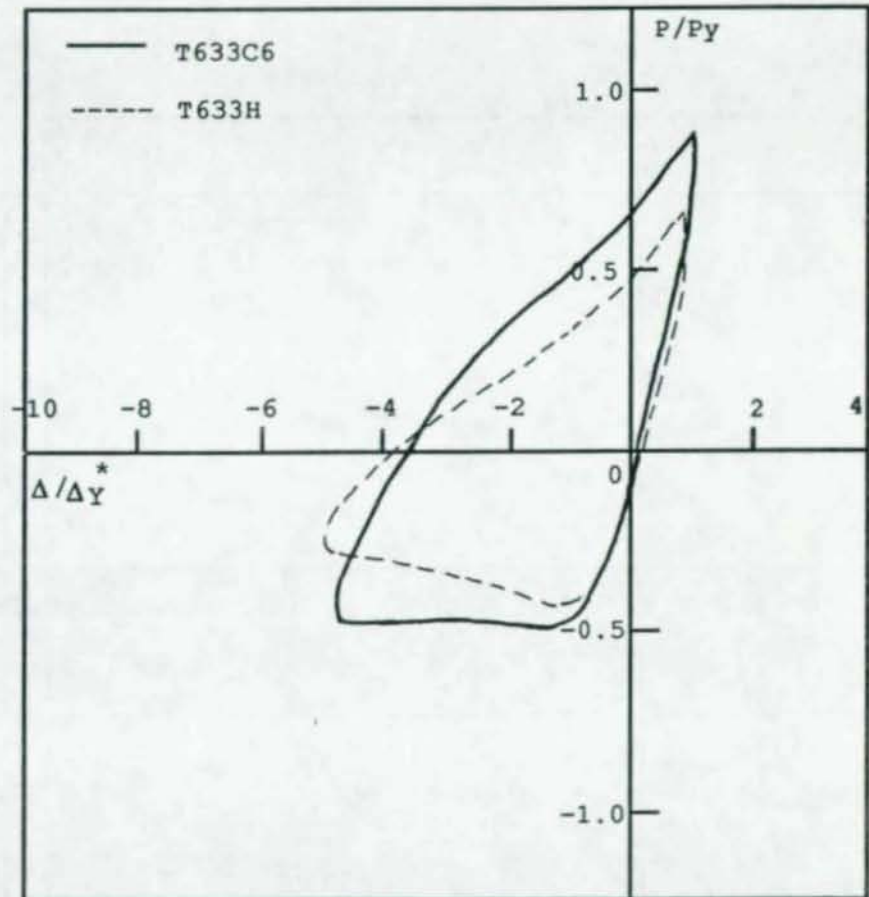


Figure B.2 Hysteresis Loops for Specimens T633H and T633C6 in Cycle 2

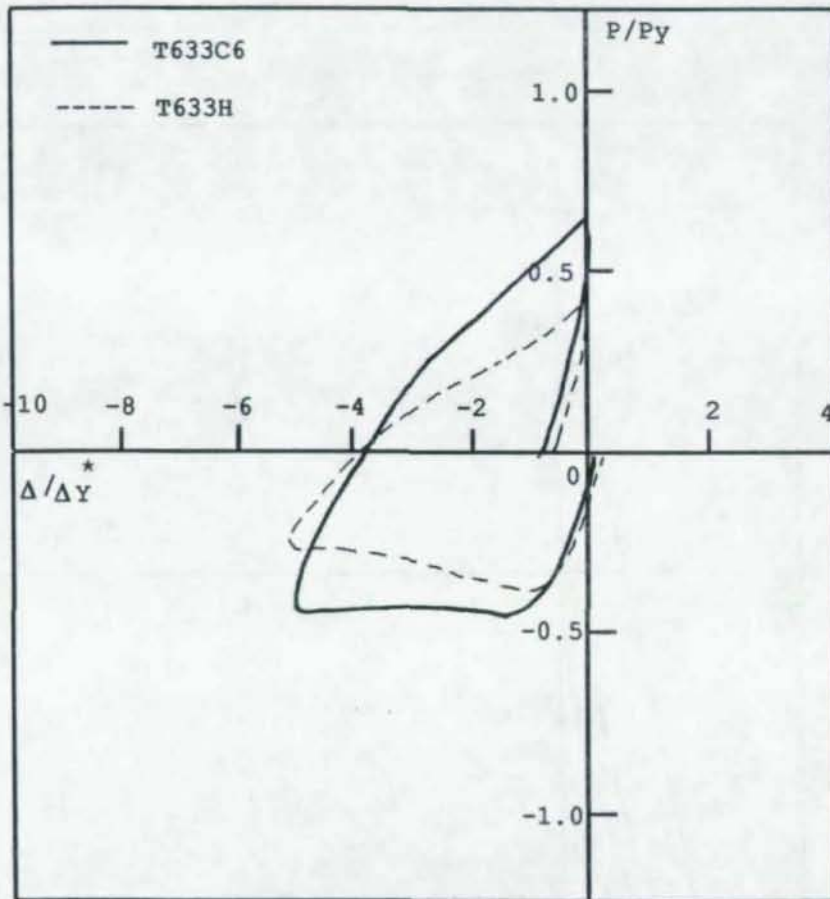


Figure B.3 Hysteresis Loops for Specimens T633H and T633C6 in Cycle 3

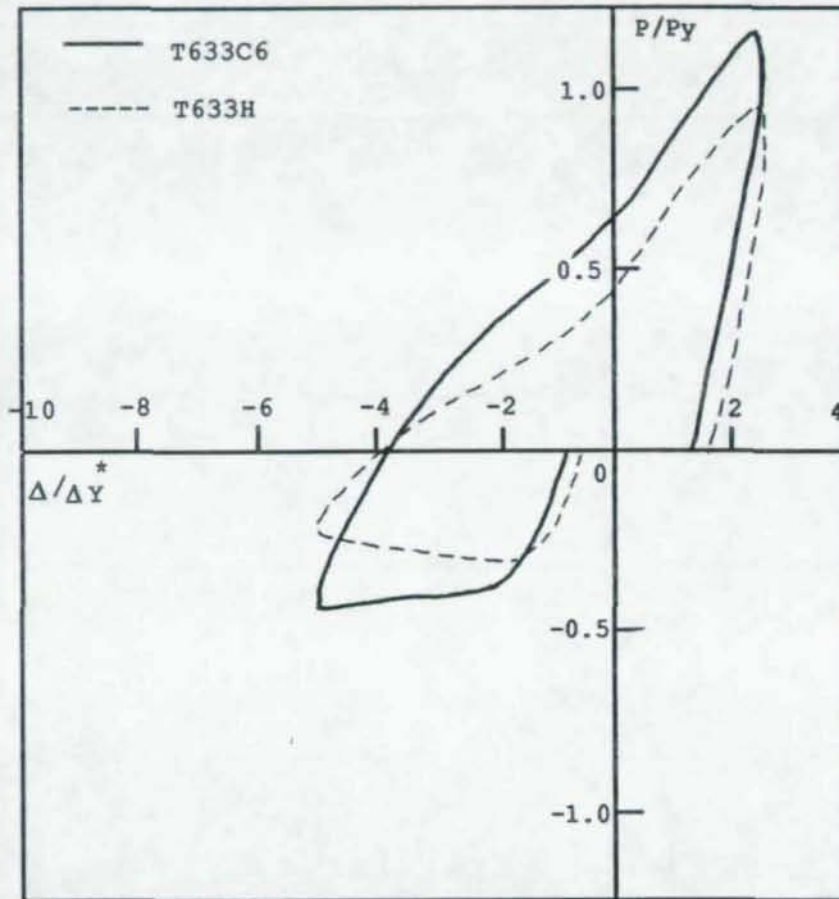


Figure B.4 Hysteresis Loops for Specimens T633H and T633C6 in Cycle 4

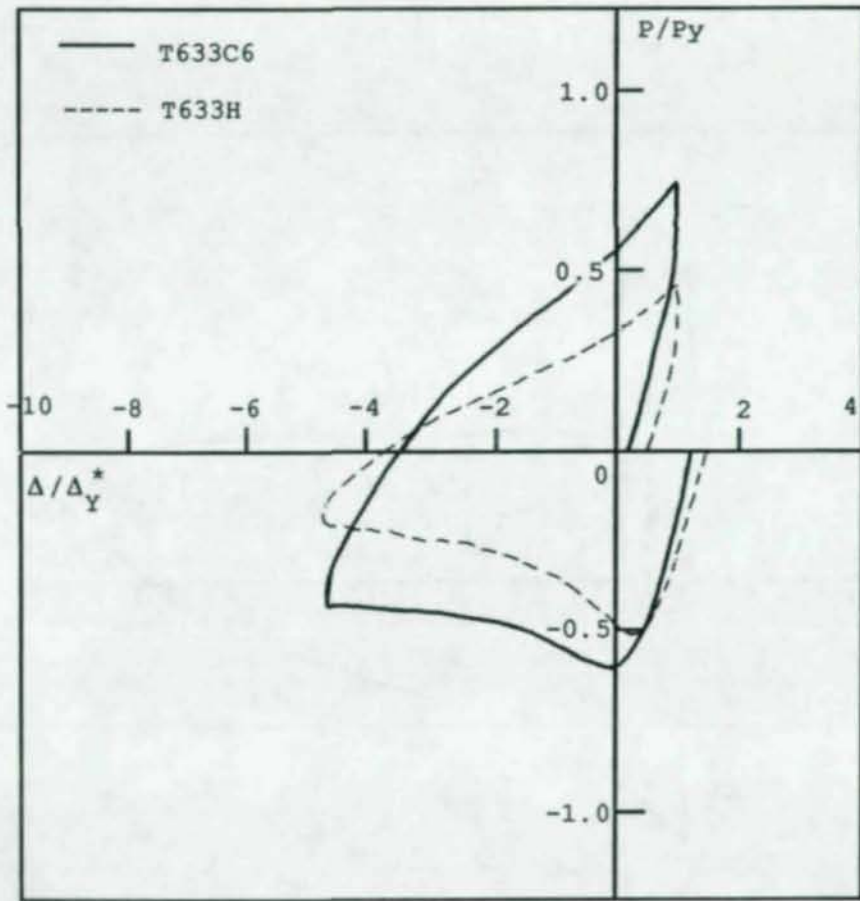


Figure B.5 Hysteresis Loops for Specimens T633H and T633C6 in Cycle 5

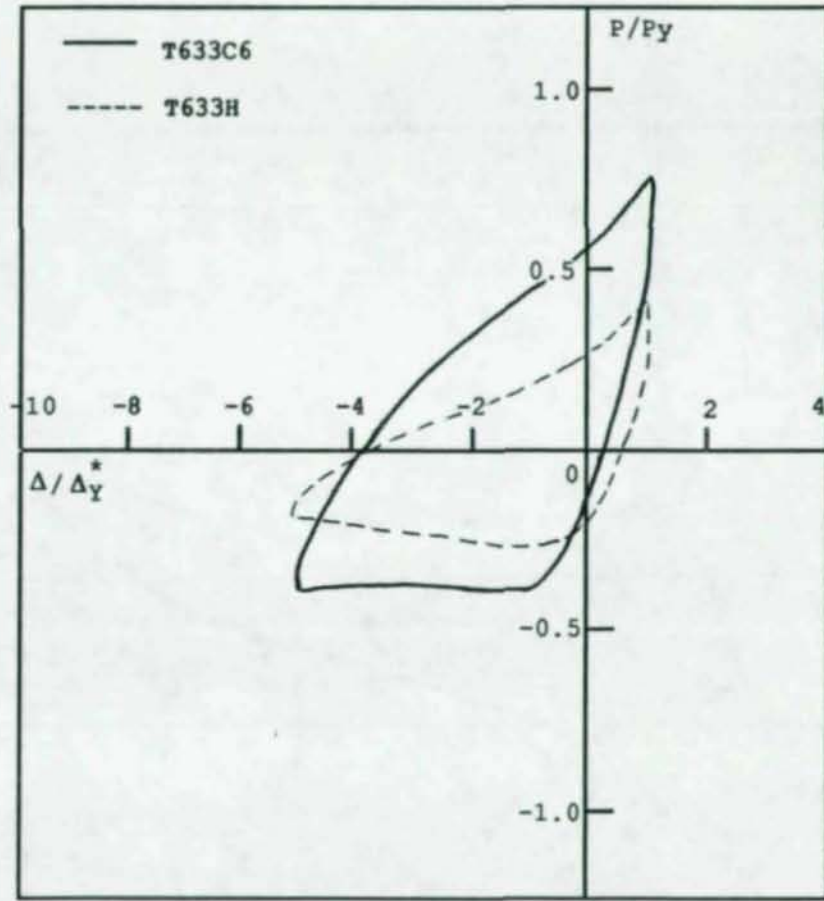


Figure B.6 Hysteresis Loops for Specimens T633H and T633C6 in Cycle 6

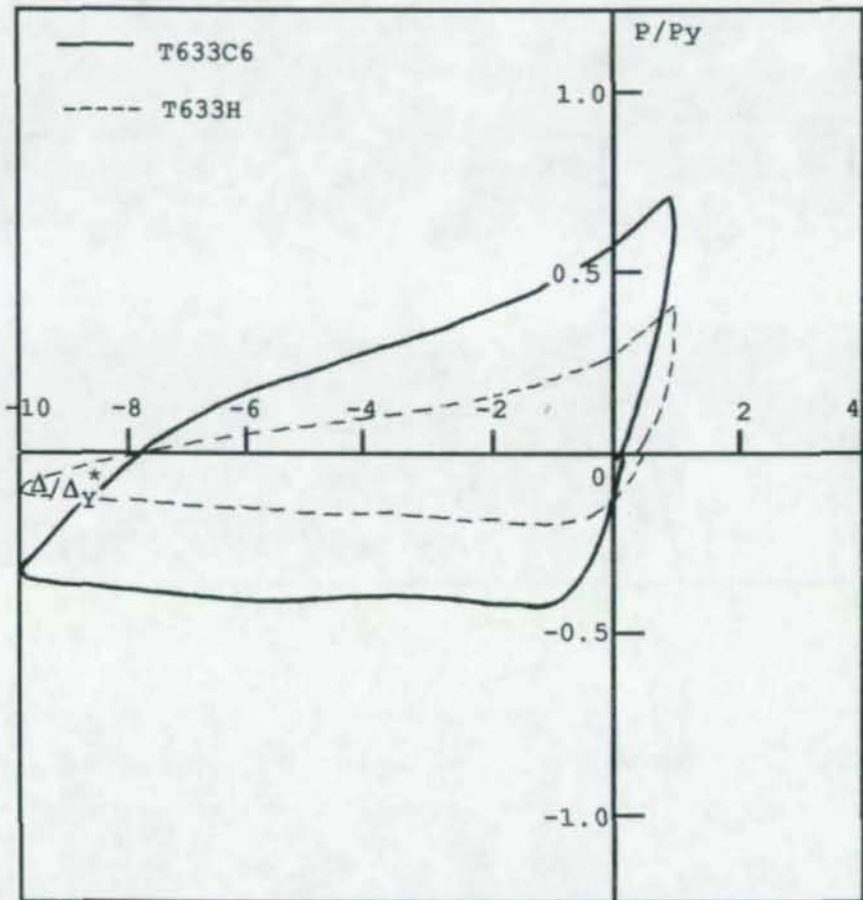


Figure B.7 Hysteresis Loops for Specimens T633H and T633C6 in Cycle 7

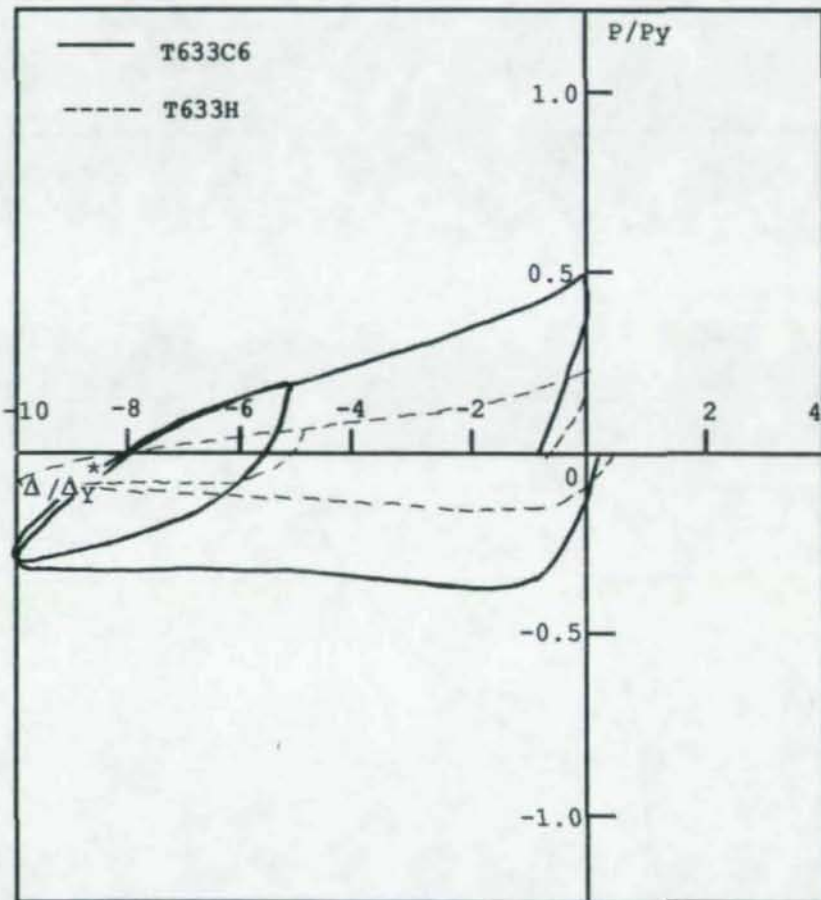


Figure B.8 Hysteresis Loops for Specimens T633H and T633C6 in Cycle 8

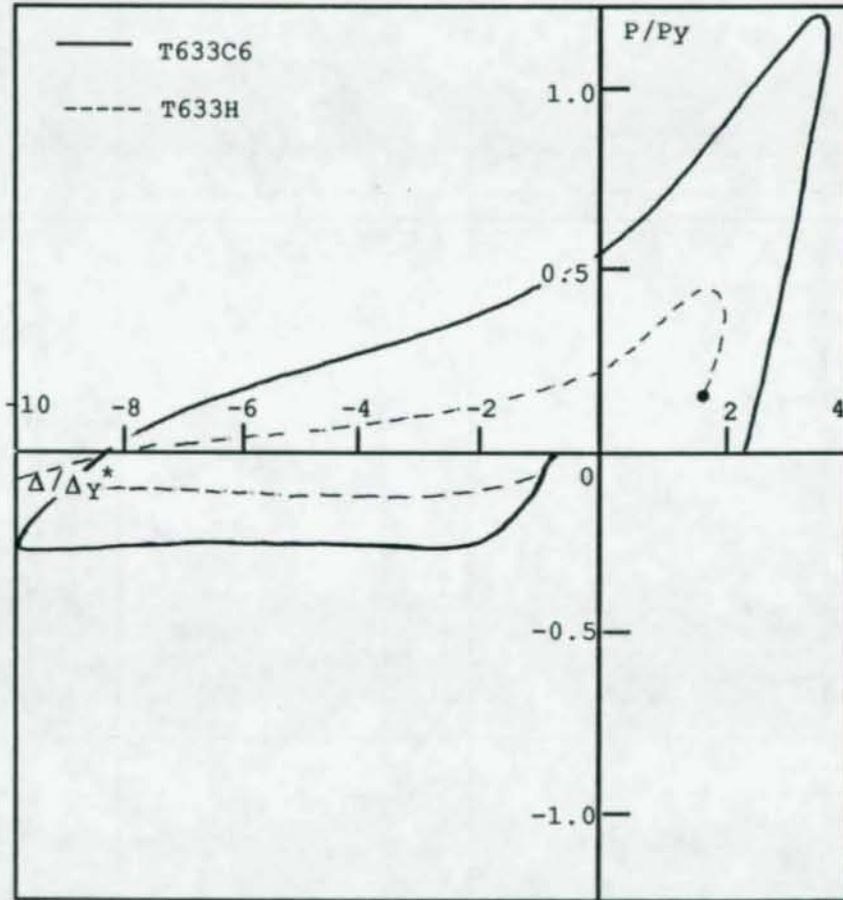


Figure B.9 Hysteresis Loops for Specimens  
T633H and T633C6 in Cycle 9

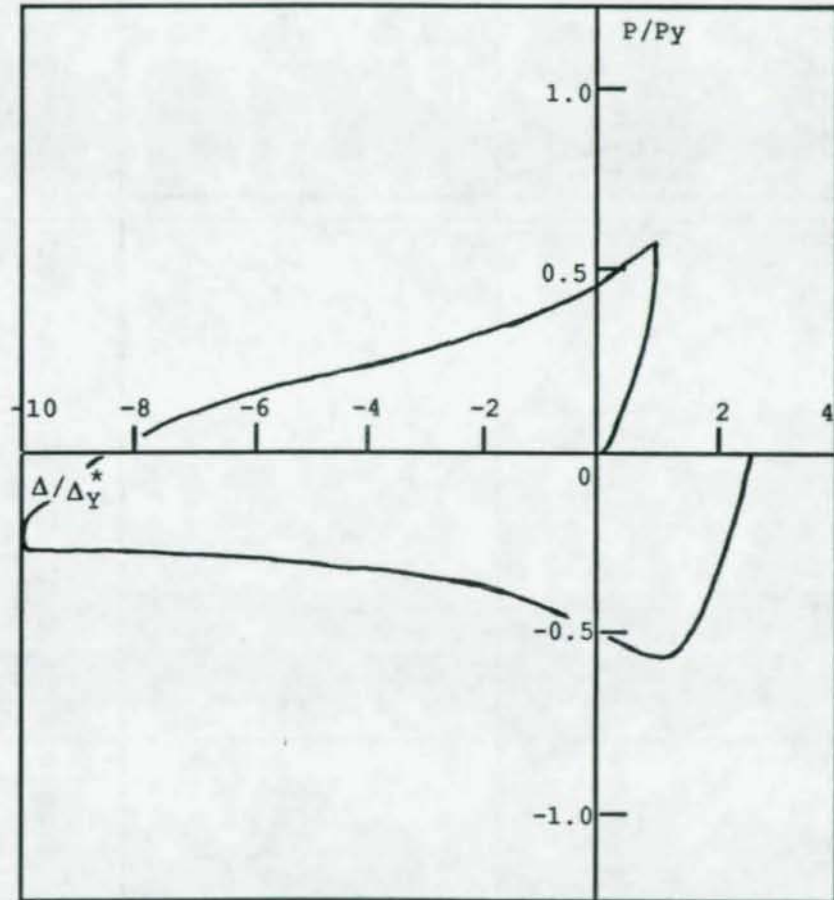


Figure B.10 Hysteresis Loop for Specimen  
T633C6 in Cycle 10

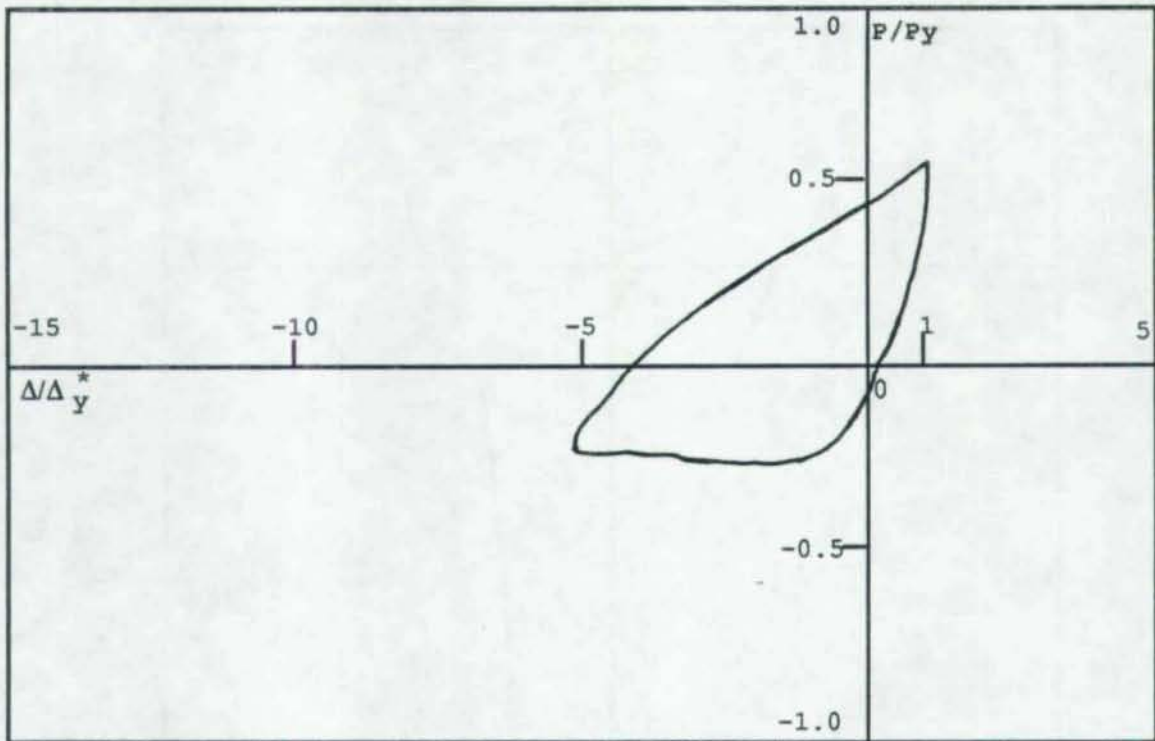


Figure B.11 Hysteresis Loops for Specimen T633C6 in Cycle 11

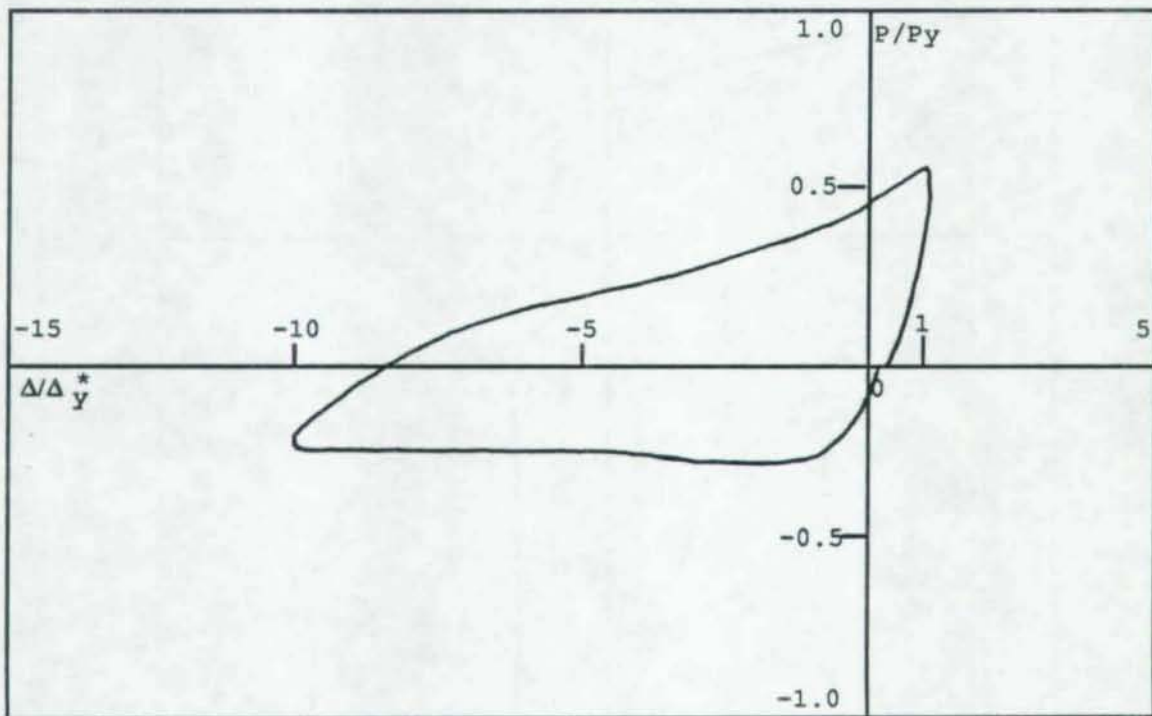


Figure B.12 Hysteresis Loops for Specimen T633C6 in Cycle 12

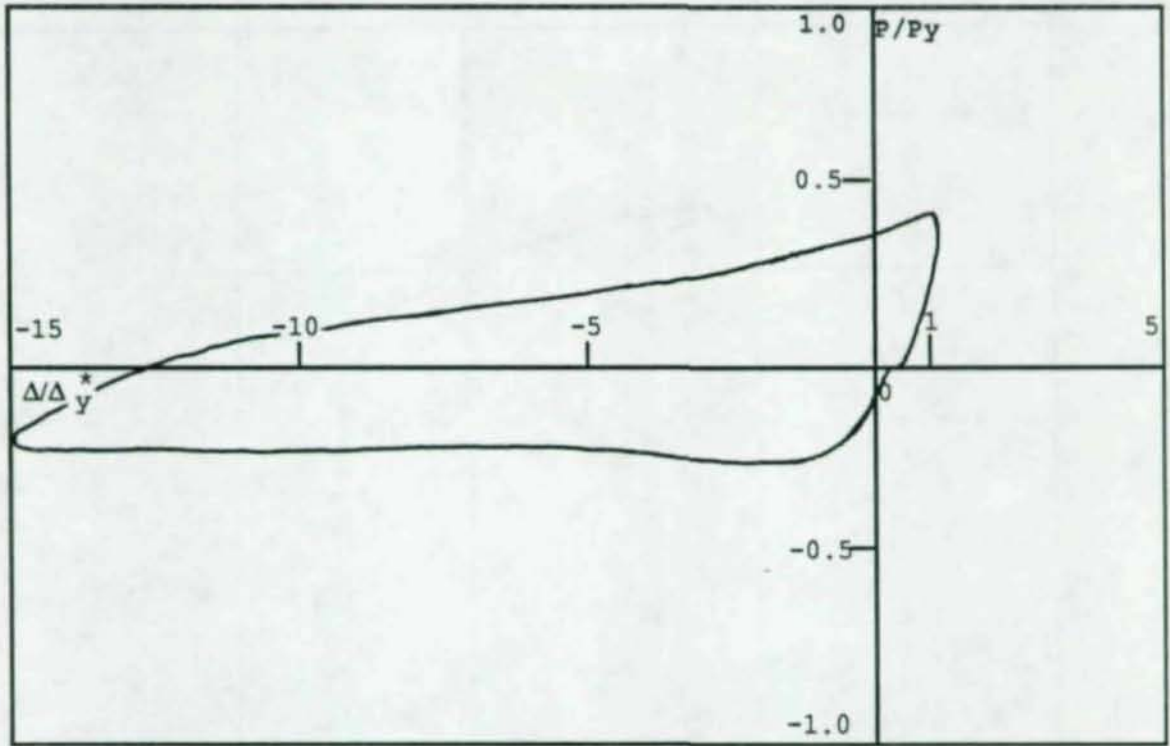


Figure B.13 Hysteresis Loops for Specimen T633C6 in Cycle 13

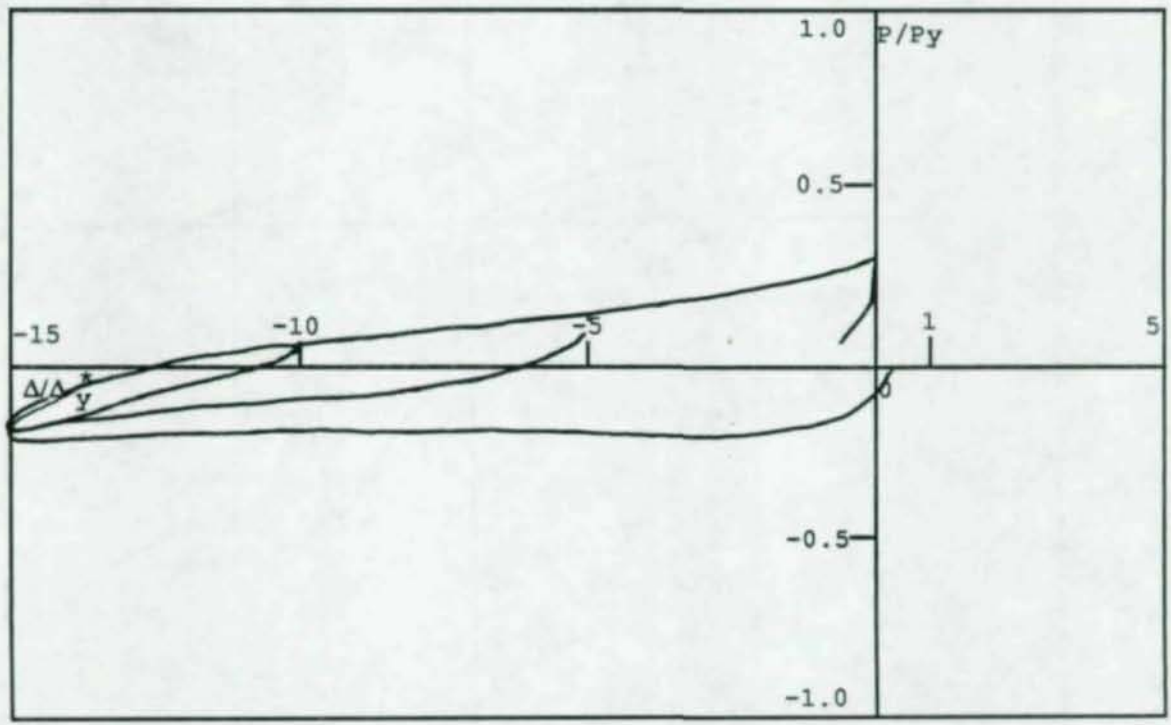


Figure B.14 Hysteresis Loops for Specimen T633C6 in Cycle 14

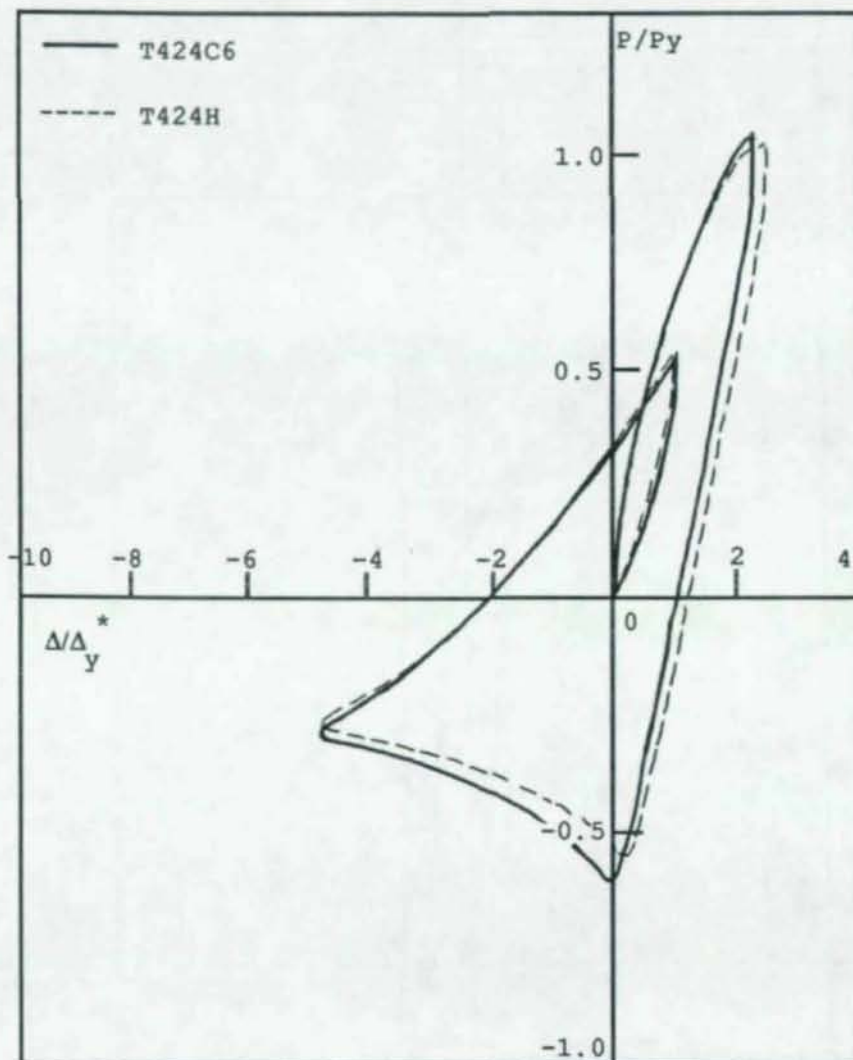


Figure B.15 Hysteresis Loops for Specimens T424H & T424C6 in Cycle 1

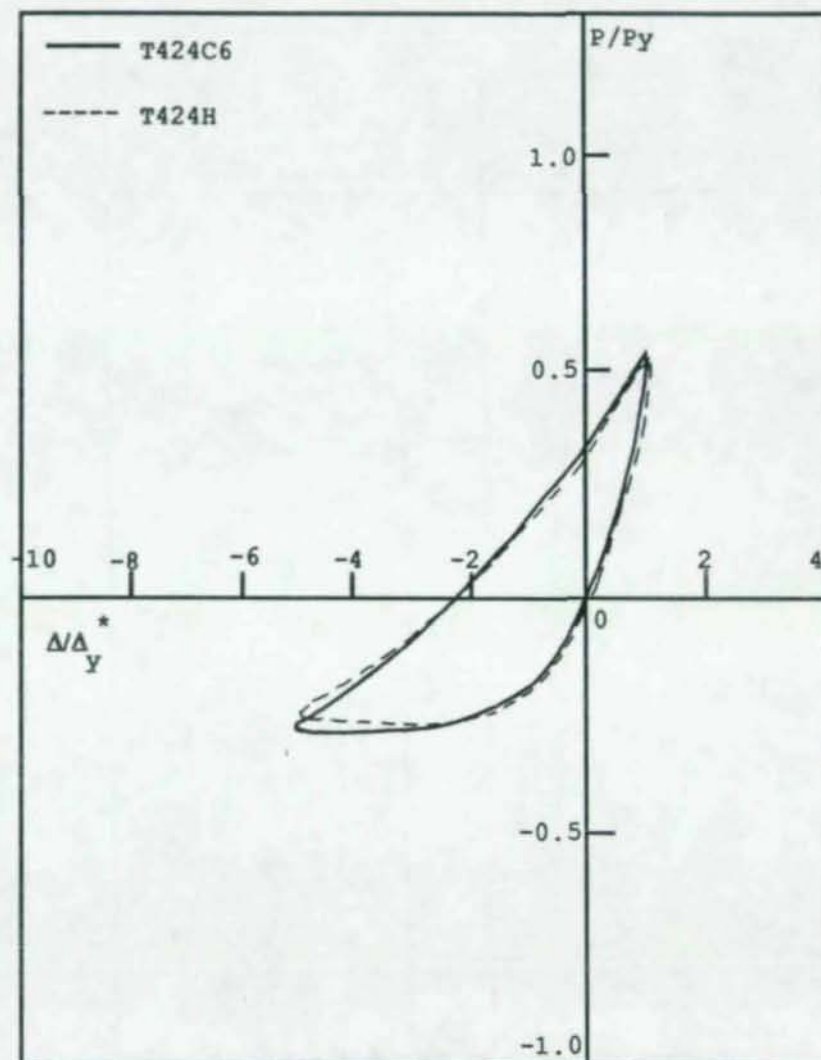


Figure B.16 Hysteresis Loops for Specimens T424H & T424C6 in Cycle 2

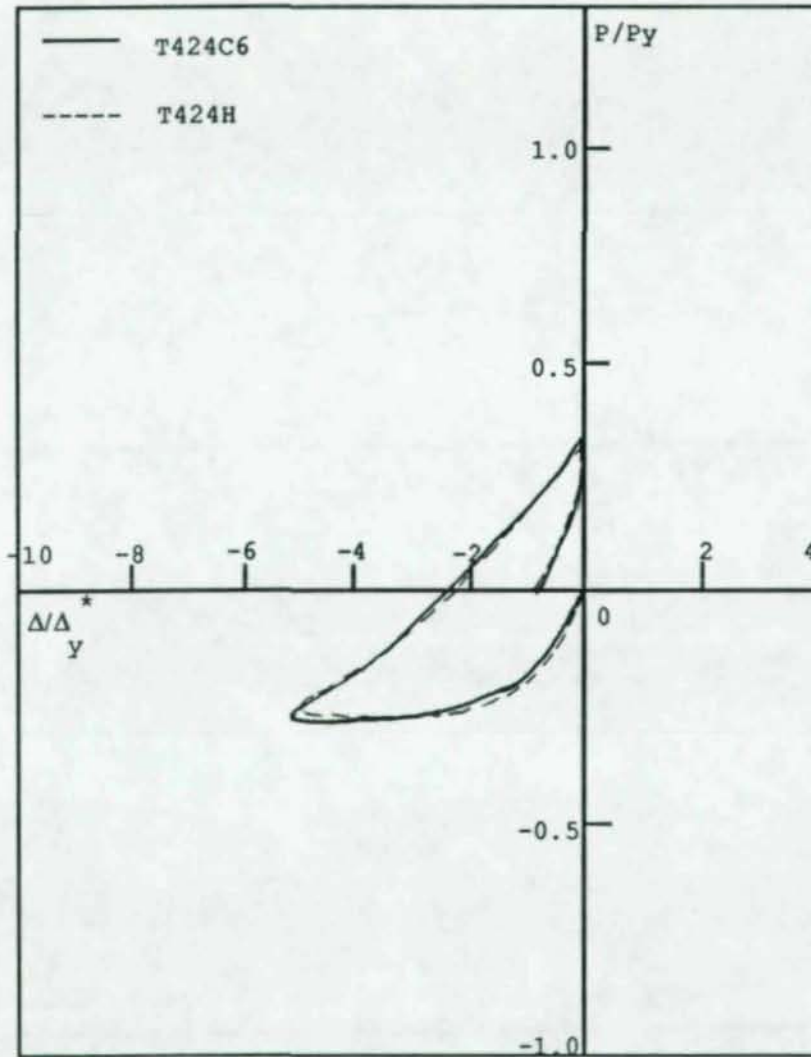


Figure B.17 Hysteresis Loops for Specimens T424H & T424C6 in Cycle 3

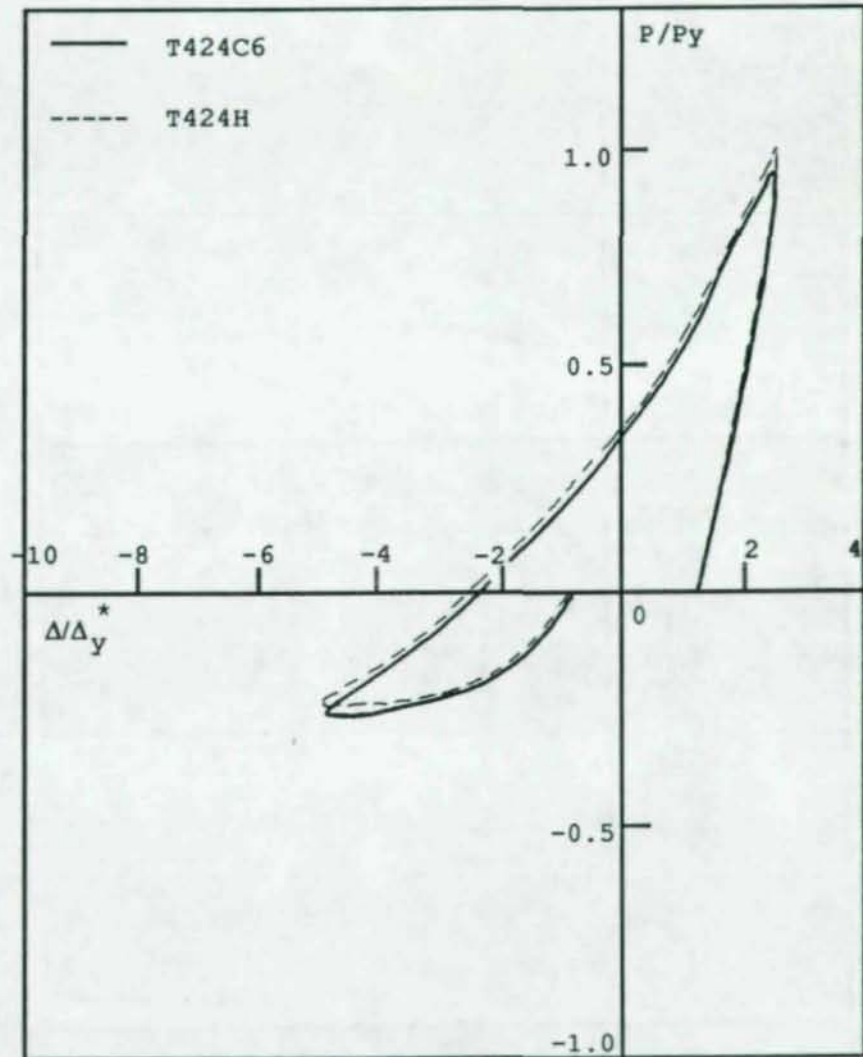


Figure B.18 Hysteresis Loops for Specimens T424H & T424C6 in Cycle 4

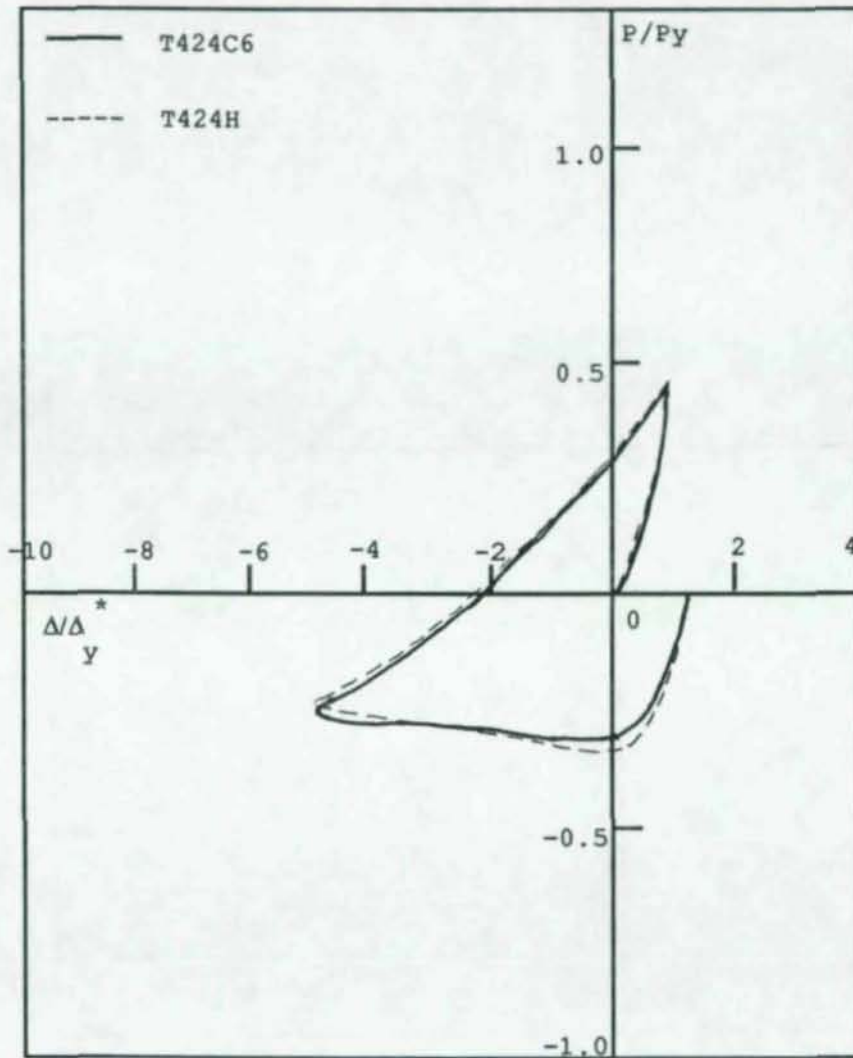


Figure B.19 Hysteresis Loops for Specimens T424H & T424C6 in Cycle 5

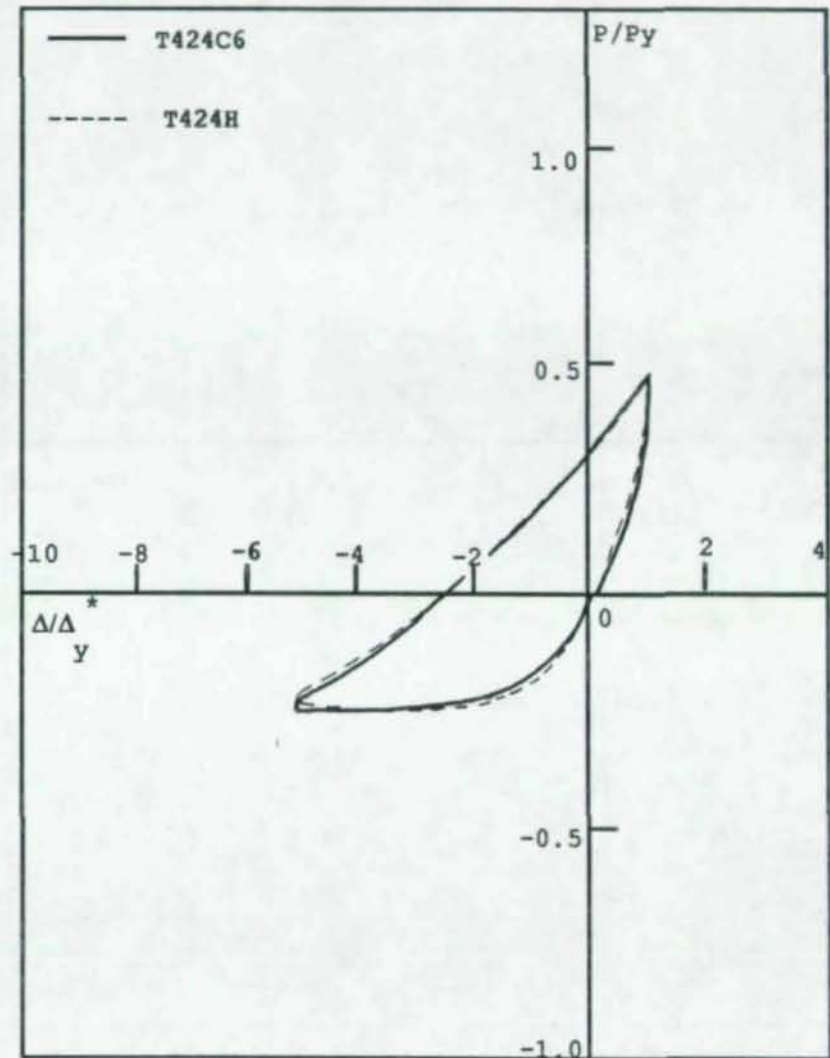


Figure B.20 Hysteresis Loops for Specimens T424H & T424C6 in Cycle 6

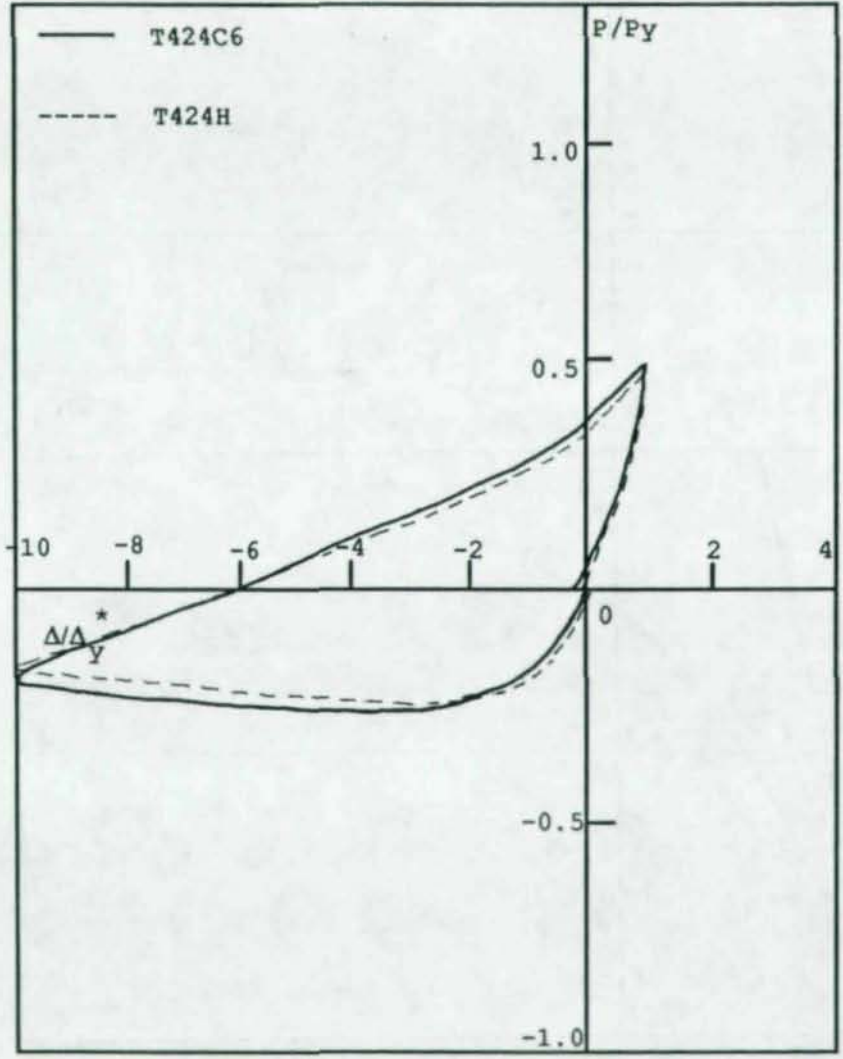


Figure B.21 Hysteresis Loops for Specimens T424H & T424C6 in Cycle 7

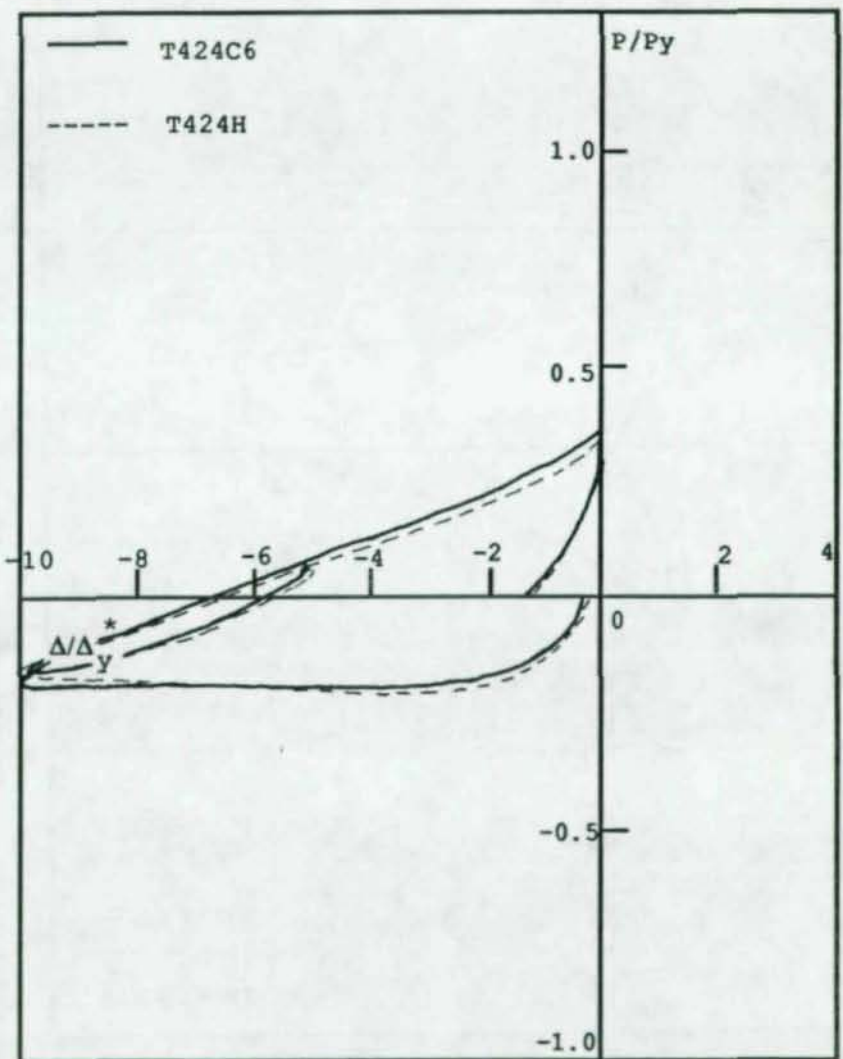


Figure B.22 Hysteresis Loops for Specimens T424H & T424C6 in Cycle 8

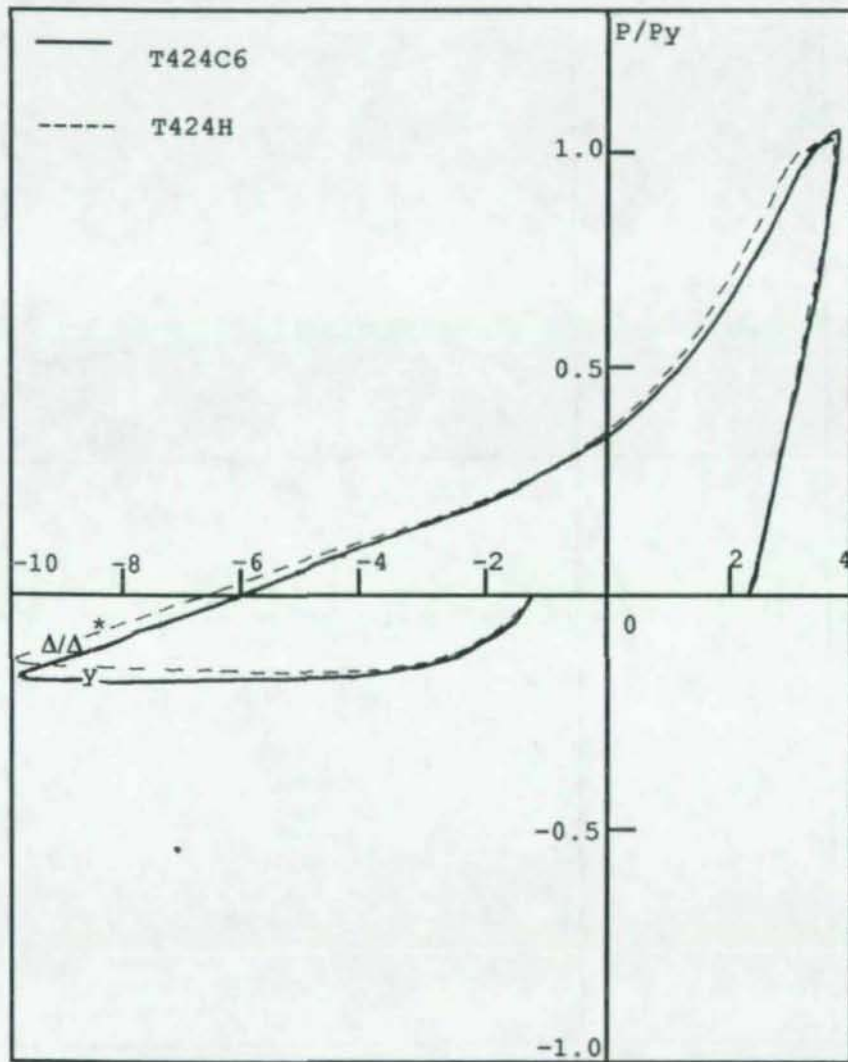


Figure B.23 Hysteresis Loops for Specimens T424H & T424C6 in Cycle 9

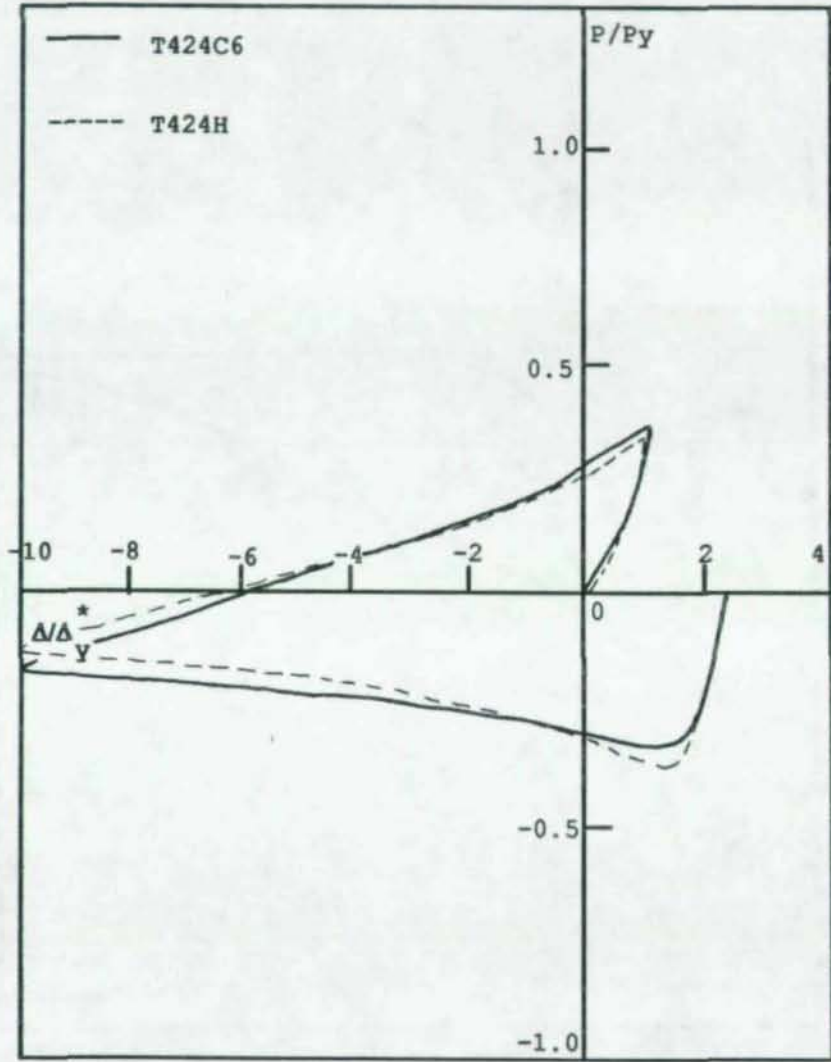


Figure B.24 Hysteresis Loops for Specimens T424H & T424C6 in Cycle 10

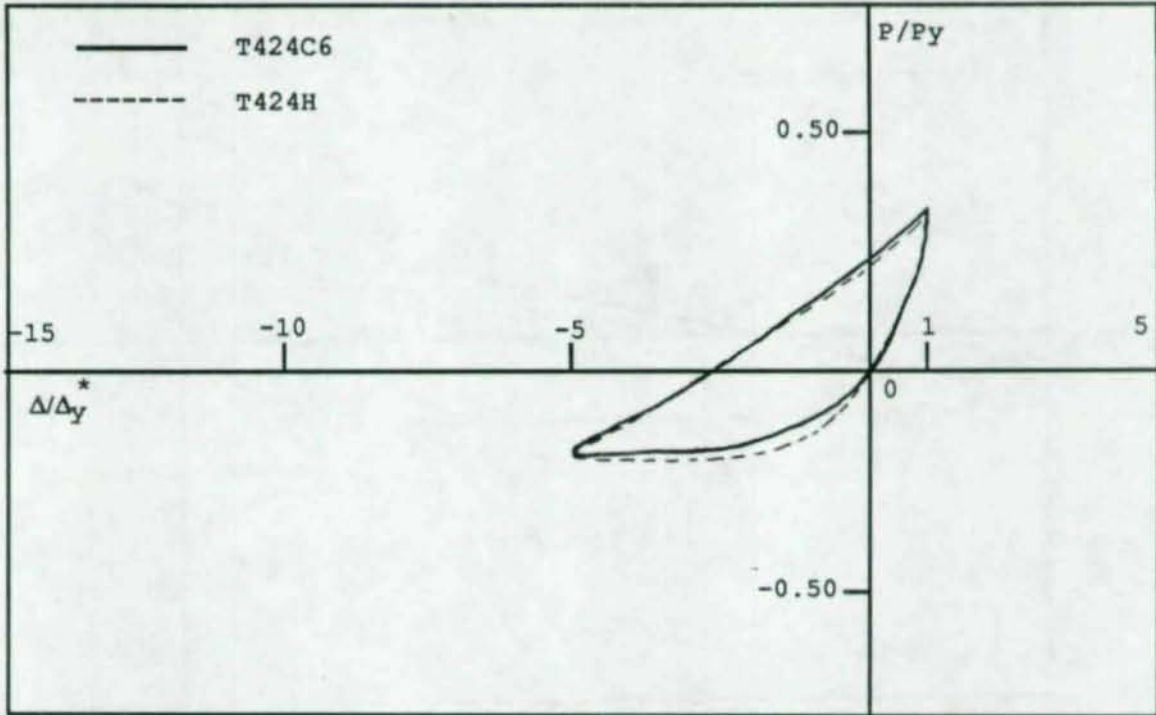


Figure B.25 Hysteresis Loops for Specimens  
T424H and T424C6 in Cycle 11

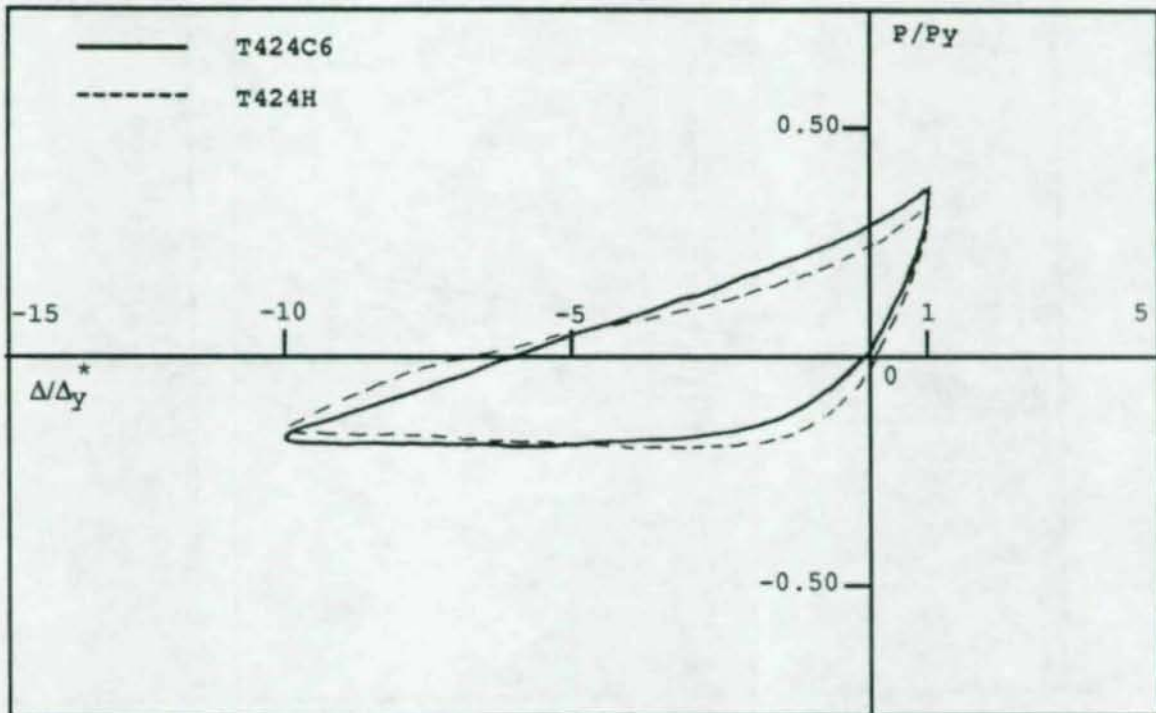


Figure B.26 Hysteresis Loops for Specimens  
T424H and T424C6 in Cycle 12

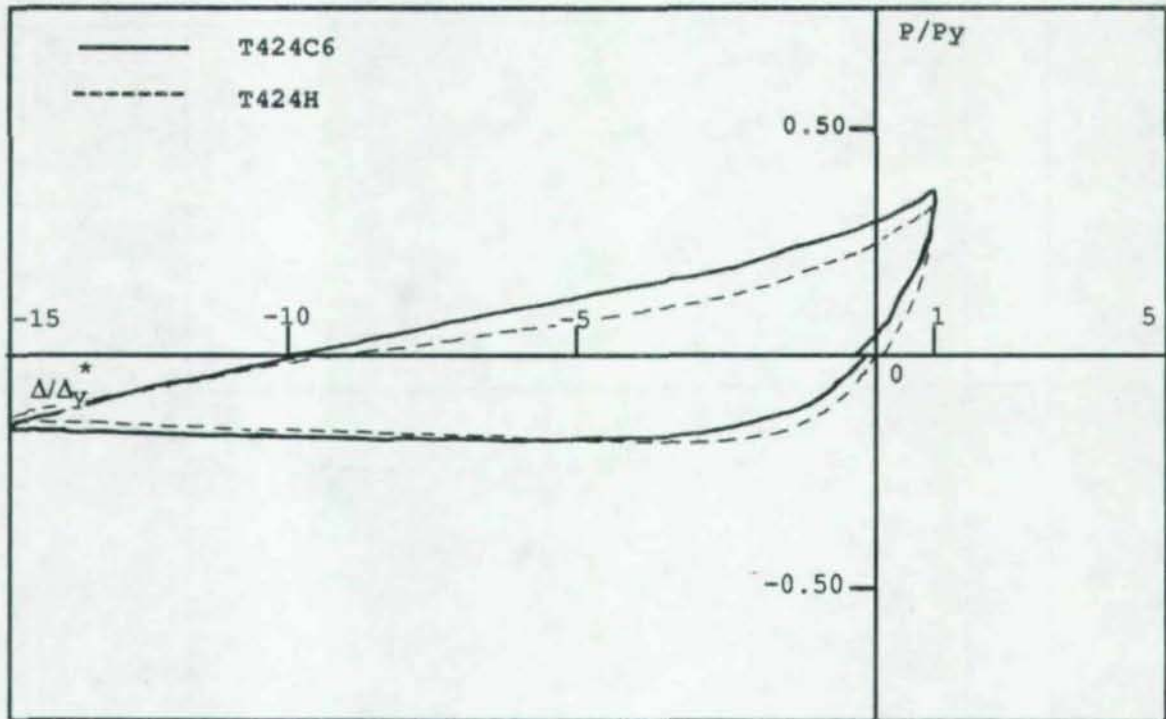


Figure B.27 Hysteresis Loops for Specimens  
T424H and T424C6 in Cycle 13

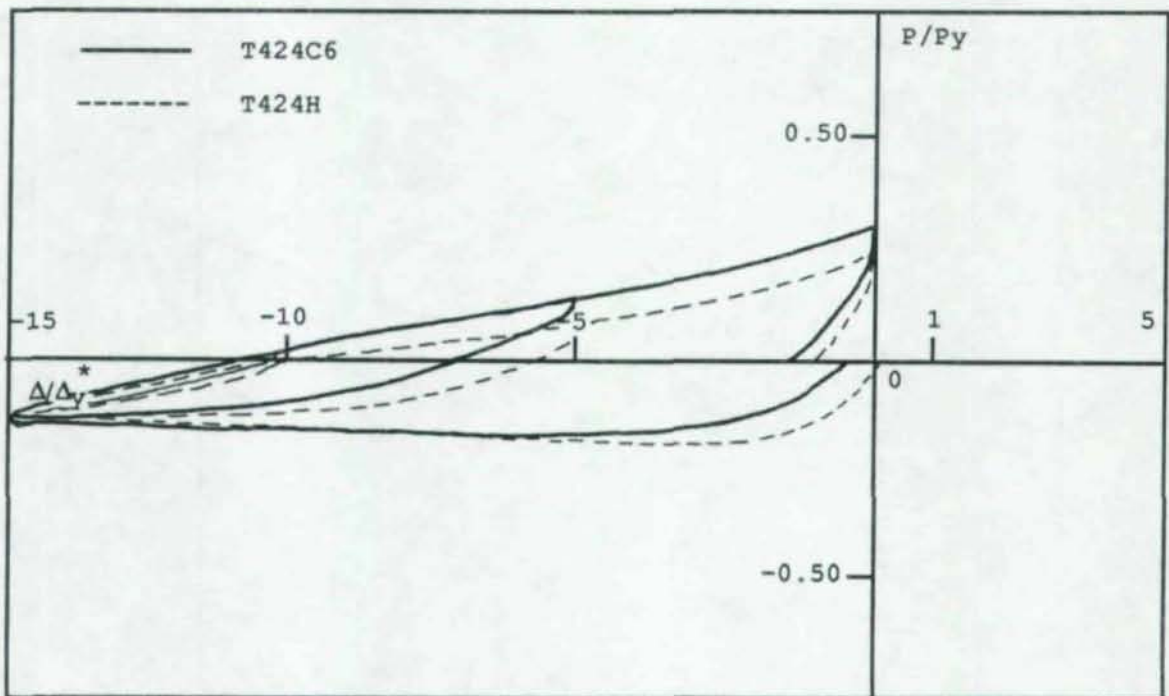


Figure B.28 Hysteresis Loops for Specimens  
T424H and T424C6 in Cycle 14

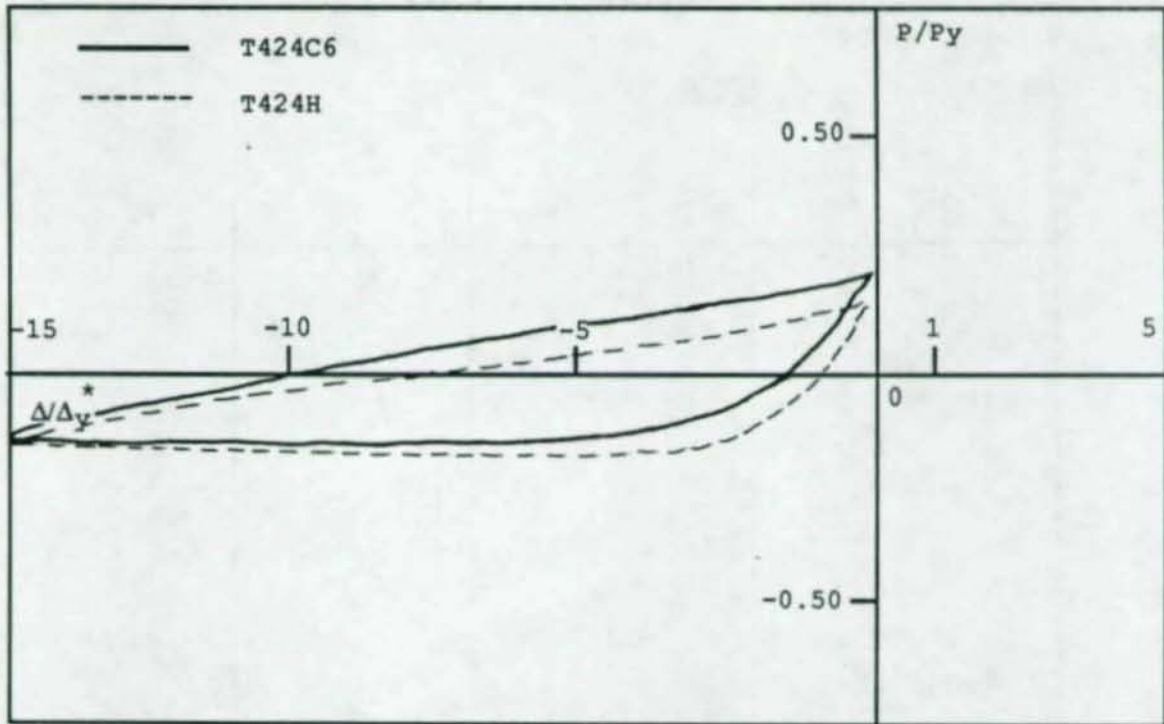


Figure B.29 Hysteresis Loops for Specimens T424H and T424C6 in Cycle 15

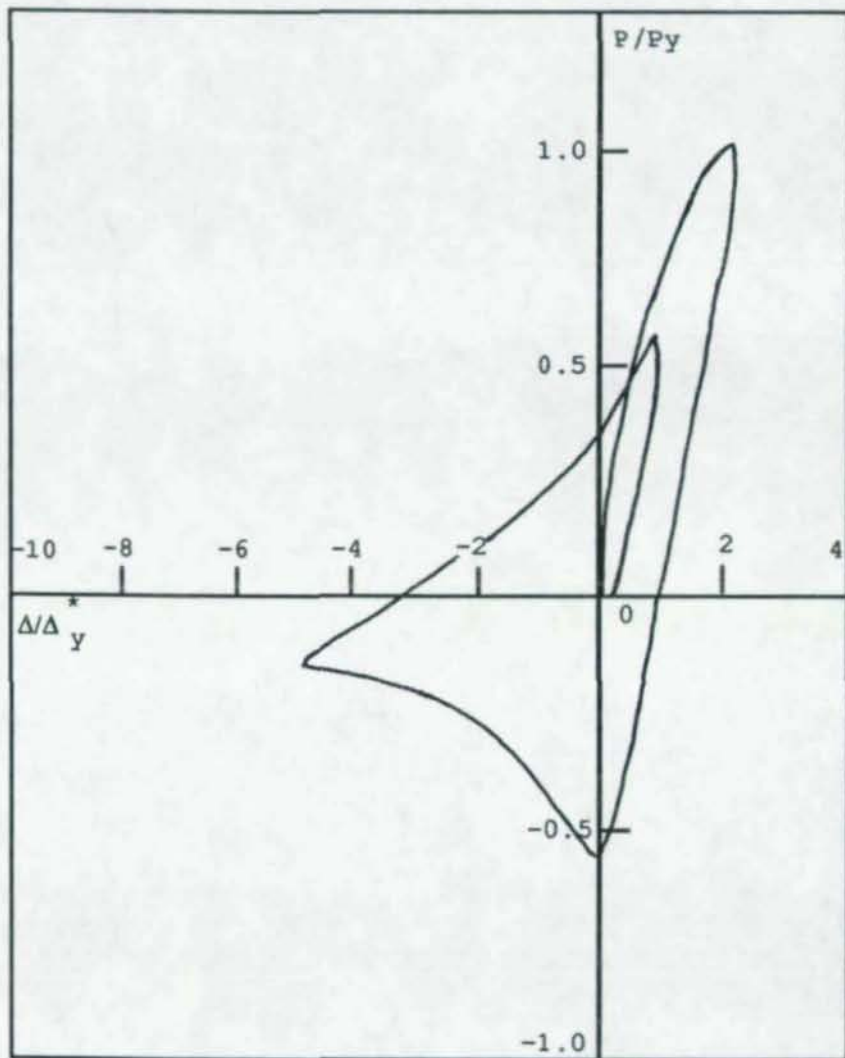


Figure B.30 Hysteresis Loops for Specimen T422H in Cycle 1

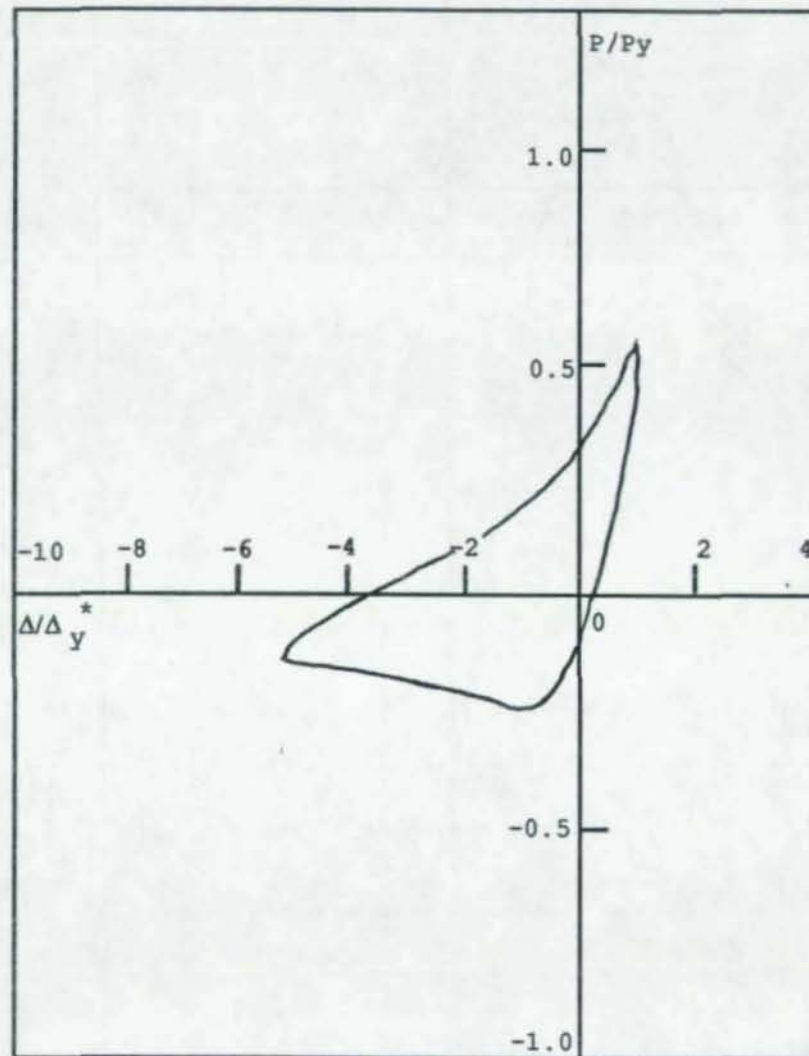


Figure B.31 Hysteresis Loops for Specimen T422H in Cycle 2

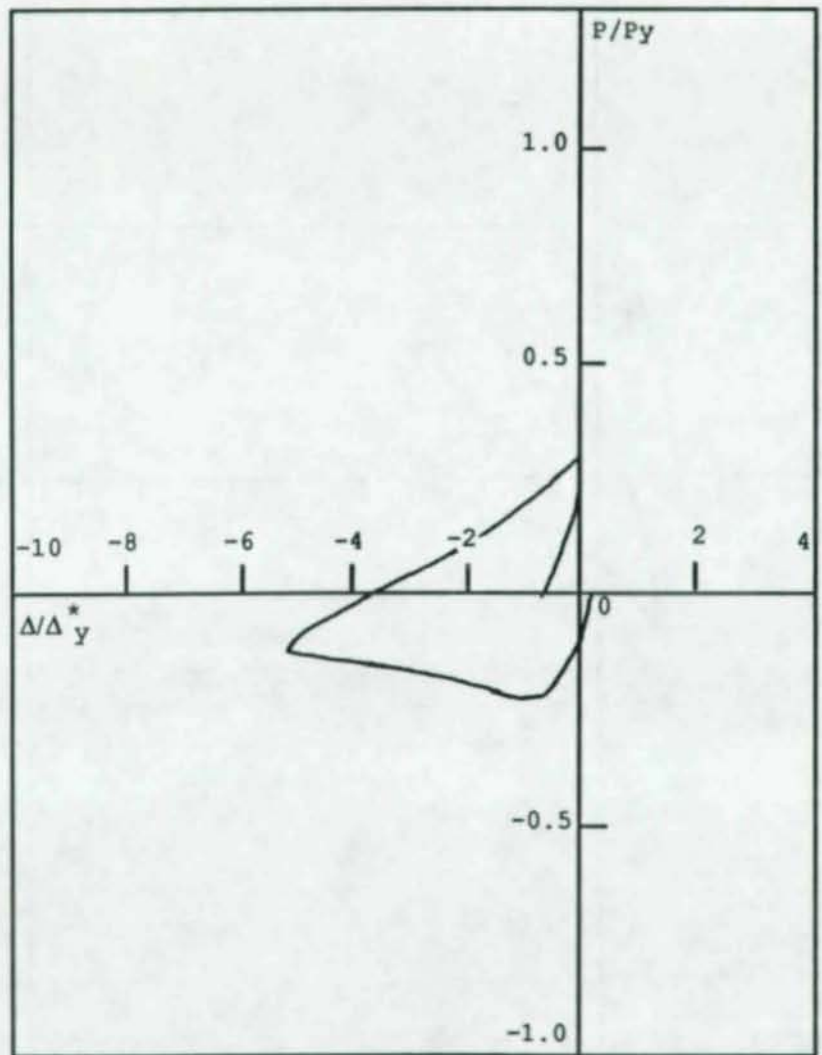


Figure B.32 Hysteresis Loops for Specimen T422H in Cycle 3

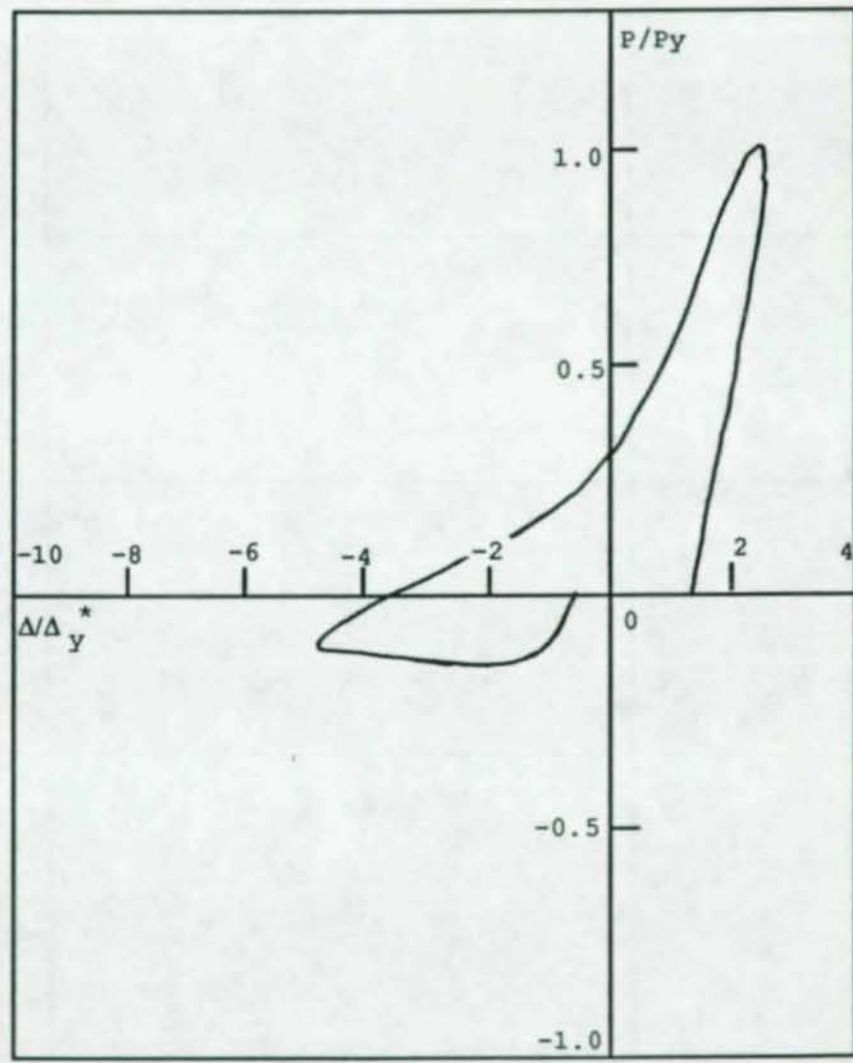


Figure B.33 Hysteresis Loops for Specimen T422H in Cycle 4

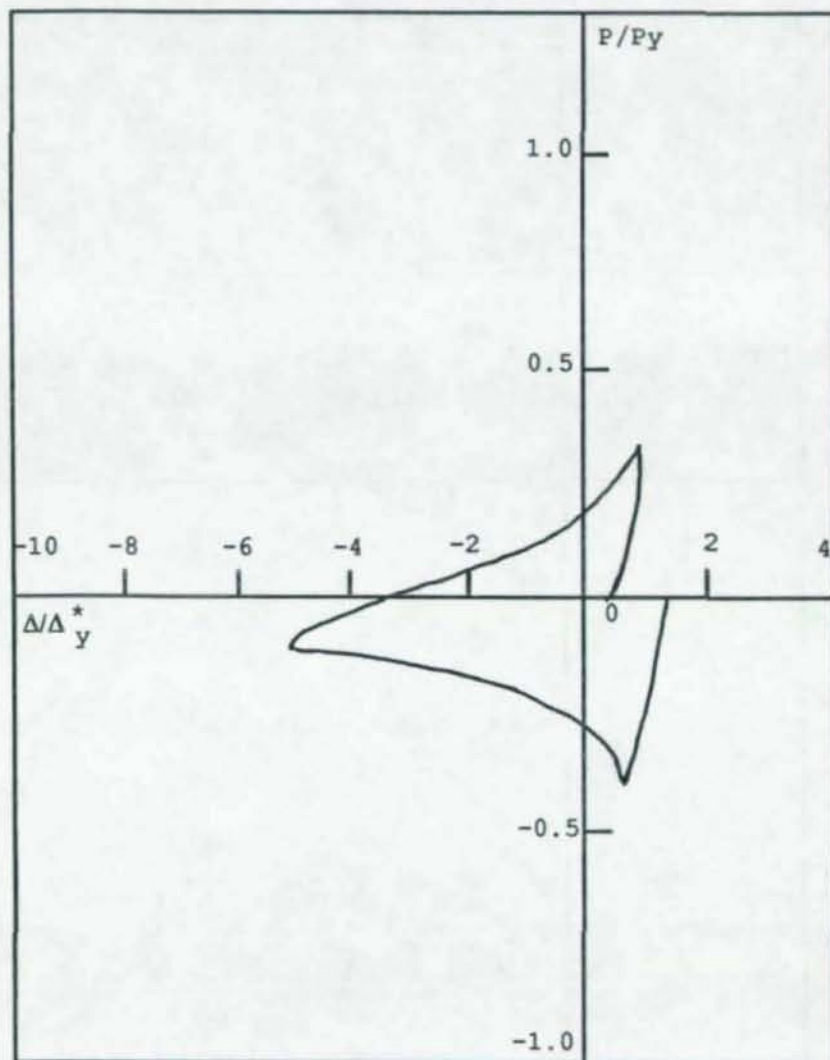


Figure B.34 Hysteresis Loops for Specimen T422H in Cycle 5

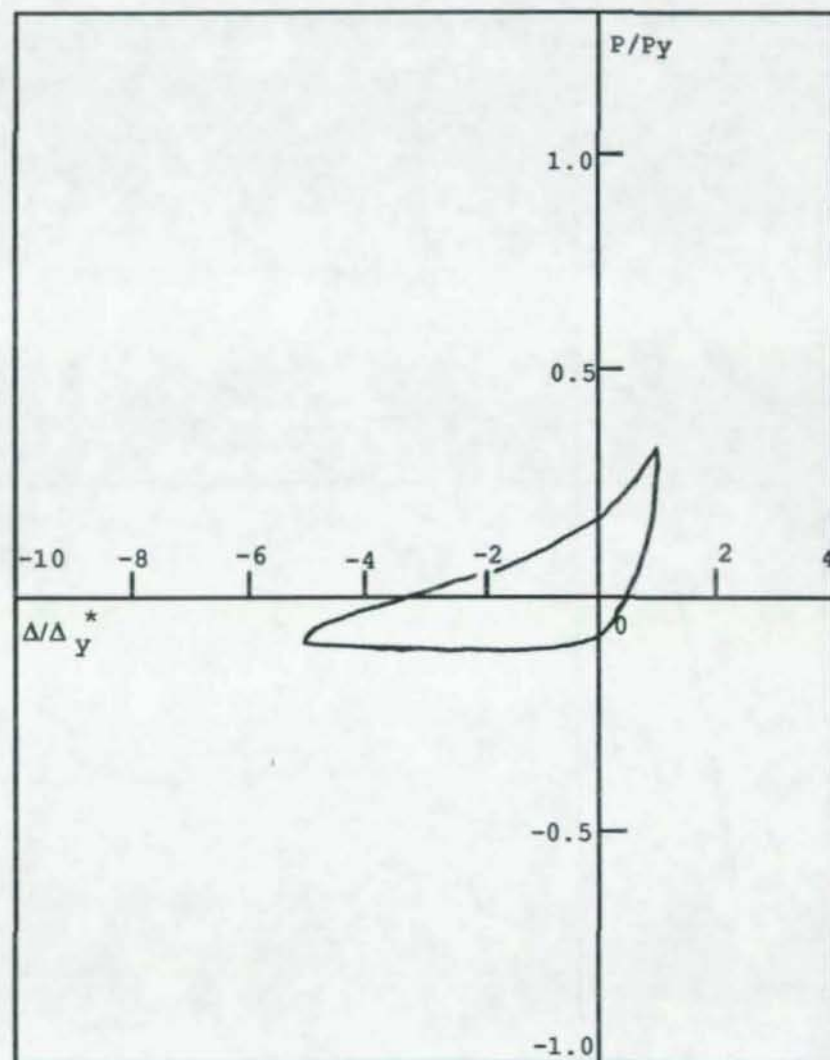


Figure B.35 Hysteresis Loops for Specimen T422H in Cycle 6

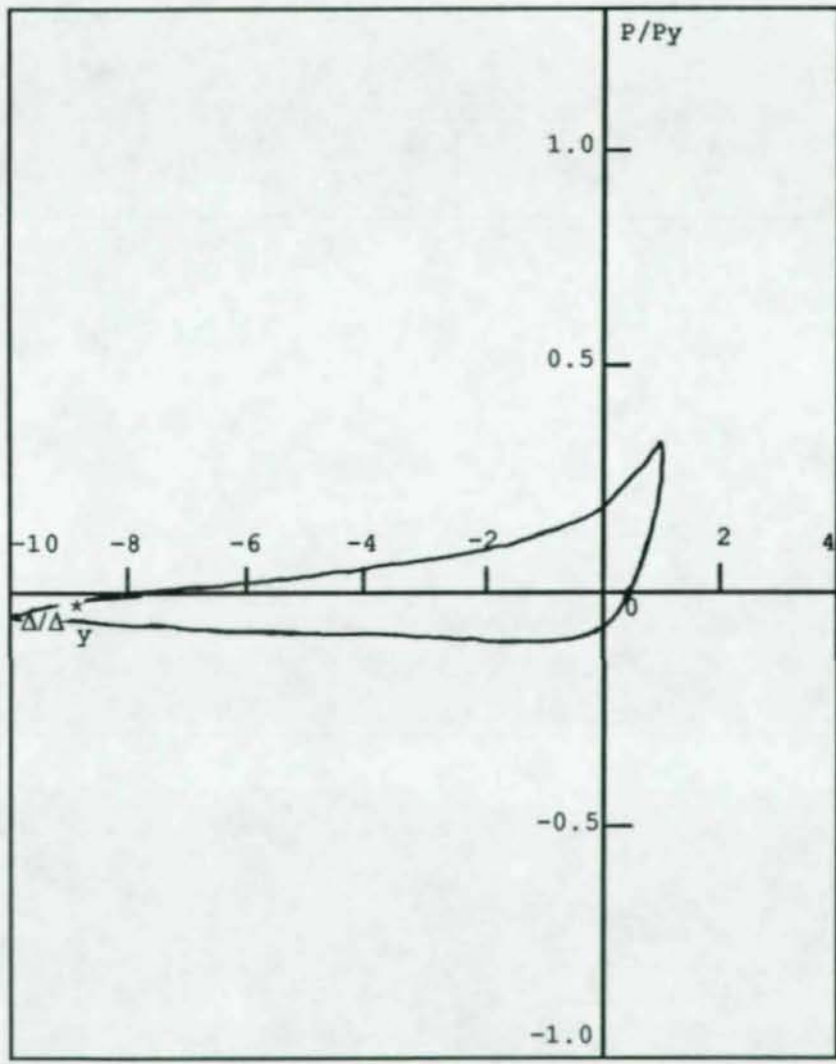


Figure B.36 Hysteresis Loops for Specimen T422H in Cycle 7

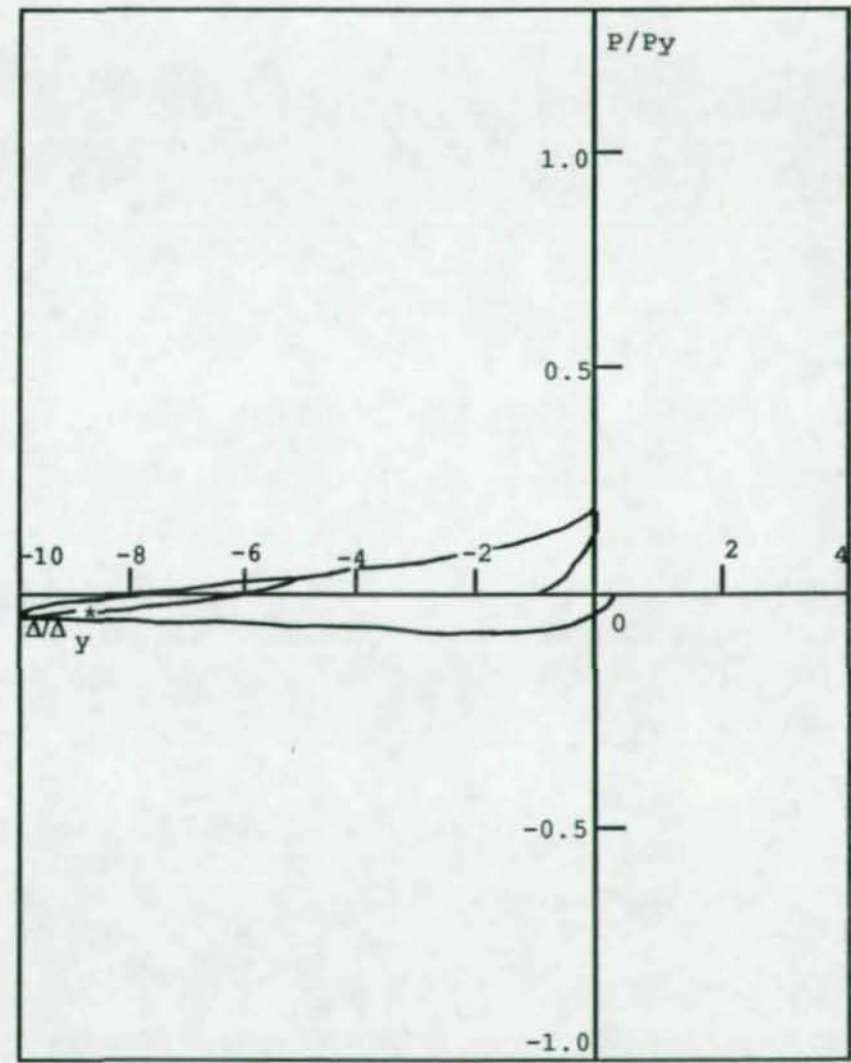


Figure B.37 Hysteresis Loops for Specimen T422H in Cycle 8

REFERENCES

## REFERENCES

1. American Concrete Institute (ACI), "Building Code Requirements for Reinforced Concrete (ACI 318-83)," ACI, Detroit, Michigan, 1983.
2. American Institute of Steel Construction, "Load and Resistance Factor Design," Chicago, Illinois, 1986.
3. American Institute of Steel Construction, "Specification for the Design, Fabrication and Erection of Structural Steel for Buildings," Chicago, Illinois, 1978.
4. Astaneh-Asl, A., and Goel, S.C., and Hanson, R.D., "Cyclic Behavior of Double Angle Bracing Members with End Gusset Plates," Report No. UMEE 82R7, Department of Civil Engineering, University of Michigan, Ann Arbor, Michigan, August, 1982.
5. Black, R.G., Wenger, W.A. and Popov, E.P., "Cyclic Inelastic Buckling of Steel Struts under Cyclic Load Reversals," Report No. UCB/ERRC-80/40, University of California, Berkeley, California, October, 1980.
6. Chen, W.F., and Atsuta, T., "Theory of Beam-Columns," (Volume I, Inplane Behavior and Design), McGraw-Hill Inc., 1976.
7. Chen, W.F., and Chen, C.H., "Analysis of Concrete-Filled Steel Tubular Beam-Columns," Report No. 370.10, Fritz Engineering Laboratory, Lehigh University.
8. El-Tayem, A.A., and Goel, S.C., "Cyclic Behavior of Angle X-Bracing with Welded Connections," Report No. UMEE 85-4, Department of Civil Engineering, The University of Michigan, Ann Arbor, Michigan, April, 1985.
9. Goel, S.C., "A Preliminary Correlation Study of the Six Story Braced Steel Test Building," Fifth JTCC Meeting, Tsukuba, Japan, February 27-29, 1984.
10. Goel, S.C., and Foutch, D.A., "Preliminary Studies and Test Results of Eccentrically Braced Full-Size Steel Structure," Sixteenth Joint Meeting U.S.-Japan Panel on Wind and Seismic Effects, National Bureau of Standards, Washington, D.C., May 15-18, 1984.

11. Goel, S.C., "Seismic Stability of Braced Steel Structures," Proceedings, Structural Stability Research Council Meeting, Washington, D.C., April 15-16, 1986.
12. Goel, S.C., and Tang, X., "Seismic Design of Steel Braced Frame," Proceeding, ASCE Structures Congress, New Orleans, September, 1986.
13. Gugerli, H. and Goel, S.C., "Inelastic Cyclic Behavior of Steel Bracing Members," Report No. UMEE 82R1, Department of Civil Engineering, The University of Michigan, Ann Arbor, Michigan, January, 1982.
14. Hanson, R.D., "Comparison of Static and Dynamic Hysteresis Curves," Journal of the Engineering Mechanics Division, ASCE, Volume No. EM5, October, 1966.
15. Higginbotham, A.B., and Hanson, R.D., "Axial Hysteretic Behavior of Steel Members," Journal of the Structural Division, ASCE, Vol. 102, No. ST7, July, 1976.
16. Ikeda, K., and Mahin, S.A., "A Refined Physical Theory Model for Predicting the Seismic Behavior of Brace Frames," Report No. UCB/EERC-84/12, University of California, Berkeley, California, July, 1984.
17. Jain, A.K., Goel, S.C., and Hanson, R.D., "Axial Hysteretic Behavior of Steel Members," Journal of the Structural Division, ASCE, Vol. 102, No. ST7, July, 1976.
18. Jain, A.K., Goel, S.C., and Hanson, R.D., "Static and Dynamic Hysteresis Behavior of Steel Tubular Members with Welded Gusset Plates," Report No. UMEE 78R3, Department of Civil Engineering, The University of Michigan, Ann Arbor, Michigan, June, 1977.
19. Kahn, L.F. and Hanson, R.D., "Inelastic Cycles of Axially Loaded Steel Members," Journal of the Structural Division, ASCE, Vol. 102, No. ST5, May, 1976.
20. Maison, B.F. and Popov, E.P., "Cyclic Response Prediction for Braced Steel Members," Journal of the Structural Division, ASCE, Vol. 106, No. ST7, July, 1980.
21. Miao, R.Y., "Analysis on Compressive Mechanism of the Composite Material of Concrete-Filled Steel Tube," Proceedings, The International Speciality Conference on Concrete Filled Steel Tubular Structures, Harbin, China, August, 1985.
22. Naaman, A.E., and Homrich, J.R., "Properties of High-Strength Fiber Reinforced Concrete," Proceeding of ACI Symposium on High Strength Concrete, H. Russel, Editor, SP-87, Detroit, 1985, pp. 233-249.

23. Nobuyuki, N., Shoichi, S., and Michio K., "Behavior of Concrete-filled Steel Tubes (Part 2; Bending Member)," 15-th Joint Meeting, UJNR, Tsukuba, May, 1983.
24. Park, R., and Paulay, T., "Reinforced Concrete Structures," John Wiley and Sons, Inc. 1975.
25. Portland Cement Association, "Design and Control of Concrete Mixtures," Twelfth Edition, Skokie, Illinois, 1979.
26. Prathuangsit, D., Goel, S.C., and Hanson, R.D., "Axial Hysteresis Behavior with Rotational End Restraints," Journal of the Structural Division, ASCE, Vol. 104, No. ST6, June, PP. 883-986.
27. Saeki, S., Minlsaku, K., and Takizawa, A., "Behavior of Concrete-Filled Steel Tubes (Part III; Beam-Column Members)," 16-th Joint Meeting, U.S.-Japan Panel on Wind Seismic Effects, UJNR, Washington, May 14-17, 1984.
28. Sakono, K., and Tomii, M., "Hysteretic Behavior of Concrete-Filled Square Steel Tubular Beam-Column Failed in Flexure," Transactions of Japan Concrete Institute, Vol. 3, 1981
29. Shah, S.P., "High Strength Concrete," Proceeding of a Workshop Held at the University of Illinois at Chicago Circle, December, 1979.
30. Singh, P., "Seismic Behavior of Braces and Braced Steel Frames," Report No. UMEE 77R1, Department of Civil Engineering, The University of Michigan, Ann Arbor, Michigan, July, 1977.
31. SSRC Task Group 20, "A Specification for the Design of Steel-Concrete Composite Columns," AISC Engineering Journal, 4th Qtr. 1979.
32. Storozhenko, L.I., "Strength and Deformation of Concrete Filled Steel Tubular Elements," Proceedings, The International Speciality Conference on Concrete Filled Steel Tubular Structures, Harbin, China, August, 1985.
33. Structural Welding Code, AWS D1.1-79., Miami, Fla.: American Welding Society, 1979.
34. Tissier, P., "Applications of HSS in France," Proceedings, International Symposium on Hollow Structural Sections, Toronto, Canada, May 25, 1977.
35. Tomii, M., and Sakino, K., "Experimental Studies on the Ultimate Moment of Concrete Filled Square Steel Tubular Beam-Columns," Trans. of A.I.J., No. 275, January, 1979.

36. Tomii, M., and Sakino, K., "Elasto-Plastic Behavior of Concrete Filled Square Steel Tubular Beam-Columns," Trans. of A.I.J., No. 280, June, 1979.
37. Tomii, M., and Sakino, K., "Experimental Studies on Concrete Filled Square Steel Tubular Beam-Columns Subjected to Monotonic Shearing Force and Constant Axial Force," Trans. of A.I.J., No. 281, July, 1979.
38. "Uniform Building Code" (UBC); International Conference of Building Officials, Whittier, California, 1976.
39. Zayas, V.A., Mahin, S.A. and Popov, E.P., "Cyclic Inelastic Behavior of Steel off Shore Structures," Report No. UCB/EERC-80/27, University of California, Berkeley, California, August, 1980.
40. Zayas, V.A., Popov, E.P., and Mahin, S.A., "Cyclic Inelastic Behavior of Tubular Steel Braces," Report No. UCB/EERC-80/16, University of California, Berkeley, California, June, 1980.
41. Zhong, S.T., "The Use of Concrete Filled Tubular Structure in China," Proceedings, The International Speciality Conference on Concrete Filled Steel Tubular Structures, Harbin, China, August, 1985.
42. Zhong, S.T., "Behavior and Strength Index of Concrete Filled Steel Tube as Composite Material under First Compression," Proceedings, The International Speciality Conference on Concrete Filled Steel Tubular Structures, Harbin, China, August, 1985.

99374